Hétérogénéité d'expression et rôles de l'E3 ubiquitine ligase TRIP12 dans la carcinogenèse pancréatique

Manon Brunet

THÈSE

En vue de l'obtention du
DOCTORAT DE L'UNIVERSITÉ DE TOULOUSE

Délivré par l'Université Toulouse 3 - Paul Sabatier

Présentée et soutenue par

Manon BRUNET

Le 20 octobre 2021

Hétérogénéité d'expression et rôles de l'E3 ubiquitine ligase TRIP12 dans la carcinogenèse pancréatique

---

Ecole doctorale : **BSB - Biologie, Santé, Biotechnologies**

Spécialité : **CANCEROLOGIE**

Unité de recherche :
CRCT - Centre de Recherche en Cancérologie de Toulouse

Thèse dirigée par
Marlène DUFRESNE et Jérôme TORRISANI

Jury

M. Patrick Jacquemin, Rapporteur
Mme Céline Gongora, Rapporteure
Mme Cécile Haumaitre, Rapporteure
Mme Julie GUILLERMET-GUIBERT, Examinatrice
Mme Marlène DUFRESNE, Directrice de thèse
M. Jérôme Torrisani, Co-directeur de thèse

Sommaire

Résumé

Le mauvais pronostic du cancer du pancréas (CP) peut s'expliquer par un diagnostic tardif et le manque de traitements efficaces. Une meilleure compréhension des mécanismes moléculaires qui régissent l'initiation, la progression et la résistance aux chimiothérapies est indispensable pour améliorer la prise en charge des patients.

TRIP12 (Thyroid hormone Receptor Interacting Protein 12) est une E3 ubiquitine ligase de la famille HECT (Homologous to the E6-AP Carboxyl Terminus). TRIP12 régule le cycle cellulaire et la stabilité chromosomique, elle intervient dans le remodelage de la chromatine, dans la réponse aux dommages à l'ADN et dans l'activation de la voie P53. L'ARNm de TRIP12 est surexprimé dans le CP. De plus, TRIP12 est impliquée dans la dégradation de PTF1a (Pancreas Transcription Factor 1a), facteur de transcription essentiel du développement et de l'homéostasie des cellules acinaires du pancréas, suppresseur de tumeur dont l'expression est perdue au cours de la carcinogénèse pancréatique. Ces données suggèrent un rôle de TRIP12 dans le CP.

Mon premier objectif de thèse était de déterminer pourquoi l'expression de TRIP12 augmente dans le CP et quelles en sont les conséquences. J'ai également émis l'hypothèse que TRIP12 joue un rôle dès l'initiation du CP. Mon second objectif de thèse était de déterminer si et comment TRIP12 contribue à la reprogrammation des cellules acinaires en cellules canalaires, première étape de la formation de lésions prénéoplasiques.

J'ai découvert que TRIP12 est nécessaire à la croissance des tumeurs pancréatiques et que son expression est variable dans les tumeurs et les lignées cellulaires dérivées de CP. J'ai démontré que l'hétérogénéité d'expression de TRIP12 dans ces lignées cellulaires s'explique 1)- par des niveaux d'ARNm différents liés à l'activité du promoteur du gène Trip12 et 2)- par une régulation différente de la protéine TRIP12 au cours du cycle cellulaire mettant en jeu la déubiquitinase USP7 et un défaut de l'export nucléaire de TRIP12. Les lignées pancréatiques ayant un taux élevé de TRIP12 répondent mieux aux agents anticancéreux mettant en évidence le rôle de TRIP12 dans la chimiosensibilité des cellules cancéreuses pancréatiques.

Par ailleurs, les résultats obtenus à partir d'un nouveau modèle murin montrent que l'invalidation conditionnelle de TRIP12 dans le pancréas au cours de l'embryogenèse n'altère pas le développement et la fonction du pancréas à l'âge adulte. Cependant, TRIP12 est capitale pour l'initiation du CP. En effet, la perte de TRIP12 dans les cellules acinaires empêche la métaplasie acino-canalaire. TRIP12 est aussi importante pour la progression du CP car son absence ralentit le développement des tumeurs engendrées par la mutation du gène Kras et la perte du gène P53.

L'ensemble de mes travaux de thèse montre que TRIP12 est un acteur décisif du CP et explique l'hétérogénéité d'expression de TRIP12 observée dans les tumeurs pancréatiques. Ces nouvelles connaissances pourraient offrir de nouvelles options thérapeutiques pour le CP où le besoin est énorme. TRIP12 est une protéine candidate de haute importance qui peut contribuer aux stratégies de thérapie par des médicaments innovants.

Abstract

The poor prognosis of pancreatic cancer (PC) is explained by a late diagnosis and lack of efficient treatments. A better understanding of the molecular mechanisms that govern its initiation, progression and resistance to most chemotherapies is essential to improve the patient care.

TRIP12 (Thyroid hormone Receptor Interacting Protein 12) is an HECT (Homologous to the E6-AP Carboxyl Terminus) type E3 ubiquitin ligase. TRIP12 regulates cell cycle and chromosome stability, it is involved in chromatin remodeling, DNA damage response and activation of P53 pathway. TRIP12 mRNA is overexpressed in pancreatic cancer. Furthermore, TRIP12 is involved in PTF1a (Pancreas Transcription Factor 1a) degradation, a transcription factor essential for the development and homeostasis of the pancreatic acinar cells. PTF1a is a tumor suppressor that is lost during pancreatic carcinogenesis suggesting a role of TRIP12 in PC.

My first thesis goal was to determine why TRIP12 expression increases during PC and what are the consequences of its increased expression. I also hypothesized that TRIP12 plays a role in the PC initiation. My second thesis goal was to determine how TRIP12 contributes to the acinar cells reprogramming into ductal cells, the first step in the preneoplastic lesions formation.

I demonstrated that TRIP12 expression is necessary for pancreatic tumor growth and its expression is variable within tumors and patients derived-cell lines. I showed that TRIP12 expression is heterogeneous in these cell lines and is explained 1) – by different mRNA levels linked to the activity of the TRIP12 promoter and 2) - by a different TRIP12 protein regulation during the cell cycle involving the deubiquitinase USP7 and a defect in TRIP12 protein nuclear export. Pancreatic cell lines with a high level of TRIP12 had a better response to anticancerous agents highlighting the role of TRIP12 in chemosensitivity.

Moreover, results obtained from a novel mouse model showed that TRIP12 conditional invalidation in the pancreas during embryogenesis does not alter the pancreas development and function in adulthood. However, TRIP12 is essential for PC initiation. Indeed, TRIP12 loss in acinar cells prevents acino-ductal metaplasia. TRIP12 is also important for cancer progression since its absence reduces tumor development mediated by Kras mutation and loss of P53.

My thesis researches demonstrated that TRIP12 is a decisive player in PC and explained the TRIP12 heterogeneity of expression observed in pancreatic tumors. This new knowledge could offer new treatment opportunities for PC where the need is huge. TRIP12 is a candidate protein of high importance which may contribute to innovative therapeutic strategies.

Liste des abréviations

A

APP-BP1: Amyloid Protein-Binding Protein 1

ARM: ARMadillo repeats

ARF: Alternative Reading Frame

ASXL1: Additional Sex Combs like 1

ATM: Ataxia-Telangiectasia-Mutated

ATR: Ataxia Telangiectasia and Rad3-related

B

BAFs: BRG-1 associated factors

BAP1: BRCA1 Associated Protein 1

BRCA1: BReast CAncer 1

BRG1: Brahma-Related Gene 1

BRM-1: BRachyury Modifier 1

53BP1: P53 Binding Protein 1

C

CagA: Cytotoxin-Associated Gene A

CDK1: Cyclin Dependent Kinase 1

CHC: Carcinome HépatoCellulaire

CKIs: Cyclin Dependent Kinase Inhibitor

CK19: Cytokeratin 19

CHK1: Checkpoint Kinase 1

CMV: CytoMégaloVirus

CP: Cancer du Pancréas

Cpa: Carboxypeptidase a

CpG: Cytosine-phosphate-Guanosine

D

DDR: DNA Damage Response

DSB: Double-Strand Break

DUB: DeUBiquitylating Enzyme

E

E6-AP: E6-Associated Protein

EED: Embryonic Ectoderm Development protein

EGFr: Epidermal Growth Factor receptor

Ela: Elastase

EMT: Epithelial–Mesenchymal Transition

ERT2: Estrogen Receptor Tamoxifen-Inducible

EZH2: Histone-lysine N-methyltransferase

F

FBXO36: F-box Only protein 36

FBW7: F-box/WD repeat-containing protein 7

FGF: Fibroblast Growth Factor

G

G_1: Gap1

G_2: Gap2

H

HECT: Homologous to the E6-AP Carboxyl Terminus

HES1: Hairy and Enhancer of Split 1

HNF1b: Hepatocyte Nuclear Factor 1 homeobox b

H. pylori: Helicobacter pylori

HPV: Human papillomavirus

I

IDR: Intrinsically Disordered Region

INK4: Inhibitor of CDK4

Ino80C: INO80 Complex subunit C

K

KO: Knock-Out

L

LAM : Leucémie Aiguë Myéloïde

M

MAC: Métaplasie acino-canalaire

MAPK: Mitogen-Activated Protein Kinase

MDM2: Mouse Double Minute 2 homolog

MPC: Multipotent progenitor cells

mTORC: Mammalian Target Of Rapamycin Complex 1

6mA: N6-MethylAdenine

N

NES: Nuclear Export Signal

Neurog3: Neurogenine 3

NHEJ: NonHomologous End Joining

Nkx6: NK6 Homeobox 1

NLS: Nuclear Localization Sequence

NPM: Nucleophosmin

NR5A2: Nuclear Receptor subfamily 5 group A member 2

NS: Nucleostemin

P

PanIN: Pancreatic Intraepithelial Neoplasia

PARylation: Poly-ADP-Ribosylation

PARP1: Poly-(ADP ribose) polymérase 1

PARPi: PARP inhibitor

PBMC: Peripheral Blood Mononuclear Cell

PDX1: Pancreatic and Duodenal Homeobox 1

PI3K: PhosphoInositide 3-Kinase

PP: Pancreatic Polypeptide cells

PP1: Protein phosphatase 1

PRC1/2: Polycomb Repressive Complex 1/2

PR-DUB : Polycomb Repressive-Deubiquitinase complex

PTF1a: Pancreas Transcription Factor 1a

R

RAP80: Receptor-Associated Protein 80

Rbp-J: Recombination signal Binding Protein for immunoglobulin kappa J region like

RBR: RING-between-RING

RE: Reticulum endoplasmic

RING: Really Interesting New Gene

RNF 8/168: Ring Finger Protein 8/168

S

SCF: SKP1, Cullin, F-box protein

SHH: Sonic Hedgehog

SOX6: SRY-Box Transcription Factor 6

SOX9: Sex-determining region Y-box 9

STAT3: Signal transducer and activator of transcription 3

SUZ12: Polycomb protein SUZ12

SWI/SNF : SWItch/Sucrose Non-Fermentable

T

TRADD: TNF-R Associated Death Domain Protein

TR-β1: Thyroid Receptor-β1

TRIP12: Thyroid hormone Receptor Interacting Protein 12

U

Ub: Ubiquitin

UBR5: UBiquitin protein ligase E3 component N-Recognin 5

UFD4: Ubiquitin Fusion Degradation 4

UPR: Unfolded Protein Response

USP7: Ubiquitin Specific Protease 7

UTR: UnTranslated Regions

W

WWE: Tryptophane-Tryptophane-Glutamate

Z

ZEB1/2: Zinc Finger E-Box Binding Homeobox 1/2

Liste des figures

Liste des tableaux

Chapitre 1 : Introduction

PARTIE 1 : L'E3 ubiquitine ligase TRIP12

I. Pourquoi TRIP12 ?

A. TRIP12 est une E3 ubiquitine ligase

Quinze protéines de séquences non apparentées, appelées TRIP (Thyroid Hormone Receptor Interacting Protein) ont été caractérisées en 1995, comme interagissant avec le domaine de liaison des ligands du récepteur aux hormones thyroïdiennes TR-β1 (Thyroid Receptor-β1) de rat.[2] Les protéines TRIP1 à TRIP11 lient le récepteur uniquement lorsque l'hormone thyroïdienne T3 est présente, les TRIP12 à TRIP15 uniquement lorsque l'hormone est absente. Cette étude montre que les TRIP présentent pour certaines, des similitudes de séquences avec des protéines connues. En particulier, la séquence de TRIP12 possède 55% d'homologie avec la partie C terminale de la protéine associée à l'oncoprotéine E6 (E6-AP).[3] La fonction de la plupart des TRIP a depuis été établie.[4]

L'ADNc de TRIP12 a été cloné antérieurement, en 1994, à partir de la lignée cellulaire myéloïde humaine KG-1. Cette séquence codante présentait une homologie partielle avec celle de la protéine UFD4 (Ubiquitin Fusion Degradation 4) de S. cerevisiae mais, n'étant pas identifiée dans la base de données GenBank, elle a été nommée KIAA0045[5] et la protéine n'a été caractérisée que dans un second temps. Une autre étude avait également identifié la similarité de séquence de la protéine avec le domaine Homologue à l'Extrémité Carboxy-Terminale (domaine HECT) de l'ubiquitine ligase E6-AP, définissant ainsi de manière structurelle TRIP12 comme une E3 ubiquitine ligase.[6]

Il a fallu attendre plus d'une décennie après son identification et sa caractérisation pour voir apparaitre les premières publications relatant les études fonctionnelles et biologiques de TRIP12. L'étude fonctionnelle de TRIP12 en 2008 a prouvé qu'il s'agissait de l'unique membre de la famille des TRIP doté d'une activité E3 ubiquitine ligase.[7] Enfin, en 2011, Kajiro *et al.* démontrent l'importance biologique de TRIP12 en publiant que son activité E3 ubiquitine ligase est essentielle pour l'embryogenèse de la souris.[8]

B. TRIP12, régulateur de l'homéostasie des cellules acineuses

Le rôle de TRIP12 dans l'homéostasie des cellules acineuses du pancréas a été envisagé après sa découverte dans l'interactome de PTF1a (Pancreas Transcription Factor 1a) par le Dr Dufresne.[9] PTF1a est un facteur de transcription impliqué dans le développement du pancréas et dans l'homéostasie du pancréas adulte par son rôle dans le maintien du phénotype acinaire (Cf : Partie II).[10,11] L'hypothèse qui a motivé la recherche de l'interactome de PTF1a est que la perte d'expression et de fonction de PTF1a observée lors de la métaplasie acino-canalaire lève un frein de transformation maligne et permet l'émergence du cancer à partir des cellules acineuses.[12] Alors qu'aucune régulation post-traductionnelle

de PTF1a n'était connue, les travaux réalisés dans mon équipe d'accueil ont ensuite démontré que TRIP12 polyubiquitine et contrôle la stabilité de PTF1a.[9]

Depuis, des études ont confirmé que PTF1a est un gène suppresseur de tumeur dont l'expression disparait durant les étapes initiatrices de la carcinogénèse pancréatique.[13] Par ailleurs, Chen *et al.* illustre que l'ARN messager de TRIP12 est surexprimé dans le cancer du pancréas.[14] L'ensemble de ces données m'a conduite à étudier le rôle de TRIP12 dans le cancer du pancréas (CP) y compris dès les étapes d'initiation.

La régulation, la structure et les fonctions physio-pathologiques de TRIP12 sont détaillées dans notre revue,[4] mais certains points sont repris dans cette première partie d'introduction afin de repositionner mon sujet de thèse.

II. Expression de TRIP12 : de l'ARNm à la protéine

A. Organisation du gène

Dans le génome humain, le gène codant pour l'ARNm de TRIP12 est situé sur le bras long du chromosome 2 au locus q36.3 **(Figure 1)**. Son gène est très conservé au cours de l'évolution à travers les espèces. L'expression de l'ARNm de TRIP12 est régie par un promoteur bidirectionnel qui initie également la transcription de l'ARNm de FBXO36 (F-Box Only protein 36) dans une direction opposée. Ce promoteur bidirectionnel de 555 pb est intégré dans une région riche en CG également appelée îlot CpG (Cytosine-phosphate-Guanosine). Aucune étude sur les régions régulatrices et le niveau de méthylation du promoteur de TRIP12/FBXO36 n'a été réalisée.

Les promoteurs bidirectionnels sont certes peu fréquents (10%) mais la conservation de ces structures au cours de l'évolution montre leur importance.[15] En effet, dans la majorité des cas, ce système permet de contrôler des gènes partageant la même régulation ou codant pour des protéines intervenant dans des processus biologiques similaires.[16] Le gène *FbxO36* code pour une protéine faisant partie du complexe d'ubiquitine ligase multiprotéique SCF (SKP1, Cullin, F-box protein). Dans ce complexe, la protéine F-Box permet la liaison des substrats à ubiquitiner.[17,18] Jusqu'à présent, les fonctions de FBXO36 sont inconnues.

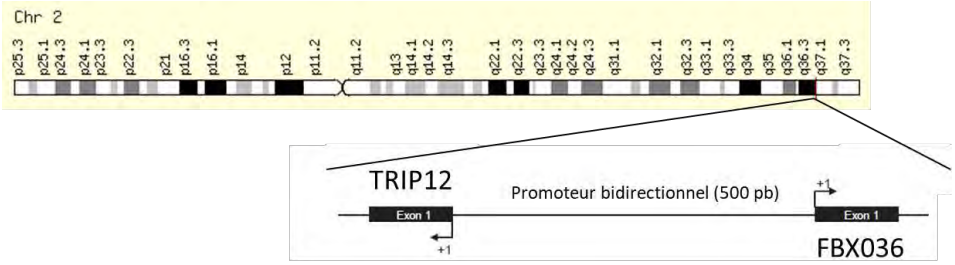

Figure 1 : Schéma représentant la position du promoteur bidirectionnel du gène *Trip12* sur le chromosome 2.

B. Structure et expression de l'ARNm de TRIP12

D'un point de vue structurel, il a été séquencé 26 variants d'épissage de l'ARNm de TRIP12 qui possèdent des similarités de composition.[4] Leur longueur varie de 9065 (variant 4) à 10492 nucléotides (variant 20) avec 41 à 43 exons. Alors que la région 5'-non traduite (5'-UTR) est formée d'environ 180 nt, la région 3'-non traduite (3'-UTR) représente environ un tiers de la longueur totale de l'ARNm (≈3700 nt), traduisant probablement une fonction de régulation de cette région **(Figure 2)**.

Figure 2 : Schéma représentant la structure de l'ARNm de TRIP12.

En fait, il existe une forme courte (340 nt) et une forme longue du 3′-UTR (3717 nt) de l'ARNm de TRIP12 en raison de la présence de deux signaux consensus de polyadénylation (PAS) induisant une terminaison de la transcription sur des régions différentes **(Figure 2)**.[19] Ces deux variants présentent une efficacité de traduction différente, la forme courte étant traduite plus efficacement que la forme longue en réponse à une activation de la voie de signalisation mTORC (mammalian Target Of Rapamycin Complex 1).[19]

Enfin, l'expression de l'ARNm de TRIP12 est ubiquitaire d'après les données disponibles sur « Human Protein Atlas » mais le niveau d'ARNm varie d'un tissu à l'autre **(Figure 3)**. Par exemple, l'ARNm de TRIP12 est fortement exprimé dans les testicules et les muscles mais faiblement exprimé dans le tissu pancréatique.[20]

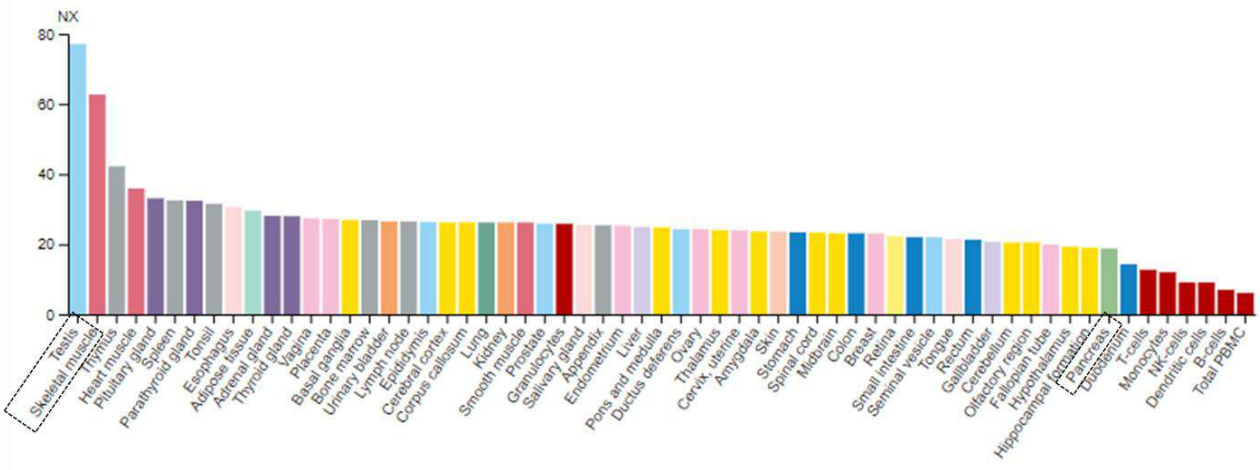

Figure 3 : Histogramme du niveau d'expression de l'ARNm de TRIP12 dans les tissus humains (adapté de *The Human Protein Atlas*).
Expression normalisée (NX) du niveau de TRIP12 référencé dans 16 types tissulaires (chaque couleur indique un type) issue des données d'analyses transcriptomiques (HPA, GTEx et FANTOM5).

C. Structure et expression de la protéine TRIP12

Les différents variants d'épissage de l'ARNm de TRIP12 permettent la génération de 14 isoformes de la protéine. Les formes longues présentent une taille comprise entre 1722 acides aminés (aa) et 2068 aa donnant naissance à une grosse protéine de poids moléculaire compris entre 189 et 227 kDa. Les isoformes de 1992 aa et 2040 aa sont les plus étudiées. Peu de formes courtes ont été caractérisées (2 protéines sur 14), leur taille est de 411 aa et de 440 aa. Mes travaux de thèse se focalisent exclusivement sur l'isoforme de TRIP12 de 1992 aa (référencée NP_004229.1), retrouvée dans l'interactome de PTF1a.[9]

- Structure protéique :

La protéine TRIP12 est structurée en plusieurs domaines caractérisés : en N-terminal, une région intrinsèquement désordonnée (IDR) identifiée dans nos travaux publiés récemment [21], puis deux domaines d'interaction protéine/protéine ARM [22] (Armadillo repeats) et WWE [23] (Tryptophane-Tryptophane-Glutamate) et le domaine catalytique HECT à l'extrémité C-terminale [24] **(Figure 4)**. Chaque domaine joue un rôle dans la fonctionnalité de TRIP12.[4]

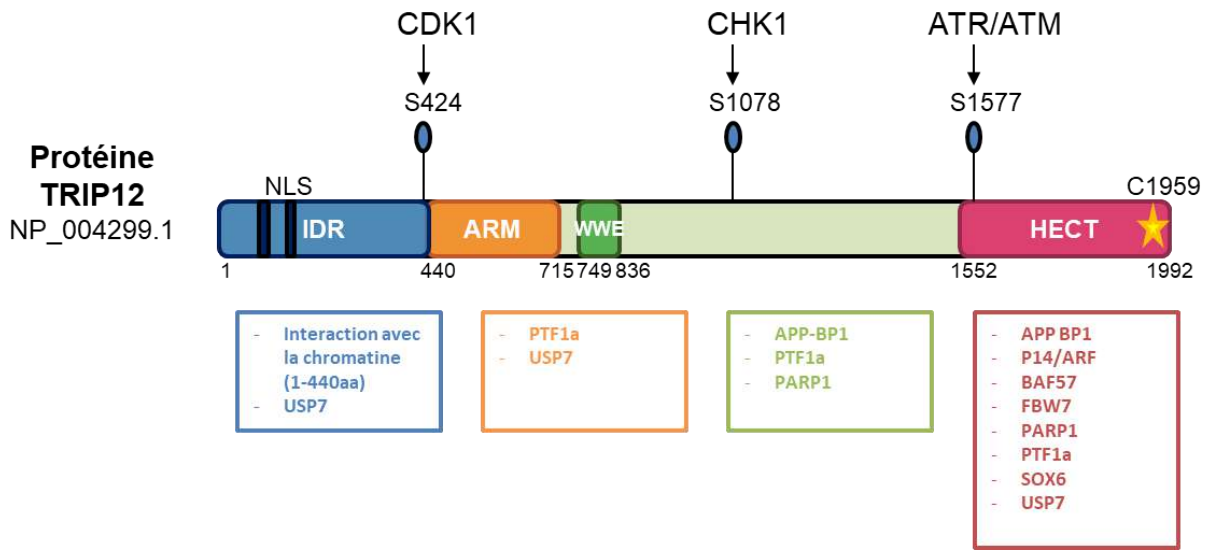

Figure 4 : Localisation des différents domaines de TRIP12 et des modifications post-traductionnelles connues dans la séquence protéique de TRIP12.
Les substrats/partenaires de TRIP12 sont indiqués sous les domaines de TRIP12 nécessaires à leur interaction. Les nombres indiquent la position des acides aminés délimitant ces domaines. La mutation de la cystéine 1959 inactivatrice de l'activité catalytique est indiquée par l'étoile jaune.

Le domaine IDR de TRIP12 est une séquence riche en acides aminés basiques située des acides aminés 1 à 440. Les IDR sont principalement impliqués dans la liaison/interaction entre les protéines, l'ARN et l'ADN [25–27] et leur présence en N-terminal favorise plus spécifiquement une interaction avec l'ADN.[27] En effet, nos travaux montrent que la déplétion du domaine de l'IDR de TRIP12 est responsable de la perte de l'interaction avec la chromatine.[21] L'IDR de TRIP12 est également nécessaire

pour son interaction avec la déubiquitinase USP7 (ubiquitin specific protease 7), mais pas suffisante car elle requiert aussi la présence du domaine ARM.[28]

Le domaine ARM, situé entre les acides aminés 437 et 715, participe aux interactions protéines/protéines. Il est connu que ces séquences jouent un rôle dans différents processus biologiques tels que l'adhésion cellule/cellule, la signalisation cellulaire, l'organisation du cytosquelette, le trafic nucléaire et l'ubiquitination.[29] Il intervient dans la reconnaissance du signal de dégradation des substrats par fusion de l'ubiquitine (UFD) chez l'homologue de TRIP12 appelée UFD4 chez la levure Saccharomyces cerevisiae.[22] Par son domaine ARM, TRIP12 interagit avec les protéines USP7 et PTF1a.

Le domaine WWE, situé entre les acides aminés 749 et 836 [4], est lui aussi essentiel aux interactions protéines/protéines. En général, les domaines WWE sont retrouvés dans la séquence des E3 ubiquitine ligases de type HECT ou RING participant ainsi au processus de dégradation des protéines par ubiquitination.[23] Le domaine WWE de TRIP12 interagit avec APP-BP1 (Amyloid Protein-Binding Protein 1)[7] et PARP1 (Poly-(ADP ribose) polymérase 1) parylée.[30] La présence du domaine WWE est aussi indispensable pour interagir avec PTF1a et entrainer sa polyubiquitination (résidu K312) pour l'adressage au protéasome.[9]

Enfin le domaine HECT est situé dans la partie C-terminale de la protéine, des résidus 1552 à 1992. Ce domaine a permis de caractériser TRIP12 comme une E3 ubiquitine ligase de type HECT possédant une activité catalytique permettant l'ubiquitination des protéines (Cf Partie I - III).[24,31] Le remplacement de la cystéine en position 1959 par un résidu alanine conduit à la perte de l'activité catalytique de ce domaine.[6]

- <u>Expression protéique</u> :

TRIP12 est ubiquitaire dans les cellules d'après les données disponibles dans les tissus humains (Human Protein Atlas). TRIP12 est exprimée à un niveau similaire dans la plupart des tissus avec un taux plus faible dans le pancréas et dans certaines glandes endocrines (surrénales, parathyroïde, thyroïde, hypophyse).

Nos travaux et les observations réalisées dans plusieurs lignées cellulaires[21,32] et tissus humains (Human Protein Atlas) décrivent la localisation de la protéine TRIP12 dans le noyau des cellules. Cette localisation nucléaire est vraisemblablement liée à la présence de deux séquences prédites de localisation nucléaire (NLS).[4] Nous avons aussi publié que la présence de TRIP12 dans le noyau dépend de la phase du cycle cellulaire : TRIP12 apparaît dans le noyau à la fin de la phase S, perdure pendant la phase G_2 et en mitose, pour disparaître en début de phase G_1 (Cf Partie I- III. C).[21]

TRIP12 peut être phosphorylée mais les conséquences de ces modifications post-traductionnelles restent, à ce jour, inconnues. En dehors des prédictions de sites de phosphorylation par analyse bio-informatique, seulement trois résidus sérine S424, S1078 et S1577 sont respectivement phosphorylés par les kinases CDK1 (Cyclin Dependent Kinase 1), CHK1 (Checkpoint Kinase 1) et ATM/ATR (Ataxia-Telangiectasia-Mutated/Ataxia Telangiectasia and Rad3-related) [33–35] **(Figure 4)**.

Seules, deux études ont montré que TRIP12 peut être ubiquitinée[36,37], processus qui est également une modification post-traductionnelle participant à la régulation de l'expression des protéines. A ce jour, l'E3 ubiquitine ligase responsable de l'ubiquitination de TRIP12 est inconnue. Cependant, il est possible que TRIP12 puisse s'auto-ubiquitiner. TRIP12 est stabilisée par la déubiquitinase USP7 (ubiquitine-specific protease-7).[36] Une boucle de rétrocontrôle est aussi observée car TRIP12 interagit avec USP7 entrainant sa polyubiquitination pour sa dégradation par le protéasome.[28]

III. Fonctions de TRIP12

TRIP12 possède de nombreuses fonctions, aussi bien dans des processus physiologiques que pathologiques, détaillées de manière exhaustive dans la revue que nous avons publiée **(§ Annexe II)**.[4] Seules les fonctions nécessaires à la compréhension de mes résultats de thèse seront abordées dans cette partie de l'introduction.

A. Rôles de TRIP12 dans l'ubiquitination des protéines

1) Généralités sur l'ubiquitination

L'ubiquitination est un processus essentiel, nécessitant de l'ATP, permettant la modification post-traductionnelle de protéines cibles pouvant conduire à leur dégradation par le protéasome 26S.[38] Elle consiste en la liaison covalente de l'ubiquitine, polypeptide de 76 aa hautement conservé (≈8,5 kDa), avec la lysine d'une protéine cible. La conjugaison canonique de l'ubiquitine implique la fixation de la glycine 76 en position C-terminale (G76) de l'ubiquitine (Ub) au groupement amine en position latérale d'une lysine du substrat protéique. Bien qu'elle soit surtout connue pour entrainer la dégradation des protéines, l'ubiquitination est aussi impliquée dans de nombreux processus cellulaires tels que le contrôle de cascades de signalisation, l'endocytose, le changement de localisation subcellulaire, les interactions protéine/protéine mais également le métabolisme, la progression du cycle cellulaire, la réponse aux dommages à l'ADN, la réponse immunitaire, le développement et le programme de mort cellulaire.[38]

L'ubiquitination est assurée par l'action concertée de trois enzymes en trois étapes. **(Figure 5)** La première étape est réalisée par l'enzyme E1 qui « active » l'ubiquitine par la formation d'une liaison thiol-ester entre la glycine C-terminale G76 de l'Ub et le résidu cystéine de l'E1. L'étape suivante, permet de transférer la molécule d'Ub de l'E1 à la cystéine de l'enzyme de conjugaison de l'Ub (E2).

L'E2 chargée interagit ensuite avec une E3 ligase qui reconnait et/ou catalyse le transfert de l'ubiquitine sur le substrat en fonction de la classe de l'enzyme E3.[39] Dans certains cas, la coopération d'une ubiquitine ligase E4 est requise permettant d'améliorer la réaction d'ubiquitination des substrats. Les E3 recrutent leurs substrats en reconnaissant une séquence spécifique appelée degron.[40]

Les ligases E3 sont classées en trois grandes classes, les RING (Really Interesting New Gene), les RBR (RING-between-RING) et les ligases HECT. Pour les E3 ligases RBR et HECT, le transfert de l'Ub implique un intermédiaire thioester avec une cystéine conservée dans le site catalytique de l'enzyme E3, correspondant respectivement au domaine Rcat ou au domaine HECT.[41,42] Par ce mécanisme, l'ubiquitine activée est transférée de l'E2 à l'E3 puis sur le substrat au niveau d'un site accepteur spécifique.[43,44] Les E3 ligases de type RING catalysent directement le transfert de l'ubiquitine conjuguée à l'E2 vers un substrat.[45]

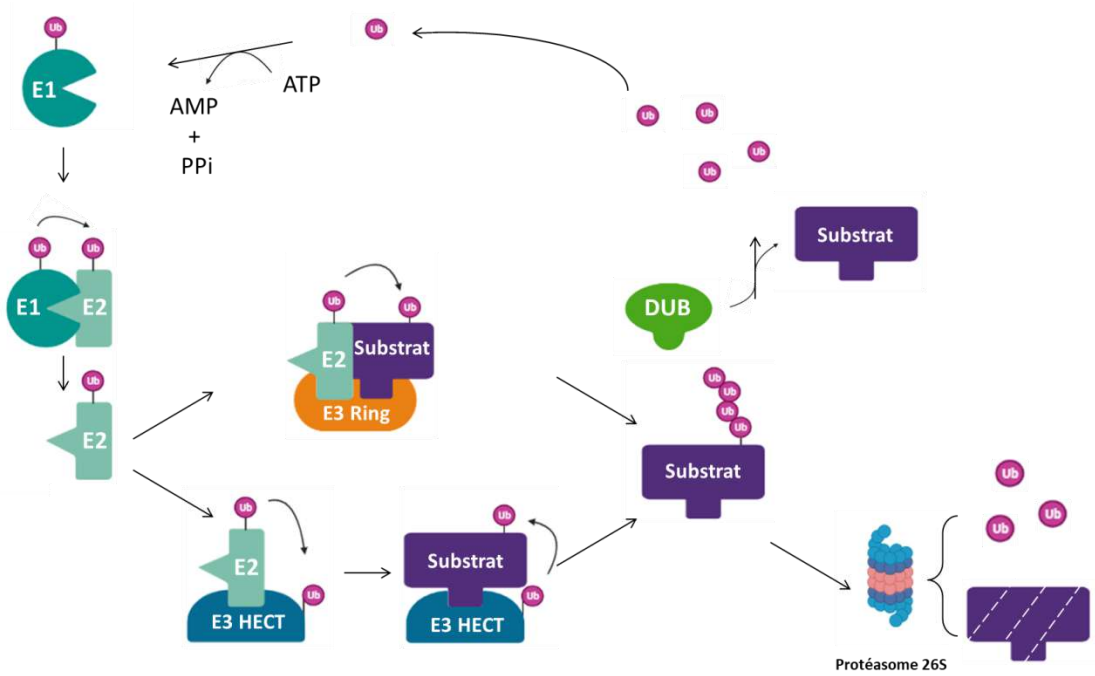

Figure 5 : Schéma représentant le mécanisme d'ubiquitination d'un substrat.
Mécanisme d'action nécessitant trois enzymes et l'ubiquitine (Ub). Les deux principales classes des E3 ligases (RING et HECT) sont représentées. Le substrat est soit adressé au protéasome 26S pour la dégradation, soit déubiquitiné par les déubiquitinases (DUB). E1 : Enzyme d'activation, E2 : Enzyme de conjugaison, E3 ubiquitine ligase.

Compte tenu du rôle clef des E3 ubiquitine ligases dans la reconnaissance et la dégradation de substrats impliqués dans la régulation et l'homéostasie des cellules, le moindre dysfonctionnement des E3 va modifier la stabilité de leurs substrats. Cela peut se traduire, par exemple, par une augmentation de l'expression de protéines à activité oncogénique aboutissant dans certains cas à des cancers.[46,47]

Les substrats peuvent être soit modifiés par une seule ubiquitine sur un site unique (monoubiquitination) ou sur plusieurs sites (multi-mono-ubiquitination), soit par des chaînes de polymère d'ubiquitine.[48] Dans ce cas, le C-terminal de la G76 d'une molécule d'Ub est lié au groupe ε-

NH_2 de l'une des sept lysines (K6, K11, K27, K29, K33, K48 ou K63) de l'ubiquitine précédente. Les chaînes poly-Ub peuvent avoir des longueurs et des topologies différentes. Il peut s'agir d'une chaine homotypique qui comprend un seul type de liaison sur la même lysine, ou hétérotypique qui comprend au sein d'un polymère des liaisons par des lysines différentes. Par exemple, la polyubiquitination liée à la lysine K48 modifie les protéines pour la destruction protéolytique par le protéasome, tandis que les liaisons non-K48 ciblent les protéines pour diverses fonctions et réponses cellulaires.[48,49] Les mono et multi-monoubiquitinations jouent uniquement un rôle dans la signalisation cellulaire, comme par exemple dans la réponse aux dommages à l'ADN, par l'ubiquitination des histones.[50]

La conjugaison de l'ubiquitine est réversible grâce à l'action des déubiquitinases (DUB).[51] Les DUB sont classées en six familles en fonction de la conservation de la séquence du domaine catalytique et comptent une centaine de protéines. La famille des USP (ubiquitine-specific proteases) est la famille qui prédomine.[52] Contrairement aux autres DUB, les USP ont la capacité de rompre toutes les liaisons d'ubiquitine.[53]

2) Les substrats connus de TRIP12

TRIP12 possède au total 77 interactants répertoriés de manière détaillée dans notre revue.[4] Ces derniers ont été identifiés par différentes approches expérimentales utilisant comme cible soit les interactants (n = 59), soit TRIP12 (n = 7) soit les deux comme appât (n = 11). Parmi les 77 interactants, seulement dix ont été caractérisés comme substrats de TRIP12. En effet, d'après les données de la littérature, TRIP12 régule la stabilité de dix substrats et promeut leur dégradation par le protéasome régulant ainsi des fonctions cellulaires comme indiqué dans le **Tableau 1**.

Substrat	**Dénomination**	**Fonction**	**Réf.**
APP-BP1	Amyloid Protein-Binding Protein 1	Neddylation	7
P14/ARF	P14/Alternate Reading Frame	Cycle cellulaire	14
ASXL1	Additional Sex Combs Like 1	Remodelage de la chromatine	54
BAF57	BRG1-Associated Factor 57	Remodelage de la chromatine	55
FBW7	F-box and WD-40 domain protein 7	Différenciation cellulaire	56
PARP1	Poly-(ADP ribose) polymerase 1	Réponse aux dommages à l'ADN	30
PTF1a	Pancreas Transcription Factor 1a	Différenciation cellulaire	9
RNF168	Ring Finger Protein 168	Réponse aux dommages à l'ADN	32
SOX6	SRY-Box Transcription Factor 6	Différenciation cellulaire	20
USP7	Ubiquitin-Specific Peptidase 7	Cycle cellulaire et réponse aux dommages à l'ADN	28

Tableau 1 : Liste des substrats connus de TRIP12 associés à leurs fonctions

B. Rôle de TRIP12 dans le remodelage de la chromatine

1) Via le contrôle de l'intégrité du complexe SWI/SNF

Composée d'histones et de l'ADN, la chromatine subit une compaction finement régulée dont la dynamique participe à divers processus tels que la transcription, la réparation et la recombinaison de l'ADN. Lorsque la chromatine est compactée, l'accessibilité des promoteurs à la machinerie transcriptionnelle est réduite se traduisant par une transcription globalement inactive des gènes.[57] A l'inverse, l'accessibilité de la chromatine peut être modifiée par le complexe SWI/SNF (SWItch/Sucrose Non-Fermentable) entrainant la libération des histones de l'ADN afin de moduler l'activité transcriptionnelle.[58] SWI/SNF (SWItch mutants/ Sucrose Non Fermenting) est un complexe multiprotéique d'une douzaine de sous-unités comprenant les ATPases BRG1 (hSWI/SNF Brahma-related Gene) et BRM-1 (BRachyury Modifier 1), qui assurent l'activité catalytique, et des protéines BAFs (BRG-1 associated factors) qui sont nécessaires pour l'activation complète du complexe. La fonctionnalité du complexe nécessite l'ensemble des sous-unités pour remodeler le positionnement des nucléosomes de manière dépendante de l'ATP. Une régulation stricte de la stœchiométrie du complexe SWI/SNF est indispensable et assurée par la dégradation par le protéasome des sous-unités libres, non liées **(Figure 6)**. Par exemple, la protéine BAF57 est stabilisée et protégée de la dégradation quand elle interagit avec BAF155.[59] TRIP12 est la principale E3 ubiquitine ligase qui polyubiquitine la fraction cellulaire libre de BAF57.[55] Par conséquent, TRIP12 contribue au « contrôle qualité » des protéines du complexe SWI/SNF.

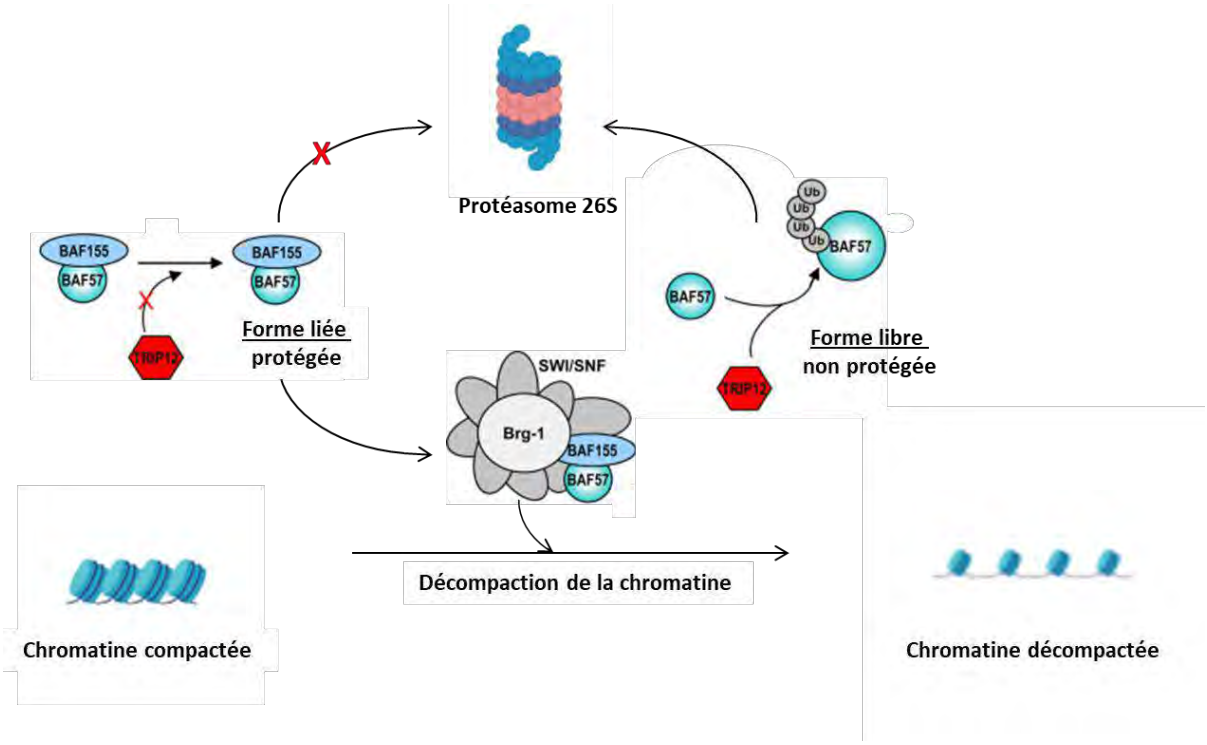

Figure 6 : Schéma de la relation entre TRIP12, BAF57 et BAF155 (Adapté de Keppler et al 2010).[55]
Lié à BAF155 ou au complexe SWI/SNF, BAF57 est protégée de l'ubiquitination, en opposition à la forme libre qui est ubiquitinée par TRIP12 et adressée au protéasome 26S en vue de sa dégradation.

2) Via la maintenance de la répression de gènes par le complexe Polycomb

Les modifications épigénétiques des bases d'ADN et des histones jouent un rôle important dans la modulation de la dynamique de la chromatine. Les histones peuvent être acétylées, méthylées, phosphorylées, ubiquitinées et sumoylées, jouant un rôle sur l'expression des gènes et dans les processus qui nécessitent un accès à l'ADN, comme la répression de la transcription.[60]

En effet, chez les mammifères, il a été récemment démontré que la méthylation de l'atome d'azote en position 6 d'une adénine (6mA) est associée à des marques répressives épigénétiques telles que la monoubiquitination sur la lysine K119 de l'histone H2A (H2AK119 Ub) et la triméthylation sur la lysine K27 de l'histone H3 (H3K27me3).[54] Ces marques répressives sont utilisées pour mettre sous silence les promoteurs, comme par exemple, lors de la différenciation des cellules souches et lors du développement embryonnaire. Ce sont les Complexes Répressifs Polycomb (PRC1 et PRC2) qui ajoutent les marques répressives.[61,62] A l'inverse, le complexe de déubiquitinase PR-DUB (Polycomb Repressive-Deubiquitinase complex), formé par les protéines ASXL1 (Additional Sex Combs like 1) et BAP1 (BRAC1 Associated Protein 1),[63] permet le retrait de l'ubiquitine du résidu K119 de l'histone H2A. La protéine BAP1 porte l'activité déubiquitinase, elle est stabilisée par ASXL1.[64] Une étude récente rapporte qu'en présence de TRIP12, ASXL1 est dégradée par polyubiquitination préservant ainsi le niveau de H2AK119Ub et la répression de certains gènes **(Figure 7)**.[54] D'autres analyses protéomiques ont identifié TRIP12 comme pouvant s'associer avec des composants du PRC2 tels que SUZ12 (Polycomb protein SUZ12), EZH2 (Histone-lysine N-methyltransferase)[65] et EED (Embryonic Ectoderm Development protein).[66] Par conséquent, TRIP12 peut ainsi contribuer à la régulation épigénétique de l'expression du génome en participant au contrôle du niveau de compaction de la chromatine.

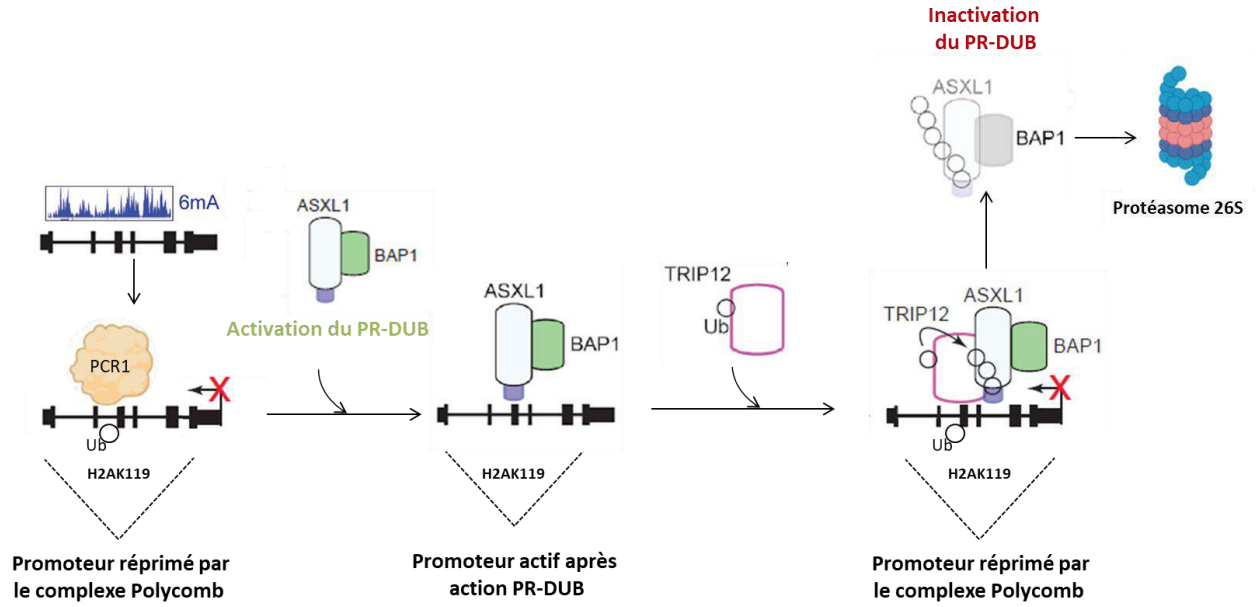

Figure 7 : Illustration du mécanisme de recrutement de TRIP12 entrainant la protéolyse d'ASXL1 et la répression de promoteurs cibles (Adaptée de Kweon et al, 2019).[54]
Suite à la méthylation de l'atome d'azote en position 6 d'une adénine (6mA) et l'ubiquitination de l'histone H2AK119 par le complexe PRC1, le complexe de déubiquitination ASXL1/BAP1 est recruté et entraine la dégradation d'ASXL1 par TRIP12. La perte d'un régulateur du complexe PR-DUB bloque son action de déubiquitinase préservant ainsi la marque répressive, H2AK119Ub, déposée par le complexe Polycomb sur la chromatine. Ub : Ubiquitine, PR-DUB : Déubiquitinase du complexe répressif Polycomb.

C. Rôle de TRIP12 dans la progression du cycle cellulaire

Pour rappel, le cycle cellulaire est un processus finement régulé qui conduit, à partir d'une cellule mère, à la naissance de deux cellules filles. De manière universelle, pour tous les organismes, le cycle cellulaire est divisé en deux grandes étapes : l'interphase et la mitose. Chez les Eucaryotes, l'interphase correspond à l'étape la plus longue du cycle cellulaire nécessaire à la préparation de la division des cellules. L'interphase est divisée en 3 étapes. La première étape appelée Gap 1 (G_1), est nécessaire pour le contrôle de la croissance cellulaire et l'intégrité du génome. S'ensuit la phase S, qui permet l'incorporation de nucléotides pour la réplication de l'ADN. Enfin, la dernière étape de l'interphase, correspond à la phase Gap 2 (G_2), étape préparatoire de la division mitotique par vérification de la réplication et de la fin de la croissance cellulaire. La division cellulaire est la phase durant laquelle les chromosomes se répartissent entre les deux cellules filles, il s'agit de la mitose. Cette phase est également très contrôlée et composée d'une succession de modifications morphologiques et biochimiques. L'entrée et la progression des cellules dans chaque phase du cycle sont régulées, en autres, par des CDK (Cyclin Dependent Kinase) qui phosphorylent les protéines kinases sur les résidus sérines ou thréonines. L'activité des kinases dépend d'autres protéines du cycle cellulaire, les cyclines, qui vont interagir et former un complexe CDK/Cycline transitoire, spécifique pour chaque phase du cycle. En plus des phosphorylations/déphosphorylations activatrices ou inactivatrices, l'activité des CDK peut être limitée par des associations transitoires à des inhibiteurs nommés CKIs (Cyclin Dependent Kinase

Inhibitor). Ainsi, $P16^{INK4A}$ qui appartient à la famille de protéines INK4 (Inhibitor of CDK4) permet la régulation uniquement de la phase G_1.

La protéine TRIP12 joue un rôle clef dans la régulation du cycle cellulaire *in vivo*.[8] Kajiro *et al.*, montrent que la mutation inactivatrice de l'activité ubiquitine ligase conduit à la létalité au stade embryonnaire E11.5 des souris mutantes homozygotes ($TRIP12^{mt/mt}$). La croissance cellulaire in vitro des cellules ES (Embryonic stem) $TRIP12^{mt/mt}$ est nettement réduite, associée à une accumulation anormale de cellules dans les phases G_2/M et sub-G_1 suite à l'induction anormale du CKI $P16^{INK4A}$ et à la stabilisation de $P14^{ARF}$ (P14/Alternative Reading Frame).

Un autre groupe a également identifié TRIP12 comme l'E3 ubiquitine ligase responsable de la dégradation de ARF et l'a renommé ULF pour Ubiquitin Ligase for ARF.[67] La protéine $P14^{ARF}$ joue un rôle majeur dans la progression du cycle cellulaire car elle régule indirectement l'activation de la voie P53 qui induit l'arrêt du cycle cellulaire **(Figure 8)**.[68] En effet, dans une cellule normale, l'action de l'E3 ubiquitine ligase MDM2 (Mouse Double Minute 2 homolog) régule le niveau de P53. Cependant en interagissant avec MDM2, ARF l'empêche de cibler P53 ce qui conduit à l'augmentation du niveau de P53 et à l'arrêt du cycle cellulaire et/ou l'apoptose.[69] En présence de TRIP12, le niveau d'expression de la protéine ARF est réduit et MDM2 déstabilise alors P53, permettant la progression du cycle cellulaire.[67]

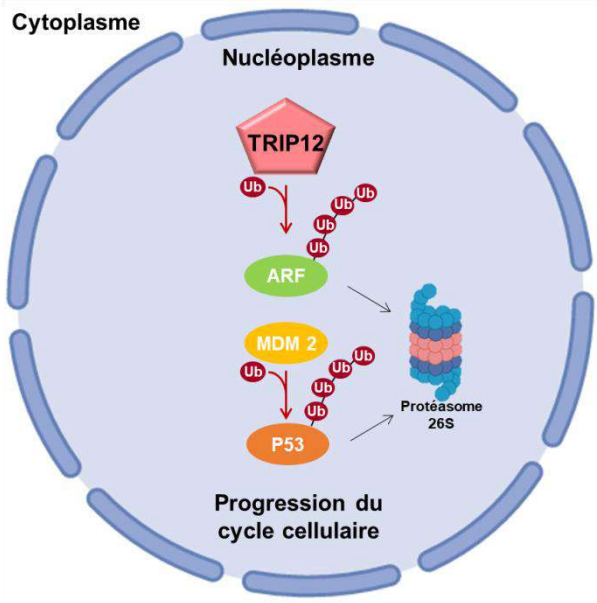

Figure 8 : Représentation schématique de la voie TRIP12, ARF et P53 (Adaptée de Brunet et al, 2021).[4]
TRIP12 contrôle directement la dégradation de ARF et indirectement celle de P53 via MDM2, contrôlant ainsi la progression du cycle cellulaire.

Plusieurs protéines interagissent avec TRIP12 ou ARF pour moduler l'inhibition de la dégradation de ARF transmise par TRIP12 conduisant alors à l'activation de la voie ARF/P53 et à l'arrêt du cycle cellulaire.

La participation de TRIP12 dans la progression du cycle cellulaire via l'ubiquitination de ARF agit telle une « barrière » contre un stress oncogénique qui dépend du niveau d'expression de c-MYC **(Figure 9)**.[70] En effet, c-MYC améliore la demi-vie de ARF en déstabilisant le complexe nucléoplasmique TRIP12/ARF.[71] De plus, TRIP12 se lie avec TRADD (TNF-R Associated Death Domain Protein), un adaptateur central dans la signalisation pro-inflammatoire.[72] Le transfert de TRADD du cytoplasme vers le noyau protège ainsi ARF de la dégradation par le protéasome.[73]

La nucléophosmine (NPM), un composant majeur des nucléoles,[74] séquestre ARF dans ce compartiment, l'isolant de l'action d'ubiquitination de TRIP12 présente uniquement dans le nucléoplasme.[14] La liaison de la nucléostémine déstabilise le complexe TRIP12/ARF dans le nucléoplasme et stabilise le complexe NPM/ARF dans les nucléoles.[75]

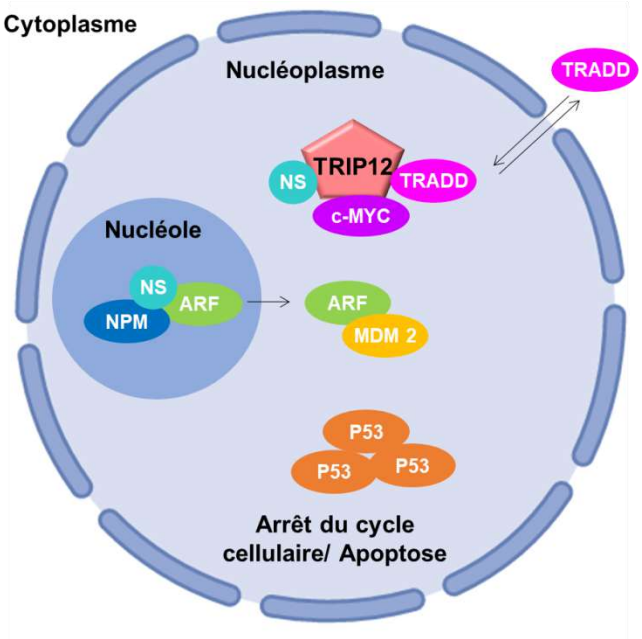

Figure 9 : Représentation schématique illustrant les régulateurs modulant la voie TRIP12, ARF et P53 (Adaptée de Brunet et al, 2021).[4]
Lié à la nucléophosmine (NPM)/nucléostémine (NS) dans le nucléole, ARF est protégé de l'action de l'E3 ligase TRIP12. Ainsi, ARF se lie et inhibe MDM2, ce qui conduit à l'accumulation de P53 et à l'arrêt du cycle cellulaire. TRIP12 interagit avec différentes protéines (NS, TNF-R Associated Death Domain Protein (TRADD), c-MYC élevés) bloquant également son interaction avec ARF dans le nucléoplasme.

TRIP12 régule aussi le cycle cellulaire indépendamment de son action sur ARF en inhibant indirectement la fonction de P53. En effet, le second substrat de TRIP12 impliqué dans la régulation de la voie ARF/P53 est la déubiquitinase USP7. USP7 stabilise directement le niveau de p53 [76] et celui de MDM2.[77] Ainsi, USP7 stabilise, via le même domaine d'interaction, à la fois TRIP12, P53 et MDM2 qui peuvent entrer en compétition en fonction du contexte cellulaire.

Si l'ensemble de ces données montre clairement que TRIP12 est étroitement impliquée dans le contrôle de la progression du cycle cellulaire, aucune étude ne s'est intéressée à la régulation de son

expression dans les différentes phases du cycle cellulaire qui conditionne cependant directement sa capacité d'interaction avec ses partenaires. Nos travaux ont révélé que TRIP12 apparaît dans le noyau des cellules à la fin de la phase S et perdure pendant la phase G_2, qu'elle interagit avec la chromatine via son IDR et coordonne l'entrée et la progression de la mitose.[21] Des études réalisées par spectrométrie de masse, ont d'ailleurs confirmé que TRIP12 est spécifiquement retenue sur la chromatine mitotique.[78] Bien qu'étroitement lié aux chromosomes pendant la mitose, TRIP12 voit son expression diminuer au début de la phase G_1, pour disparaitre du noyau à la fin de la phase G_1 et au début de la phase S.[21] Lorsque TRIP12 atteint un seuil maximal d'expression c'est-à-dire en fin de phase G_2 et en mitose, son rôle est optimal sur ses substrats (ARF, USP7) afin de réguler la progression du cycle cellulaire.

D. Rôle de TRIP12 dans la réponse aux dommages à l'ADN

Plusieurs études ont rapporté l'implication de TRIP12 dans le contrôle de la réparation des dommages à l'ADN qui varie en fonction du contexte cellulaire, des substrats de TRIP12 et du type de cassures.

1) Via la voie de signalisation ARF/P53

Dans une cellule en conditions normales, le cycle cellulaire est régulé par des points de contrôle activés par exemple par des stimuli génotoxiques. En réponse à un dommage de l'ADN, l'activation en amont des kinases ATM-CHK2 et ATR-CHK1 module la phosphorylation de P53 entrainant la séparation des protéines MDM2 et P53. L'augmentation du niveau de P53 déclenche un double contrôle de la voie de réparation des dommages à l'ADN (DDR) et l'arrêt du cycle cellulaire.[68,79] Ces deux voies de régulation sont interconnectées et souvent dérégulées dans les cancers.[80]

Dans ce contexte, les régulateurs de TRIP12 au cours du cycle cellulaire vont également être recrutés pour moduler l'action de l'E3 ligase en fonction du dommage, favorisant cette fois l'arrêt du cycle. En effet, la protéine c-MYC est surexprimée en réponse aux dommages à l'ADN induits par la doxorubicine, favorisant indirectement l'accumulation de p53 et une réponse apoptotique.[70] De manière similaire, l'invalidation de TRIP12 dans des fibroblastes embryonnaires de souris (MEF) atténue la dégradation de ARF favorisant l'apoptose en réponse aux dommages à l'ADN. Ainsi, la stabilité de ARF module clairement la réponse apoptotique dépendante de la voie P53.

Le second régulateur de l'action de TRIP12, la nucléophosmine (NPM), est également modulé en réponse à l'activation de la DDR. En effet, la kinase ATM active la protéine phosphatase 1 (PP1), qui, à son tour, déphosphoryle la protéine nucléolaire NPM inhibant son interaction avec ARF. De ce fait, la kinase ATM permet la polyubiquitination de ARF par TRIP12,[81] et ainsi le blocage de la réponse apoptotique après dommages à l'ADN. De façon intéressante, une étude a identifié la sérine S1577 de TRIP12 comme phosphorylée par les kinases ATM/ATR, suggérant que les modifications post-

traductionnelles sont vraisemblablement nécessaires et régulatrices pour l'implication antinomique de TRIP12 dans le mécanisme de réparation des dommages à l'ADN.[35]

2) Via le contrôle de l'ubiquitination des histones

L'ubiquitination des histones joue un rôle crucial dans le recrutement des protéines responsables de la détection et de la réparation des dommages à l'ADN (voir ci-après). TRIP12 est un régulateur direct et indirect de la stabilité des histones qui permet d'éviter une ubiquitination excessive de la chromatine en réponse à un dommage de l'ADN.

TRIP12 participe directement à l'ubiquitination des histones en réponse à un dommage à l'ADN.[82] En effet, UFD4 (homologue de TRIP12 chez la levure) appartient au complexe Ino80C (INO80 Complex Subunit C), un complexe constitué de cinq E3 ubiquitine ligases (Rad6, Bre1, PEP5, RSP5), qui contribue à l'épuisement des histones du noyau. La perte d'UFD4 associée à celles de Rad6 et PEP5 favorise la persistance des histones sur la chromatine ce qui compromet la décompaction de la chromatine. En réduisant le pool d'histones, TRIP12 diminue indirectement la compaction de la chromatine et facilite le recrutement des acteurs de la réparation de l'ADN.

TRIP12 et UBR5 sont deux protéines qui régulent indirectement l'ubiquitination des histones après l'induction de dommages à l'ADN par cassure double brin (DSB). [32] L'E3 ubiquitine ligase RNF8 (Ring Finger Protein 8) monoubiquitine les histones H2A et H2AX (K63) au niveau des sites endommagés.[83] La réaction d'ubiquitination est ensuite amplifiée par un autre facteur clé de la DDR, RNF168 une E3 ubiquitine ligase permettant la formation de chaînes de polyubiquitination (chaînes K63).[84] L'action concertée de ces protéines agit comme une plateforme permettant d'orchestrer le recrutement de facteurs de signalisation de réparation, tels que 53BP1 (P53 Binding Protein 1) et le complexe RAP80/BRCA1 (Receptor-Associated Protein 80/Breast Cancer 1).[85] TRIP12 est l'E3 ubiquitine ligase impliquée dans la stabilité de RNF168. Dans des conditions physiologiques, TRIP12 et UBR5 contrôlent la quantité de RNF168 nécessaire pour restreindre l'ubiquitination des histones autour des lésions de l'ADN. Cependant, une déplétion de TRIP12 et UBR5 provoque une accumulation de RNF168 en quantité excessive qui amplifie l'ubiquitination des histones au-delà des sites DSB. Le signal d'ubiquitination est essentiel car dans le cas où RNF168 se propage au-delà de la zone endommagée en polyubiquitinant les histones H2A et H2AX, il y a séquestration des molécules effectrices de la réparation, 53BP1 et BRCA1. La rétention de ces effecteurs sur un site d'ADN non endommagé empêche leur recrutement sur des sites d'ADN qui nécessiteraient une réparation. Un déséquilibre dans la régulation de l'ubiquitination des histones conduit à des lésions non réparées qui peuvent être délétères pour la cellule.

3) Via la déubiquitinase USP7

Il est admis que la déubiquitinase USP7 joue un rôle majeur dans la réponse aux dommages de l'ADN en stabilisant l'expression de protéines clés telles que P53 et RNF168.[77,86] TRIP12 interagit avec USP7 et le polyubiquitine pour sa dégradation par le protéasome.[28] Par conséquent, la dégradation d'USP7 par TRIP12 affecte les niveaux de P53, 53BP1 et CHK1 qui sont des régulateurs importants de la DDR. En effet, suite à une lésion de l'ADN, les kinases ATM et ATR phosphorylent MDM2 qui perd son affinité pour USP7, ceci permet la déubiquitination de P53 et augmente sa stabilité. En revanche, lorsque TRIP12 est exprimée, le niveau d'USP7 est réduit favorisant la déstabilisation de P53.

De plus, les rôles opposés de TRIP12 et USP7 dans la régulation du niveau de RNF168 et le contrôle mutuel de leur expression sont importants pour induire une réparation efficace. En effet, USP7 se lie à RNF168 dans le but d'éviter sa dégradation par le protéasome[86] mais à l'inverse TRIP12 polyubiquitine RNF168 pour induire sa perte.[32] Il est important de rappeler que TRIP12 est également stabilisée par USP7 via une boucle de rétrocontrôle.[36] Ce rétrocontrôle réciproque est finalement une balance essentielle pour assurer une bonne gestion de la réparation des dommages à l'ADN via le contrôle de la quantité de RNF168.

4) Via la polyubiquitination de PARP1

Une étude publiée l'année dernière montre que TRIP12 ubiquitine PARP1 pour sa dégradation par la protéasome.[30] Les protéines appelées poly(ADP-ribose) polymérases participent à la formation de polymères de molécules d'ADP-ribose à la surface de protéines cibles, mécanisme appelé Poly-ADP-Ribosylation (PARylation).[87] La PARylation intervient dans la régulation de la réparation de l'ADN et dans la dynamique de la chromatine.[88,89] PARP1 est un partenaire-clé dans la reconnaissance des cassures de l'ADN. Son activité est impliquée dans le recrutement précoce de facteurs facilitant entre autres la réparation des DSB.[90] En effet, un déficit ou l'inhibition de PARP1 entraîne une activation retardée des protéines impliquées dans la DDR telles que la phosphorylation des histones H2AX ou celle de P53 normalement induites en réponse à l'activation d'ATM.[91] De plus, des souris déficientes des gènes PARP1 et ATM présentent une létalité embryonnaire, suggérant un rôle essentiel de PARP1 dans la DDR et la prolifération cellulaire. [92] Les travaux de Gatti *et al.* démontrent que l'interaction de TRIP12 avec PARP1 via le domaine WWE favorise la polyubiquitination de PARP1 et sa dégradation par le protéasome.[30] Comme pour RNF168, TRIP12 empêche l'accumulation supra-physiologique de PARP1 au niveau du dommage.

Ces données de la littérature montrent que la forte implication de TRIP12 dans les mécanismes de réparation des dommages de l'ADN. Toutefois, ces différentes études révèlent que TRIP12 peut être à la fois une protéine activatrice ou inhibitrice de la réponse aux dommages à l'ADN en fonction du contexte cellulaire et du substrat.

E. Rôle dans la différenciation cellulaire

La différenciation cellulaire est un mécanisme par lequel les cellules en division changent de fonction et/ou de phénotype. Elle implique la régulation coordonnée des gènes par une multitude de voies de signalisation. Compte tenu du rôle de TRIP12 dans la régulation des complexes Polycomb et SWI/SNF, la perturbation de l'expression de TRIP12 peut entrainer la dérégulation globale de l'expression des gènes nécessaires au développement et à la régénération. De plus, l'activité E3 ubiquitine ligase de TRIP12 régule des facteurs clés de l'homéostasie et de la différenciation cellulaire.

TRIP12 est essentielle au développement embryonnaire de la souris.[8] En effet, le mutant homozygote inactif de TRIP12 entraine un retard de développement visible dès le stade embryonnaire 8.5 (E8.5) corrélé à la diminution du nombre de somites. Il est également observé un défaut dans la formation des structures placentaires dans les souris mutantes. Ces malformations conduisent à une létalité embryonnaire à E11.5.

Par ailleurs, TRIP12 participe à la régénération cellulaire par le recrutement de cellules souches chez le planaire d'eau douce Schmidtea mediterranea.[20] En effet, ce ver est capable de remplacer la perte des cellules en induisant le renouvellement cellulaire en conditions normales ou lors de la perte tissulaire grâce à la capacité de régénération de ses cellules souches adultes appelées néoblastes. L'orthologue de TRIP12 appelé « smed-TRIP12 », exprimé dans les néoblastes, est essentiel pour l'établissement et le maintien des tissus postérieurs de Schmidtea mediterranea.

Le facteur de transcription SOX6 (SRY-Box Transcription Factor 6) est une cible de TRIP12 chez les mammifères.[20] Ce facteur est essentiel pour l'homéostasie des cellules musculaires. Exprimé dans les somites au cours de l'embryogenèse, SOX6 coordonne la différenciation des fibres musculaires en agissant comme un suppresseur transcriptionnel des fibres lentes de l'embryon de la souris. La diminution de TRIP12 dans des lignées cellulaires dérivées de myotubes entraîne une augmentation du niveau de la protéine SOX6 et une dérégulation de l'homéostasie des fibres musculaires via une modification de l'expression génique liée à l'augmentation de SOX6.

De plus, TRIP12 dégrade des substrats tels que PTF1a et FBW7 (F-box/WD repeat-containing protein 7), régulateurs de la différenciation des cellules pancréatiques. L'étude de Hanoun *et al.* montre que TRIP12 polyubiquitine et provoque la dégradation du facteur de transcription PTF1a (Pancreas Transcription Factor 1a).[9] Le groupe de Behrens élucide le mécanisme par lequel TRIP12 dégrade FBW7 appartenant au complexe d'E3 ubiquitin ligase SCF et qui permet la reconnaissance du substrat. FBW7 est capable de s'auto-ubiquitiner via le complexe SCF sur les résidus K404 et K412, mais la présence de TRIP12 est nécessaire pour la polyubiquitination K11 et l'adressage au protéasome.

IV. Rôles de TRIP12 dans le cancer

A. Altérations du gène et de l'ARNm de TRIP12

L'analyse de la base de données cBioPORTAL qui référencie toutes les mutations connues dans la littérature et le nombres de copies altérées dans le génome (ou CNA pour copy number alteration) montre que la mutation du gène de TRIP12 est retrouvée dans moins de 3% des gènes mutés dans les cancers. Par comparaison, la fréquence de mutation de TP53 est de 35,2%. Au total, le gène Trip12 est muté dans 6 types de cancer à des fréquences variables, sur différents sites référencés dans le **Tableau 2**.

Cancer	Mutation	Exon	Type de mutation	Fréquences (%)	Réf
Adénocarcinome colorectal	c.3583delT (p.S1195LfsX24)	24	Délétion, instabilité micro satellitaire	3,1% (1/32)	93
Adénocarcinome gastrique	c.273InsA (p.P92TfsX8)	3	Insertion, instabilité micro satellitaire	3,7% (1/27)	
Adénocarcinome pulmonaire	g.230670518 G>C	16	Faux sens	75% (9/12)	94
Cancer du sein	g.230467943 C>A	Intron (entre exon 1 et 2)	Substitution		95
Carcinome anal	c.592C>T (p.S197F)	3	Faux sens	15% (3/20)	96
	c.4783C>T (p.R1595X)	33	Non-Sens		
	c.5462_5469del	37	Délétion		
Leucémie myéloïde aiguë pédiatrique	TRIP12-NPM1	20	Fusion	1,44% (2/139)	97

Tableau 2 : Caractérisation des mutations du gène Trip12 retrouvées dans certains cancers.

Cependant, ces données obtenues à partir de petites cohortes ne permettent pas d'établir une relation de causalité entre la présence de ces mutations et les cancers évoqués ci-dessus. De plus, les analyses restent descriptives sans recherche des conséquences fonctionnelles de ces mutations.

Le constat est le même pour le niveau d'ARNm de Trip12 dans les cancers avec peu d'analyses de ce niveau de régulation. En 2010, Chen *et al.* ont montré que le niveau d'ARNm de Trip12 est significativement augmenté dans le cancer du sein à partir d'une cohorte de 53 tissus tumoraux comparativement à 6 tissus sains.[14] Les bases de données telles que GEPIA (Gene Expression Profiling Interactive Analysis) répertorient le niveau d'ARNm de gènes de chaque cancer et les comparent à ceux des tissus normaux correspondants dans des cohortes plus conséquentes. Cette base de données montre une variabilité du niveau de Trip12 selon le type de cancer. L'ARNm de Trip12 est significativement surexprimé dans seulement le lymphome diffus à grandes cellules B, le cholangiocarcinome, le cancer du thymus et l'adénocarcinome pancréatique. A l'inverse, le niveau de Trip12 est significativement diminué dans les tumeurs des cellules germinales testiculaires **(Figure 10)**. L'analyse d'une grande

cohorte (1085 tissus tumoraux pour 112 tissus sains) ne montre pas de différence de niveau de l'ARNm de Trip12 dans le cancer du sein remettant en cause les résultats de Chen *et al.*

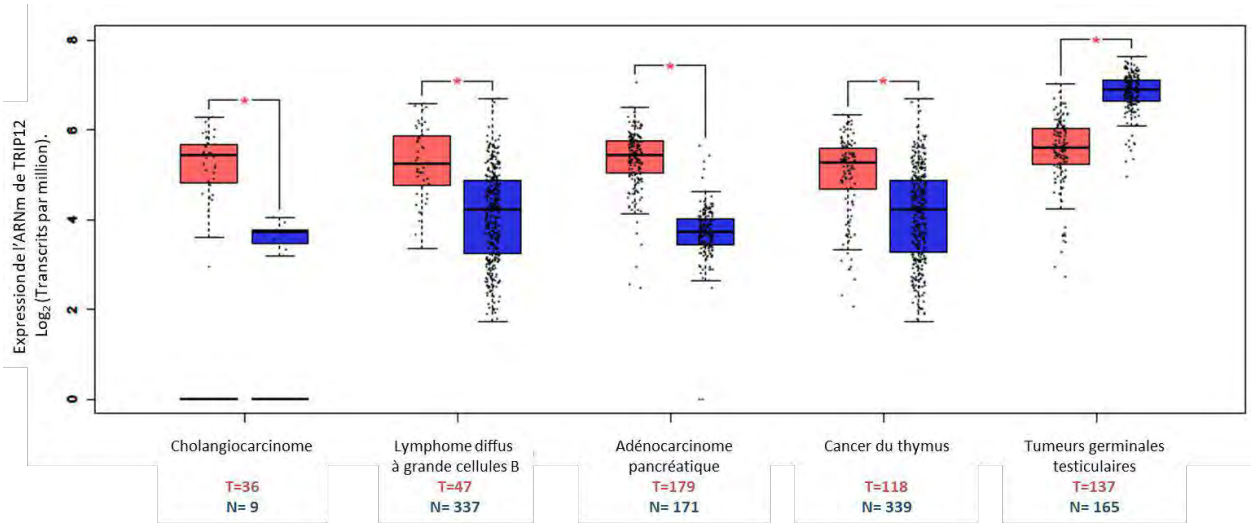

Figure 10 : Niveaux d'expression de l'ARNm de TRIP12 dans 5 types de cancer.
Le niveau d'ARNm de Trip12 est obtenu par RNAseq à partir des données disponibles dans la base de données GEPIA. Chaque point représente un échantillon, la barre noire horizontale représente la moyenne. Les différences statistiquement significatives entre les échantillons normaux (en bleu) et tumoraux (en rose) sont représentées par un astérisque rouge (test ANOVA avec une valeur $q < 0,01$).

Les mécanismes responsables de l'altération du niveau de l'ARNm de Trip12 dans les échantillons tumoraux restent largement inconnus. Une seule étude s'est intéressée à l'épissage alternatif de TRIP12 dans les cas de leucémie myéloïde aiguë (LAM).[98] En effet, l'analyse par RNA-seq de cellules mononucléées du sang périphérique (PBMC) a montré l'augmentation de l'isoforme de Trip12 ayant subi un épissage de l'exon 3 chez une patiente atteinte de LAM après traitement et rémission complète. Compte tenu du rôle essentiel de TRIP12 en tant que régulateur de la voie de signalisation ARF/P53, les auteurs suggèrent (sans mécanisme explicatif) que l'épissage alternatif de son ARNm pourrait de manière indirecte induire l'activation de la voie P53 et l'apoptose des cellules à croissance aberrante contribuant à la rémission.

B. Altération de l'expression protéique de TRIP12

Les données disponibles sur l'expression de la protéine TRIP12 dans le cancer sont encore moins abondantes que celles décrites pour le niveau d'ARNm. Le niveau protéique dans les tissus humains, référencé dans le « Human Protein Atlas », indique un niveau d'expression variable de TRIP12 selon le type de cancer. TRIP12 est retrouvée avec une fréquence élevée dans les cancers ORL, le cancer des testicules, et chez les patients atteints de gliome **(Figure 11)**.

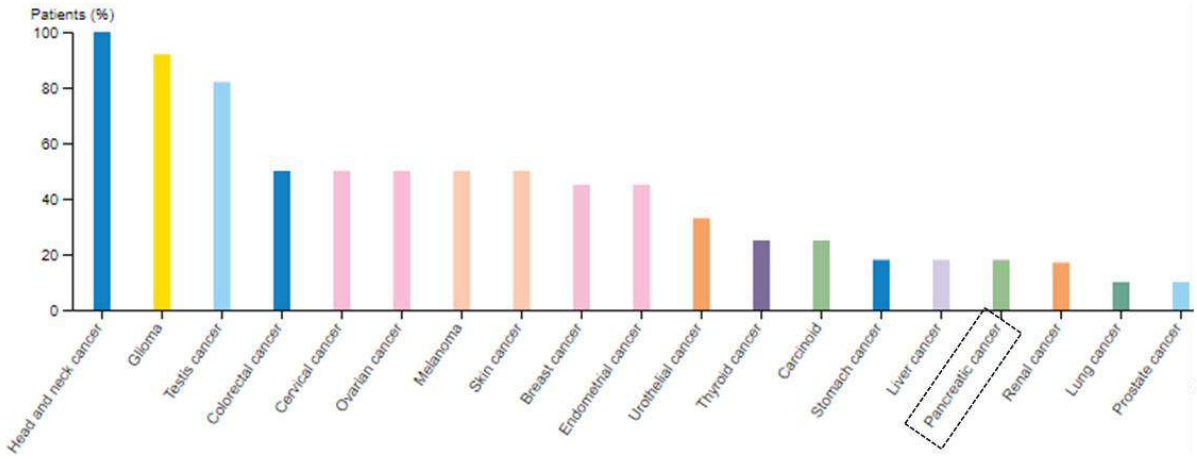

Figure 11 : Expression protéique de TRIP12 en pourcentage dans les cancers référencés dans la base de données GEPIA.
Le niveau protéique de TRIP12 est déterminé par analyse immunohistochimique de tissue microarray (TMA) d'après les données disponibles dans la base de données « The Human Protein Atlas ». L'expression en pourcentage est définie en normalisant l'expression dans 20 tissus cancéreux différents comparés à celle de 44 tissus normaux.

Dernièrement, il a été montré qu'un fort niveau de TRIP12 dans les tumeurs du sein améliore la survie sans métastases des patientes.[99] Le séquençage de l'ARN révèle que les cellules appauvries en TRIP12 ont acquis des traits mésenchymateux tels que la perte de polarité cellulaire et une motilité cellulaire accrue. L'expression ectopique de TRIP12 dans ces cellules les sensibilise à l'anoïkis, une mort cellulaire par perte de contact cellulaire. Dans cette étude, TRIP12 bloque l'EMT en inhibant l'expression du gène ZEB1/2, par un mécanisme qui reste encore à démontrer, et serait un suppresseur potentiel de la progression dans le cancer du sein.

Les événements moléculaires conduisant à l'altération de l'expression de la protéine TRIP12 sont peu étudiés. La déubiquitinase USP7 est surexprimée dans le carcinome hépatocellulaire (CHC) et requise pour la prolifération des lignées cellulaires dérivées du CHC.[36] D'un point de vue mécanistique, en réponse à la surexpression d'USP7, la protéine TRIP12 est stabilisée et ubiquitine ARF pour sa dégradation afin de promouvoir la prolifération des cellules dérivées du CHC. Fait intéressant, les auteurs établissent que TRIP12 et USP7, lorsqu'ils sont surexprimés, sont des marqueurs indépendants de mauvais pronostic du CHC. L'interaction entre ces deux partenaires, l'importance de USP7 dans la stabilité de TRIP12 et l'impact sur la voie P53 sont également retrouvés dans trois lignées de carcinome gastrique (AGS, CNE2Z, HCT-116).[37]

TRIP12 est surexprimée uniquement dans les cancers gastriques infectés par la bactérie Helicobacter pylori (H. pylori).[100] Cette bactérie est un des agents pathogènes humains courants et est reconnue comme un facteur de malignité gastrique.[101] L'infection par H. Pylori des lignées cellulaires dérivées de cancer gastrique induit l'expression de la protéine TRIP12 en impliquant le facteur de virulence CagA (Cytotoxin-Associated Gene A).[100] La surexpression de TRIP12 a pour conséquence la dégradation de la protéine ARF par polyubiquitination qui conduit à une inhibition de l'autophagie dans les cellules gastriques.

Enfin, le niveau de TRIP12 est le reflet du taux de réponse aux traitements pour certains cancers. En effet, les patients atteints de carcinomes ORL infectés par le virus du papillomavirus humain (HPV-positif) répondent mieux à la radiothérapie avec une survie globale plus élevée que ceux ayant un carcinome sans infection virale (HPV-négatif).[102] Suite à l'infection au HPV, la surexpression de P16 provoque la déstabilisation de TRIP12. Le mécanisme à l'origine de la perte de TRIP12 n'est pas encore connu. Cependant, compte tenu de la fonction inhibitrice de TRIP12 dans la DDR, la diminution de TRIP12 entraine la surexpression de RNF168, qui augmente à son tour l'ubiquitination incontrôlée des histones. La taille des foyers de réparation des dommages reconnus par 53BP1 est amplifiée et persiste 24h après l'irradiation, reflétant une réparation des cassures de l'ADN déficiente. La régulation à la baisse de TRIP12 sensibilise ainsi les cellules HPV positives à la radiothérapie. Inversement, chez 18 patients positifs pour le HPV, la surexpression de TRIP12 est associée à un faible taux de survie après radiothérapie. Ainsi, dans le cas de réponse à la radiothérapie, TRIP12 pourrait être un marqueur de prédiction de réponse aux traitements.

Le niveau de la protéine TRIP12 pourrait aussi fournir un marqueur utile pour la sensibilité aux inhibiteurs de PARP (PARPi).[30] En effet, les réponses à cette thérapie sont prometteuses, mais les prédictions de réponse aux traitements basées sur l'abondance sur la chromatine et/ou l'expression de PARP1 dans la cellule ne sont pas assez précises. De manière remarquable, le niveau de la protéine TRIP12 est négativement corrélé avec l'abondance de la protéine PARP1 dans deux cohortes de patientes atteintes d'un cancer du sein ou de l'ovaire.[30] En effet, TRIP12 cible et réduit la présence de PARP1 au niveau de la chromatine en la polyubiquitinant et ainsi limite le « piégeage » de PARP1 par PARPi.

PARTIE 2 : Le pancréas

I. Structure et fonction du pancréas

A. Notions générales d'anatomie

Le pancréas est un organe qui pèse en moyenne 80g chez l'homme adulte. Il se situe dans la cavité abdominale avec une localisation rétropéritonéale. Le pancréas s'étend de la courbe en forme de C du duodénum (tête), passe derrière l'estomac (corps) et se termine au hile de la rate (queue) (**Figure 12**). Compte tenu de sa localisation, l'exploration médicale de cet organe est difficile.

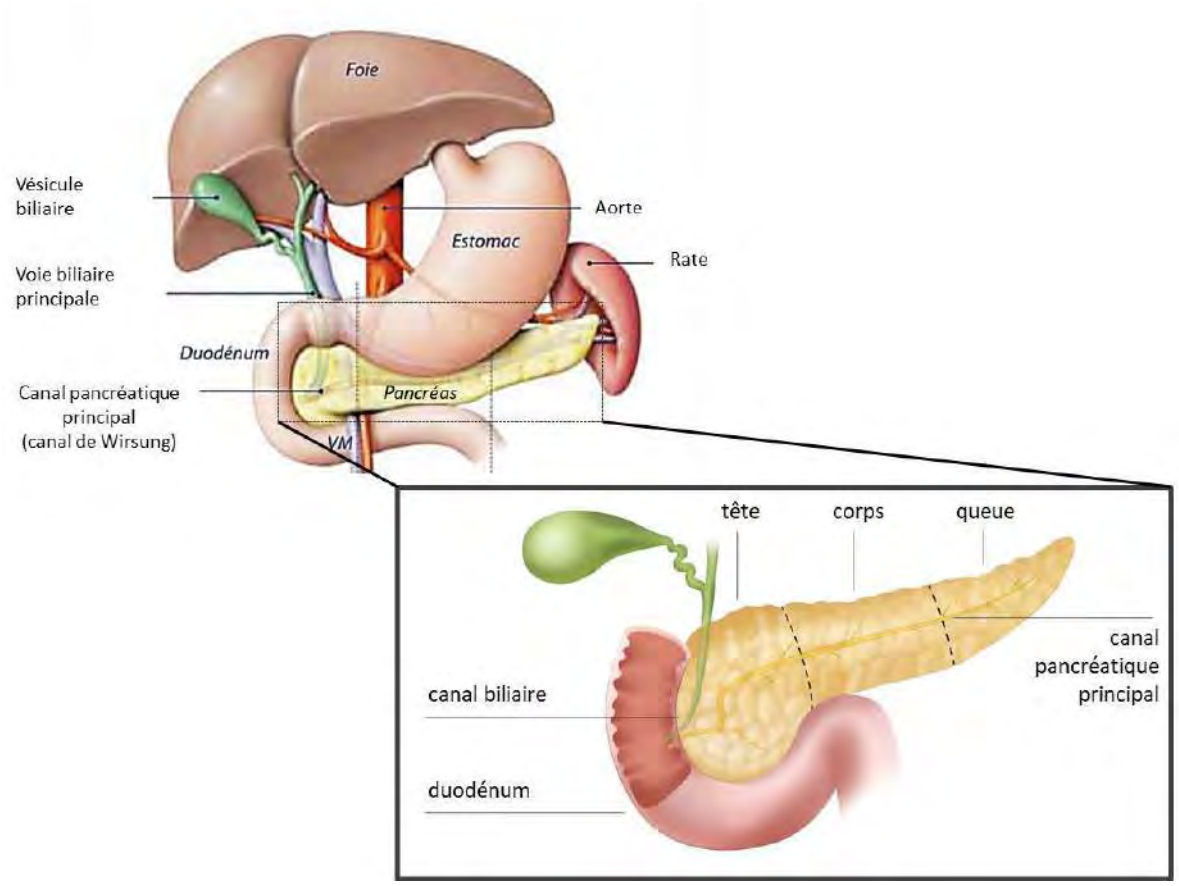

Figure 12 : Schéma représentant la localisation du pancréas et la forme de la glande.
Adapté de « Le cancer du pancréas en question » Paris, fondation ARCAD de T Andre et P Hammel, 2014 www.fondation arcad.org et de « the Hirshberg Foundation for Pancreatic Cancer Research » site : www.pancreatic.org.

B. Physiologie du pancréas

Le pancréas est un organe amphicrine c'est-à-dire qu'il possède deux fonctions : une fonction exocrine (tissu acineux et canalaire) et une fonction endocrine (îlots de Langerhans) **(Figure 13)**. Ces deux compartiments fonctionnels jouent un rôle essentiel et complémentaire dans le métabolisme des nutriments facilitant la digestion des nutriments et participant à l'homéostasie de la glycémie.

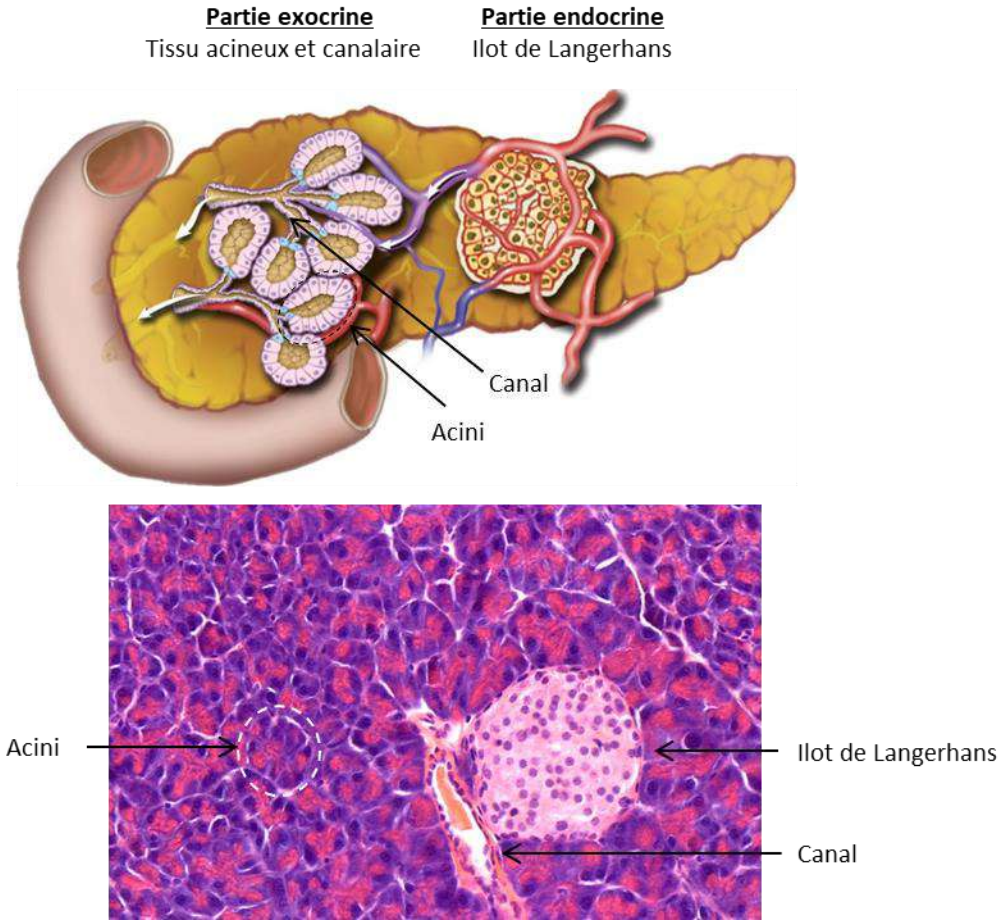

Figure 13 : Représentation histologique du pancréas exocrine et endocrine.
Schéma (en haut) montrant les 2 composantes du pancréas, le pancréas exocrine constitué d'acini et de canaux et la partie endocrine comprenant les ilots de Langerhans (Adapté de *Pandol, 2011*).[103] En bas, figure une coupe de pancréas de souris (coloration en H/E) repositionnant les structures histologiques du pancréas.

1) Compartiment endocrine

Dispersé dans le tissu acineux, le compartiment endocrine du pancréas est organisé en îlots de Langerhans hautement vascularisés et innervés, constituant environ 1 à 2 % du pancréas. Ces structures sont composées de cinq types cellulaires distincts produisant différentes hormones peptidiques. Les cellules α produisent le glucagon, une hormone hyperglycémiante. Les cellules β sont responsables de la synthèse et de la sécrétion de l'insuline, hormone hypoglycémiante. Les cellules δ sécrètent la somatostatine, qui inhibe la sécrétion d'insuline et de glucagon. Les cellules ε produisent la ghréline, hormone qui déclenche la sensation d'appétit et les cellules PP sécrètent le polypeptide pancréatique (PP) qui limite les sécrétions biliaires et pancréatiques. Ces hormones jouent un rôle unique et essentiel en régulant le métabolisme des nutriments impliqués dans la glycémie, la coordination de la digestion et l'appétit.

2) Compartiment exocrine

Le pancréas exocrine est constitué d'un réseau de cellules canalaires élaboré qui se termine par les cellules acineuses. Ce réseau représente 95% de la masse du pancréas. Les acini sont constitués de plusieurs cellules acineuses polarisées et compartimentées permettant une organisation autour d'une lumière centroacineuse.[104] Sur la membrane basolatérale se trouvent les récepteurs d'hormones et de neurotransmetteurs qui stimulent la sécrétion des enzymes.[105] Au pôle basal de la cellule, se localisent le noyau ainsi qu'un réticulum endoplasmique (RE) rugueux abondant pour la synthèse des protéines **(Figure 14)**. La région apicale de la cellule contient des granules de zymogène, lieu de stockage des enzymes digestives. La surface apicale de la cellule acineuse possède également de nombreuses microvillosités dans la lumière centroacineuse. Au niveau des microvillosités et dans le cytoplasme sous-jacent à la membrane plasmique apicale est présent un réseau d'actine filamenteuse impliquée dans l'exocytose du contenu des granules de zymogène. [106,107] La sécrétion se fait dans la lumière de l'acinus connectée au système canalaire. Les jonctions serrées entre les cellules acineuses assurent la cohésion des cellules entres elles et séparent le compartiment basolatéral du compartiment luminal. Les complexes jonctionnels assurent également le passage paracellulaire de l'eau et des ions.

L'épithélium canalaire est constitué de cellules cubiques ou pyramidales en fonction de leur localisation dans l'architecture du réseau canalaire. Ces cellules sont pourvues d'abondantes mitochondries qui produisent l'énergie nécessaire au transport des ions **(Figure 14)**.[108] Au niveau du pôle apical des cellules se trouvent les transporteurs et canaux ioniques impliqués dans la sécrétion des ions chlore et bicarbonate.[109] Les cellules canalaires expriment spécifiquement de la cytokératine 19 (CK19), de l'anhydrase carbonique II et des mucines MUC1 et MUC6.

À la jonction entre l'acinus et le système canalaire se trouvent les cellules centroacineuses présentant une morphologie cellulaire et des profils transcriptionnels distincts et spécifiques. Les cellules centroacineuses sont plus petites que les cellules acineuses, de forme cuboïde (≈10 µm de diamètre), avec un rapport nucléocytoplasmique élevé et de longs prolongements cytoplasmiques qui permettent le contact avec d'autres cellules.[110] Elles possèdent des caractéristiques à la fois de cellules acineuses et canalaires. Le rôle des cellules centroacineuses reste à l'étude, mais certains auteurs suggèrent que celles-ci pourraient représenter des cellules pancréatiques multipotentes progénitrices[111] potentiellement impliquées dans la régénération du tissu exocrine.[112]

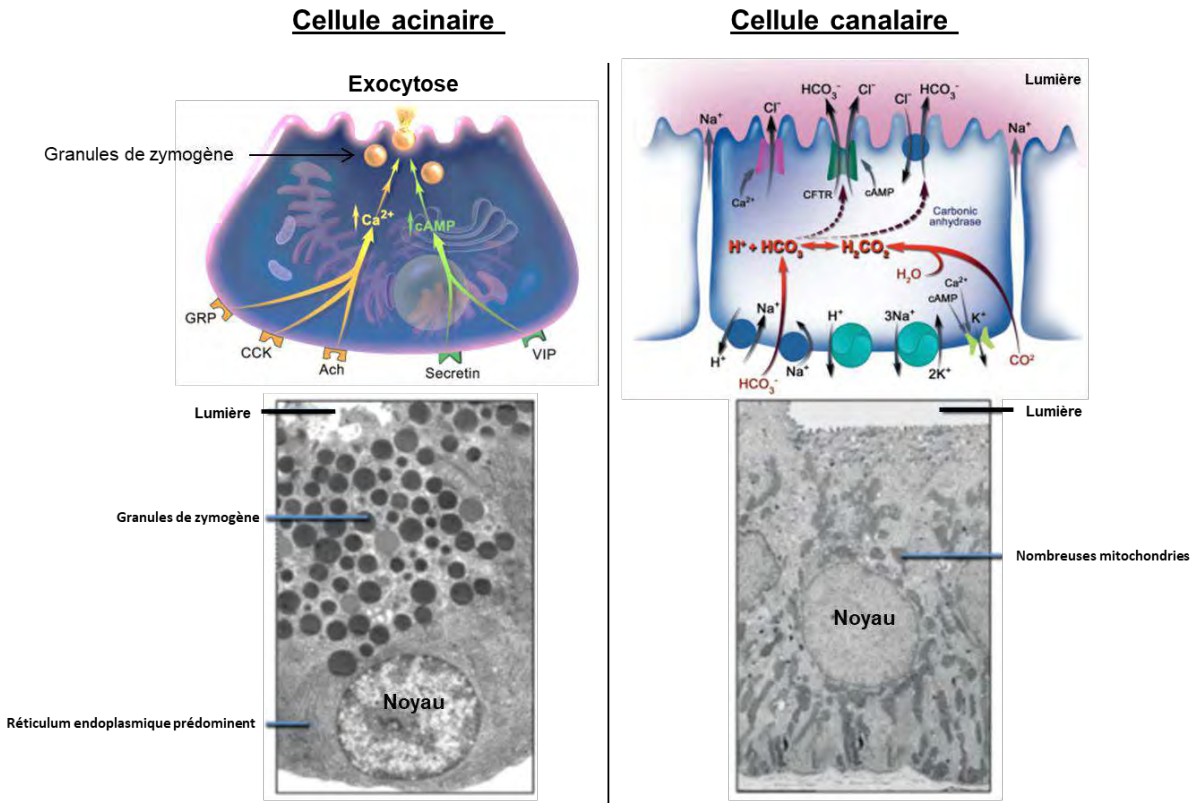

Figure 14 : Schéma des cellules constituant le compartiment exocrine.
Schéma de la cellule acineuse (en haut à gauche) et de la cellule canalaire (en haut à droite) avec les voies de signalisation spécifiques de l'exocytose et du transport des enzymes vers la lumière du canal excréteur (Adapté de *Pandol, 2011*).[103] En bas, images de microscopie électronique de la cellule acineuse (à gauche) et de la cellule canalaire (à droite).

Les cellules acineuses synthétisent et sécrètent des proenzymes protéolytiques (trypsine, chymotrypsine, carboxypeptidase, élastase), des désoxyribonucléases et des ribonucléases (DNAse et RNAse), de l'amylase et de la lipase.[113] La majorité de ces enzymes digestives est synthétisée dans un état inactif, appelé proenzyme, et conservée à pH acide dans les granules de zymogène protégeant ainsi les cellules acineuses de l'autodigestion. Le transport et le relargage des granules de zymogène sont régulés par un mécanisme d'exocytose dépendant de l'action d'hormones peptidiques et de neurotransmetteurs. Les cellules acineuses possèdent des récepteurs spécifiques de chaque sécrétagogue (cholécystokinine, acétylcholine, sécrétine, VIP (Vasoactive Intestinal Peptide)) localisés en position basolatérale. Leur activation entraine une cascade de signalisation intracellulaire, soit par la libération de calcium par le RE (CCK et Ach) ou par l'augmentation de l'AMPc (sécrétine et VIP), qui provoque l'exocytose.

Le contenu sécrétoire acineux riche en proenzymes, catalyse la dégradation des glucides, des protéines et des lipides après sécrétion et activation par les sucs gastriques dans le duodénum. Pour cela, les proenzymes sécrétées par les cellules acineuses dans le réseau canalaire au niveau des cellules centroacineuses sont transportées via le réseau hautement ramifié de petits canaux intralobulaires convergeant vers des canaux interlobulaires plus gros qui se déversent dans le canal pancréatique

principal de Wirsung et le canal accessoire de Santorini débouchant dans le duodénum. Les cellules canalaires sécrètent également des molécules inorganiques (bicarbonate, sodium, potassium et chlore).

C. Organogenèse du pancréas

Les outils génétiques tels que les modèles murins génétiquement modifiés ont permis d'identifier les étapes majeures et les principaux facteurs qui gouvernent l'organogenèse du pancréas. Le développement embryonnaire du pancréas murin possède des similitudes avec celui du pancréas humain.

1) Mise en place des bourgeons pancréatiques

Le pancréas dérive du feuillet endodermique et se forme à partir de deux bourgeons, ventral et dorsal qui deviendront les régions pré-pancréatiques.[114] La partie ventrale du pancréas est située au niveau de l'endoderme antérieur près des futurs progéniteurs hépatiques, alors que le pancréas dorsal se forme à partir de cellules endodermiques postérieures **(Figure 15-A)**.

A partir de 8,5 jours de développement embryonnaire (E8.5) chez la souris, avant même l'apparition des bourgeons pancréatiques, se met en place une cascade de voies de signalisation qui dépend des tissus environnants. Cette signalisation permettra d'orienter la mise en place du bourgeon ventral et du bourgeon dorsal le long de l'axe antéro-postérieur. En effet, la voie Sonic Hedgehog (SHH) est inhibée de manière régionalisée par la présence de la notochorde au niveau du bourgeon dorsal, sécrétant l'activine et le Fibroblast Growth Factor 2 (FGF2). Suite à la mise en place de l'aorte dorsale et des veines vitellines, le bourgeon pancréatique dorsal émerge du duodénum à E9.[115] Le bourgeon pancréatique ventral est induit par des signaux du mésoderme qui répriment la signalisation FGF. Les signaux de régionalisation sont ainsi différents pour le bourgeon dorsal et le bourgeon ventral qui émergent respectivement à E9 et à E9.5. A E8.5, le gène homéotique Pancreatic and Duodenal Homeobox 1 (PDX1), essentiel à la différenciation de tous les types cellulaires pancréatiques,[116] est exprimé dans les cellules progénitrices pancréatiques multipotentes (MPC) des deux bourgeons pancréatiques **(Figure 15-B)**.

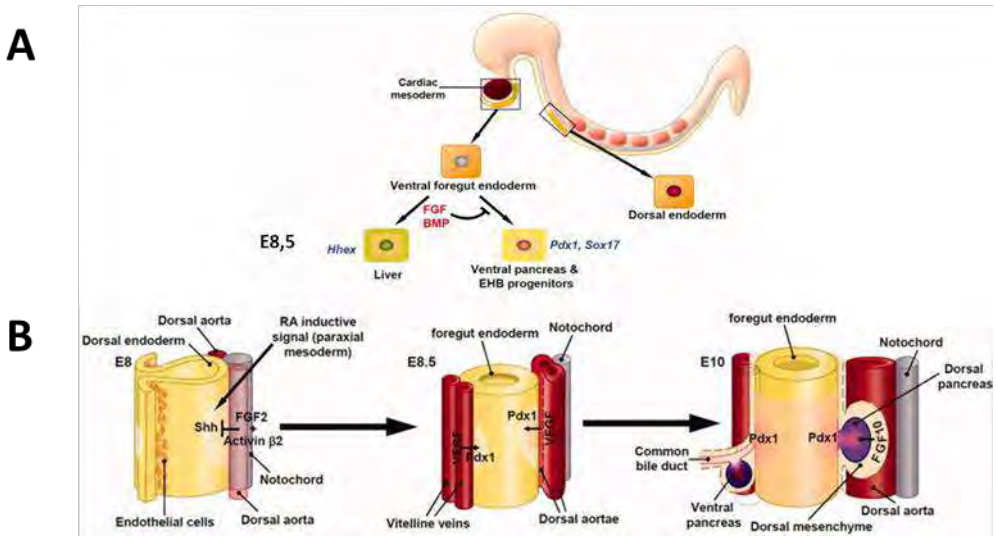

Figure 15 : Mise en place des ébauches embryonnaires endodermiques pré-pancréatiques dorsale et ventrale
A- Modélisation de l'influence de la signalisation dérivant du mésoderme dans la mise en place des domaines pancréatiques. B- Coupe sagittale des ébauches embryonnaires endodermiques pré-pancréatiques dorsale et ventrale à E8,5 exprimant PDX1, régulateurs transcriptionnels (en bleu) et signalisation moléculaire (en rouge). Schéma adapté de la revue Pan et Wright, 2011. [116]

Le niveau d'expression du gène PDX1 est fortement régulé pour maintenir l'identité pancréatique. D'une part, la perte de fonction homozygote de PDX1 provoque une agénésie pancréatique complète malgré la formation initiale de bourgeons épithéliaux.[117] D'autre part, le maintien de l'expression de PDX1 dans des souris transgéniques, conduit à la formation d'un pancréas atrophié dans lequel les cellules acineuses sont remplacées par des structures canalaires.[118]

La voie Notch est importante dans la mise en place des MPC car elle permet de coordonner et de réguler la différenciation des MPC qui vont ensuite donner naissance aux cellules acineuses, canalaires et endocrines. Les MPC expriment plusieurs facteurs de transcription dont les principaux sont PDX1, PTF1a, SOX9 (Sex-determining region Y-box 9) et HNF1b (Hepatocyte nuclear factor 1 homeobox B). L'inactivation de HES1 (Hairy and enhancer of split 1) ou de SOX9 provoque une hypoplasie pancréatique.[119,120] L'invalidation génétique (knock-out) homozygote de PTF1a provoque une agénésie pancréatique ventrale complète et une structure rudimentaire en forme de canal en position dorsale chez la souris.[121] Les embryons de souris déficients en HNF1b présentent une agénésie du pancréas, avec un bourgeon dorsal transitoire exprimant PDX1 mais pas PTF1a, montrant que HNF1b est nécessaire pour la spécification du pancréas.[122] L'expression spatio-temporelle de ces facteurs est finement régulée car ils vont jouer plusieurs rôles aux différentes étapes du développement du pancréas.

2) Spécification des lignages cellulaires pancréatiques

La spécification des différents lignages pancréatiques est marquée par deux grandes étapes. Tout d'abord, la transition primaire, qui se déroule entre E9.5 et 12.5, vise à induire la spécification des progéniteurs endodermiques pancréatiques en précurseurs multipotents (MPC) proliférants. Puis, la

transition secondaire entre E12.5 et 15.5, qui est marquée par un changement morphogénétique drastique, permet l'élaboration de l'épithélium pancréatique différencié.

a. Transition primaire (E9.5 – 12.5)

Les principaux événements de cette transition comprennent des modifications morphologiques structurelles. En premier lieu, la prolifération active des cellules progénitrices du bourgeon pancréatique pour générer un épithélium pseudo-stratifié formé d'un nombre déterminé de précurseurs multipotents. Puis, la formation de plusieurs lumières appelées microlumières et d'un réseau canalaire ramifié dans chaque bourgeon à E10.5. Suite à la rotation du duodénum (à E11.5), il y a rapprochement des deux ébauches prépancréatiques qui fusionnent en un seul organe formant un réseau tridimensionnel.[123] Un changement morphologique est ensuite visible et finalisé à E12.5, correspondant à l'étape nommée ségrégation des domaines. Il s'agit de l'étape initiatrice de la différenciation cellulaire.

Une expression différentielle à la fois spatiale et temporelle des gènes est nécessaire à la mise en place des domaines « Tip » (E9.5) et « Trunk » (E10.5). En effet, les extrémités des bourgeons pancréatiques deviendront les domaines « Tip », associés à l'expression de PDX1, PTF1a, c-Myc et Cpa (Carboxypeptidase).[124,125] Les structures internes appelées domaines « Trunk » sont associées à l'expression de Nkx6 (NK6 Homeobox 1), SOX9, HES1, HNF6. Les modèles transgéniques de lignage ont prouvé que les cellules acineuses sont issues des cellules « Tip » alors que les cellules endocrines et canalaires sont issues des cellules « Trunk ».[126,127] La voie Notch est primordiale pour induire la mise en place des domaines « Tip » et « Trunk ». En effet, Murtaugh *et al.* ont montré qu'en réponse à une activation élevée de la voie Notch, le niveau du facteur de transcription Nkx6 est augmenté inhibant directement la transcription du facteur PTF1a. L'absence de l'expression de PTF1a favorise alors une différenciation en précurseur de type « Trunk ».[128] Ainsi, les facteurs PTF1a et Nkx6 sont responsables de la spécification des lignages cellulaires pancréatiques grâce à leur capacité transcriptionnelle corépressive **(Figure 16)**.[129]

b. Transition secondaire

Cette étape marquée par une importante expansion de l'épithélium commence à E13. Elle est caractérisée, dans un premier temps, par la différenciation des précurseurs « Tip » et « Trunk » en cellules pancréatiques matures (cellules acineuses, cellules canalaires, et cellules endocrines). Dans un second temps, le pancréas acquiert sa structure arborescente.

Le complexe trimérique PTF1 joue un rôle clé dans les cellules de la partie « Tip ». PTF1 est formé de la protéine bHLH PTF1a, d'une autre protéine bHLH ubiquitaire (protéine E) et de la protéine RBP-J ou de son paralogue RBP-JL. $PTF1^{RBPJ}$ est essentiel pour la formation des MPC à l'origine de tous les types cellulaires du pancréas. $PTF1^{RBPJ}$ active l'expression de RBP-JL et facilite la formation

du complexe transcriptionnel PTF1^{RBPJL} appelé PTF1a-L. Le programme transcriptionnel permettant la maturation des progéniteurs acineux en cellules exocrines matures sera alors activé par PTF1a-L à E15.5.[130] PTF1a-L est ainsi le facteur majeur synchronisant le programme transcriptionnel acineux. Cependant, il n'est pas suffisant pour induire cette différenciation puisque l'expression ectopique de PTF1A-L dans les cellules PDX1+ ne permet pas une différenciation prématurée du compartiment acineux, mais bloque le développement des précurseurs « Trunk ».[131] Ces cellules acineuses expriment également des facteurs de transcription spécifiques tels que NR5A2 (Nuclear receptor subfamily 5 group A member 2) et MIST1. En effet, NR5A2, une cible transcriptionnelle de PTF1a, coopère avec PTF1a-L dans l'activation des gènes nécessaires à la mise en place du phénotype acinaire.[132,133] Il a aussi été prouvé que l'expression de MIST1 permet la différenciation terminale de la lignée acinaire en mettant en place l'exocytose des granules de zymogène. Son absence entraîne le développement de cellules acineuses peu différenciées, avec un défaut de polarité et l'incapacité de faire l'exocytose des granules de zymogènes.[134]

A la différence du domaine « Tip » donnant naissance à un seul type cellulaire, la partie « Trunk » est bipotente et conduit à la différenciation de la lignée canalaire et de la lignée endocrine. En réponse à un faible niveau de signalisation de la voie Notch, l'expression de Neurog3 (Neurogénine 3) est induite dans une sous-partie du domaine « Trunk » qui amorcera la différenciation des cellules endocrines[135]. En revanche, en réponse à l'activation de la voie Notch, les progéniteurs du domaine « Trunk » qui n'expriment pas de Neurog3, se différencient par défaut en cellules canalaires.[136] La voie Notch favorise également l'activation de HES1 et de SOX9 régulant ainsi le niveau de Neurog3.[137] Les facteurs de transcription tels que SOX9, HES1, HNF1b exprimés dans les progéniteurs « Trunk » sont conservés au sein des cellules canalaires, ils sont exclus des progéniteurs de la lignée endocrine **(Figure 16)**.[116,125,138–140]

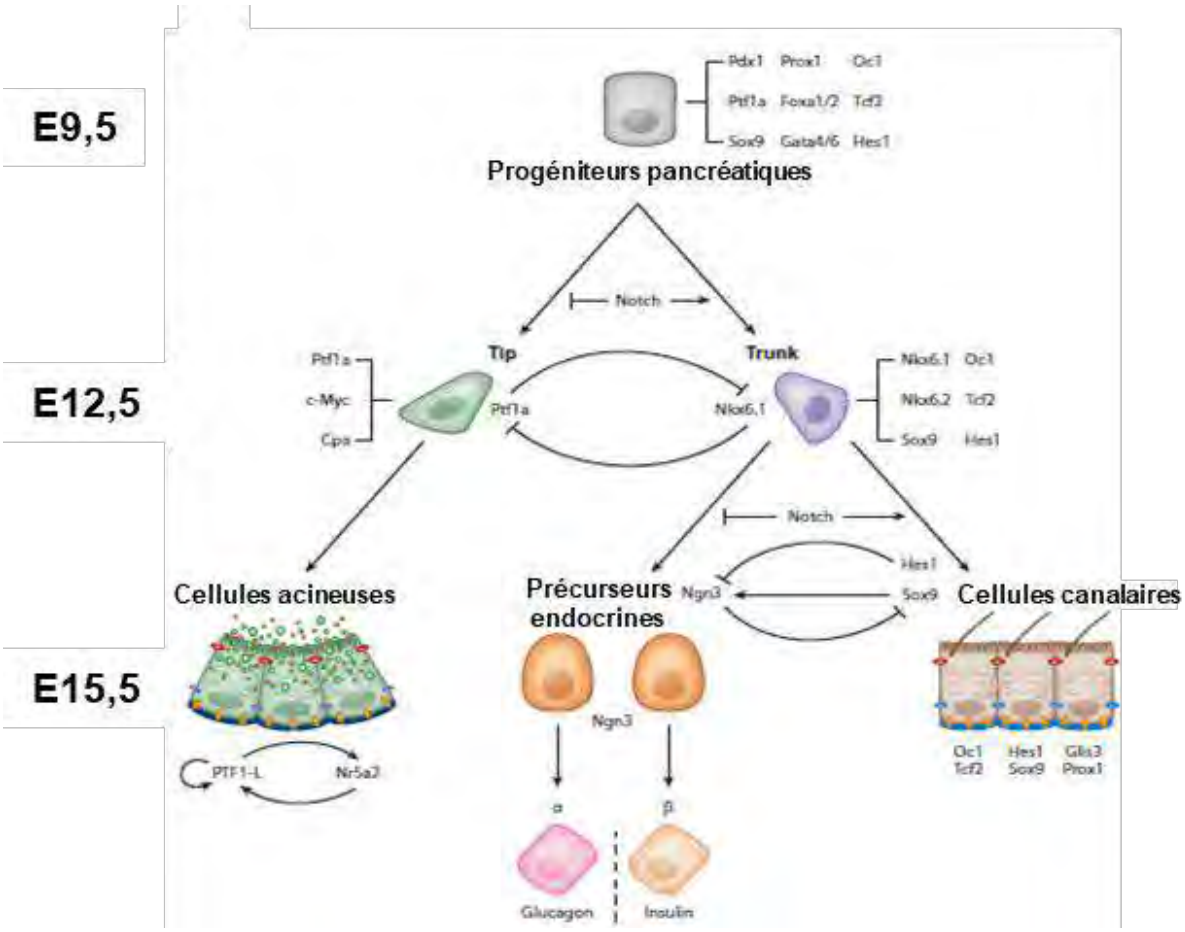

Figure 16 : Modèle simplifié de la spécification du devenir des cellules issues des bourgeons pancréatiques.
Différenciation des progéniteurs pancréatiques multipotents (MPC) situés dans les bougeons pré-pancréatiques ventraux et dorsaux. Au début de la transition secondaire, la ségrégation des cellules des extrémités appelées « Tip » et les cellules du tronc « Trunk » dépend de la voie de signalisation Notch. La spécification des lignées cellulaires acineuses, canalaires et endocrines est régie par l'expression de facteurs de transcriptions spécifiques des types cellulaires décrite dans le texte. (Adapté de *Shih et al, 2013*[125])

En parallèle de la différenciation cellulaire, se met également en place la tubulogenèse pancréatique à partir de la transition secondaire jusqu'à la naissance. Cette étape est contrôlée par la division des progéniteurs acineux « Tip » qui subissent d'importants phénomènes de remodelage induisant l'extension, la croissance et la hiérarchisation de l'arbre canalaire.[141] Cette organisation topologique est visible à partir de E15.5 avec des amas cellulaire acineux fusionnés autour des extrémités du réseau canalaire **(Figure 17)**.

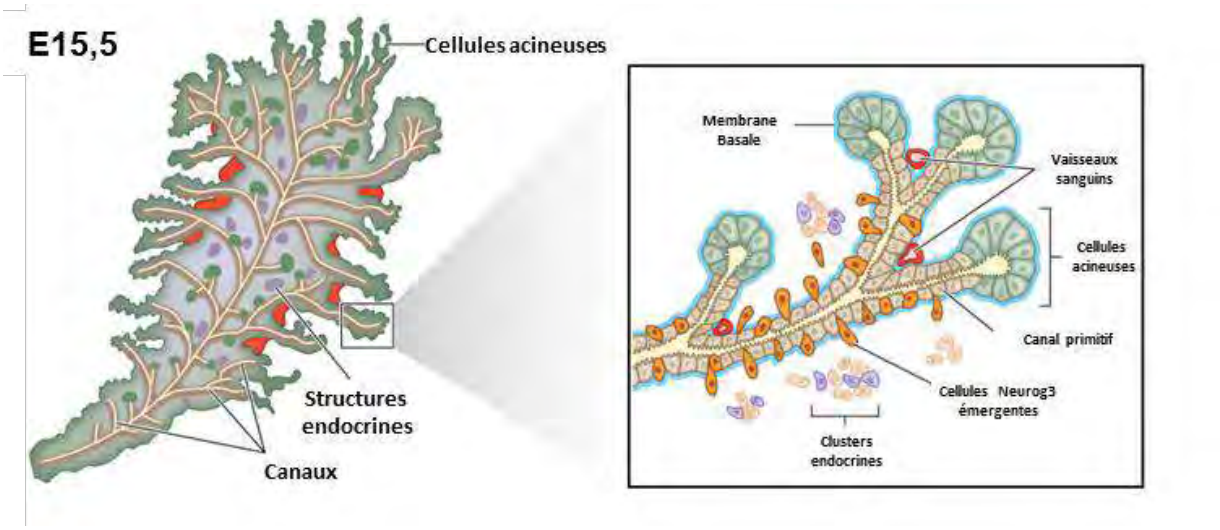

Figure 17 : Représentation de la tubulogenèse du pancréas au stade embryonnaireE15.5
Hiérarchisation de l'arbre canalaire se remodelant progressivement en un épithélium monocouche constitué de canaux primitifs très ramifiés et de cellules acineuses nouvellement différenciées. Les précurseurs endocrines exprimant Neurog3 (cellules en orange dans l'encart) migrent pour former des amas de cellules endocrines. Les vaisseaux sanguins sont intercalés entre les branches naissantes de l'arbre canalaire pancréatique. (Adapté de *Shih et al, 2013*[125])

La différenciation et la maturation du tissu exocrine se poursuivent pendant les premières semaines de la période post-natale. Les îlots de Langerhans adoptent leur forme caractéristique juste après la naissance et leur nombre augmente considérablement pendant les deux premiers mois.

II. La métaplasie acino-canalaire

Les cellules acineuses sont des usines à production d'enzymes digestives, la quantité de protéines produite n'est égalée par aucun autre type cellulaire dans l'organisme. Cette production intense engendre un haut niveau de stress physiologique qui peut être accentué par différents stimuli anormaux (comme l'alcool ou le tabac).[142] Malgré toutes ces perturbations (endogènes et exogènes), le maintien de l'homéostasie de cet organe est possible grâce à la grande plasticité des cellules pancréatiques permettant de résister à un stress soutenu et d'éviter la mort cellulaire. Ce paragraphe vise à expliquer de manière détaillée la découverte du mécanisme à l'origine de cette plasticité ainsi que les voies à l'origine de la régulation.

A. Plasticité des cellules exocrines du pancréas

Depuis 30 ans, différentes études ont prouvé que les cellules acineuses pancréatiques sont plastiques aussi bien chez l'homme que chez la souris. Leur changement phénotypique a tout d'abord été observé en 1990 après mise en culture d'acini obtenus après digestion enzymatique de pancréas de souris[143], puis en 1992 à partir de cultures d'acini de pancréas humain réséqué par chirurgie.[144] Ces

expériences montrent la perte rapide en deux jours des marqueurs des cellules acineuses associée avec l'augmentation réciproque des marqueurs canalaires en absence d'apoptose.[144–146] Ces premières observations ont ensuite été confirmées chez le rongeur (rat, souris).[147,148]

Le phénotype des cellules acineuses mises en culture n'est pas stable et le changement d'environnement est perçu comme un stress favorisant la métaplasie acino-canalaire (MAC), c'est-à-dire la transformation des cellules acinaires en cellules canalaires. La MAC se fait par transdifférenciation. D'un point de vue étymologique, la transdifférenciation est un processus dans lequel un type cellulaire différencié qui a des fonctions précises se convertit en un autre type cellulaire complètement différent ayant d'autres fonctions.[149] La MAC ne se fait pas par transdifférenciation directe. En effet, dans un premier temps, les cellules métaplasiques acineuses se dédifférencient en cellules cuboïdes intermédiaires avant d'adopter un phénotype canalaire **(Figure 18)**. Dans ces cellules intermédiaires, l'expression des marqueurs acineux diminue mais perdure, celle des marqueurs de différenciation et des marqueurs canalaires augmente **(Figure 19)**. Par ailleurs, la MAC est transitoire et s'accompagne d'une phase de redifférenciation, c'est-à-dire d'une réversion phénotypique en cellules acineuses. Dans mon manuscrit de thèse les termes MAC et transdifférenciation seront utilisés comme synonymes. En absence d'oncogène, ce mécanisme est réversible, il peut être inhibé par l'utilisation du nicotinamide par exemple.[148]

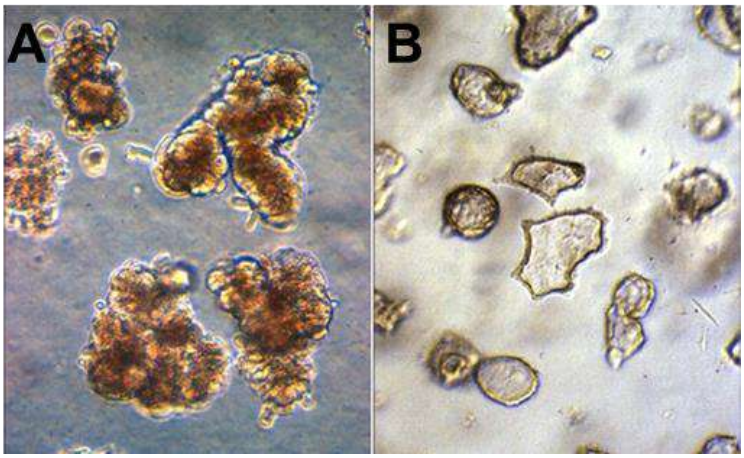

Figure 18 : Métaplasie acino-canalaire de cellules acineuses pancréatiques murines.
Images de cellules acineuses directement après ensemencement (J0, image A), subissant la métaplasie acino-canalaire cinq jours après mise en culture (image B). (Adaptée de *Means et al*,.[150])

La plasticité des cellules acineuses a aussi été envisagée pour régénérer les cellules β du pancréas chez les patients diabétiques en alternative à la transplantation d'îlots de Langerhans. Ainsi, il a été mis en évidence que les cellules acineuses ont la capacité de se transdifférencier en nouvelles cellules β, sécrétrices d'insuline.[151,152] De même, les acini peuvent se trandifférencier en hépatocytes.[153]

Les preuves du changement phénotypique des cellules acinaires pancréatiques ont été fournies grâce au développement de lignées de souris génétiquement modifiées permettant de suivre le devenir des cellules acineuses en culture par lignage cellulaire. L'étude réalisée par Means *et al*. utilise la

recombinaison d'un allèle rapporteur lacZ par une recombinase Cre active dans les acini pour suivre le devenir de ces cellules. L'expression de β-galactosidase démontre ainsi qu'après mise en culture et stimulation de la voie des récepteurs de l'EGF (EGFR), les cellules acineuses murines se transdifférencient en cellules canalaires.[150] Lors de leur mise en culture, les cellules exprimant la β-galactosidase sont positives pour l'amylase et négatives pour les cytokératines. Après cinq jours, le marquage β-galactosidase persiste dans les cellules de type canalaire qui n'expriment alors plus d'amylase et présentent un marquage cytokératine, reflet de la transdifférenciation cellulaire.

Le changement phénotypique des cellules acineuses humaines en cellules qui expriment des marqueurs canalaires spécifiques, tels que CK19, SOX9 et l'anhydrase carbonique II a également été démontré expérimentalement par le lignage cellulaire.[154] La co-transduction des cellules exocrines humaines à l'aide de deux vecteurs adénoviraux (Ad-CMV-LSL-EGFP et Ad-Amy-Cre) a permis l'expression de GFP spécifiquement dans les cellules acineuses sous la dépendance du promoteur amylase. Ces cellules se transforment en cellules acinaires exprimant la GFP et deviennent positives pour le marquage cytokératine 19 après 7 jours de mise en culture.

Ainsi dans le pancréas, la transformation du tissu acineux différencié en tissu canalaire différencié, de morphologie, de fonction et de physiologie différentes est appelée métaplasie acino-canalaire.[155,149]

B. Pourquoi la métaplasie joue-t-elle un rôle clef dans l'homéostasie pancréatique ?

La plasticité des cellules exocrines du pancréas est notamment observée lors de la pancréatite, atteinte inflammatoire du pancréas exocrine qui survient à la fois dans des formes aiguës et chroniques. La pancréatite aiguë se distingue des autres maladies gastrointestinales par la détection des enzymes pancréatiques telles que l'amylase et la lipase dans la circulation sanguine.[156]

Cependant, l'étude de la régénération du tissu exocrine chez l'homme est limitée car seule une minorité de patients peuvent être opérés par résection chirurgicale. A partir de ces tissus nécrotiques, il a été caractérisé la présence de fibrose, d'un infiltrat immunitaire et de structures de type canalaire.[154,157] Les expériences de lignage cellulaire réalisées dans des modèles murins de pancréatite expérimentale ont largement prouvé que les cellules acineuses contribuent à ce changement morphologique.[158]

La majorité des formes de pancréatite sont bénignes et se résolvent sans incident en quelques jours ou quelques semaines traduisant ainsi l'importance de la plasticité des cellules acineuses. A l'inverse, un défaut de plasticité entraine des formes nécrosantes, plus graves, pouvant conduire à la mort. La pancréatite chronique se caractérise par l'absence d'enzymes circulantes reflétant l'atrophie des cellules acineuses pancréatiques.[159] Ces deux pathologies sont finalement liées car une pancréatite aigüe dont l'inflammation persiste et qui ne peut se résorber évolue vers une maladie chronique.[156]

L'utilisation de modèles murins a permis de caractériser la cinétique de la pancréatite. En réponse à un stress exogène (comme l'alcool), les enzymes digestives sont sécrétées en quantité trop abondante sur une longue période, entraînant une autodigestion de l'organe qui s'accompagne de nécrose et d'inflammation (phase aigüe). Le mécanisme de dédifférenciation des cellules acineuses a été observé en réponse à différents modèles de lésion pancréatique in vivo (traitement chimique tel que la caeruléine ou traitement chirurgical tel que la ligature du canal pancréatique).[160] Majoritairement utilisée, l'injection de caeruléine, un analogue de la cholécystokinine, est l'une des techniques les plus simples. Les premières études réalisées sur des préparations d'acini *in vitro*, par Williams *et al.* en 1978, démontrent que l'administration de caeruléine à faible dose induit la sécrétion d'amylase.[161] En revanche, cette sécrétion est complètement aberrante en réponse à des doses supramaximales[161] entrainant tout d'abord l'apoptose de certaines cellules acineuses et une cascade de signalisation pro-inflammatoire (cytokines telles que TNF-α, IL-6) favorisant le recrutement de macrophages et de neutrophiles.[162] Des études in vivo ont ensuite permis de renforcer ces résultats et de nommer cette étape la phase d'initiation.[163] Durant cette phase, une hyperamylasémie dans le sérum est observée une heure après la dernière injection de caeruléine en raison de la fuite paracellulaire des enzymes digestives par les acini endommagés dans la circulation sanguine.[164] Il s'ensuit une phase de dédifférenciation des cellules acineuses résiduelles, induite par la diminution de l'expression des enzymes digestives et des marqueurs acineux que sont l'amylase, l'élastase, MIST1, NR5A2 et PTF1a, de la réexpression des protéines canalaires telles que CK19, MUC1, SOX9, HNF1b et de l'expression des marqueurs progéniteurs comme PDX1 et HES1 **(Figure 19)**.[165–167] Enfin, une phase de régénération tissulaire permettant la restauration complète du compartiment acinaire est visible une à deux semaines après une pancréatite aiguë chez la souris induite par caéruléine.[150,168]

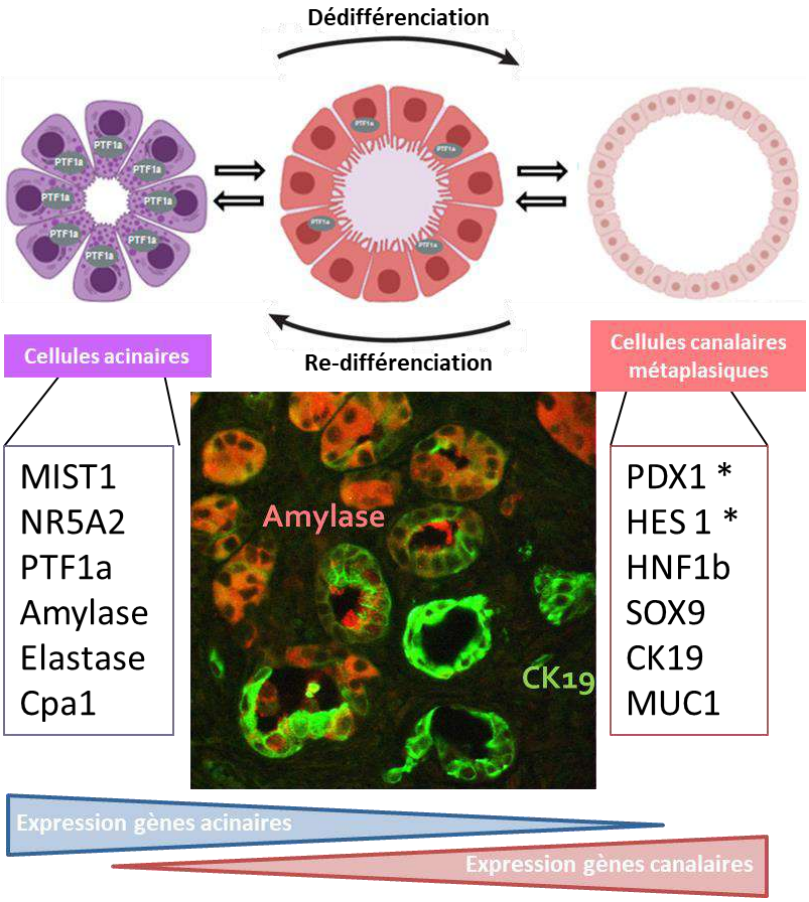

Figure 19 : Mécanismes moléculaires et structuraux de dédifférenciation des cellules acineuses en cellules canalaires.
Schéma représentant le processus de métaplasie (en haut) durant lequel les cellulaires acineuses acquièrent un phénotype de cellules canalaires, caractérisé morphologiquement par des cellules cuboïdes et une lumière élargie. Au niveau moléculaire, ce changement phénotypique s'accompagne d'une perte de l'expression des gènes acineux et des enzymes digestives au profit de l'expression des gènes canalaires et de la réexpression de gènes des progéniteurs pancréatiques (notés par un *).

Donc les cellules les plus abondantes du pancréas, les acini, que l'on croyait différenciées de façon irréversible, ont une plasticité la plus élevée parmi les cellules qui constituent le compartiment exocrine[169,166] afin de préserver l'intégrité du pancréas exocrine. Les cellules acineuses par leur fonction de cellules progénitrices facultatives préservent l'homéostasie exocrine du pancréas.

C. Voies qui régissent la métaplasie acino-canalaire

Toutes les lignées épithéliales du pancréas adulte proviennent de précurseurs communs initiés au cours du développement (Cf Partie 2 – I. C). Au cours de la MAC, les cellules acineuses réactivent des programmes induits pendant le développement pour se dédifférencier en cellules de type progénitrices facultatives, pouvant ensuite se spécifier en cellules canalaires permettant la régénération du tissu. Ce mécanisme nécessite une combinaison de régulation sur trois niveaux : la réexpression de gènes clés ou masters gènes, la régulation de voies de signalisation et des modifications épigénétiques.[169]

1) Les masters gènes

a. Les facteurs de transcription acineux

Plusieurs facteurs de transcription tels que PTF1a, MIST1 et NR5A2 contribuent à préserver l'identité et l'état différencié des cellules acineuses. En revanche, leur délétion génétique dans des modèles murins conduit à la dédifférenciation et à la MAC.

Par exemple, le complexe PTF1 joue un rôle central non seulement dans le maintien de la différenciation des cellules acineuses, mais aussi dans leur fonction en régulant la production d'enzymes digestives.[170] Dans le pancréas adulte, le complexe PTF1 est un facteur de transcription trimérique formé par PTF1a, RBPJ-L et une protéine E. Sous cette conformation, le recrutement de p300/CREB (une histone acétyltransférase) est alors possible, acétylant PTF1a pour améliorer son activité transcriptionnelle.[10,171] Dans le pancréas adulte, PTF1a, contrôle son expression et celle des autres composants constituant le complexe PTF1 par une boucle d'autorégulation positive.[130]

Le niveau de PTF1a dans la cellule acineuse est finement contrôlé. En effet, après une pancréatite aiguë induite par injection de caeruléine, la perte de PTF1a est observée 6h post-injections.[172] Sa réexpression est ensuite nécessaire afin de régénérer le compartiment acinaire. Ces données sont également corroborées par le fait que l'invalidation de PTF1a à l'âge adulte est suffisante pour induire la MAC.[13] De plus, l'homéostasie du niveau de PTF1a est modulée par une régulation épigénétique favorisant sa mise en silence pendant la MAC chez la souris.[173] (Cf Partie 2 ; II-C.2.c)

NR5A2 en coopérant avec le complexe PTF1, maintient également l'identité des cellules acineuses adultes. En effet, il interagit avec des motifs de liaison en amont de certains gènes spécifiques de la différenciation acineuse, tels que celui de la carboxypeptidase A2 (*Cpa2*) et de l'élastase 1 (Elas).[132] NR5A2 contrôle également l'expression de NrOb2, répresseur transcriptionnel du promoteur de c-jun exprimé dans les acini. De manière similaire à PTF1a, la délétion du gène du récepteur nucléaire NR5A2, accélère la transdifférenciation des acini en canal après inclusion en matrigel™ et exacerbe la formation de MAC après induction de pancréatite.[174,175] L'analyse transcriptomique de cellules acineuses hétérozygotes pour NR5A2 révèle un réarrangement de la transcription des gènes suite à la diminution d'expression de NR5A2 qui non seulement conduit à une diminution de l'expression des gènes spécifiques de la différenciation acinaire mais favorise aussi la mise en place d'un programme pro-inflammatoire.[175] En fait, le repositionnement à l'échelle du génome de NR5A2 et du co-activateur AP-1 formé de c-jun et de Fos stimule l'expression de gènes inflammatoires.[175] La capacité régénératrice du pancréas, perdue suite à la perte de NR5A2, est restaurée après la déplétion uniquement du gène Jun, montrant un lien entre ces voies.[175]

Enfin, MIST1 est également un acteur dans le maintien de l'identité et de l'organisation des cellules acineuses adultes.[176] MIST1 est un facteur bHLH qui fonctionne sous forme homodimérique. Dans les cellules acineuses, MIST1 régule la polarité apico-basale, la formation des jonctions communicantes et le bon positionnement des granules de zymogène et l'exocytose.[177] Lorsque l'homodimérisation de MIST1 est bloquée dans les cellules acineuses, une prédisposition pour une conversion en un phénotype canalaire[134] associée à une expression accrue de SOX9[178] et à l'activation des voies de signalisation EGFR et Notch.[179] Enfin, la perte de MIST1 entraine la diminution de l'expression du gène p21 augmentant ainsi le potentiel prolifératif des cellules.[180,181] De ce fait, la perte de fonction de MIST1 conduit à l'épuisement des jonctions communicantes, à la perte de polarité, à la dédifférenciation des acini ainsi qu'à la MAC.[134,178]

b. Les facteurs de transcription canalaires

Fait intéressant, l'activation ectopique de facteurs de transcription canalaires peut être également à l'origine du processus métaplasique. En effet, en conditions inflammatoires, la réexpression des facteurs SOX9 et HNF6 est induite spécifiquement dans les cellules acineuses subissant la métaplasie.[182] La surexpression de SOX9 dans les cellules progénitrices pancréatiques entraîne une aggravation de la MAC chez les souris adultes.[183]

Le facteur de transcription nucléaire hépatocytaire 1b (HNF1b), possède aussi une fonction cruciale dans la différenciation des cellules canalaires épithéliales participant au processus métaplasique.[184] La perte de HNF1b dans les cellules canalaires entraîne une pancréatite chronique et une néoplasie tissulaire.[184] Ainsi, à l'âge adulte, sa fonction est nécessaire dans le maintien du phénotype canalaire pour l'homéostasie du compartiment exocrine en cohérence avec son rôle pendant le développement du pancréas.

Enfin, le facteur de transcription embryonnaire PDX1 est également ré-exprimé pendant la MAC.[166,185] Une augmentation du niveau de PDX1 est nécessaire au cours de la métaplasie durant la phase de régénération cellulaire pour rétablir l'état différencié en cellules acineuses.[166,185] D'ailleurs, l'expression prolongée de PDX1 dans les cellules acineuses dès les stades embryonnaires provoque une MAC qui nécessite l'activation de la voie STAT3 (Signal transducer and activator of transcription 3), voie impliquée dans la réponse inflammatoire. [118]

Ces données soutiennent le paradigme selon lequel l'identité des cellules pancréatiques est orchestrée par plusieurs réseaux transcriptionnels dominants finement contrôlés. Divers acteurs sont ainsi impliqués pour moduler la plasticité des cellules acineuses.

2) Les voies de signalisation qui régissent la métaplasie acino-canalaire

Des voies de signalisation sont modulées au cours de la MAC telles que les voies MAPK, PI3K et des voies de l'embryogenèse pancréatique sont réactivées dans ce contexte.

a. La voie MAPK

La cascade de signalisation, appelée protéine kinase activée par les mitogènes (MAPK) (appelée également voie ERK), est une voie effectrice importante qui intervient notamment dans la régulation de la prolifération cellulaire.[186]

La voie MAPK est soumise à des phosphorylations séquentielles de protéines qui sont initiées par la protéine RAS. Il a été démontré que cette voie est requise pour la dédifférenciation des cellules acineuses.[187] En effet, elle est activable par le récepteur aux facteur de croissance épidermique (EGFR) liant les facteurs de croissance TGFα et EGF reconnus comme molécules initiatrices de la MAC.[188] L'activation de la voie MAPK induit une métaplasie à la fois *ex vivo* (acini humains[154] et murins[150]) et *in vivo* dans de multiples modèles transgéniques murins.[189,190] Durant la transdifférenciation, la voie MAPK activée, entraine la régulation de l'expression génique de SOX9 par le complexe c-Jun/ NFATc1/4 (Nuclear factor of activated T-cells). Il a été prouvé que le traitement avec des inhibiteurs de kinase de l'EGFR tel que l'Erlotinib, bloque la métaplasie acino-canalaire dans les cellules acineuses exprimant l'oncogène $Kras^{G12D}$ ex vivo.[191] Enfin, des études montrent que le ciblage pharmacologique des kinases de la voie telle que MEK ou la perte de son expression, inhibent également la transdifférenciation des acini.[192,193] En effet, l'inhibition par voie systémique de la MEK par le Trametinib, entraîne la perte de la capacité de prolifération du pancréas et perturbe la restauration du compartiment exocrine.

Ces données mettent clairement en évidence le rôle de la voie de signalisation MAPK dans l'induction et le maintien de la métaplasie des cellules acineuses en canaux.

b. La voie PI3K/AKT

La voie PI3K/AKT est un nœud de signalisation majeur qui participe à la régulation des fonctions cellulaires.[194] La plasticité des cellules acineuses au cours de la métaplasie est régie par la protéine p110, sous unité catalytique de la kinase PI3K. En effet, la signalisation p110α est nécessaire pour la reprogrammation des cellules acineuses en régulant la morphologie cellulaire in vivo et in vitro via la petite GTPase Rho et le contrôle du cytosquelette d'actine.[195] La perte de cette sous-unité par inhibition pharmacologique ou par invalidation génétique bloque la MAC.[195] Inversement, l'expression transgénique d'une forme constitutivement active de p110α favorise le développement de la MAC.[196] La transdifférenciation des cellules acineuses induite par la voie PI3K régule également la voie de

signalisation ERK1/2. Par ailleurs, la seule perte de PTEN, régulateur négatif de la signalisation PI3K, dans le pancréas augmente la métaplasie et le nombre de structures canalaires.[197] Enfin, l'expression d'un allèle constitutivement actif de Akt1 conduit également à la MAC.[198]

Ainsi, la voie PI3K est essentielle dans le processus de MAC. L'homéostasie de cette signalisation est cruciale car elle peut contribuer à une métaplasie irréversible. Cependant, les patients atteints d'un CP porteur d'une mutation du gène PIK3 représentent un faible pourcentage (2 à 3 %). Cela suggère que l'augmentation de l'activité PI3K pourrait être principalement obtenue par la voie de signalisation MAPK pouvant être régulée de manière constitutivement active par l'oncogène $Kras^{G12D}$.

c. Les voies de signalisation de l'embryogénèse

Des études ont prouvé que la réactivation des voies de signalisation embryonnaire telles que Notch et Wnt, sont réactivées au cours de la MAC. Au cours du développement des organes, notamment du pancréas, le récepteur Notch est activé suite à l'interaction du récepteur avec son ligand (Jagged-1), entraînant l'activation d'une protéase (γ-sécrétase) qui clive la partie intracellulaire du récepteur appelé NICD. Celui-ci ainsi libéré est transféré vers le noyau, modulant l'expression de gènes cibles tels que HES1, PTF1a et MIST1.[199]

Les travaux de Esni *et al.* ont montré que l'activation ectopique de Notch dans les acini en culture inhibe la différenciation acinaire en bloquant l'activité du complexe PTF1.[200] Par ailleurs, l'altération de la voie Notch (soit par invalidation conditionnelle du récepteur Notch, soit par l'inhibition de la γ-sécrétase) est associée à une régénération du pancréas exocrine déficiente après induction d'une pancréatite aiguë par traitement à la caéruléine.[201] Enfin, la voie Notch est également modulée par un régulateur négatif, NUMB. La perte de ce dernier entraine une dédifférenciation des cellules acineuses et un défaut de régénération en réponse à une pancréatite aigüe.[202]

De manière similaire à la voie Notch, la voie Wnt/β-Cat contribue au développement du compartiment acinaire[203] et est réactivée durant la MAC. La protéine β-caténine est requise pour régénérer ce compartiment et favorise la dédifférenciation des cellules acineuses.[204] La déficience en β-caténine bloque la MAC des acini de souris isolés ex vivo.[205]

Dans les cellules acineuses normales, la transdifférenciation en cellules canalaires est donc contrôlée par des mécanismes réversibles impliquant l'activation synergique des voies de signalisation MAPK, PI3K/Akt, Wnt et Notch **(Figure 20)** régulant à leur tour l'expression de gènes cibles.

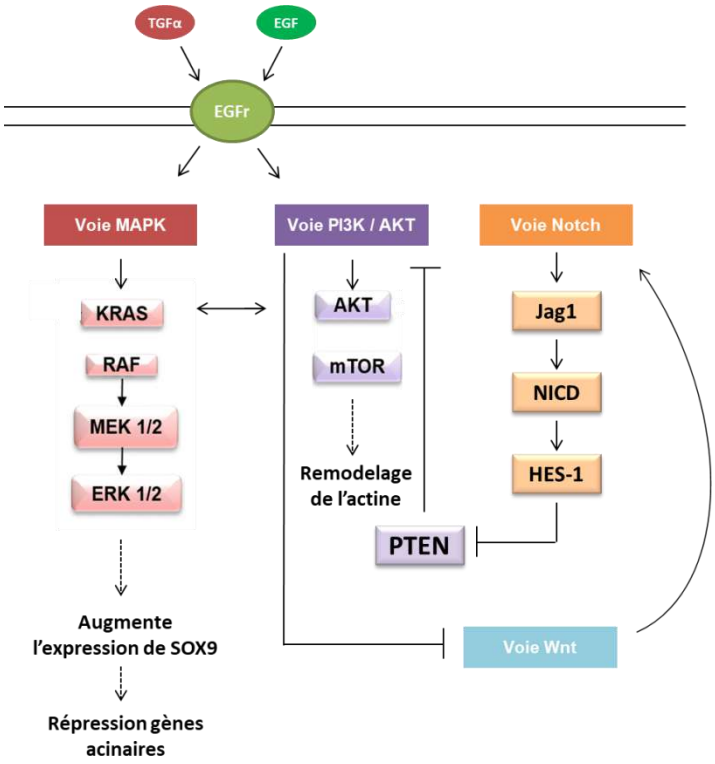

Figure 20 : Les signalisations MAPK, Wnt, Notch et PI3K/Akt sont impliquées dans la MAC.

3) Remodelage de la chromatine

Comme décrit précédemment, la MAC est un mécanisme qui nécessite l'arrêt de l'expression des gènes impliqués dans la différenciation des cellules acineuses et l'activation de l'expression des gènes des canaux et des progéniteurs.[165] Depuis quelques années, plusieurs études ont prouvé que les modifications épigénétiques telles que l'acétylation et la méthylation des histones, ainsi que le recrutement du complexe de remodelage SWI/SNF participent à la régulation de l'expression génique observée durant ce processus **(Figure 21)**.[206]

a. <u>Le complexe SWI/SNF</u>

L'invalidation du gène codant pour la protéine BRG1, sous unité catalytique du complexe de remodelage SWI/SNF **(§ Partie 1 ; III- B.1)**, dans des cellules acineuses à l'âge adulte atténue la MAC.[207] Ainsi, BRG1 est essentiel à l'induction de la transdifférenciation en activant l'expression de SOX9. En effet, l'immunoprécipitation de la chromatine (ChIP) d'acini isolés a révélé que BRG1 se lie aux régions promotrices de SOX9, permettant le recrutement de PDX1 au niveau de cette région pour induire l'expression de SOX9 dans les acini au cours de la MAC. Dans les modèles murins invalidés du gène Brg1, la MAC est réduite par l'absence de fonctionnalité du complexe SWI/SNF sur l'expression des gènes canalaires. Cependant, l'effet de la perte de BRG1 est spécifique du type cellulaire. En effet, si son expression est nécessaire pour la formation de lésions à partir de cellules acineuses adultes, la

perte de BRG1 est requise pour la formation de lésions à partir de cellules canalaires pancréatiques adultes.[208]

De plus, des modifications épigénétiques spécifiques régulant l'expression de gènes pro-inflammatoires tel que l'IL6 ont été identifiées en réponse à la déplétion du gène Brg1 dans un contexte de pancréatite aiguë chez le rat. Après injection d'un acide biliaire conduisant à une pancréatite aiguë, une augmentation rapide et transitoire de l'acétylation des histones H3K14, H3K27 et H4K5 est visible une heure post injection, régulée par le recrutement de BRG-1 activant l'expression de gènes cibles.[209] Puis, l'augmentation de la méthylation des histones est observée 6h après la fin des injections en particulier celle de l'histone 3 sur le résidu K4 permettant un remodelage de la chromatine réprimant l'expression de gènes pro-inflammatoires tels que l'IL6. Ainsi BRG1, régulateur du complexe SWI/SNF, engendre des modifications épigénétiques essentielles pour activer différemment l'expression de gènes inflammatoires nécessaires au cours de la métaplasie.

Parmi les composants protéiques variables du complexe SWI/SNF, les protéines ARID (ARID1A, ARID1B, ARID2) participent aussi, en tant que sous unités du complexe de remodelage.[210] ARID1A participe à la structure de la chromatine et à son accessibilité en contrôlant la position du nucléosome et la modification des histones.[211] ARID1A est nécessaire au maintien de l'identité et à l'activité des cellules acineuses en réponse à une lésion.[212] En effet, l'arrêt de la production d'ARID1A dans ces cellules bloque la production des enzymes digestives et entraine un changement phénotypique. La réduction d'ARID1A diminue également l'accessibilité de la chromatine au niveau des promoteurs spécifiques des gènes acineux (PTF1a, NR5A2),[213] limitant l'expression des facteurs de transcription acineux et redirigeant le destin des cellules acineuses en cellules canalaires par l'enrichissement des motifs de PDX1. Une étude récemment publiée confirme le rôle d'ARID1A dans la MAC en tant que régulateur de la plasticité acinaire afin de résister aux lésions du pancréas induites par la caéruléine.[214] La perte d'ARID1A est également associée à une augmentation de l'expression de l'interleukine-6 (IL6) transmise par régulation épigénétique dans les cellules acineuses murines qui présentent un enrichissement de l'acétylation de H3K27 dans les régions promotrices distales du promoteur de l'IL6.[214]

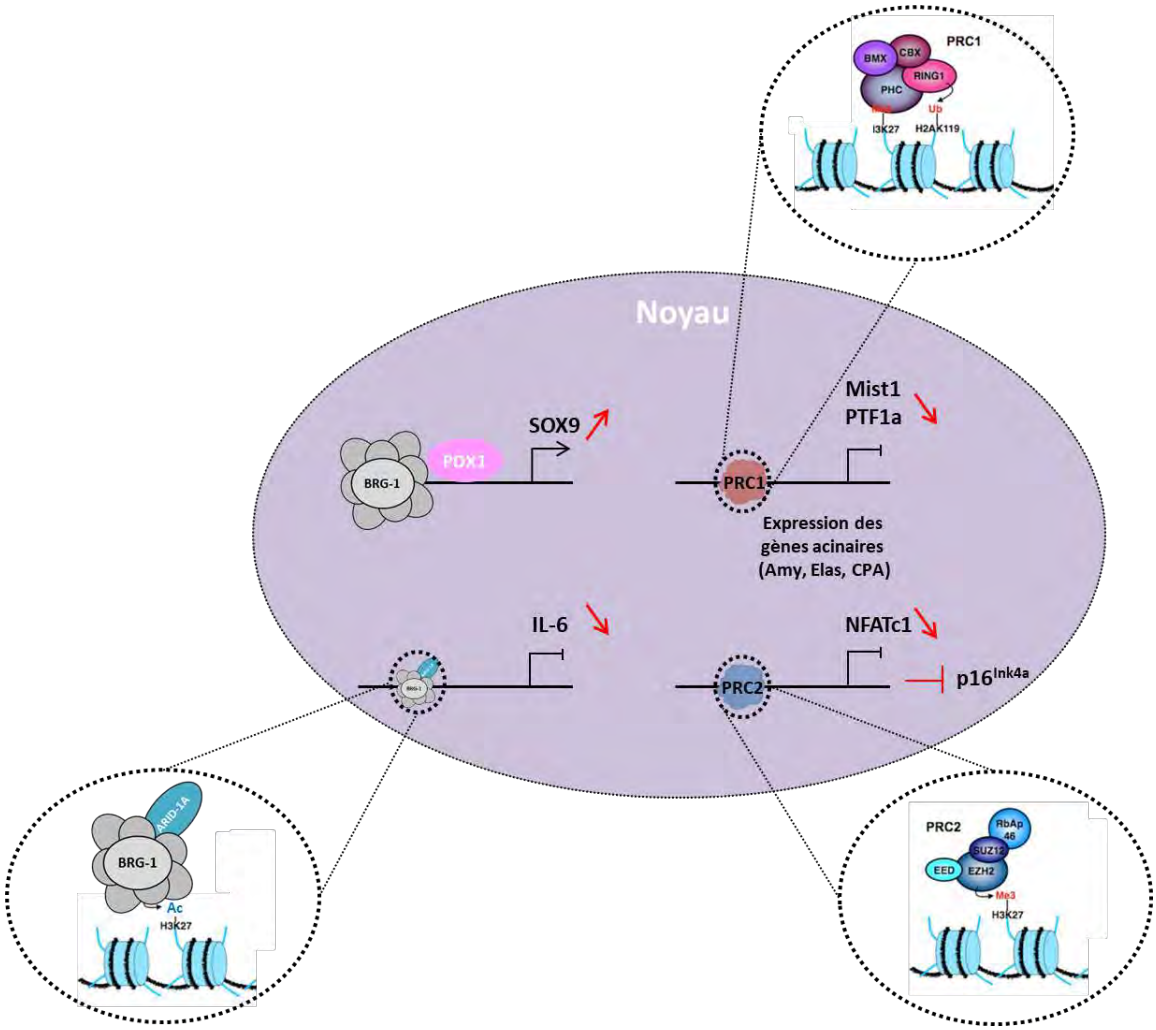

Figure 21 : Exemples de régulations épigénétiques de la MAC.

b. Le complexe Polycomb

Le complexe Polycomb **(§ Partie 1 ; III- B.2)**, composé des deux sous unités PRC1 et PRC2,[215] est un autre système capable de réguler l'expression des gènes durant la MAC. Au cours de ce mécanisme, les marques répressives des histones H3K27me3 et H2AK119ub sont augmentées au niveau des promoteurs des gènes codant pour les facteurs exprimés dans les cellules acineuses (PTF1a et RBPJ-L).[216,217] Benitz *et al*., se sont particulièrement intéressés au rôle du complexe PRC1, spécifiquement par l'étude de RING1B, dans la régulation épigénétique des facteurs de transcription des cellules acineuses. Au cours de la MAC, les marques répressives telles que H2AK119ub sont enrichies au niveau des promoteurs de PTF1a et RBPJ-L entrainant la perte d'expression des gènes impliqués dans la différenciation acinaire.[217] A l'inverse, dans les souris invalidées du gène RING1B, ces modifications épigénétiques répressives sont nettement réduites favorisant l'expression des gènes impliqués dans la différenciation acinaire réduisant ainsi la MAC.

De plus, le complexe PRC2 est aussi nécessaire à la régénération du compartiment exocrine via la surexpression d'EZH2.[218] La perte de fonction d'EZH2 altère les capacités régénératrices des cellules

qui subissent une MAC en modifiant leurs capacités de prolifération. Des analyses par immunoprécipitation de chromatine montrent que EZH2 réprime le gène $p16^{Ink4a}$ (inhibiteur de CDK). La perte de fonction d'EZH2, favorise l'expression soutenue de $p16^{Ink4a}$ dans les cellules métaplasiques bloquant leur prolifération et leur redifférenciation en acini. Ce défaut de régénération, induit par la perte d'EZH2, est entièrement restauré par la délétion de $p16^{Ink4a}$ dans le pancréas.[218] Une étude a également prouvé que EZH2 régule de manière épigénétique l'expression de NFATc1, régulant lui-même en retour l'expression de $p16^{Ink4a}$ pendant la régénération pancréatique.[219] La perturbation de ce mécanisme par perte génétique d'EZH2 ou par l'expression ectopique de NFATc1 empêche la bonne régénération du pancréas.

Les exemples cités (RING1B et EZH2) illustrent l'importance du complexe Polycomb au cours de la métaplasie, cependant d'autres régulateurs épigénétiques possèdent également des fonctions dans ce processus tels que KDM6A, Setd2 et Setdb.[220–222] Ces données soutiennent l'idée que la reprogrammation épigénétique à grande échelle est nécessaire en désactivant sélectivement et collectivement les gènes acinaires permettant la transition vers des cellules canalaires.

4) Conclusion sur les voies impliquées dans le mécanisme de MAC

Au cours de la MAC, les modifications épigénétiques participent au contrôle fin de l'expression des gènes, eux même sous la dépendance de voies de signalisation intracellulaire. Ces processus agissent en synergie, le moindre dysfonctionnement peut conduire à une MAC anormale.

Il est important de préciser que toutes les cellules acineuses ne sont pas équivalentes mais qu'il existe une hétérogénéité au sein de cette population prouvée par RNA-Seq de cellules individuelles.[223–225] Les populations d'acini qui prolifèrent sont différentes selon le stress induit. En réponse à la caeruléine, une sous-population positive pour BMI1 double en 5 jours, tandis que les cellules acineuses positives pour la stathmine 1 augmentent jusqu'à 30% la population acineuse.[223,226] Après une pancréatectomie, les cellules acineuses positives pour Dclk1, représentant 0,1 à 0,5% de la population acinaire au repos, peuvent repeupler l'ensemble des lobes pancréatiques nouvellement formés.[227] Ces résultats montrent que le degré de contribution des cellules acineuses pour repeupler l'épithélium pancréatique après une lésion est variable et que ces cellules se comportent comme des populations de progéniteurs facultatifs distinctes.[223,226,227]

Ainsi, longtemps représenté comme un lot de cellules très peu variable, l'hétérogénéité intercellulaire des acini est à prendre en compte au cours de la métaplasie en plus des voies qui régissent ce mécanisme.

D. Rôle de la MAC dans l'initiation du CP

Le suivi de la transformation cellulaire chez l'humain étant impossible, seules les observations histologiques faites sur les tissus réséqués de patients atteints de cancer sont disponibles. Les études montraient historiquement une morphologie et l'expression de marqueurs de cellules canalaires en faveur d'une origine du cancer à partir du compartiment canalaire. En moins de deux décennies, les modèles murins génétiquement modifiés ont accéléré les découvertes et bousculé les certitudes sur les étapes initiatrices du CP.

L'expression d'une forme mutée du gène Kras ($Kras^{G12D}$) dans les cellules progénitrices embryonnaires pancréatiques mime la pathologie humaine en induisant la MAC et des lésions prénéoplasiques pancréatiques de type PanIN (Pancreatic Intraepithelial Neoplasia).[228–230]

De nombreuses études, répertoriées dans le **Tableau 3**, ont prouvé que l'expression du mutant $Kras^{G12D}$ spécifiquement dans les cellules acinaires, sous le contrôle de différents promoteurs tels que ceux de l'élastase ou de MIST1, est suffisante pour induire successivement la MAC et l'apparition de PanIN chez la souris.[231]

GEM model	Tumor initiation	Targeted cell type	Lesions (incidence %)			Observations	References
			PanIN	PDAC	MET		
Elastase-TGF-α	Prenatal	Acinar	100	10	No	KrasG12D accelerates progression of mPanIN lesions to PDAC	Wagner et al., 2001
Pdx1-Cre; K-Ras+/LSLG12D	Prenatal	Acinar, CAC, ductal, endocrine	100	100	Yes	Impossibility to asses cell of origin	Hingorani et al., 2003
Ptf1a-Cre; K-Ras+/LSLG12D	Prenatal	Acinar, CAC, ductal, endocrine	100	100	Yes	Impossibility to asses cell of origin	Hingorani et al., 2003
Elastase-tTA; Tet-O-Cre; K-Ras+/LSLG12Vgeo	Prenatal	Acinar	90	10	No	Pancreatitis accelerates PanIN development.	Guerra et al., 2007
Nestin-Cre; K-Ras+/LSLG12D	Prenatal	Acinar, acinar precursors	100	No	No	Short survival due to CNS complications. PDAC in the context of pancreatitis.	Carriere et al., 2007
Elastase-tTA; Tet-O-Cre; K-Ras+/LSLG12Vgeo plus caerulein	Postnatal (8 weeks)	Acinar	100	20	No	PanIN development requires pancreatitis.	Guerra et al., 2007
Elastase-CreER; K-Ras+/LSLG12D	Postnatal (6 weeks)	Acinar	36	NA	No	Leaky system. Short term study.	De La O et al., 2008
Elastase-CreERT2; K-Ras+/LSLG12D	Postnatal (6 weeks)	Acinar	63	No	No	PanIN development does not require pancreatitis.	Habbe et al., 2008
Mist1-CreERT2; K-Ras+/LSLG12D	Postnatal (6 weeks)	Acinar	30	No	No	PanIN development does not require pancreatitis.	Habbe et al., 2008
Pdx1-CreER; K-Ras+/LSLG12D	Postnatal (8 weeks)	Endocrine	55	Rare	No	The system may target acinar and precursor cells.	Gidekel-Friedlander et al., 2009
proCPA1CreERT2; K-Ras+/LSLG12D	Postnatal (3 weeks)	Acinar	10	No	No	PanIN development require pancreatitis in older mice (5–8 weeks): PanIN in 33% mice.	Gidekel-Friedlander et al., 2009
RipCreER; K-Ras+/LSLG12D	Postnatal (2–8 weeks)	Insulin expressing cells	0	No	No	Cooperation with pancreatitis	Gidekel-Friedlander et al., 2009

MET (metastasis); NA: not analyzed.

Tableau 3 : Tableau synthétique des modèles murins génétiquement modifiés exprimant une forme constitutivement active de la protéine Kras.
Adapté de la revue Guerra et al, 2013.[231]

Actuellement, il est admis et démontré dans les modèles murins que le CP peut être initié dans plusieurs types cellulaires. Cependant, les travaux de Kopp *et al.* démontrent que les cellules acineuses sont environ 100 fois plus sensibles à la transformation par l'oncogène $Kras^{G12D}$ que ne le sont les cellules canalaires.[127] Le lignage cellulaire prouve qu'en conditions de stress lié à l'oncogène $Kras^{G12D}$, ces cellules hautement plastiques vont changer d'apparence et former, via la MAC, des canaux évoluant en PanIN de grade de plus en plus élevé jusqu'au stade de tumeur **(Figure 22)**.[232]

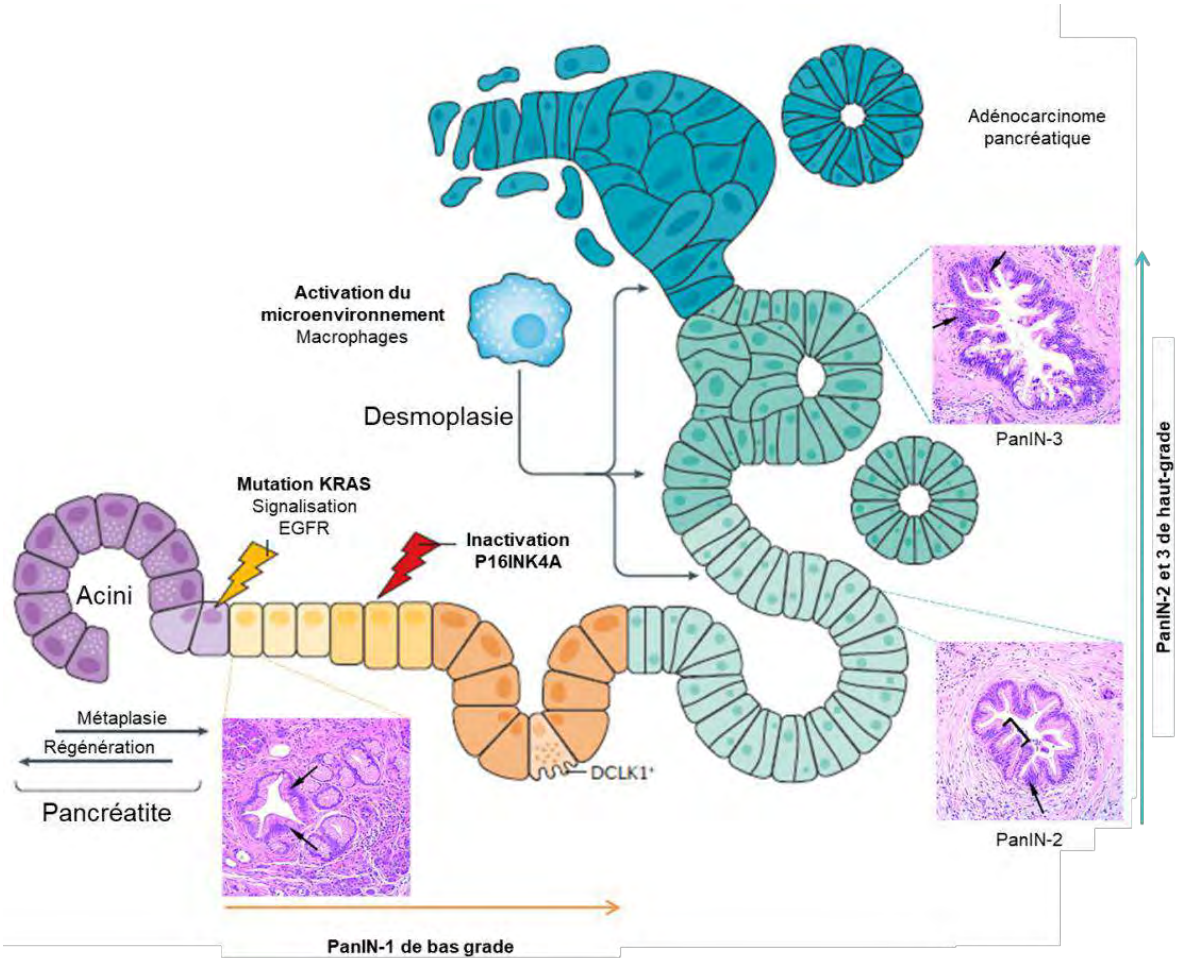

Figure 22 : Modèle linéaire de la progression des acini en PanIN aboutissant au cancer pancréatique.
Au cours de la pancréatite, la MAC est un processus réversible qui devient irréversible en présence de la mutation oncogénique de $Kras^{G12D}$, conduisant à l'apparition de lésions précancéreuses appelées PanIN. Ces PanIN sont répertoriées en trois grades PanIN-1 à 3 comme illustré. L'activation oncogénique de $Kras^{G12D}$ entraine une activation de la voie EGFR, aboutissant à la formation de lésions de type PanIN-1. Ces lésions de bas grade constituent un épithélium monostratifié formé de cellules cylindriques avec un cytoplasme riche en mucus et un noyau rond localisé au pôle basal. L'inactivation de l'inhibiteur de CDKN2A (appelé P16INK4) induit une perte de la sénescence cellulaire permettant la progression vers des lésions de haut grade. L'acquisition de mutations génétiques supplémentaires est nécessaire pour induire l'apparition de PanIN-2 et 3 et le développement d'un adénocarcinome pancréatique. Les PanIN-2 se caractérisent par l'apparition d'un épithélium pseudo-stratifié en cours de formation et des noyaux de forme irrégulière qui ne sont plus localisés au pôle basal. Enfin, les PanIN-3, sont caractérisées par des cellules de forme irrégulière formant un épithélium pseudo-stratifié cribriforme avec des bourgeonnements cellulaires vers la lumière. Adapté de la revue Storz, 2017[232] et Iacobuzio- Donahue, 2012[233].

Ainsi, en présence de l'oncogène $Kras^{G12D}$, le mécanisme physiologique réversible de la métaplasie, essentiel pour la réparation du tissu pancréatique, peut-être l'événement initiateur de la tumorigénèse pancréatique.[192,234] La MAC est dans ce cas irréversible. Tout facteur ou situation déstabilisant le phénotype acinaire, augmentant la plasticité des acini et favorisant la MAC, est potentiellement considéré comme promoteur de la formation de PanIN en association avec la mutation $Kras^{G12D}$.[232] L'inactivation du gène PTF1a rend ainsi les cellules acineuses intrinsèquement plus sensibles à la transformation en cellules canalaires.[13] A l'inverse, la réintroduction de facteurs préservant le phénotype acinaire (MIST1, PTF1a) peut outrepasser l'effet de la mutation $Kras^{G12D}$ en inhibant la MAC et la formation de PanIN.[192] De plus la réintroduction de PTF1a au stade de PanIN ramène les

cellules vers un état différencié de cellules acineuses, bloquant ainsi l'initiation de la tumorigénèse.[235] Au contraire, tout facteur favorisant l'expression de gènes canalaires entraine la MAC. Dès les stades prénéoplasiques, l'expression de SOX9 est élevée et corrélée avec une activation accrue de la voie EGFR. De même, l'absence de ce régulateur réduit la signalisation de l'EGFR et la mise en place des lésions pancréatiques chez la souris.[236]

La mutation $Kras^{G12D}$ à elle seule est insuffisante pour conduire au développement du CP.[237] L'induction d'une pancréatite dans les modèles murins exprimant une forme mutée de $Kras^{G12D}$ dès l'embryogenèse ou dans les acini à l'âge adulte amplifie la formation des lésions précancéreuses et accélère la carcinogenèse.[183,238] La pancréatite est d'ailleurs un facteur de risque reconnu pour le développement du CP chez l'homme.[239,240] En revanche, cette synergie n'existe pas si la mutation du gène Kras se fait dans le compartiment canalaire. Il est important de préciser que la MAC induite en réponse à une pancréatite aigüe ou chronique n'est pas suffisante à elle seule pour initier des lésions précancéreuses de types PanIN.[241] En absence de pancréatite, la perte de fonction d'un suppresseur de tumeurs est souvent nécessaire pour que les lésions prénéoplasiques progressent jusqu'au stade tumoral. Néanmoins, à ce jour il n'existe pas encore de preuve formelle d'une évolution séquentielle linéaire des PanIN jusqu'au stade tumoral.[242]

III. Caractéristiques de l'adénocarcinome du pancréas humain

A. Notions générales

1) Epidémiologie

Au niveau mondial, en 2020 le nombre de cancer du pancréas est estimé à environ 495 000 cas, tout âge et sexe confondus, avec un nombre de décès d'environ 466 000 par an.[243] Le CP est classé au 12ème rang des cancers les plus fréquents et au 7ème rang des causes de mortalité par cancer dans le monde. En revanche, au sein de l'Union Européenne, il est estimé que le CP deviendra bientôt la troisième cause de décès par cancer et dépassera à ce titre le cancer du sein.[244] Malgré l'amélioration de la survie globale à 5 ans, qui est passée de 5 % dans les années 1990 à 9% en 2021 aux États-Unis et en Europe, le taux de survie pour le CP reste faible. [245,246] La plupart des patients sont diagnostiqués tardivement à un âge médian de 71 ans et seulement 20 % des diagnostics surviennent avant 60 ans.[247,248] Enfin, à l'échelle mondiale, le taux d'incidence du CP a tendance à être un peu plus élevé chez les hommes que chez les femmes, en particulier chez les personnes de moins de 75 ans.[249]

Le faible taux de survie est dû au stade avancé de la maladie au moment du diagnostic rendant impossible l'exérèse de la tumeur. Mais, parmi les patients diagnostiqués précocement et pouvant bénéficier d'une résection chirurgicale, le taux de survie à 5 ans reste malgré tout faible (15 à 25 %).[250]

Dans 90 % des cas, le CP est un adénocarcinome canalaire pancréatique.[251] L'apparition de ce cancer est influencée par divers facteurs de risques.

2) Facteurs de risques

Les facteurs de risque connus comprennent des facteurs « modifiables » comme le tabac, l'alcool, l'obésité ou encore la pancréatite non héréditaire et des facteurs « non modifiables » comme le terrain héréditaire **(Tableau 4)**.[252]

Facteurs de risques		**Risque associé**	**Réf.**
Modifiables	Cigarette	~ 1,7 fois plus de risque par rapport aux personnes n'ayant jamais fumé	[253]
	Obésité	~ 1,6 fois plus de risque chez les personnes obèses par rapport à celles de poids normal	[254]
	Alcool	Risque 1,6 fois plus élevé chez les personnes qui consomment > 6 verres par jour par rapport à celles qui consomment moins d'un verre par jour	[255]
	Pancréatite	Risque accru de 2 à 3 fois chez les personnes atteintes de pancréatite chronique de longue date	[240]
Non modifiables	Hérédité familiale	Risque variable en fonction du nombre de parents au premier degré atteints. Risque augmentant jusqu'à 32 fois plus si trois parents au premier degré ou plus ont déjà été diagnostiqués.	[256,257]

Tableau 4 : Facteurs de risques connus du CP
Tableau adapté de la revue "Pancreatic cancer epidemiology: understanding the role of lifestyle and inherited risk factors" de Alison P. Klein.[252]

Une seule étude à ce jour a montré par une enquête prospective européenne le lien entre le mode de vie et l'incidence du CP.[258] Le score définissant le mode de vie comprend 5 critères dont le tabagisme, l'alcool, l'activité physique, l'adiposité et l'alimentation. L'adhésion à un mode de vie sain est inversement associée au risque de développer un CP. En effet, les estimations suggèrent que les fumeurs sont environ deux fois plus susceptibles de développer un CP par rapport aux non-fumeurs. Cependant, il n'a pas été identifié de signature génétique unique pour le CP liée au tabagisme contrairement à d'autres tumeurs malignes.[253] De plus, les données de la cohorte du National Institutes of Health montrent que les patients en surpoids ou obèses (indice de masse corporelle [IMC] ≥30 kg/m²) ont une probabilité accrue de développer ce cancer par rapport aux patients ayant un IMC normal.[254] La pancréatite chronique liée à une alimentation trop riche ou un excès d'alcool, (Cf Partie 2 : II-B) est également à l'origine d'un dysfonctionnement du pancréas et favorise l'apparition du CP.[240]

Enfin, des facteurs non modifiables sont aussi répertoriés, tel que le diabète de type 2, dont l'apparition après 50 ans pourrait être un signe avant-coureur du CP.[259] Par ailleurs, les formes de CP héréditaires représentent 5 à 10 % des nouveaux cas.[256] Les patients présentant des facteurs de risque familiaux ont un risque 9 fois plus élevé de développer un CP que ceux sans antécédent. Ce risque est 32 fois plus élevé si trois parents au premier degré ou plus ont déjà été diagnostiqués.[257] Dans les formes héréditaires, des syndromes spécifiques et des mutations germinales (BRCA, CDKN2A…) sont

également associés à un risque accru de développer un CP par rapport à la population générale.[260,261] Ceux-ci sont résumés dans le **Tableau 5**.

Syndrome	**Gênes**	**Risque relatif par rapport à la population générale**	
		Chen et al [260]	Del Chiaro et al [261]
Cancer héréditaire du sein et de l'ovaire	BRCA1	1.6-4.7	
	BRCA2	2.2-5.9	
Syndrome de Peutz-Jeghers	STK11	76.2-139.0	132.0
Pancréatite héréditaire	PRSS1	53-87	50-70
Mélanome familial atypique multiple	CDKN2A	14.8-80.0	34-39
Cancer colorectal héréditaire sans polypose	MMR	0.0-10.7	4.7

Tableau 5 : Risque relatif de développer un CP associé à des syndromes spécifiques

B. Le diagnostic

Dans la majorité des cas, les patients présentent peu de symptômes caractéristiques de la pathologie. En effet, les patients ont des douleurs épigastriques ou dorsales, des nausées, des ballonnements, une sensation de plénitude abdominale ou une modification de la consistance des selles qui peuvent être interprétés comme des pathologies bénignes, retardant le diagnostic à des stades avancés de la maladie.[262,263] Ceci explique la minorité de patients ayant recours à une chirurgie.

L'apparition des symptômes dépend également de la localisation de la tumeur dans le pancréas. Environ 60 à 70 % des tumeurs pancréatiques sont localisées dans la tête du pancréas et sont plus susceptibles de causer une obstruction biliaire, conduisant à un ictère indolore (jaunisse). A l'inverse, les tumeurs de la queue du pancréas peuvent souvent se développer sans entrave en raison de peu de contact anatomique, retardant souvent le diagnostic.

Il n'existe pas de biomarqueur circulant spécifique du PDAC. La détection d'une tumeur, basée sur le diagnostic par imagerie, permet une première stratification des tumeurs et une meilleure prise en charge du patient. En effet, l'imagerie est une étape nécessaire dans le diagnostic pouvant s'effectuer par échographie abdominale, imagerie par résonance magnétique (IRM), tomodensitométrie thoraco-abdomino-pelvienne (TDM TAP), échoendoscopie, tomographie par émission de positons (TEP).

Cette première étape est utile pour valider la présence de la tumeur, cependant elle n'est pas suffisante pour identifier et caractériser l'agressivité tumorale. Cela nécessite la réalisation d'une biopsie et le diagnostic par un(e) anatomopathologiste **(Tableau 6)**.[264] Les CP sont très variables entres les individus, ils sont classés en plusieurs stades et en fonction de trois critères cliniques définis (Taille de la tumeurs (T), l'invasion ganglionnaire (N) , diffusion de métastases (M))[265].

Stade IA	**T1**	**N0**	**M0**
Stade IB	**T2**	**N0**	**M0**
Stade IIA	**T3**	**N0**	**M0**
Stade IIB	**T1-T3**	**N1**	**M0**
Stade III	**Tout T** **T4**	**N2** **Tout N**	**M0** **M0**
Stage IV	**Tout T**	**Tout N**	**M1**

Tableau 6 : Synthèse des différents stades de CP en fonction de la classification morphologique.
Adapté de la revue générale « Cancer du pancréas », Neuzillet et al, 2021. [264]
T= Taille de la tumeur, mesurée dans sa plus grande dimension avec T1=Tumeur ≤ 2 cm, T2=Tumeur > 2 et ≤ 4 cm, T3= Tumeur > 4 cm, T4= Tumeur envahissant l'axe cœliaque l'artère mésentérique supérieure et/ou l'artère hépatique commune. N= Adénopathies régionales, invasion ganglionnaire avec des sous classes : N0= Pas de métastase ganglionnaire régionale, N1= 1 à 3 ganglions régionaux métastatiques, N=2 ≥ 4 ganglions régionaux métastatiques. M= statut métastatique avec 2 sous types : M0= Pas de métastase à distance, M1 Présence de métastase(s) à distance.

C. Traitements actuels

A ce jour, le traitement ayant une efficacité la plus élevée reste la chirurgie combinée à un traitement de chimiothérapie (Folfirinox ou Gemcitabine).[266] Cependant, il est important de rappeler que seulement 20% des patients peuvent avoir recours à cette chirurgie.

Pour la majorité restante, il existe différents protocoles de traitements en fonction des caractéristiques tumorales qui sont à visée palliative (réduire la douleur) et tendent à prolonger la survie des patients.

Actuellement, quatre protocoles de traitements sont disponibles :

- Pour les patients ayant une tumeur résécable, afin d'éviter une rechute, une chimiothérapie adjuvante (Folfirinox, cocktail de quatre composés : l'acide folinique, 5-fluorouracile, irinotécan, oxaliplatine) est préconisée pendant 6 mois post chirurgie.
- Pour les patients ayant une tumeur résécable dite « limite », une première ligne de chimiothérapie ou de radiothérapie, dite thérapie néo-adjuvante, est mise en place dans le but de diminuer la taille de la tumeur avant une éventuelle intervention chirurgicale. Les principales chimiothérapies dans ce cas sont également des combinaisons telles que la gemcitabine (le traitement standard de référence) en association avec le Folfirinox ou le cisplatine ou le Nab-Placlitaxel.
- Les patients présentant des tumeurs localement avancées, sans métastases ne peuvent pas être opérés chirurgicalement. Cependant, un cycle de chimiothérapie associé à la radiothérapie est envisageable. Dans les cas où le patient est en bon état général, il peut bénéficier d'une monothérapie, le Folfirinox ou des traitements combinant Gemcitabine et Nab-Placlitaxel par

exemple. Pour les patients en mauvais état général, seules les monothérapies sont administrées tels que la Gemcitabine ou le 5-FU.

- Enfin dans le cas où les tumeurs sont à un stade métastatiques, les seuls traitements envisagés dans le but de soulager les douleurs et les symptômes, sont l'administration de la Gemcitabine en première intention ou le Folfirinox améliorant significativement la survie mais sont associés à de nombreux effets secondaires.

Divers essais cliniques sont en cours visant à cibler des mécanismes plus larges souvent dérégulés dans ce cancer tels que le ciblage des mécanismes de détection des dommages à l'ADN (ex : inhibiteur de PARP), le microenvironnement (ex : inhibiteurs des checkpoint immunitaires), ou encore par ciblage du stroma afin d'augmenter la distribution de la thérapie (ex : Losartan). L'idée d'un traitement adapté spécifiquement en fonction des patients est une option thérapeutique envisagée actuellement au vu de l'hétérogénéité des tumeurs pancréatiques.

D. Que sait-on réellement sur le CP ?

Les tumeurs pancréatiques sont histologiquement très différentes. La plupart des adénocarcinomes canalaires pancréatiques proviennent de PanIN évoluant par l'acquisition d'altérations génétiques en un adénocarcinome canalaire pancréatique. Une minorité d'adénocarcinome canalaire pancréatique provient de lésions kystiques tels que les néoplasmes mucineux papillaires intracanalaires (IPMN) ou les cystadénomes mucineux (MCN).[267] Ces différences sont le reflet de l'hétérogénéité de l'origine cellulaire qui va subir une transformation cellulaire conduisant au développement de tumeurs pancréatiques différentes.

Le développement des tumeurs issues des PanIN nécessite des mutations génétiques supplémentaires à la mutation du gène Kras. Les mutations fréquemment retrouvées en plus de l'activation de la protéine Kras conduisent à l'inactivation de suppresseur de tumeurs tels que $p16^{INK4A}$, p53 et SMAD4 favorisant une prolifération cellulaire incontrôlée. Ces mutations et leurs incidences sont référencées dans le **Tableau 7**.

Gene	Fonction	Altération génique	Incidence	Réf.
Kras	GTPase liée à la membrane	Substitution principalement dans le codon 12 (G12D, G12V et G12R)	95 %	[268]
P16/CDKN2A	Suppresseur de tumeur / Régulateur du cycle cellulaire	Délétion homozygotes. Mutation intragénique. Méthylation épigénétique du promoteur.	98%	[269]
TP53	Suppresseur de tumeur / Régulateur « Check point »	Mutation non-sens	50-70%	[270]
SMAD4	Suppresseur de tumeur / Régulateur de la voie TGFβ	Délétion homozygote Mutation non-sens	55%	[271]

Tableau 7 : Synthèse des altérations génétiques les plus fréquemment retrouvées dans le CP.

Une liste plus détaillée des mutations retrouvées dans le CP a ensuite été répertoriée par l'analyse d'une cohorte comprenant 24 échantillons de tumeurs de patients par séquençage.[272] Cette étude démontre que ces mutations ciblent spécifiquement 12 voies moléculaires essentielles pour l'homéostasie cellulaire **(Figure 23)**. La signature génétique est donc spécifique à chaque tumeur, reflet d'une forte hétérogénéité entres les patients.

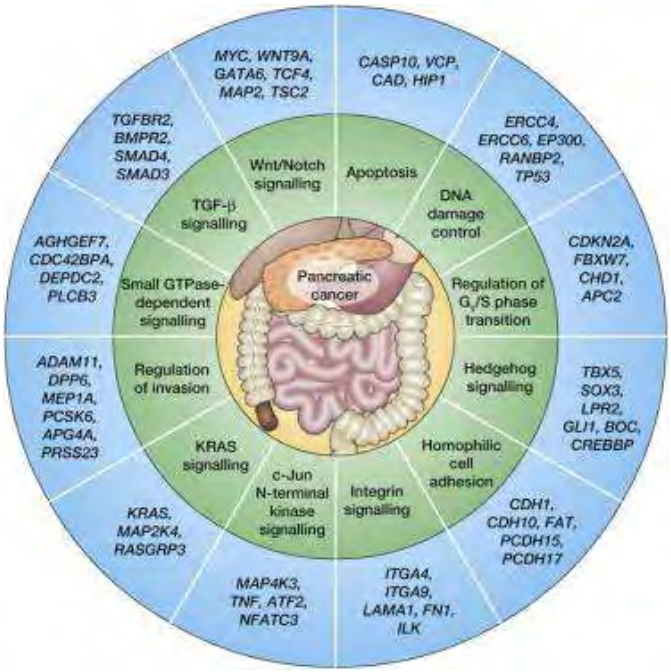

Figure 23 : Mutations associées aux 12 voies moléculaires altérées dans le cancer du pancréas.
Représentation graphique de l'hétérogénéité des mutations et des 12 voies moléculaires identifiées à partir d'une cohorte de 24 patients atteints de cancer du pancréas. Adapté de *Jones et al.*, 2008.[272]

Fait intéressant, les effets pro-oncogéniques de la mutation Kras associée à celle de P53 (par exemple) sont variables en fonction du compartiment ciblé (acinaire ou canalaire).[273] Dans les canaux, la mutation Kras est sans effet. Néanmoins, associée à la mutation P53, elle entraine le développement d'un CP. Dans ce contexte, les tumeurs ne semblent pas passer par un stade transitoire de PanIN contrairement aux tumeurs issues des cellules acinaires. Ainsi, le schéma de progression néoplasique diffère, en fonction du type cellulaire dans lequel les mutations sont exprimées, source d'hétérogénéité entres les individus.

Les variations inter-tumorales observées au niveau de l'ADN sont également présentes au niveau de l'ARN. La stratification des cancers à l'aide de la signature « ARN », déjà disponible en routine pour le cancer du sein par exemple, pourrait être une opportunité pour adapter les traitements des patients sur des thérapies ciblées.

Plusieurs études ont tenté de stratifier les cas de CP sur la base des données d'expression de l'ARNm. Notamment, *Collisson et al*. ont défini un système de classification, comprenant trois sous-types : classique, quasi-mésenchymateux et de type exocrine.[274] Dans une autre étude, *Moffitt et al.* ont

proposé une méthode de stratification alternative qui catégorise les PDAC en cellules tumorales (classiques et basales) et un sous-types spécifique stromal (normaux et activés).[275] En 2016, *Bailey et al.* et l'International Cancer Genome Consortium (ICGC) ont identifié quatre sous-types : progéniteur pancréatique, squameux, ADEX (Aberrantly Differentiated Endocrine Exocrine) et immunogène.[276] Enfin, Puleo et ses collègues ont proposé un autre système, composé de sous-types classiques purs, classiques immunitaires, desmoplastiques, activés par le stroma et de type basal pur, en utilisant un plus grand nombre d'échantillons provenant de plusieurs cohortes. Les sous-types tumoraux ont également été examinés par des analyses protéomiques et métabolomiques. Bien qu'elles ne soient pas aussi approfondies que les études transcriptomiques, ces études mettent également en évidence des sous types similaires à ceux retrouvées par analyse transcriptomique **(Figure 24)**.[274–277]

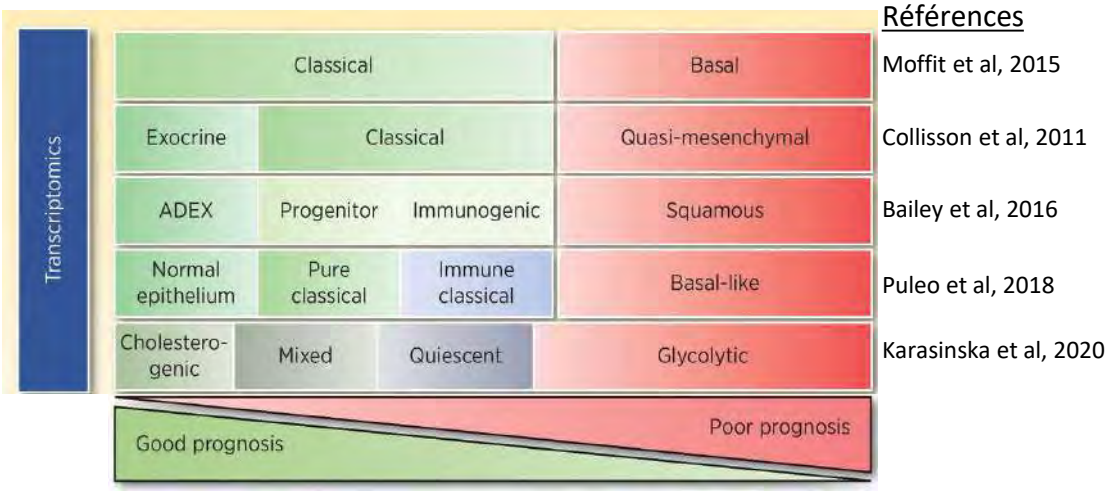

Figure 24 : Différents sous types de CP en fonction de leurs signatures transcriptomiques.
Les sous-types moléculaires de PDAC proposés par diverses études, basées sur des analyses transcriptomiques, sont classés chronologiquement de haut en bas. Les couleurs assorties représentent des signatures similaires. La survie des patients s'aggrave de gauche à droite. Adapté de la revue « Molecular Subtypes of Pancreatic Cancer: A Proteomics Approach », Thakur et al, 2021.[278]

Chaque sous-type moléculaire est corrélé avec un pronostic plus ou moins bon. En effet, le sous-type avec un meilleur pronostic correspond à un sous type qualifié de « classique »[274,275] ou « d'immunogène »[276] ou encore immunitaire classique et desmoplastique[277] en fonction des études.

Enfin, il a également été mis en évidence une instabilité génétique entres les cellules issues du la tumeur primaire et celles issues des métastases, cela définit l'hétérogénéité intra-tumorale.[279] Cette variabilité semble être initiée aux stades précoces de la carcinogenèse, associée à une évolution clonale qui va également être visible au stade métastatique. La masse tumorale n'est pas une structure homogène mais un ensemble de sous populations cellulaires pressentant des mutations différentes.[280] Ainsi, la variabilité de colonisation des métastases s'accompagne d'une variabilité génétique liée non seulement aux clones cellulaires dont elles sont issues mais aussi de leur adaptation à la pression environnementale de l'organe colonisé.

Le sous-typage moléculaire du CP n'en est qu'à ses balbutiements car l'importance de la stratification moléculaire réside dans l'optique d'améliorer la prise en charge des patients. L'identification des voies altérées permettrait d'orienter les recherches et futurs essais thérapeutiques afin de découvrir des traitements adaptés pour chaque signature moléculaire en tenant compte de l'hétérogénéité inter et intratumorale des tumeurs pancréatiques. L'idéal serait d'avoir pour chaque patient un traitement spécifique dépendant de la « carte d'identité » de la tumeur. Cependant, les applications cliniques sont restées stagnantes en raison de plusieurs obstacles. En effet, les méthodologies de classification sont basées sur des analyses de regroupement, ainsi il est difficile de prédire le risque individuel d'un patient avec une « carte d'identité tumorale » spécifique. En outre, les méthodologies utilisées dans ces précédentes études (puces à ADN, le séquençage d'ARN (RNA-seq)…) devraient être utilisées pour une caractérisation du sous type mais elles sont cliniquement inappropriées en raison de la complexité de leur mise en œuvre, de leur coût élevé et de leur longue durée d'exécution.

Chapitre 2 : Résultats expérimentaux

PARTIE 1 : Objectifs des travaux de thèse

J'ai réalisé ma thèse dans une équipe qui axe ses recherches depuis plusieurs années vers le développement de nouvelles approches thérapeutiques pour le CP.

L'objectif de ma thèse était d'identifier comment la surexpression de TRIP12 peut participer à l'initiation et la progression de la carcinogenèse pancréatique. Pour cela mes travaux de thèse se sont articulés en 2 parties et les résultats expérimentaux que j'ai obtenus ont permis la rédaction de deux publications présentées dans ce chapitre **(§II)**.

Les données scientifiques ayant motivé l'étude de TRIP12, les hypothèses sur son rôle dans la carcinogenèse pancréatique cancer et le lien entre les 2 articles sont détaillés ci-dessous.

TRIP12 est une E3 ligase exprimée de manière ubiquitaire dans l'organisme. Les données de la littérature démontrent son implication dans plusieurs processus biologiques essentiels altérés dans le cancer. Elles indiquent aussi que la dérégulation de l'expression de TRIP12 peut avoir des conséquences sur le pronostic et la réponse aux thérapies de cette pathologie **(§ Chapitre 1 - Partie 1)**.

I. Role de TRIP12 dans la carcinoégènese pancréatique

Les tumeurs pancréatiques se caractérisent par une grande hétérogénéité phénotypique et moléculaire inter-patients.[274–277] Les bases de données indiquent que le niveau de l'ARNm de TRIP12 est augmenté dans le PDAC. De plus, le TRIP12 est muté dans certains clones résistants chez des patients atteints de CP en récidive. En effet, des mutations somatiques de TRIP12 ont été localisées au niveau des sites d'épissage chez deux patients qui ont récidivé alors que la tumeur primitive ne présentait aucune mutation.[281]

Nous avons démontré que la protéine TRIP12 est régulée au cours du cycle cellulaire et impliquée dans la progression des cellules en mitose.[21] Au vu des différentes fonctions connues de TRIP12, il était logique de s'interroger sur la régulation de TRIP12 au cours de la carcinogenèse pancréatique car aucune étude n'avait été réalisée dans ce contexte.

Le premier objectif de ma thèse a été de déterminer pourquoi l'expression de TRIP12 augmente dans le cancer du pancréas et quelles en sont les conséquences sur la chimio-sensibilité des cellules cancéreuses.

Ces travaux constituent la partie principale de ma thèse et font l'objet de la rédaction d'un article en cours de finalisation intitulé : « ***Altered cell cycle regulation of the E3 ubiquitin ligase TRIP12 leads to its over-expression and chemosensitivity of pancreatic cancer cells*** », **§ Chapitre 2 ; II- A**.

II. Role de TRIP12 dans l'initiation et la progression du PDAC

Il est important de préserver la stabilité du programme de différenciation des cellules acineuses car il constitue une barrière protectrice contre le CP. En effet, ce programme qui, lorsqu'il est maintenu, bloque les effets de la mutation $Kras^{G12D}$, a des fonctions de suppresseur de tumeur.[13,179] De nombreuses preuves expérimentales issues de la littérature suggèrent un rôle de TRIP12 dans les voies de régulation de la métaplasie acino-canalaire (Figure 25).

TRIP12 polyubiquitine des substrats qui sont des facteurs de transcription essentiels pour le maintien du phénotype des cellules exocrines du pancréas tels que PTF1a et FBW7 **(§ Partie 1 ; III-E)**.[13,56] La perte de PTF1a favorise la dédifférenciation cellulaire, la MAC et le développement des tumeurs pancréatiques en présence de l'oncogène $Kras^{G12D}$.[13,282] TRIP12 pourrait ainsi participer à la perte du programme de différenciation cellulaire par des régulations post traductionnelles de facteurs.

Par ailleurs, TRIP12 participe au remodelage de la chromatine, comme décrit dans le **§ Partie 1 ; III- B**. TRIP12 cible BAF57 et ASXL1 des régulateurs clefs appartenant respectivement aux complexes SWI/SNF et Polycomb. De plus, EZH2 et SUZ12, deux régulateurs du complexe Polycomb PRC1 figurent parmi les interactants identifiés de TRIP12.[4] Ces complexes de remodelage sont essentiels au cours de la métaplasie acino-canalaire pour la reprogrammation qui nécessite la répression du programme de différenciation acinaire et l'activation de l'expression de facteurs des cellules canalaires.[217,283] TRIP12 influence la dynamique de la chromatine par son action sur le PR-DUB (Polycomb Repressive-Deubiquitinase complex), il est donc logique de s'interroger sur le rôle potentiel de TRIP12 dans la reprogrammation cellulaire se produisant au cours de la MAC. En ciblant ASXL1, TRIP12 déstabilise le complexe PR-DUB et empêche le retrait des marques répressives K119 Ub-H2A.[54] TRIP12 pourrait ainsi intervenir dans la régulation épigénétique de la MAC et contribuer à réprimer le programme de différenciation des acini.

Il est légitime de s'interroger sur le rôle potentiel de TRIP12 dans la signalisation activée au cours de la MAC. La signalisation MAPK est nécessaire au changement de phénotype des cellules acineuses.[187] Par ailleurs, les capacités prolifératrices des cellules métaplasiques sont requises durant la régénération cellulaire. TRIP12 régule le cycle cellulaire par le contrôle indirect de la voie P53. **(§ Partie 1 ; III- C)**. Kras et MAP2K3 (protéine impliquée dans la voie MAPK) sont des interactants connus de TRIP12.[4] Enfin, toute perturbation de l'expression de TRIP12 est source de défauts de ségrégation chromosomique et d'altération de la prolifération cellulaire altérée qui pourraient bloquer la phase de régénération de la MAC.[21]

Le second objectif de mes travaux de thèse était de déterminer si TRIP12 contribue aux étapes d'initiation du PDAC en intervenant dans la reprogrammation des cellules acinaires en cellules canalaires et quelles sont les conséquences sur la carcinogenèse pancréatique. Ce projet a nécessité la génération d'un nouveau modèle murin transgénique permettant l'invalidation conditionnelle de

TRIP12 dans le pancréas. L'étude descriptive de l'impact de l'invalidation du gène Trip12 de l'embryogenèse à la carcinogenèse a constitué la deuxième partie des résultats expérimentaux. Ce travail nécessitera des analyses mécanistiques essentielles à la compréhension du phénotype obtenu dans ce modèle. Il fait néanmoins l'objet de l'ébauche d'un second article intitulé : « ***Loss of the E3 ubiquitin ligase TRIP12 inhibits Acinar to Ductal Metaplasia, Development of Pancreatic Intraepithelial Neoplasia and Proliferation of Tumor Cells in Mice*** », **§ Chapitre 2 ; II- B**. La discussion de cet article est donc surtout consacrée aux expériences complémentaires qui sont envisagées pour la finalisation de ce travail.

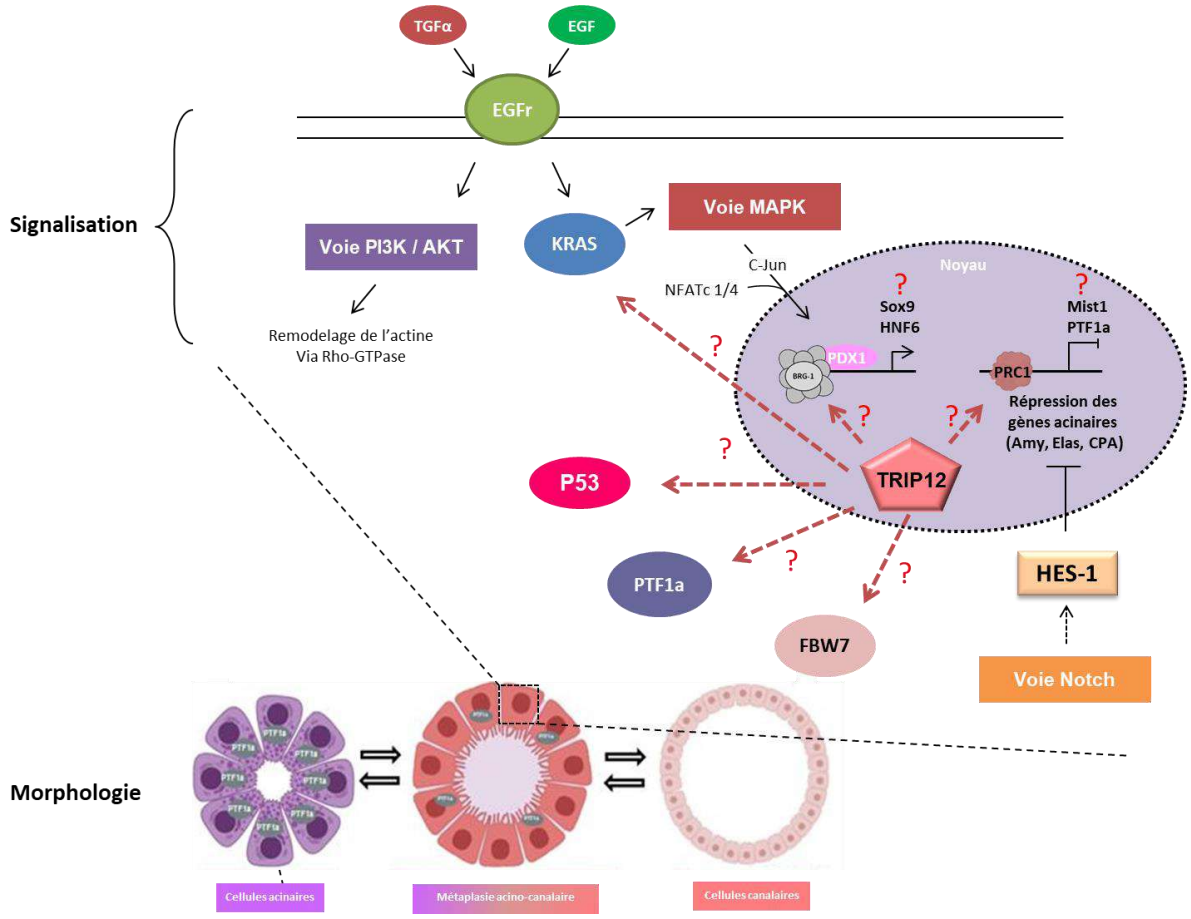

Figure 25 : Schéma illustrant les rôles potentiels de TRIP12 dans le mécanisme de métaplasie acino-canalaire.
TRIP12 possède différentes fonctions pouvant être impliquées dans la conversion des cellules acineuses (en violet) en cellules métaplasiques (en rouge). En effet, au niveau de la chromatine, TRIP12 pourrait participer à la régulation de l'expression des gènes acinaires en modulant indirectement l'ubiquitination des histones H2AK119, régulées par le complexe Polycomb (PRC1), et ainsi réprimer l'expression de PTF1a. Par sa fonction régulatrice du complexe SWI/SNF, il pourrait déstabiliser le complexe BRG1-BAF et ainsi réduire l'expression des gènes canalaires. Par ailleurs, par son action d'E3 ligase, TRIP12 pourrait participer à la dégradation de PTF1a ou encore de FBW7, tous deux impliqués dans la différenciation cellulaire, lesquels favorisent la MAC lorsqu'ils sont perdus. Enfin, la présence de TRIP12 modulerait l'expression de ARF réduisant ainsi les niveaux de P53 et favoriserait la prolifération cellulaire. Etant donné ses interactants connus, TRIP12 pourrait également intervenir dans la régulation de la voie Ras, voie de signalisation qui interagit avec la voie PI3K.

PARTIE 2 : Publications

I. Article 1 : *"Altered cell cycle regulation of the E3 ubiquitin ligase TRIP12 leads to its over-expression and chemosensitivity of pancreatic cancer cells"*

En préparation

Altered cell cycle regulation of the E3 ubiquitin ligase TRIP12 leads to its over-expression and modifies the chemosensitivity of pancreatic cancer cells.

LIST OF AUTHORS: Manon BRUNET [1], Dorian LARRIEU [1], Claire VARGAS [1], Naïma HANOUN [1], Laetitia LIGAT [1], Guillaume LABROUSSE [1], Lucrèce DAGNON [1], Julie LESCURE [1], Julie BONZOM [1], Hubert LULKA [1], Charley LAGARDE [2], Janick SELVES [1,2], Pierre CORDELIER [1], Marlène DUFRESNE [1†] and Jérôme TORRISANI[1†].

INSTITUTION :

[1] Université de Toulouse, INSERM, Université Toulouse III-Paul Sabatier, Centre de Recherches en Cancérologie de Toulouse, Toulouse, France.

[2] Département de Pathologie, Institut Universitaire du Cancer Toulouse Oncopole, CHU Toulouse, France.

[†] **Corresponding author:** Marlène Dufresne (marlene.dufresne@inserm.fr) and Jérôme Torrisani (Jerome.torrisani@inserm.fr)

ABSTRACT.

Pancreatic cancer is among the worse cancers in the world with a 5 year-survival rate lower than 8 %. This poor prognosis is explained by a lack of efficient treatment or early diagnosis but above all by an incomplete understanding of molecular mechanisms that govern its initiation, progression and resistance to most therapies. Among molecular processes, ubiquitination system is often altered in cancers. The E3 ubiquitin ligase TRIP12 (Thyroid hormone receptor interacting protein) has been involved in the regulation of p53 stability and DNA damage repair but also responsible of the degradation of the Pancreas Transcription Factor 1A, essential for the maintenance of acinar cells.

In this study, we reveal a heterogeneity of TRIP12 protein expression in human pancreatic tumors that is also observed in pancreatic cancer-derived cell lines. We first show that TRIP12 expression is required for PDAC-derived cell growth by controlling E2F-target genes. Second, we demonstrate that TRIP12 heterogeneity results from a combination of different levels of regulation. They mainly include the activity of a bi-directional promoter that controls Trip12 mRNA level and the variation of TRIP12 expression during cell cycle. More importantly, we demonstrate that the level of TRIP12 in PDAC-derived cell lines modifies their sensitivity to a DNA damage-inducing drug.

KEY WORDS: Pancreatic cancer, TRIP12, E3 ubiquitin ligase, cell cycle, DNA repair, chemotherapy sensitivity.

INTRODUCTION.

The ubiquitin-mediated degradation pathway is often deregulated in cancers **(Senft, Qi, and Ronai 2018)**. Among the proteins involved in this pathway, the protein TRIP12 (Thyroid hormone Receptor Interacting Protein 12) belongs to E3 ubiquitin ligase family with HECT domain (Homologous to the E6-AP Carboxyl Terminus). It participates in the control of major biological processes such cell proliferation, chromatin remodeling and DNA damage repair by controlling the stability of key proteins such as ARF (Alternative Reading Frame)**(Chen et al. 2013; 2010)**, SOX6 **(An, Ganio, and Hagiwara 2013)** and BAF57 (Brg1 associated factor 57)**(Keppler and Archer 2010)**, RNF168 (Ring Finger Protein 168) **(Gudjonsson et al. 2012)**, PARP1 (Poly-ADP-ribose polymerase 1) **(Gatti et al. 2020)** among others **(Brunet et al. 2020)**. TRIP12 expression is positively correlated with a poor prognosis in cellular hepatocellular carcinoma **(Cai et al. 2015)** and affects the radio-sensitivity of HPV (human papilloma virus)-positive head and neck squamous carcinoma **(Wang et al. 2017; Molkentine et al. 2020)**. It also constitutes a potential marker of response to PARP inhibitors in BRCAness patients (**Gatti et al. 2020)**. We showed that TRIP12 expression is tightly regulated during cell cycle and is required for mitotic processing and chromosome stability **(Larrieu et al. 2020)**. Little is known on the regulation of TRIP12 stability with the exception that the deubiquitinase USP7 (Ubiquitin Specific Peptidase 7) protects TRIP12 against proteasome degradation **(Georges et al. 2018; Cai et al. 2015)**.

Pancreatic cancer is the fourth cause of death by cancer in Western countries with 5 year-survival rate below 10% **(Siegel, Miller, and Jemal 2020)**. This poor prognosis is explained by an absence of early diagnosis markers and efficient therapies. Treatment with gemcitabine is often used for palliative goals. FOLFIRINOX and Nab-Paclitaxel are frequently proposed to metastatic patients. PARP inhibitors therapies have recently emerged for a subset of patients with deficiency in DNA damage repair systems **(Sahin et al. 2016)**. Despite important research efforts, a great majority of patients do not respond to the different chemotherapies **(Duconseil et al. 2015)**. It is therefore urgent to better understand the mechanisms that control pancreatic cancer progression and their sensitivity to chemotherapies.

Pancreatic tumors take their origin from different cellular types **(Storz and Crawford 2020)** and are characterized by a high phenotypic and molecular heterogeneity between patients **(Bailey et al. 2016)**. It is reported that TRIP12 controls the stability of key-proteins involved in the determining of cellular types at the origin of pancreatic cancer. Indeed, TRIP12 targets the degradation of FBW7 (F-box and WD-40 domain), the substrate recognition component of SCF (SKP1, CUL1 and F-box protein complex) ubiquitin ligase **(Khan et al. 2021)**. FBW7 is a major regulator of pancreatic ductal cell fate and a known tumor suppressor gene in a subset of PDAC patients **(Zhang et al. 2016)**. Moreover, we demonstrated that TRIP12 ubiquitinates PTF1a (Pancreas specific Transcription Factor 1a) and induces its proteasomal degradation. PTF1a, a transcription factor essential for pancreas development, functions as a tumor suppressor by its role as a gatekeeper of pancreatic acinar phenotype **(Hanoun et al. 2014)**. Moreover, TRIP12 is overexpressed in pancreatic cancer tissues **(Chen et al. 2010)**.

Due to its implication in cellular functions in pancreatic cancer development and mechanisms of chemoresistance, TRIP12 level of expression and modes of regulation in human pancreatic tumors needed to be explored. In this study, we demonstrate that TRIP12 protein is heterogeneously expressed in human pancreatic tumors which is also observed in PDAC-derived cell lines. We show that TRIP12 expression is required for PDAC-derived growth *in vitro* and *in vivo* as it is necessary for E2F-regulated genes. We show that Trip12 mRNA level is controlled by a bidirectional promoter and explains in some extent the heterogeneous expression of TRIP12 protein in PDAC-derived cell lines. Additionally, we demonstrate that a variation of TRIP12-cell cycle regulation greatly participates in TRIP12 heterogeneity in PDAC-derived cell lines. More importantly, we show that TRIP12 expression level influences the sensitivity of PDAC-derived cell lines to DNA damage inducing drug.

MATERIALS AND METHODS.

Cell culture and treatments.
hPNE cells were a gift for Dr M. Ouellette (University of Nebraska Medical center, Omaha, USA) **(Lee et al. 2003)**. BxPC-3 (ATCC® CRL-1687™), Capan-1 (ATCC® HTB79™), Capan-2 (ATCC® HTB80™), MiaPACA-2 (ATCC® CRL-1420™) and PANC-1 (ATCC® CRL-1469™) cell lines were obtained for the American Tissue and Cells Collection and cultured as previously described **(Delpu et al. 2013)**. Gaussia Luciferase MiaPACA-2 cell line was previously described **(Delpu et al. 2013)**. BxPC-3 cells were treated with lovastatin (60 µM; Sigma-Aldrich) for 24h for late G_1-phase enrichment, with aphidicolin (1 µM; Sigma-Aldrich) for 24h for early S-phase enrichment. For G_2-phase enrichment, BxPC-3 cells were subject to a 18h-treatment with thymidine (2mM; Sigma-Aldrich), released in complete medium for 5h followed by a 3h-treatment with Ro3306 (9 µM; Tocris). MiaPACA-2 cells were seeded at 80% of confluence and cultured in 0.1% fetal calf serum (FCS)-supplemented medium for 72h for late G_1-phase enrichment, with thymidine (2mM) for two periods of 18h spaced by a 8h-period in complete culture medium for early S-phase enrichment. For G_2-phase enrichment, MiaPACA-2 cells were treated with Ro3306 (9 µM) for 24h.
Cell lines were treated with 5-ethynyl-2'-deoxyuridine (EdU) (10 µM, Life technologies) for 20 min. Cells in S phase were visualized using Click-it® EdU Alexa Fluor® 647 imaging kit (Life technologies).
BxPC-3 and Capan-1 cells were treated with leptomycin B (50 ng/ml; Sigma Aldrich) for 20h.
MiaPACA-2 cells at ~50% of confluence were treated with the USP7 inhibitor P22077 (25 µM; Selleckchem) for 20h. Doxorubicin was purchased from Sigma-Aldrich.
For USP7 depletion, three different siRNAs (#1 5'-CCCAAAUUAUUCCGCGGCAAA-3'; #2 5'-AAGCGUCCCUUUAGCAUUAUU-3'; #3 5'-GCAUAGUGAUAAACCUGUAUU-3') at 50 nM and a control siRNA (Ambion) were transfected using siPORT NeoFX™ reagent (Ambion) diluted into OPTI-MEM® medium (Invitrogen). SiRNA transfections were repeated after 24h. Subsequent analysis were performed 48h-post-transfection.

Antibodies.
All the antibodies and dilutions used in this study are listed in **Supplemental Table 1**.

Immunohistochemistry on human pancreatic cancer macro-array.
A human pancreatic cancer macro-array was obtained from the department of pathology (Pr. J Selves, Cancer University Institute of Toulouse) following ethical procedures. It contains 23 human samples (21 pancreatic adenocarcinomas, 1 intraductal papillary mucinous neoplasm (IPMN) and 1 mucinous carcinoma). Samples were processed using EnVision Flex kit (DakoCytomation) with a pretreatment at pH 9 on a DAKO Autostainer link 48. TRIP12 antibody (Sigma-HPA036835) was used at a dilution of 1/200. The intensity of TRIP12 nuclear staining in pancreatic adenocarcinoma samples was graded as weak, moderate and strong by four different observers (M.B., J.S. M.D. and J.T.)

Immunofluorescence.
Enriched and asynchronous cell populations treated or with EdU-treated grown on glass cover slips were fixed, permeabilized with IntraStain reagent (DAKO) following supplier's instructions and followed by a 30 min-incubation with Protein Block reagent (DAKO). Cells were incubated overnight at 4°C with appropriate primary antibodies **(Suppl Table 1)** diluted in Antibody Diluent reagent (DAKO). After PBS wash, cells were incubated with appropriate AlexaFluor®488, 555 coupled secondary antibodies (ThermoFisher) **(Suppl Table 1)** for 2h at room temperature. EdU incorporation was visualized using the Click-it® EdU Alexa Fluor® 647 Imaging kit (Life technologies) following supplier's instructions. Nuclei were stained with DAPI (1 µM, Euromedex). Cover slips were mounted on microscope slide using Fluorescent Mounting™ medium (DAKO), visualized using LSM 780 confocal microscope (Zeiss) and analyzed using ZEN 2.3 software. Nuclear TRIP12 fluorescence intensity was determined using a FIJI macro-command. The classification of cells in the different phases of the cell cycle was previously described **(Larrieu et al. 2020)**.

CGH array

Genomic DNA of the different cell lines was extracted using the DNeasy QIAGEN kit. Comparative Genomic Hybridization (CGH) array was performed using Cytoscan HD kit (Life technologies). Microarray chips were prepared according to manufacturer's instructions and scanned using Affymetrix Scanner (Affymetrix GeneChip Scanner 3000 7G System). Data are analyzed using Chas software (Applied biosystem).

Trip12 promoter deletion constructs.

pGL_3-MCS-Firefly Luciferase/pCMV-Renilla Luciferase plasmid was generated by inserting *BamH* I/*Bgl* II fragment of pRL-CMV plasmid (Promega) into pGL_3 Basic plasmid (Promega) at *BamH* I site. Genomic DNA fragment corresponding *Trip12/FbxO36* bi-directional promoter (GRCh38.p13 Chr2 position 229921874 to 229922496) and *Cxcr4* promoter (GRCh38 Chr2 position 136118060 to 136118339) were amplified by PCR from BxPC-3 genomic DNA using *Trip12* and *Cxcr4* promoter primers **(Suppl Table 2)** and cloned into pGem-T plasmid (Promega). *Trip12/FbxO36* and *Cxcr4* promoters were subsequently inserted into pGL_3-MCS–Firefly Luciferase/pCMV-Renilla plasmid in both orientations at *Kpn* I/*BamH* I and *Kpn* I restriction sites, respectively. *Trip12/FbxO36* promoter successive deletion constructs were generated by site-directed mutagenesis (Stratagene® mutagenesis kit) **(Suppl Table 2)** . All construct sequences were verified by automatic sequencing.

shRNA lentiviral plasmids and lentiviral production.

The following lentivirus shRNA lentiviral plasmids were purchased from Sigma-Aldrich: pLKO1-TRC1 non mammalian shRNA control SHC002-target sequence CAACAAGATGAAGAGCACCAA, ShTRIP12#1 pLKO1-TRC1 TRCN0000022374-target sequence CCTGAGTCAAGGAAACATGTT, ShTRIP12#2 pLKO1-TRC1 TRCN0000022375-target sequence CCGGAGTTTGAATCCACCTTT and ShTRIP12#3 pLKO1-TRC1 TRCN0000273210-target sequence CCACTACTCAGTCACCTAAAT. Lentiviral particle production using LentiSmart reagents (Cayla, Invivogen) was previously described **(Larrieu et al. 2020)**.

RNA extraction and RT-qPCR.

Total RNA was isolated from cell lines with Trizol® reagent (ThermoFisher) according to supplier's instructions. RNA concentration was measured with a NanoDrop ND-1000 spectrophotometer (ThermoScientific). The RevertAid minus H (company) kit was used according to the manufacturer's recommendations with 2 µg of total RNA. cDNA samples were diluted 1 into 100. qPCR duplicates were carried out using 2 µL of diluted cDNA in a 20 µL-reaction using Sso Fast EvaGreen® reagent (BioRad) following supplier's instructions on a StepOne Plus™ Real-Time PCR system (Applied BioSystems). Relative amount of mRNA was calculated by the comparative threshold cycle (Ct) method as $2^{-\Delta Ct}$, where ΔCt=Ct target mRNA – Ct geometric mean of GAPDH, β-Actin and cyclophilin A **(Suppl Table 2)**. Amplification efficacy was verified for every sets of primers. A specific protocol was performed for the quantification of short and long form of *Trip12* mRNA. Primers were tested on RT reaction in absence of Reverse Transcriptase to detec genomic DNA contamination. *Trip12* mRNA total amount was quantified using Exon 10-11 primers and the long form using 3-'UTR primers **(Suppl Table 2)**, the quantity of the short form was determined by the difference between the total amount of *Trip12* mRNA and the long form.

Flow cytometry.

Cells were fixed in 70% ethanol during the exponential growth phase for asynchronous cells or after treatments for cell-cycle enriched populations. Fixed cells were treated with RNAse A (10 µg/mL) and propidium iodide (20 µg/mL) (Sigma-Aldrich) for 15 min at 37°C. Data were acquired using the MACS Quant® VYB cytometer (Miltenyi Biotech) and cell cycle distribution was analyzed with MACS Quant and ModFit software.

Chromatin Immunoprecipitation.
MiaPACA-2 and Capan-1 cells were incubated with formaldehyde (1%; Sigma-Aldrich) for 8 min. Chromatin was immunoprecipitated by an anti-acetylated lysine 9 histone 3 antibody or non-immune rabbit IgG **(Suppl Table 1)** using EpiQuik™ Chromatin Immunoprecipitation kit (Epigentek) following manufacturer's instructions. The recovered DNA was subjected to PCR amplification using five sets of primers **(Suppl Table 2)**. Semi-quantitative PCR was performed using Sso Fast EvaGreen reagent (BioRad) following supplier's instructions on a StepOne Plus™ Real-Time PCR system (Applied BioSystems). Amplification efficiency was verified for each set of primers. The relative binding of K9H3 antibody to the target sequences was determined by dividing the calculated amount of precipitated DNA by the amount of that sequence in the input DNA.

Sodium bisulfite mapping.
Using EZ DNA methylation kit (Zymo Research) for bisulfite treatment. PCR conditions: between 30-60 ng of bisulfited DNA. PCR with AmpliTaq Gold (Perkin Elmer). 95°C 5 min, 40 cycles of 95°C 30 s, 50.4°C for 30 s, 72°C for 30 s and final extension 72°C for 8 min. with TRIP12 primers **(Suppl Table 2)**. PCR products (366 bp) were subsequently inserted into pCR2.1 cloning vector (Invitrogen) and sequenced using standard M13 Forward and Reverse primers using an automatic sequencer.

Luciferase activity measurement.
Different PDAC-derived cell lines were seeded at 2.10^4 cells/well of a 48 well-dish and transiently transfected 24h later with 0.5 µg of reporter plasmids using polyethyleneimine (PEI) reagent (PolyPlus) with a ratio N/P=10. After 48h, cells were lysed with Cell Lysis Buffer (Promega). Renilla and firefly luciferase activity was measured using Luciferase kit (Promega) and CLARIOstar luminometer (BMG LABTECH). Firefly luciferase activity was normalized by renilla luciferase activity.

Orthotopic graft in SCID mice
All protocols including animals were approved by the ANEXPLO ethic committee (Protocol number: 10/1037/10/14). Gaussia Luciferase MiaPACA-2 shScr and shTRIP12#1 (2.10^6 cells/injection) were injected into the pancreas of SCID mice. Luciferase activity was determined after injection of colenterazine (Promega) every 4-5 days post-injection as previously described **(Delpu et al. 2013)**.

Agilent microarray gene expression and gene sets enrichment analysis (GSEA).
Four MiaPACA-2 and PANC-1 ShScr and ShTRIP12#1 clones were isolated by serial dilution. Total RNA was extracted using Trizol® reagent (Life technologies) (see above). *Trip12* mRNA depletion in each ShTRIP12 clones was verified by qRT-PCR as described above. Total RNA was hybridized on Agilent SurePrint G3 Human GE V2 8x60K microarrays. Adjustment of the estimated significance level to account for multiple hypothesis testing (Benjamini-Hochberg adjusted value). The Gene Expression Omnibus (GEO) (http://www.ncbi.nlm.nih.gov/geo) accession numbers corresponding to our data sets are GSE147717 (PANC-1) and GSE 147549 (MiaPACA-2). Gene set enrichment analysis (GSEA) was performed using the Broad Institute platform (version 4.0.1) with a number of permutation of 1000. P value and a false discovery rate (FDR) were set at 0.001. Fifty gene sets relative to the Hallmarks repertory from Molecular Signature DataBase (MsigDB) were analyzed using the GSEA pre-ranked method.

Western blot analysis.
Cytosolic protein fraction was isolated using a lysis buffer containing Tris-HCl (pH 7.5) 10 mM, $MgCl_2$ 1.5 mM, KCl 5 mM, DTT 0.5 mM, Nonidet™-P40 0.5% and PMSF 0.5mM supplemented with Protease Inhibitor Cocktail (Sigma-Aldrich). Soluble nuclear protein fraction was isolated using a lysis buffer containing Tris-HCl (pH 7.5) 20 mM, NaCl 400 mM, Glycerol 0.025%, $MgCl_2$ 1.5 mM, DTT 0.5 mM, PMSF 0.5 mM, EDTA 0.2 mM and Protease Inhibitor Cocktail. Protein quantity was determined using Bradford assay. 30-50 µg of nuclear proteins were loaded onto a 10% SDS-PAGE and transferred on nitrocellulose membrane using TransBlot apparatus (BioRad). Membranes were subsequently

incubated with TBS Tween-20® 0.01% + 5% fat milk for 1h and with indicated antibodies **(Suppl Table 1)** overnight at 4°C. Membranes were incubated with appropriate HRP-coupled secondary antibodies **(Suppl Table 1)**. Protein abundance was visualized using Clarity™ Western ECL substrate, ChemiDoc™ XRS+ device and ImageLab™ software (BioRad).

Protein-protein interaction network analysis.
The STRING database v11 (https://string-db.org) was used to map the physical interaction networks of proteins encoded by the MsigDB Hallmark E2F-target gene set (n=195), TRIP12 depleted-PANC-1 (n=138) and TRIP12-depleted MiaPACA-2 (n=113) leading edge E2F-target genes obtained from GSEA. Networks were obtained with the following active interaction sources: text mining, experiments, databases with a minimum required interaction score of 0.700 (high confidence).

Cell viability assay.
TRIP12-depleted or control MiaPACA-2 cells were seeded at 4.10^3 cells/well of a 96-well plate. After 24h, the cells are treated with indicated doses of doxorubicin (Sigma). After 24h, 20 µL of MTS reagent (Cell Titer 96® AQueous One Solution cell proliferation assay, Promega) were added. The optical density at 490 nm was measured after 1h-incubation at 37°C, 5% CO_2 using the CLARIOstar plate reader (BMG LABTECH).

Statistical analysis.
In vitro data were analyzed by 2-tailed, unpaired Student's t-test using a multiple statistics Graph Pad Prism 9 software package and a difference was considered significant when p value was lower than 0.05. Mean values are given ± SEM. Number of independent experiments is indicated in the figure legends. *, ** and *** indicate a p value <0.05, 0.01 and 0.001, respectively.

RESULTS.

1. TRIP12 protein is heterogeneously expressed in human pancreatic tumors and PDAC-derived cell lines.

TRIP12 is involved in the degradation of key-proteins that leads to pancreatic cancer initiation **(Khan et al. 2021; Hanoun et al. 2014)**. Nevertheless, little is known on TRIP12 expression in pancreatic tumors. Immunohistochemistry experiments revealed a great heterogeneity of TRIP12 expression in a collection of 21 human pancreatic tumors in which 6 samples display a weak TRIP12 expression, 8 an intermediate expression and 7 a high TRIP12 expression. **(Fig. 1A and Table 1)**.

Table 1.

Case number	Gender	Age	Grade	Differentiation state	TRIP12 expression
P13.19943	F	57	Low	High	+
P13.19946	M	64	Low	Moderate	+
P14.369	F	72	Low	High	+
P11.10243	F	66	Low	High	+
P11.8368	M	71	Low	High	+
P12.12800	F	53	High	Anaplasia	+
P13.19938	M	59	High	Low	++
P13.19939	F	64	Low	Moderate	++
P13.19940	M	59	Low	High	++
P14.366	F	64	Low	High	++
P14.368	M	72	Low	Moderate	++
P14.365	M	77	Low	Moderate	++
P11.12821	M	59	Low	Moderate	++
P11.12520	F	76	Low	High	++
P13.19941	M	66	Low	High	+++
P13.19944	F	72	Low	Moderate	+++
P13.19947	M	42	Low	High	+++
P13.19948	F	59	Low	High	+++
P14.364	F	69	Low	High	+++
P12.10905	F	74	High	Low	+++
P12.13329	F	78	Low	High	+++

Clinical data of 21 patients corresponding to pancreatic tumors that constitute the tissue microarray. The protein expression of TRIP12, age, sex, cell grade and differentiation status of each patient are indicated. The quantification score corresponds to the percentage of TRIP12 nuclear positive cells multiplied by an intensity score evaluated from 0 to 3. A score between 0 and 100 is considered as a weak expression (+), between 100 and 200 as moderate (++) and between 200 and 300 as a strong expression (+++).

A great heterogeneity was also observed in human PDAC-derived cell lines. Indeed, as a nuclear protein, we measured by immunofluorescence the percentage of TRIP12 nuclear positive cells in BxPC-3, Capan-1, Capan-2, PANC-1 and MiaPACA-2 cell lines **(Fig. 1B and C)**. The percentage of TRIP12 nuclear positive cells in BxPC-3 and Capan-1 in only 23.1 % and 23.2 %, respectively, while it reaches 66.6% in MiaPACA-2 cells. This disparity of expression was confirmed by Western blot analysis where

TRIP12 expression in BxPC-3 cells is significantly lower than the one in MiaPACA-2 cells **(Fig. 1D)**. We previously showed that TRIP12 is required for cell division **(Larrieu et al. 2020)**. Interestingly, the cell lines with a low TRIP12 expression (ex: BxPC-3 and Capan-1) display a lower growth rate compared to the other cell lines **(Fig. 1E)** reinforcing the notion that TRIP12 is necessary for the growth of PDAC-derived cell lines.

2. The depletion of TRIP12 affects the growth of TRIP12 high expressing PDAC-derived cells.

To study the importance of TRIP12 in the growth of PDAC-derived cells, we generated TRIP12 depleted-PANC-1 and MiaPACA-2 stable cell lines using three different ShRNAs **(Fig. 2A and 2B)**. PANC-1 and MiaPACA-2 cell lines were chosen as they express a high level of TRIP12 protein. The main consequence of TRIP12 depletion is a significant inhibition of cellular growth and a decreased capacity to form colonies **(Fig. 2C and 2D)**. The growth inhibition in response to TRIP12 depletion was also observed *in vivo* after orthotopic injection in murine pancreas **(Fig. 2E and 2F)**. These results demonstrate the requirement of TRIP12 in the proper growth of the PDAC-derived PANC-1 and MiaPACA-2 cells.

3. TRIP12 preferentially controls E2F-regulated genes implicated in G_2/M transition.

To decipher the mechanisms by which TRIP12 affects PDAC-derived cell growth, transcriptomic analyses were performed on TRIP12-depleted PANC-1 and MiaPACA-2 cells using ShTRIP12#1. Analysis of gene set enrichment on differentially expressed genes in response to TRIP12 inhibition was performed. Among the 50 hallmarks gene sets (Molecular Signatures database-MSigDB), eight were retrieved statistically enriched in TRIP12 depleted-PANC-1 cells and five in TRIP12-depleted MiaPACA-2 cells **(Table 2)**. Interestingly, the four negatively enriched pathways in TRIP12-depleted PANC-1 cells were all retrieved in TRIP12 depleted-MiaPACA-2 cells **(Fig. 3A)**. These four gene sets belong to the Hallmark Proliferation process category **(Liberzon et al. 2015)**. Among the 195 genes of the E2F target gene set (MSigDB E2F target genes), 138 and 113 are leading edge genes in PANC-1 and MiaPACA-2 cells, respectively **(Fig. 3B and Suppl Table 3)**. Interestingly, 90 genes are commonly repressed in absence of TRIP12 in both cell lines **(Fig. 3B)**. The repression of a subset of E2F-target genes was also measured using ShTRIP12#2 and #3 **(Fig. 3C)**. E2F transcription factor family is known to control the transcription of different sets of gene involved in G_1-to-S, G_2-to-M transition and DNA damage repair **(Kent and Leone 2019)**. Transcription level of these genes are temporally regulated during the cell cycle. Physical protein interaction network (STRING) of the 195 E2F target genes clearly depicts the two functional networks implicated in G_1-to-S (DNA replication and DNA repair) and G_2-to-M (G2/M transition of mitotic cycle and Chromosome segregation) transitions **(Fig. 3D, left panel)**. We performed the same STRING analysis with the 113 leading edge genes in TRIP12 depleted-MiaPACA-2 cells and observed that these commonly E2F target repressed genes are preferentially involved in G_2-to-M transition **(Fig. 3D, right panel)**. Similar results were observed in TRIP12 depleted-PANC-1 leading edge genes **(Suppl Fig. S1)**. Moreover, the consequences of a TRIP12 depletion in MiaPACA-2 cells leads to an accumulation of cells in S and G_2 phases associated to a decrease in the proportion of cells in G_1 phase **(Fig. 3E)**. Altogether, these results suggest that TRIP12 is required for the transcription of genes involved in G_2-to-M transition and a proper cell division.

Table 2.

TRIP12 depleted-PANC-1		TRIP12 depleted-MiaPACA-2	
Pathways	**NES**	**Pathways**	**NES**
Interferon α response	2.45	K ras signaling	1.69
Interferon γ response	2.05		
TNF-α signaling via NFKB	1.99		
Epithelial mesenchymal transition	1.91		
E2F targets	-2.99	E2F targets	-2.12
G_2/M checkpoint	-2.64	MYC targets V1	-2.11
MYC targets V1	-2.51	MYC targets V2	-2.09
MYC targets V2	-2.23	G_2/M checkpoint	-1.96

Nominal p value and FDR q-value < 0.001
NES: normalized enrichment score

4. A bi-directional promoter-controlled mRNA level partially explains TRIP12 protein expression heterogeneity in PDAC-derived cell lines.

We decided to investigate the molecular mechanisms that could explain the variation of TRIP12 protein expression in the different PDAC-derived cell lines. T*rip12* mRNA level was measured in the different cell lines **(Fig. 4A)**. Variable *Trip12* mRNA level between the different cell lines was revealed. Among them, *Trip12* mRNA level is higher in MiaPACA-2 and PANC-1 cell lines comparatively to BxPC-3, Capan-1 and Capan-2 cell lines. These results were highly similar with those available from the Broad Institute Cancer Cell Line Encyclopedia (CCLE) **(Suppl Fig. S2)**.

No chromosomic large alterations (deletion, duplication) encompassing *Trip12* gene was detected in any of the tested PDAC-derived cell lines **(Suppl Fig. S3)**. Bio-informatic analysis of *Trip12* genomic DNA region suggested that *Trip12* mRNA expression is controlled by a 555 bp-bidirectional promoter that also controls *FbxO36 (F-box only protein 36)* mRNA level in the head-to-head opposite direction **(Fig. 4B and Suppl Fig. S4)**. Moreover, we noticed that genomic DNA region containing *Trip12* promoter is embedded in a CpG island (1753 bp). In cancer cells, DNA hypermethylation is often responsible of promoter silencing of tumor suppressor genes **(Nishiyama and Nakanishi 2021)**. Bisulfite mapping analysis revealed that *Trip12* promoter region is not methylated in any of the tested cell lines **(Suppl Fig. S5)** demonstrating that DNA hypermethylation is not responsible of *Trip12* mRNA variation.

In parallel, a study reported the existence of *Trip12* mRNA variants with a short or a long 3'-UTR (3'-Untranslated Region) that display different translation efficiency; the short form being more efficiently translated than the long form **(Chang et al. 2015)**. The quantification of the proportion of *Trip12* mRNA short and the long forms in our different cell lines did not reveal significant changes between the cell lines that could explain the heterogeneity of TRIP12 protein expression **(Suppl Fig. S6)**. Functional studies using luciferase reporter constructs confirmed a bi-directional activity of *Trip12/FbxO36* promoter in the different PDAC-derived cell lines when compared to an unidirectional CXCR4 (CXC chemokine receptor type 4) promoter **(Fig. 4C)**. More importantly, *Trip12*/*FbxO36* promoter activity correlates to *Trip12* mRNA level **(Fig. 4A)**. Moreover, ChIP-qPCR analyses showed that endogenous *Trip12* promoter is more associated to transcriptionally active histone marks (acetylated K9-H3) in *Trip12* mRNA-high expressing MiaPACA-2 cells than in Capan-1 cells **(Fig. 4D)**. To identify important regulatory sequences in *Trip12/FbxO36* bi-directional promoter, PhastCons (UCSC genome browser) analysis revealed the presence of several highly conserved regions **(Fig. 4B)**. Successive deletion analysis of *Trip12/FbxO36* promoter showed that the conserved region located between -186/-249 nt (relatively to *Trip12* transcriptional start site +1) is required for a maximal transcriptional of *Trip12* promoter activity (but not in *FbxO36* orientation) **(Fig. 4E and Suppl Fig. S4)**.

Altogether, our results demonstrate that a bi-directional promoter controls *Trip12* mRNA level and participates to *Trip12* heterogeneity at a mRNA level in our tested PDAC-derived cell lines. Nevertheless, the difference between low and high TRIP12-expressing cell lines at the mRNA level (~

2.5 fold between BxPC-3 and MiaPACA-2 **(Fig. 4A)**) does not entirely explain the difference measured at the protein level (~26 fold between BxPC-3 and MiaPACA-2, **Fig. 1D**). This suggested the implication of another levels of regulation in TRIP12 protein heterogeneity.

5. Variation of the TRIP12 cell cycle regulation in PDAC-derived cell lines.

We recently demonstrated that the TRIP12 presence in the nucleus is tightly dependent to the cell cycle in HelaS3 cancer cells **(Larrieu et al. 2020)**. Logically, we decided to investigate TRIP12 cell cycle regulation within our PDAC-derived cell lines of interest by an approach described in **Suppl Fig. S7**. We determined the percentage of TRIP12 nuclear positive cells in each phase of the cell cycle **(Fig. 5A and 5B)**. In low TRIP12 protein expressing BxPC-3 and Capan-1 cells, TRIP12 is weakly present in the nucleus of cells in early G_1, late G_1 and early S phases. TRIP12 protein appears in the nucleus of late S and G_2 phase-cells. In contrast, in moderate TRIP12 expressing Capan-2 and PANC-1 cells, while TRIP12 is still highly present in late S and G_2 phase-cells, we observed a significant increase of TRIP12 nuclear positive cells in early G_1 cells. This heterogeneity of TRIP12 cell cycle regulation is even more visible in the high TRIP12 expressing-MiaPACA-2 cells in which TRIP12 is frequently present in the nucleus of cells in early G_1 and late G_1 phases in addition to those in late S and G_2 phases.

To ascertain whether this heterogeneous cell cycle regulation of TRIP12 could explain the difference of its protein expression **(Fig. 1D)**, we precisely established the distribution in the cycle of the five asynchronous PDAC-derived cell lines **(Fig. 5C)**. We noticed that the cells in late G_1 phase represent approximately 40% in all cell lines. However, the proportion of cells in late S and G_2 phases in MiaPACA-2 cell line is ~2 times higher than in the other cell lines. Combined with the findings in **Fig. 5A and 5B**, the heterogeneous expression of TRIP12 protein in PDAC-derived cell lines measured in **Fig. 1D** can be mainly explained by not only a higher proportion of late S and G_2-phase cells in MiaPACA-2 cells but above all by a high presence of TRIP12 in the nucleus of cells in early and late G_1 phase.

The variation in TRIP12 protein expression during the cell cycle in TRIP12 low-expressing BxPC-3 and TRIP12 high-expressing MiaPACA-2 cells was confirmed using cell populations enriched in late G_1, early S- and G_2-phases **(Fig. 5D and 5E)**. This variation was not observed at the mRNA level in the same enriched population **(Fig. 5F)**. Indeed, *Trip12* mRNA level remains constant in the different enriched cell populations which it is not the case for the *Cyclin B1* mRNA that is known to be increased in G_2 phase.

6. Nuclear export and the deubiquitinase USP7 implication in TRIP12 cell cycle regulation.

Although we showed that TRIP12 protein is tightly regulated during the cell cycle, the mechanisms involved remained unexplained. Interestingly, we noticed a cytoplasmic localization of TRIP12 in 20.6% of BxPC-3 and in 8.2 % of Capan-1 cells in early G_1 phase. The early G_1-TRIP12 cytoplasmic localization was not observed in any phases in the other cell lines **(Fig. 6A and 6B)**. This observation suggested the requirement of a nuclear export of TRIP12 into the cytoplasmic compartment for a subsequent degradation. This hypothesis was verified by a treatment of BxPC-3 and Capan-1 with the CRM1-inhibitor leptomycin B that significantly increases the percentage of TRIP12 nuclear positive cells in early G_1 cells **(Fig. 6C)**. These results are in favor of rapid degradation of TRIP12 in early G_1 phase in low expressing cell lines (BxPC-3 and Capan-1). In contrast, TRIP12 protein expression persists in the nucleus of early G_1, late G_1 and in some extent in early S phase in TRIP12 moderate and high expressing cell lines such as Capan-2, PANC-1 and MiaPACA-2.

It is also reported that TRIP12 protein stability is controlled by the deubiquitinase USP7 (Ubiquitin Specific Peptidase 7) in different cell lines (**Cai et al. 2015; Georges et al. 2018**). Immunofluorescence analysis revealed that the USP7 protein is more frequently present in the nucleus of MiaPACA-2 cells in early G_1 and G_1 phase comparatively to BxPC-3 cells **(Fig. 6D)**. In parallel, we measured the effect of a USP7 pharmacological inhibition **(Fig. 6E)** or a siRNA-depletion. We previously ensured that the different treatments did not dramatically modify the cell cycle distribution **(Suppl Fig. S8)**. In contrast, they lead to a significant decreased expression of TRIP12, the level of CHK1 (Checkpoint Kinase 1), a well-known USP7 target being used as a positive control **(Alonso-de Vega,**

Martín, and Smits 2014) (Fig. 6E). Altogether, these results suggest that USP7 presence in the nucleus participates in the cell cycle regulation of TRIP12 in PDAC-derived cell lines.

7. TRIP12 protein expression modulates drug sensitivity of PDAC-derived cell lines.

We further decided to study the consequences of TRIP12 expression variation in PDAC-derived cell lines. TRIP12 was reported to inhibit DNA damage repair involving different molecular mechanisms (RNF168 and PARP1) **(Gudjonsson et al. 2012; Gatti et al. 2020)**. Interestingly, data obtained from Genomics of Drug Sensitivity in Cancer website show that TRIP12-high expressing MiaPACA-2 cells are the more sensitive to a multitude of DNA damage causing-drugs comparatively to the TRIP12-low expressing Capan-1 and BxPC-3 cells suggesting that TRIP12 expression level might participate to chemotherapy sensitivity **(Fig. 7A)**. We confirmed this hypothesis by demonstrating that a depletion of TRIP12 decreases the sensitivity of PANC-1 and MiaPACA-2 cells to increasing doses of doxorubicin **(Fig. 7B)**. This result suggests that TRIP12 expression level in PDAC-derived cells could be a potential indicator of chemosensitivity.

DISCUSSION.

The E3 ubiquitin ligase TRIP12 has been involved in several important biological processes altered in cancers **(Brunet et al. 2020)**. In this study, we unveil a high heterogeneity of TRIP12 expression within PDAC samples. Data available in human Protein Atlas (www.proteinatlas.org) support our findings. We also measured a high heterogeneity of TRIP12 expression within PDAC-derived cell lines which provided us relevant cellular models to elucidate to causes of TRIP12 protein heterogeneity. Interestingly, we found that the cell lines with the lowest TRIP12 expression level (BxPC-3 and Capan-1) also display the lowest histological grade **(Sipos et al. 2003)** and growth rates. Subsequently, we showed that, TRIP12 is necessary for PDAC-derived cell growth. Indeed, the depletion of TRIP12 considerably reduces the growth capacity of TRIP12-moderate and high expression PANC-1 and MiaPACA-2 cells, respectively. Transcriptomic approaches demonstrated that TRIP12 depletion dramatically repressed the expression genes targeted by the transcription factor E2F. It is known that E2F transcription family controls the expression of genes implicated in G_1-S and G_2/M transition **(Bracken et al. 2004)**. More interestingly, our analysis revealed that TRIP12 depletion impacts more specifically the expression of E2F-target genes involved in G_2-M transition such as SMC4, Aurora A/B suggesting that TRIP12 participates in the proper expression of genes necessary for G_2-M transition. This observation parallels with the fact that TRIP12 expression is tightly regulated during the cell cycle **(Larrieu et al. 2020)**. Indeed, TRIP12 is absent in the nucleus of cells in late G_1 and early S phases. Its nuclear expression dramatically increases in late S late to reach a maximum in G_2 phase. Therefore, it is likely that TRIP12 participates more specifically to the expression of genes necessary for the transition G_2-M. The next issue will be to elucidate whether TRIP12 is directly or indirectly implicated in the regulation of this subset of genes. Is it by directly interacting with chromatin at the E2F sites and/or by controlling the stability of a key-protein that directly controls E2F genes?

Then, we took advantage of our PDAC-derived cellular models to decipher the mechanisms responsible to the heterogeneity of TRIP12 expression. We determined that *Trip12* mRNA level is controlled by the activity a bidirectional promoter that also controls *FbxO36* (F-box Only protein 36) mRNA level and correlated in some extent to TRIP12 protein level. Bidirectional promoters are often used by organisms to co-regulated genes implicated in the same biological processes **(Wakano et al. 2012)**. Although FBXO36 protein functions are largely unknown, Fbx protein family is implicated SCF (SKP, Cullin, F-box containing complex) degradation complex **(Kipreos and Pagano 2000)**. We further discovered that highly conserved regions within *Trip12/Fbx036* promoter participate to its maximal transcriptional activity. Bioinformatics analysis revealed the putative binding sites of numerous transcription factors such as PDX1, HNF1 (Hepatic Nuclear Factor) (Data not shown). The identification of *Trip12/FoxO36* promoter-regulatory transcription factors in PDAC-derived cell lines might provide precious information on Trip12 mRNA regulation. Although we observed a variation in Trip12 mRNA expression within the PDAC-derived cell lines that correlated with TRIP12 protein expression, this variation could not totally explain the level of TRIP12 protein in the different cell lines.

Therefore, we investigated other mechanisms that could explain such TRIP12 heterogeneity in PDAC-derived cell lines. We previously showed that TRIP12 protein expression is tightly regulated in the cell cycle **(Larrieu et al. 2020)**. Highly expressed in the nucleus of HelaS3 cells in late S and G_2 phases, TRIP12 rapidly disappears from the nucleus in early G_1 to become absent in late G_1 and early S phases. We observed that in low TRIP12-expressing cell lines (BxPC-3 and Capan-1), TRIP12 nuclear presence follows the same cell cycle-dependent regulation. Interestingly, we noticed that, during mitotic exit, TRIP12 is exported from the nucleus that is experimentally blocked by a CRM1 (Chromosomal Maintenance 1)-inhibitor, the leptomycin B. The localization of TRIP12 in the cytoplasm in a subset of early G_1 cells suggest a rapid degradation of TRIP12 in the cytoplasm. A similar type of regulation was reported for key-proteins such as $p27^{(Kip1)}$ that is degraded in the cytoplasm of G_1 cells by a Kip1 ubiquitination-promoting complex upon CRM1 mediated-nuclear export **(Kamura et al. 2004)**. In contrast, in moderate and high TRIP12 expressing cell lines, we did not observe a cytoplasmic localization of TRIP12 but rather a high presence of TRIP12 in the nucleus of late G_1 cells suggesting a default of nuclear export in these cell lines. Despite the presence of a putative nuclear export sequence

(NES) (aa 900 aa/ELM resource), putative KEN box (aa 1496-1570/UniProt resource) and Destruction boxes (aa 859–867 and aa 1546–1554/ELM resource), the molecular mechanisms that control TRIP12 nuclear export in early G_1 and degradation in the cytoplasm remain to be discovered. Post-translational modifications are likely implicated in this process although we cannot exclude that a protein-protein interaction with a nuclear partner retains TRIP12 in the nucleus like it is the case for another ubiquitin ligase BRCA1 (Breast Cancer protein 1), that is maintained in the nucleosol by the association with the protein BARD1 (BRCA1-associated RING domain protein 1) **(Fabbro et al. 2002)**. Moreover, we showed that the deubiquitinase USP7 might participate in the TRIP12 cell cycle regulation. Indeed, we can speculate that the presence of USP7 in the nucleus of early G_1-phase PDAC cells stabilizes TRIP12 and retains it in the nuclear compartment.

In summary, our study demonstrates that the heterogeneity of TRIP12 expression in PDAC-derived cell lines is explained by a combination of different levels of regulation. A remaining question is whether this variation in TRIP12 cell cycle regulation is also observed in primary tumors. In any case, it is important to be cautious with *Trip12* mRNA level in biological tissues for clinical investigation as it may not reflect the level of TRIP12 protein.

Several studies have reported the implication of TRIP12 in the control of DNA damage repair. However, the mechanisms involved and the consequences on chemotherapy sensitivity greatly depend of the cellular context, the TRIP12 substrates and the type of DNA damage inducers. For instance, TRIP12 was initially shown to repress NHEJ-mediated repair capacity (and HR in a lower extent) by triggering the degradation of the ubiquitin ligase RNF168 **(Gudjonsson et al. 2012)**. In this study, a depletion of TRIP12 decreased the sensitivity of cells to irradiation. In contrast, Gatti *et al.* demonstrated that, in HR and BRCA1/2 proficient cells, TRIP12 regulates PARP1 turnover which is implicated in DNA repair and genome stability. In this context, the authors showed that a TRIP12 loss increases the sensitivity of cancer cells to PARP inhibition in a PARP1 dependent manner **(Gatti et al. 2020)**. The protein FBW7 (F-Box/WD repeat-containing protein 7) is a substrate adaptor for the E3 ubiquitin ligase complex SKP1-CUL1-F-Box (SCF) that targets several oncoproteins for degradation. FBW7 acts as a tumor suppressor genes and is significantly mutated in pancreatic carcinogenesis **(Zhang et al. 2016)**. A recent study showed that TRIP12 enhances the degradation of FBW7 by branched K11-linked ubiquitination. In this case, a depletion of TRIP12 leads to FBW7-dependent downregulation of MCL1 (Myeloid Cell Leukemia 1) protein and enhanced sensitivity to taxol of cancer cells **(Khan et al. 2021)**. In our study, we observed that a high expression of TRIP12 PDAC-derived cell lines is associated to a higher sensitivity to different types of DNA damage-inducing drugs. Inversely, a depletion of TRIP12 decreases their sensitivity to doxorubicin. Moreover, we demonstrate that a high expression of TRIP12 is mostly due to its presence in late G_1 cells. We can therefore speculate that the aberrant presence of TRIP12 in G_1 cells could inhibit their capacity of NHEJ-mediated DNA damage repair. Overall, TRIP12 protein expression could be used as a potential indicator of drug sensitivity in a pancreatic cancer context.

In addition to its function in DNA damage response, TRIP12 is also described as a regulator of key-proteins involved in the control of cell proliferation (*i.e.*: p14/Arf, p53) and differentiation (i.e.: SOX6, PTF1A). Our study show that TRIP12 protein expression is associated with the growth capacity and the histological grade of PDAC-derived cell lines. Moreover, TRIP12 is implicated in the regulation of chromatin remodeling, a major biological process in pancreatic cancer initiation **(Hank and Liss 2018)**. It would be of interest to determine whether the heterogeneity of TRIP12 expression could influence the initiation and/or the progression of pancreatic cancer. For this purpose, the establishment of murine model of pancreatic carcinogenesis with a specific deletion of Trip12 gene in the pancreas could help to address this important question.

ACKNOWLEDGEMENTS.
We thank the platform ANAPATH (IUCT-O), the animal facility (UMS 006) and the histology platform (I2MC). We also thank the imaging, cytometry and geno-transcriptomics platforms of the Cancer Research Center of Toulouse (CRCT). We thank the GET-TRI platform (INRAE-Saint Martin du Touch). We thank Drs F. Larminat (Institute of Pharmacology and Structural Biology of Toulouse), A. Cammas, JS. Hoffmann research groups (CRCT) for ample scientific discussions and D. Arvanitis (Institute of Metabolic and Cardiovascular Diseases (I2MC)) for English proof reading of the manuscript.

Fundings: This project was funded by the Fondation Toulouse Cancer Santé (TCS 2018CS079) and the Ligue Régionale contre le Cancer-Midi-Pyrénées. M. BRUNET and C. VARGAS PhD fellowship was funded by the University Paul Sabatier of Toulouse and the Ligue Nationale contre le Cancer. D. LARRIEU PhD fellowship was funded by the Ligue Nationale contre le Cancer.

I declare that the authors have no competing interests or other interests that might be perceived to influence the results and/or discussion reported in this paper.

DATA AVAILABILTY.
The datasets generated during and/or analyzed during the current study are available from the corresponding author on reasonable request.

AUTHOR CONTRIBUTIONS STATEMENT.

M.B.: acquisition, analysis and interpretation of data, writing of the manuscript
D.L.: acquisition, analysis and interpretation of data
C.V.: acquisition, analysis and interpretation of data
N.H.: acquisition of data
L.L.: acquisition of data and analysis
L.D.: acquisition of data and analysis
J.L.: acquisition of data
J.B.: acquisition of data
H.L.: acquisition of data
C.L.: acquisition of data
J.S.: substantial contributions to the conception and analysis
P.C.: substantial contributions to the conception
M.D.: substantial contributions to the conception and design of the work
J.T.: conception and design of the work, acquisition, analysis and interpretation of data, writing of the manuscript

FIGURE LEGENDS.

Figure 1: Heterogeneous expression of TRIP12 protein in human pancreatic tumors and PDAC-derived cell lines.

A- Representative images obtained by immunocytochemistry on tumor microarray of human pancreatic tumors displaying a weak, moderate and strong TRIP12 expression. The insets emphasize on cancerous cells.
B- TRIP12 protein nuclear expression was visualized by immunofluorescence in five human PDAC-derived cell lines. The different cell lines were fixed during exponential phase of growth. Nuclei were counterstained with DAPI.
C- The percentage of nuclear TRIP12-positive cells was quantified in five human PDAC-derived cell lines using Fiji software. The quantification was performed on over than 300 cells obtained from three separate experiments. Results are expressed as mean (±SEM).
D- TRIP12 protein expression in five PDAC-derived cell lines was determined by Western blot analysis. GAPDH protein level was used for normalization. The image is representative of at least three separate experiments. The quantification is expressed as the mean (±SEM) of three different experiments.
E- Cell growth of PDAC-derived cell lines was determined by cell counting every 24h during 72h. The results are expressed as growth rate compared to T=0h and represent the mean (±SEM) of three separate experiments.

Figure 2: The depletion of TRIP12 affects the growth of TRIP12 high expressing PDAC-derived cells.

A- Trip12 mRNA level in PANC-1 and MiaPACA-2 cells stably expressing three different shRNAs directed against Trip12 mRNA (ShTRIP12#1, #2, #3) was measured by qRT-PCR and compared to its level in PANC-1 and MiaPACA-2 expressing a control shRNA (ShScr). GAPDH, β-Actin and cyclophilin A mRNA levels were used for normalization. Results are expressed as a percentage (±SEM) of Trip12 mRNA level in PANC-1 and MiaPACA-2 control cells (set as 100%) and are the mean of at least four separate experiments. * indicates a p value < 0.05.
B- TRIP12 protein level in PANC-1 and MiaPACA-2 cells stably expressing three different shRNAs directed against Trip12 mRNA (ShTRIP12#1, #2, #3) was measured by Western blot analysis and compared to its level in PANC-1 and MiaPACA-2 expressing a control shRNA (ShScr). PCNA protein level was used for normalization. The image is representative of three separate experiments. The graphs represent the quantification of protein levels. The results are expressed as a percentage (±SEM) of TRIP12 protein level in PANC-1 and MiaPACA-2 control cells (set as 100%) and are the mean of at least three separate experiments. * indicates a p value < 0.05.
C- Cell growth rate of TRIP12 depleted-PANC-1 and MiaPACA-2 was determined by cell counting. Cell were seeded at 5.10^5 cells/well and counted every 24h for 72h. Results are expressed as mean (±SEM) compared to t=0h (set as 1). * indicates a p value < 0.05.
D- Colony formation assay was performed TRIP12 depleted-PANC-1 and MiaPACA-2. Cells were seeded at 10^3 cells per 10 cm-plate. After 9-14 days, colonies were stained using Cristal violet. The graphs represent the quantification of colony number using Fiji software. The results are expressed as mean (±SEM) compared to obtained from at least three separate experiments. * indicates a p value < 0.05.
E- In vivo growth of TRIP12 depleted and control MiaPACA-2 cells was determined after orthotopic implantation in the pancreas of Nude mice. Gaussia Luciferase (GLuc) stably expressing MiaPACA-2 cells were stably transfected with ShTRIP12 or Scr shRNA using lentiviral transduction. Luciferase activity in blood was measured every 4-6 days during 29 days. The results represent the luciferase activity (RLU) in four mice per conditions. The inset represents the level of TRIP12 protein in ShScr and ShTRIP12 GLuc MiaPACA-2 cells determined by Western blot analysis. PCNA protein level was used as loading control.

F- Weight and volume of ShScr and ShTRIP12 GLuc MiaPACA-2 tumors were measured after 29 days. The results are expressed as mean (±SEM) of four tumors for each conditions.

Figure 3: TRIP12 depletion affects preferentially the expression of genes implicated in G_2/M transition.

A- Graphical representation of E2F target, G_2/M checkpoint, c-myc targets V1 and V2 gene set enrichments after TRIP12 depleted-PANC-1 and MiaPACA-2 cell transcriptomic analysis using GSEA software with a nominal p value <0.001 and a false discovery rate (FDR) < 0.001. NES Stands for Normalized Enrichment Score.
B- Venn diagram representation of E2F target, G_2/M checkpoint, c-myc targets V1 and V2 leading edge genes in TRIP12-depleted PANC-1 and MiaPACA-2 cell transcriptomic analysis.
C- *Birc5*, *Tmpo* and *Tk1* mRNA expression in PANC-1 cells stably expressing three different shRNAs directed against Trip12 mRNA (ShTRIP12#1, #2, #3) was measured by qRT-PCR and compared to its level in PANC-1 expressing a control shRNA (ShScr). GAPDH, β-Actin and cyclophilin A mRNA levels were used for normalization. Results are expressed as a percentage of Trip12 mRNA level in PANC-1 control cells (set as 100%) and were obtained from three separate experiments.
D- Physical interaction networks of proteins encoded by the E2 target gene set (n=195, left panel) and the TRIP12 depleted-MiaPACA-2 E2F target leading edge genes (n=113, right panel). The analysis was performed using STRING software. Nodes represent proteins. The edges indicate that the proteins are part of a physical complex. The line thickness indicates the strength of data. Colored nodes represent proteins that belong to the Gene Ontology biological processes indicated on the figure.
E- Cell cycle distribution of TRIP12 depleted (ShTRIP12 #1, #2 and #3) and control (ShScr) MiaPACA-2 cells measured by flow cytometry after propidium iodide treatment. The results are expressed as percentage of cells in the different phase of the cell cycle and are the mean (±SEM) of at least four separate experiments. * a p value < 0.01.

Figure 4: A bi-directional promoter-controlled mRNA level partially explains TRIP12 protein expression heterogeneity in PDAC-derived cell lines.

A- *Trip12* mRNA expression in indicated PDAC-derived cell lines was determined by qRT-PCR using two different sets of primers. *Gapdh*, *β-Actin* and *Cyclophilin A* mRNA levels were used for normalization. Results were obtained from four separate experiments and expressed as percentage (±SEM) of hPNE control cell line (set as 100%).
B- Graphical representation of *Trip12/FbxO36* gene organization. Positions of Exon 1 (black boxes) of *Trip12* and *FbxO36* genes on human chromosome 2 (2q36) was obtained from the UCSC genome browser (genome.ucsc.edu) **(Suppl Fig. S4)**. Transcriptional start sites are represented by an arrow and (+1). Red boxes correspond to highly conserved sequences in Vertebrates determined by PhastCons analysis. The green box represents the location of a CpG island containing 150 dinucleotides CG. Primers used for bidirectional promoter cloning, bisulfite mapping and ChiP-PCR analyses are symbolized by arrows. ATG represents the translation start codon.
C- Measurement of transcriptional activity of Trip12/FbxO36 bidirectional promoter. Trip12/FbxO36 promoter in both orientation was inserted in Firefly luciferase reporter plasmid (top panel) and transfected in the indicated cell lines (left panel). Comparatively, unidirectional CXCR4 promoter activity was similarly measured in MiaPACA-2 cells (Right panel). Firefly luciferase activity was measured and normalized to Renilla luciferase activity. Results are expressed as percentage of activity of control plasmid (100%). They represent the mean (±SEM) of three separate experiments.
D- Enrichment of acetylated lysine 9 Histone 3 (H3K9) on *Trip12/FboxO36* bidirectional promoter was in MiaPACA-2 and Capan-1 cells was determined ChIP-PCR. The graph represents the IP/input ratio on five different loci on *Trip12/FbxO36* genomic region. The results are expressed as mean (±SEM) of three separate experiments. The position of ChIP-PCR primers (A, B, C, D and E) are illustrated in Fig. 4B.

E- Transcriptional activity *Trip12/FbxO36* promoter deletion constructs was determined in PANC-1 cells. Firefly luciferase activity was measured and normalized to Renilla luciferase activity. Results are expressed as percentage of activity of *Trip12* and *FbxO36* control plasmids (set as 100%). They represent the mean (±SEM) of three separate experiments.

Figure 5. Variation of TRIP12 cell cycle regulation in PDAC-derived cells.

A- Representative images of TRIP12 protein cellular localization during the different phases of the cell cycle in asynchronous BxPC-3, Capan-1, Capan-2, PANC-1 and MiaPACA-2 cell population. The method to categorize cells in the different phases of the cell cycle is described in **Suppl Fig. S7**. Nuclei were counterstained with DAPI.
B- The percentage of nuclear TRIP12 positive cells in the different phase of the cell cycle was determined in indicated PDAC-derived cell lines by immuno-fluorescence as described in Material and Methods section. The graph represents the percentage of TRIP12 nuclear positive cells and expressed as the mean (±SEM) obtained over more than 500 cells from at least two separate experiments.
C- The distribution of asynchronous PDAC-derived cell lines in the different phases of cell cycle was determined by immuno-fluorescence as described in Material and Methods section. The graph represents the percentage of cells and expressed as the mean (±SEM) obtained over more than 700 cells from at least two separate experiments.
D- Cell cycle distribution of BxPC-3 and MiaPACA-2 enriched cell population in G_1, Early S and G_2 phases. Cells were enriched in the cell cycle phases following indicated treatments. Enrichment level was measured by flow cytometry after propidium iodide incorporation. The graph represents the percentage of cells in the different phases of the cell cycle and are expressed as the mean (±SEM) of at least three separate experiments.
E- TRIP12 protein expression in BxPC-3 and MiaPACA-2 enriched cell population in G_1, Early S and G_2 phases was determined by Western blot analysis. CYCLIN B1 level was used control of enrichment. GAPDH level was used as loading control. The images were obtained from the same experiment and are representative of at least three separate experiments.
F- *Trip12* mRNA level in BxPC-3 and MiaPACA-2 enriched cell population in G_1, Early S and G_2 phases was determined by RT-qPCR. Two sets of primers (Exon 10-11 and Exon 35-36) were used to determine *Trip12* mRNA expression. *Gapdh*, *β-Actin* and *Cyclophilin A* mRNA levels were used for normalization. *Cyclin B1* mRNA level was used as control of enrichment. Results were obtained from at least three separate experiments and expressed as percentage (±SEM) of *Trip12* mRNA level in G_1 enriched cell population (set as 100%).

Figure 6. Nuclear export and the deubiquitinase USP7 participates in TRIP12 cell cycle regulation.

A- Representative images of TRIP12 cytoplasmic localization in BxPC-3 and Capan-1 cells in early G_1 phase by immunofluorescence. Nuclei were counterstained with DAPI.
B- Percentage of TRIP12 cytoplasmic positive PDAC-derived cells in early G_1 phase. The graph represents the mean (±SEM) of three separate experiments over more than 350 early G_1 cells.
C- Percentage of TRIP12 nuclear positive BxPC-3 and Capan-1 cells in early G_1 phase treated with leptomycin B (50 ng/ml) or a vehicle for 20h was determined by immunofluorescence. Nuclei were counterstained with DAPI. The results are expressed as mean (±SEM) of two separate experiments on over 100 cells.
D- The percentage of nuclear USP7 positive cells in the different phase of the cell cycle was determined in MiaPACA-2 and BxPC-3 cell lines by immuno-fluorescence as described in Material and Methods section. The graph represents the percentage of USP7 nuclear positive cells and expressed as the mean (±SEM) obtained over more than 200 cells from one experiment.
E- TRIP12 and USP7 protein expression in MiaPACA-2 in response to USP7 inhibition was determined by Western blot analysis. Cells treated with the USP7 inhibitor P22077 (25 µM) for 20h. CHK1 protein

level was used as a positive control. GAPDH protein level was used as loading control. The images were obtained from the same experiment and are representative of 3three different experiments.
F- TRIP12 and USP7 protein expression in MiaPACA-2 in response to USP7 depletion by siRNA was determined by Western blot analysis. MiaPACA-2 cells were double-transfected with three different siRNA (50 nM) for 48 h. CHK1 protein level was used as a positive control. GAPDH protein level was used as a loading control. The images are representative of three different experiments.

Figure 7. TRIP12 protein expression controls drug sensitivity of PDAC-derived cell lines.

A- Sensitivity expressed as the half inhibitory concentration (IC50 in µM) of 30 PDAC-derived cell lines to the indicated drugs was obtained from Genomics of Drug Sensitivity in Cancer (www.cancerxgene.org) website. The different cell lines are represented as empty circles with the exception of BxPC-3, Capan-1 and MiaPACA-2 cell lines that are represented as blue, yellow and red filled circles, respectively.
B- Doxorubicin sensitivity of TRIP12-depleted PANC-1 (left panel) and MiaPACA-2 cells (right panel) was measured by MTS assay. Cells were seeded and treated 24h later with the indicated doses of doxorubicin for 24h. The graph represents a percentage of viable cells compared to control MiaPACA-2 cells (ShScr) set as 100%. Results are expressed as mean (±SEM) obtained from at least three separate experiments.

Figure 1

A

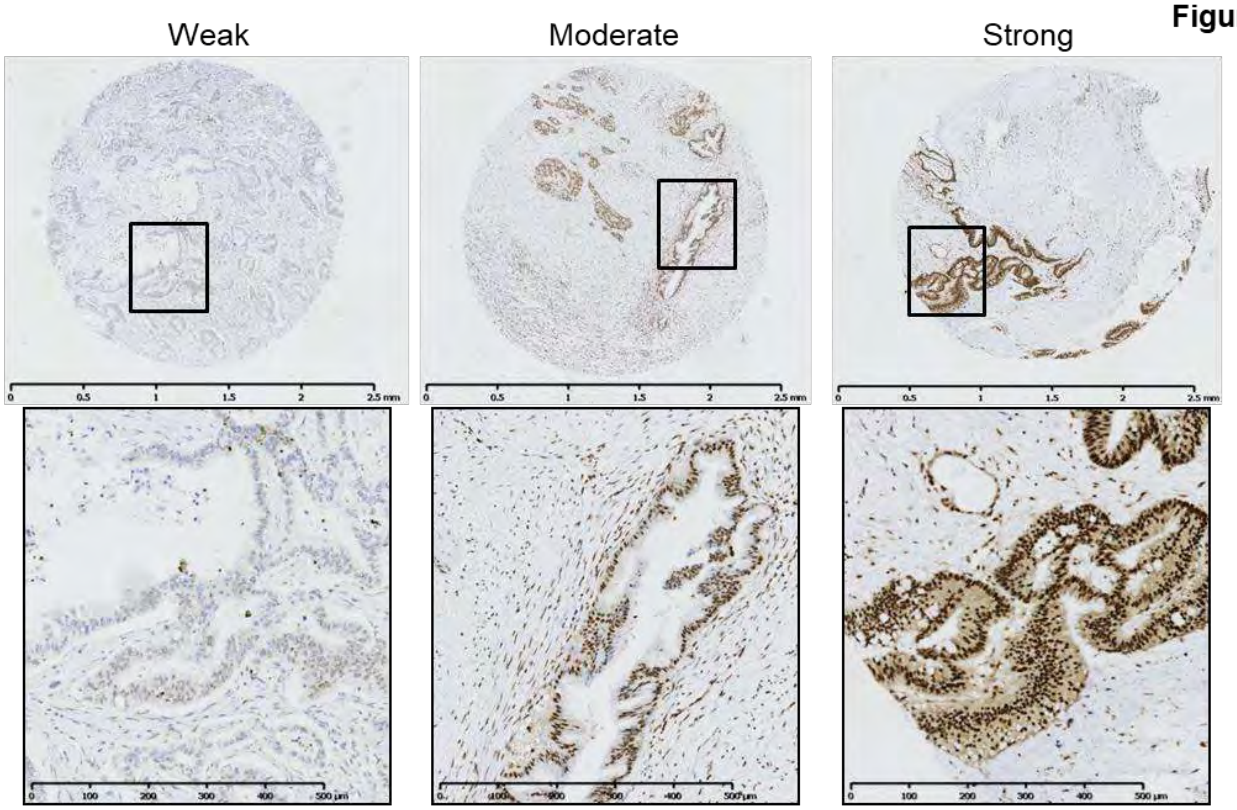

A- Representative images obtained by immunocytochemistry on tumor tissue microarray of human pancreatic tumors displaying a weak, moderate and strong TRIP12 expression. The insets emphasize on cancerous cells.

B

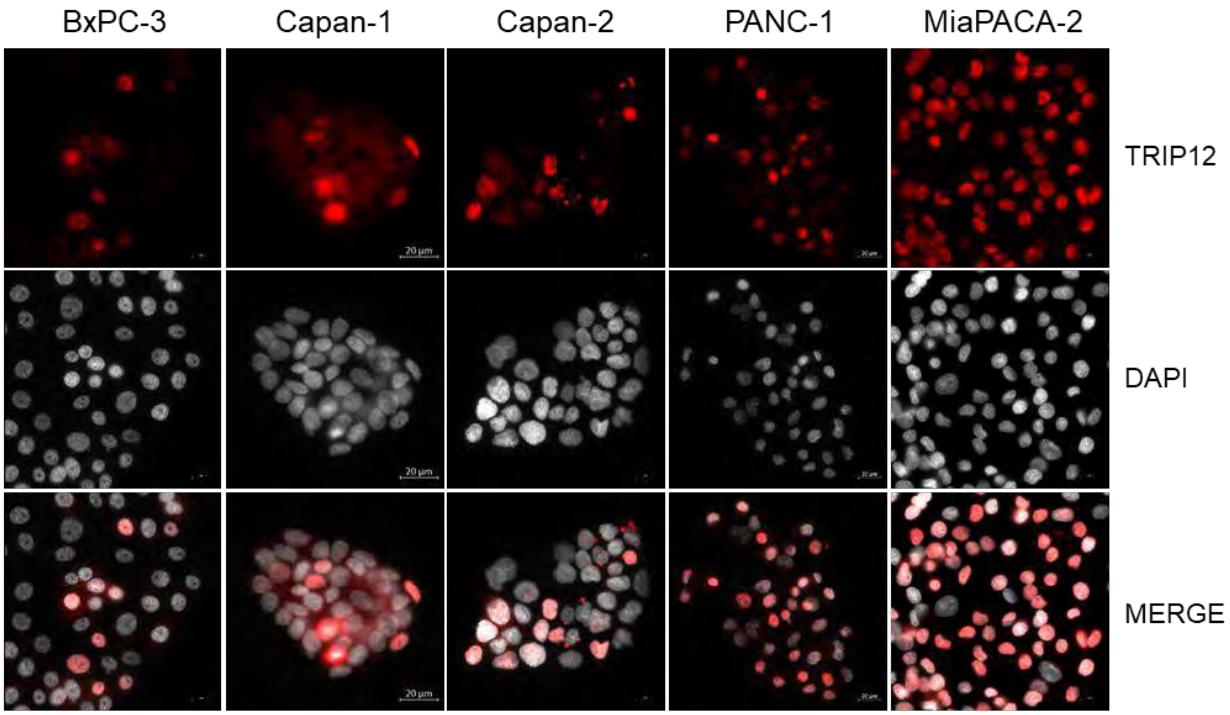

B- TRIP12 protein nuclear expression was visualized by immunofluorescence in five human PDAC-derived cell lines. The different cell lines were fixed during exponential phase of growth. Nuclei were counterstained with DAPI.

Figure 1

C

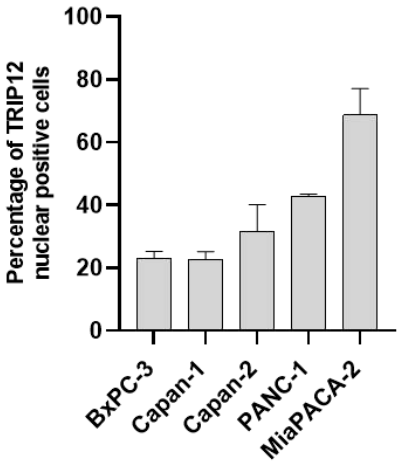

C- The percentage of nuclear TRIP12-positive cells was quantified in five human PDAC-derived cell lines using Fiji software. The quantification was performed on over than 300 cells obtained from three separate experiments. Results are expressed as mean (± SEM).

D

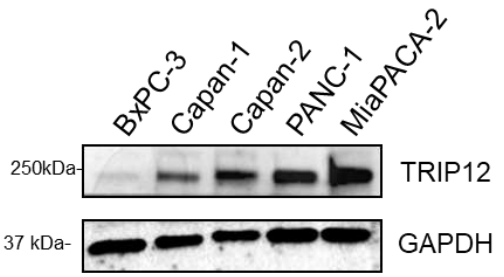

D- TRIP12 protein expression in five PDAC-derived cell lines was determined by Western blot analysis. GAPDH protein level was used for normalization. The image is representative of at least three separate experiments. The quantification is expressed as the mean (±SEM) of three different experiments.

E

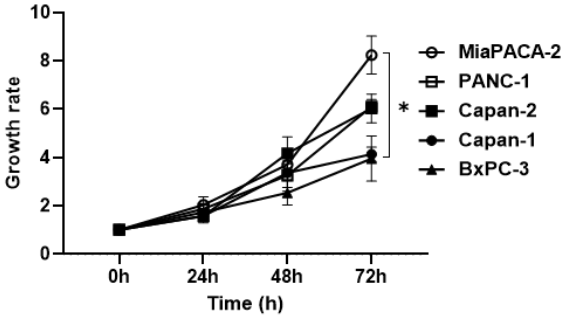

E- Cell growth of PDAC-derived cell lines was determined by cell counting every 24h during 72h The results are expressed as growth rate compared to T=0h and represent the mean (±SEM) of three separate experiments.

Figure 2

A

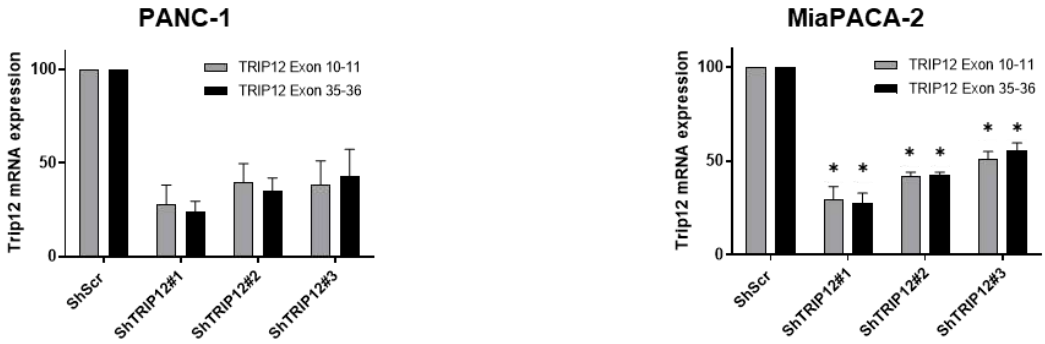

A- Trip12 mRNA level in PANC-1 and MiaPACA-2 cells stably expressing three different shRNAs directed against Trip12 mRNA (ShTRIP12#1, #2, #3) was measured by qRT-PCR and compared to its level in PANC-1 and MiaPACA-2 expressing a control shRNA (ShScr). GAPDH, β-Actin and cyclophilin A mRNA levels were used for normalization. Results are expressed as a percentage (±SEM) of Trip12 mRNA level in PANC-1 and MiaPACA-2 control cells (set as 100%) and are the mean of at least four separate experiments. * indicates a p value < 0.05.

B

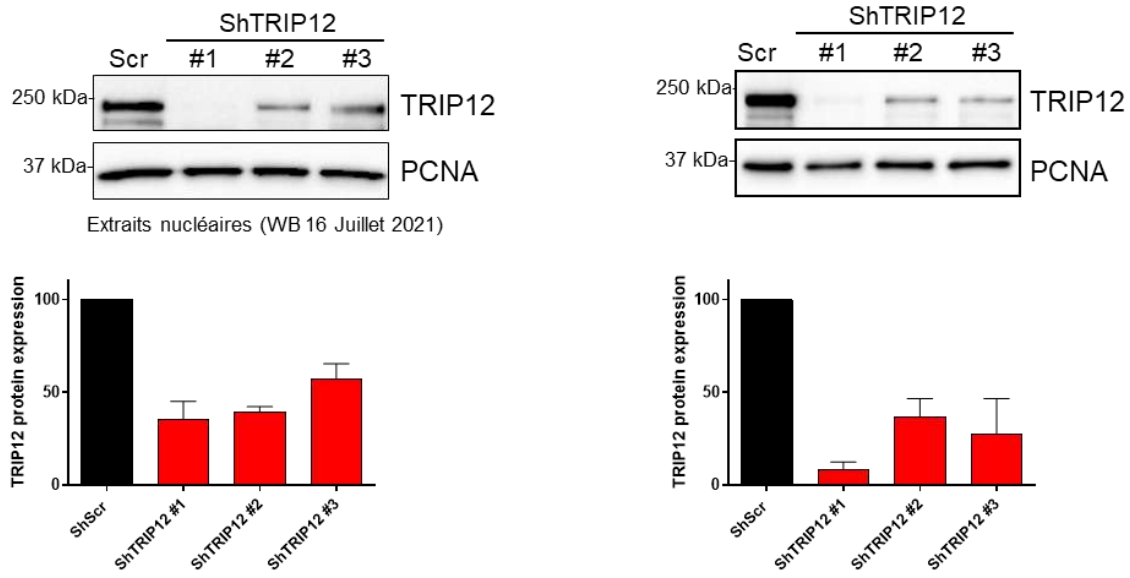

B- TRIP12 protein level in PANC-1 and MiaPACA-2 cells stably expressing three different shRNAs directed against Trip12 mRNA (ShTRIP12#1, #2, #3) was measured by Western blot analysis and compared to its level in PANC-1 and MiaPACA-2 expressing a control shRNA (ShScr). PCNA protein level was used for normalization. The image is representative of three separate experiments. The graphs represent the quantification of protein levels. The results are expressed as a percentage (±SEM) of TRIP12 protein level in PANC-1 and MiaPACA-2 control cells (set as 100%) and are the mean of at least three separate experiments. * indicates a p value < 0.05.

C

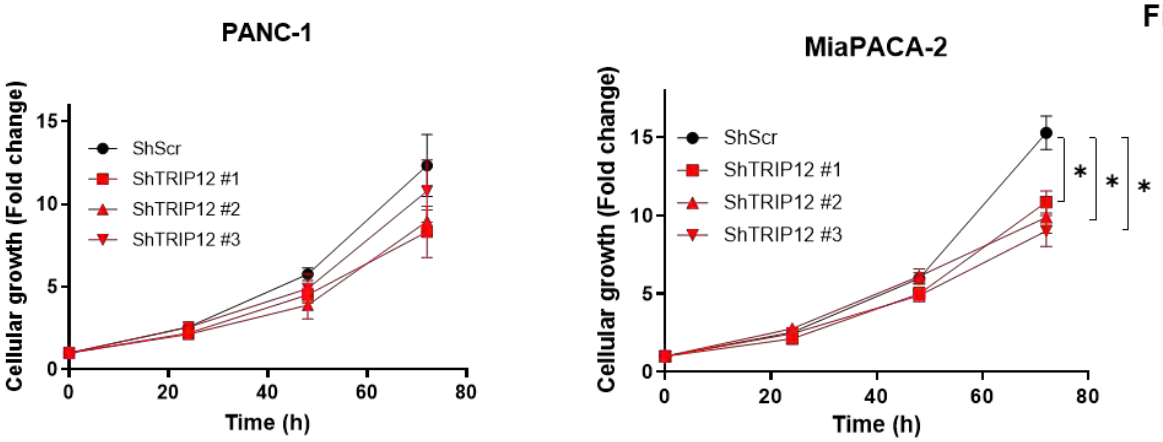

C- Cell growth rate of TRIP12 depleted-PANC-1 and MiaPACA-2 was determined by cell counting. Cell were seeded at 5.10^5 cells/well and counted every 24h for 72h. Results are expressed as mean (±SEM) compared to t=0h (set as 1). * indicates a p value < 0.05.

D

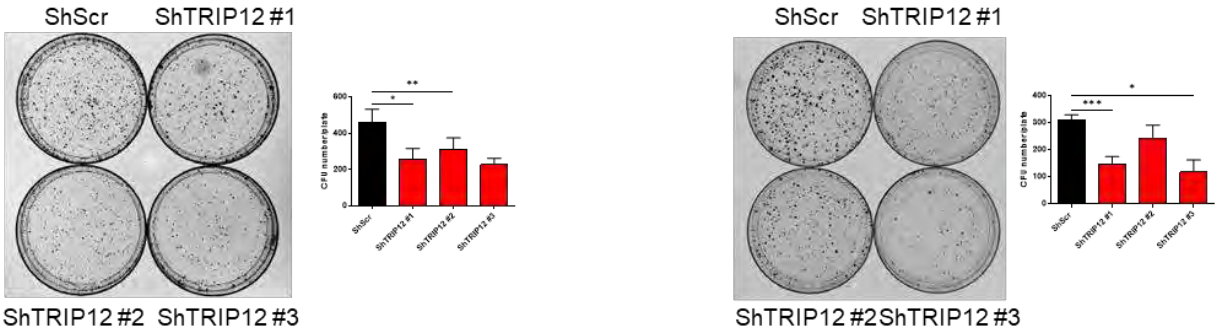

D- Colony formation assay was performed TRIP12 depleted-PANC-1 and MiaPACA-2. Cells were seeded at 10^3 cells per 10 cm-plate. After 9-14 days, colonies were stained using Cristal violet. The graphs represent the quantification of colony number using Fiji software. The results are expressed as mean (±SEM) compared to obtained from at least three separate experiments. * indicates a p value < 0.05.

Figure 2

E

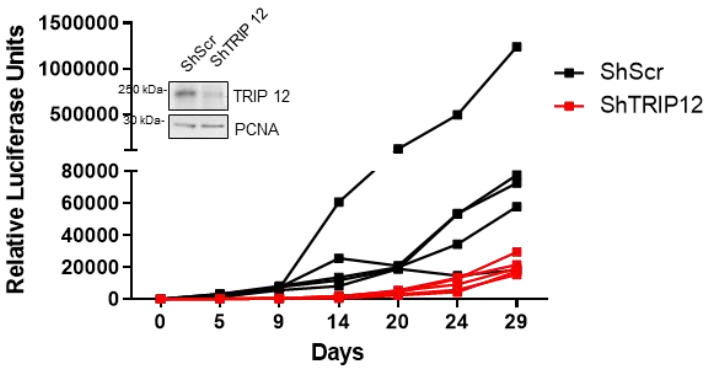

E- In vivo growth of TRIP12 depleted and control MiaPACA-2 cells was determined after orthotopic implantation in the pancreas of Nude mice. Gaussia Luciferase (GLuc) stably expressing MiaPACA-2 cells were stably transfected with ShTRIP12 or Scr shRNA using lentiviral transduction. Luciferase activity in blood was measured every 4-6 days during 29 days. The results represent the luciferase activity (RLU) in four mice per conditions. The inset represents the level of TRIP12 protein in ShScr and ShTRIP12 GLuc MiaPACA-2 cells determined by Western blot analysis. PCNA protein level was used as loading control.

F

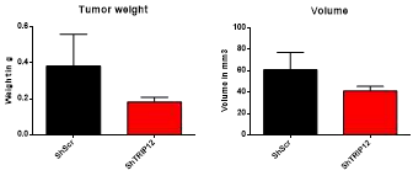

F- Weight and volume of ShScr and ShTRIP12 GLuc MiaPACA-2 tumors were measured after 29 days. The results are expressed as mean (±SEM) of four tumors for each conditions.

Figure 3

A

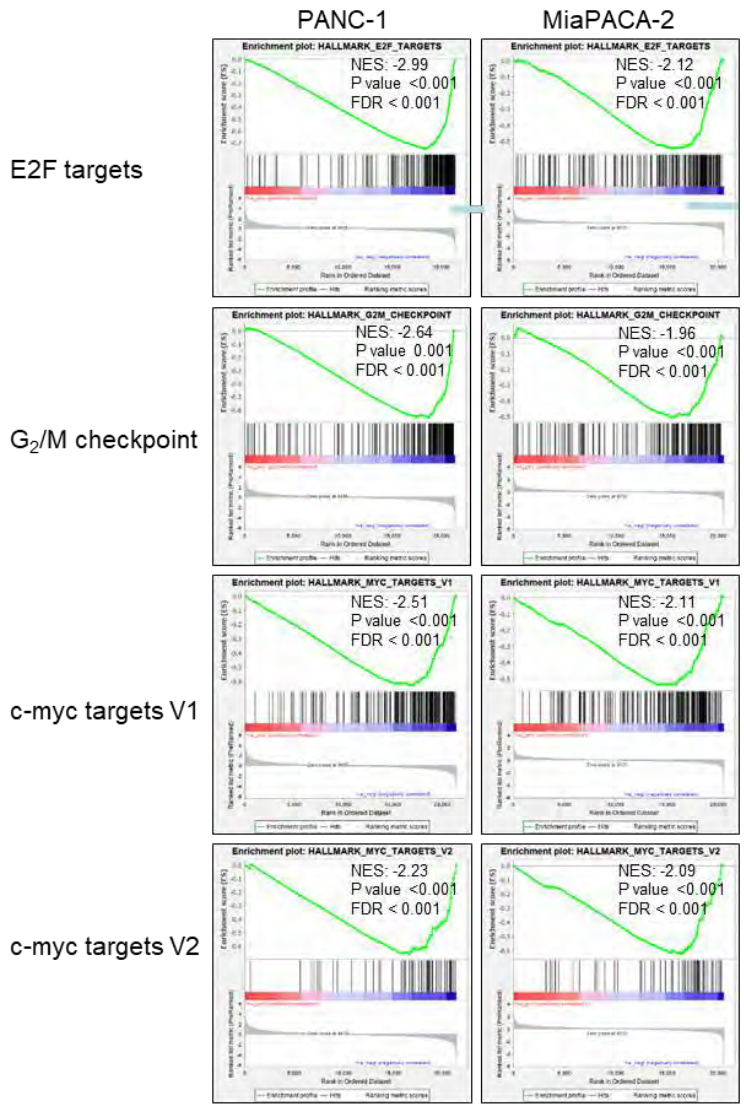

B

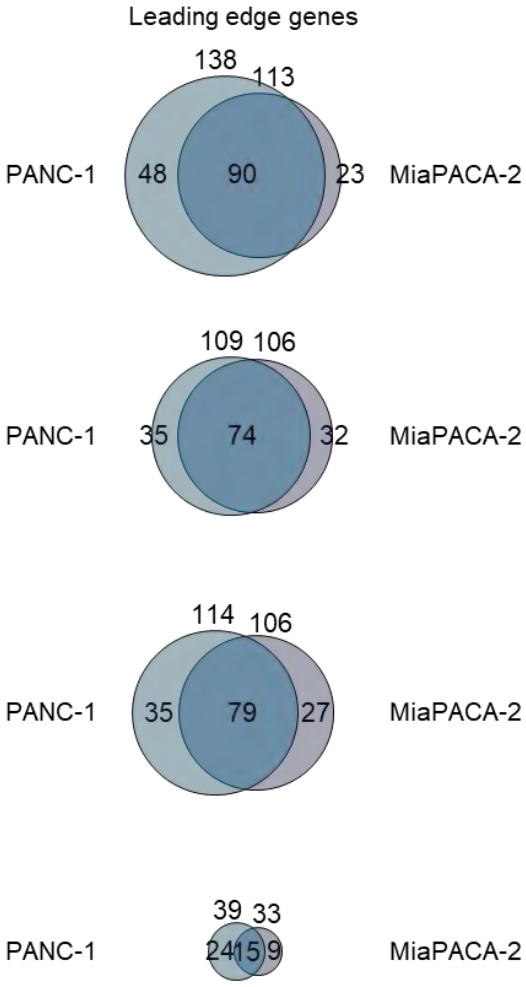

A- Graphical representation of E2F target, G_2/M checkpoint, c-myc targets V1 and V2 gene set enrichments after TRIP12 depleted-PANC-1 and MiaPACA-2 cell transcriptomic analysis using GSEA software with a nominal p value <0.001 and a False Discovery Rate (FDR) < 0.001. NES Stands for Normalized Enrichment Score.

B- Venn diagram representation of E2F target, G_2/M checkpoint, c-myc targets V1 and V2 leading edge genes in TRIP12-depleted PANC-1 and MiaPACA-2 cell transcriptomic analysis.

C

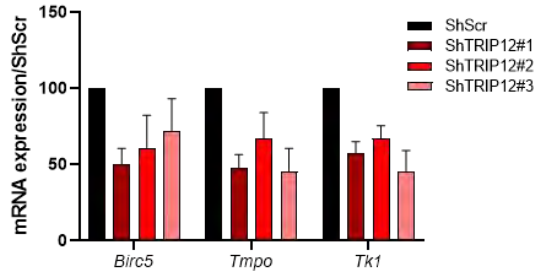

C- Birc5, Tmpo and Tk1 mRNA expression in PANC-1 cells stably expressing three different shRNAs directed against Trip12 mRNA (ShTRIP12#1, #2, #3) was measured by qRT-PCR and compared to its level in PANC-1 expressing a control shRNA (ShScr). GAPDH, β-Actin and cyclophilin A mRNA levels were used for normalization. Results are expressed as a percentage of Trip12 mRNA level in PANC-1 control cells (set as 100%) and were obtained from three separate experiments.

Figure 3

D

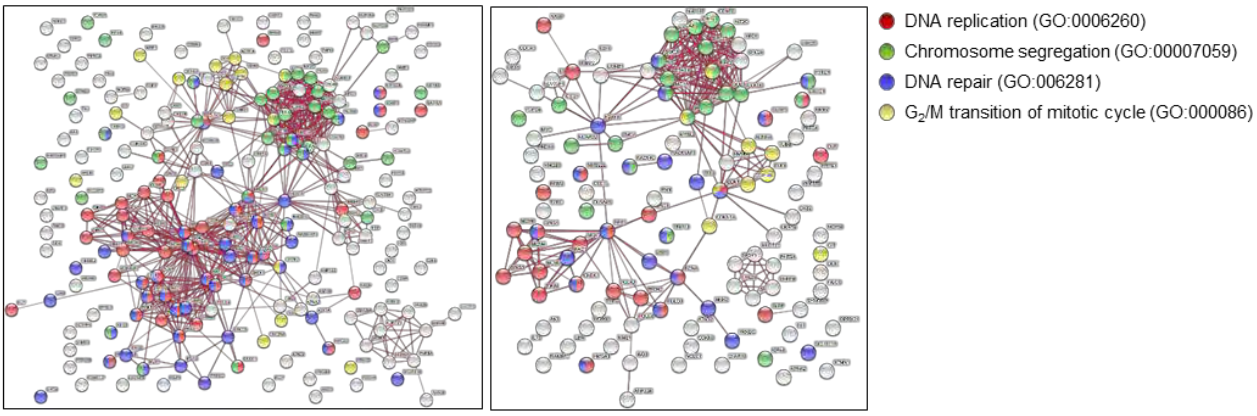

D- Physical interaction networks of proteins encoded by the E2 target gene set (n=195, left panel) and the TRIP12 depleted-MiaPACA-2 E2F target leading edge genes (n=113, right panel). The analysis was performed using STRING software. Nodes represent proteins. The edges indicate that the proteins are part of a physical complex. The line thickness indicates the strength of data. Colored nodes represent proteins that belong to the Gene Ontology biological processes indicated on the figure.

E

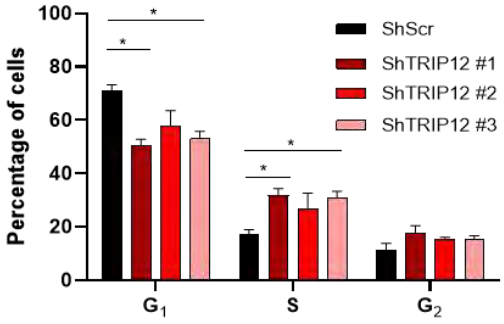

E- Cell cycle distribution of TRIP12 depleted (ShTRIP12 #1, #2 and #3) and control (ShScr) MiaPACA-2 cells measured by flow cytometry after propidium iodide treatment. The results are expressed as percentage of cells in the different phase of the cell cycle and are the mean (±SEM) of at least four separate experiments. ** and *** indicate a p value < 0.01 and 0.005, respectively.

Figure 4

A

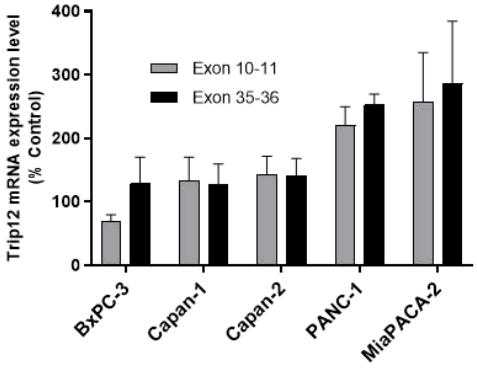

A- Trip12 mRNA expression in indicated PDAC-derived cell lines was determined by qRT-PCR using two different sets of primers. *Gapdh*, *b-Actin* and *Cyclophilin A* mRNA levels were used for normalization. Results were obtained from four separate experiments and expressed as percentage (±SEM) of hPNE control cell line (set as 100%).

B

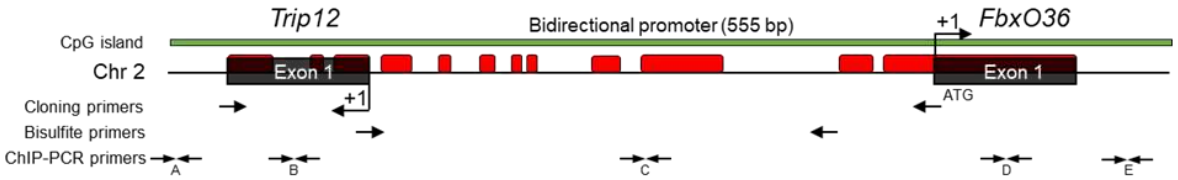

B- Graphical representation of *Trip12/FbxO36* gene organization. Positions of Exon 1 (black boxes) of *Trip12* and *FbxO36* genes on human chromosome 2 (2q36) was obtained from the UCSC genome browser (genome.ucsc.edu)**(See Suppl Fig. S4)**. Transcriptional start sites are represented by an arrow and (+1). Red boxes correspond to highly conserved sequences in Vertebrates determined by PhastCons analysis. The green box represents the location of a CpG island containing 150 dinucleotides CG. Primers used for bidirectional promoter cloning, bisulfite mapping and ChiP-PCR analyses are symbolized by arrows. ATG represents the translation start codon.

C

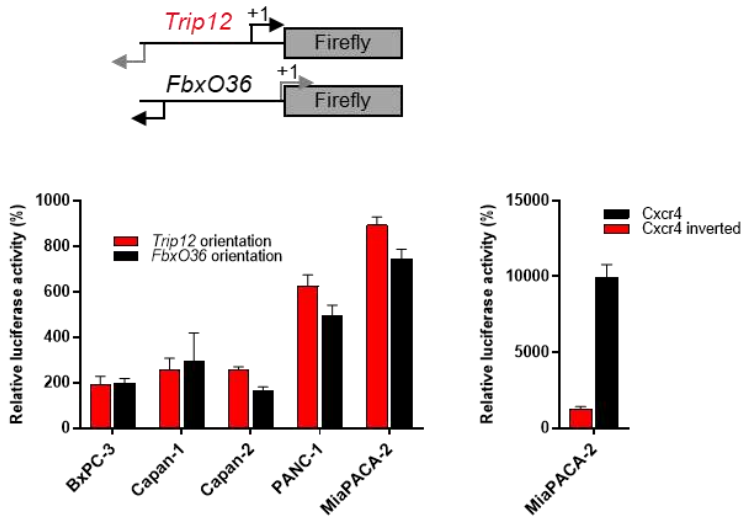

C-Measurement of transcriptional activity of Trip12/FbxO36 bidirectional promoter. Trip12/FbxO36 promoter in both orientation was inserted in Firefly luciferase reporter plasmid (top panel) and transfected in the indicated cell lines (left panel). Comparatively, unidirectional CXCR4 promoter activity was similarly measured in MiaPACA-2 cells (Right panel) . Firefly luciferase activity was measured and normalized to Renilla luciferase activity. Results are expressed as percentage of activity of control plasmid (100%). They represent the mean (±SEM) of three separate experiments.

D

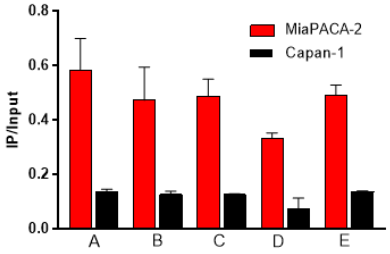

D- Enrichment of acetylated lysine 9 Histone 3 (H3K9) on *Trip12/FboxO36* bidirectional promoter was in MiaPACA-2 and Capan-1 cells was determined ChIP-PCR. The graph represents the IP/input ratio on five different loci on *Trip12/FbxO36* genomic region. The results are expressed as mean (±SEM) of three separate experiments. The position of ChIP-PCR primers (A, B, C, D and E) are illustrated in Fig. 4B.

E

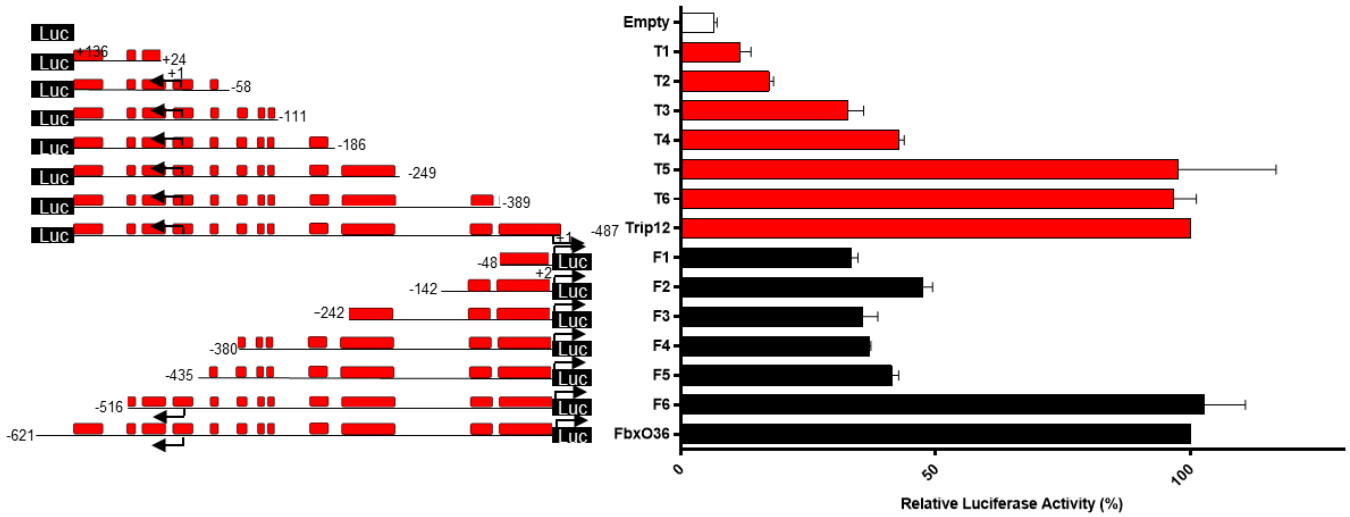

E- Transcriptional activity *Trip12/FbxO36* promoter deletion constructs was determined in MiaPACA-2 cells. Firefly luciferase activity was measured and normalized to Renilla luciferase activity. Results are expressed as percentage of activity of *Trip12* and *FbxO36* control plasmids (set as 100%). They represent the mean (±SEM) of three separate experiments.

Figure 5

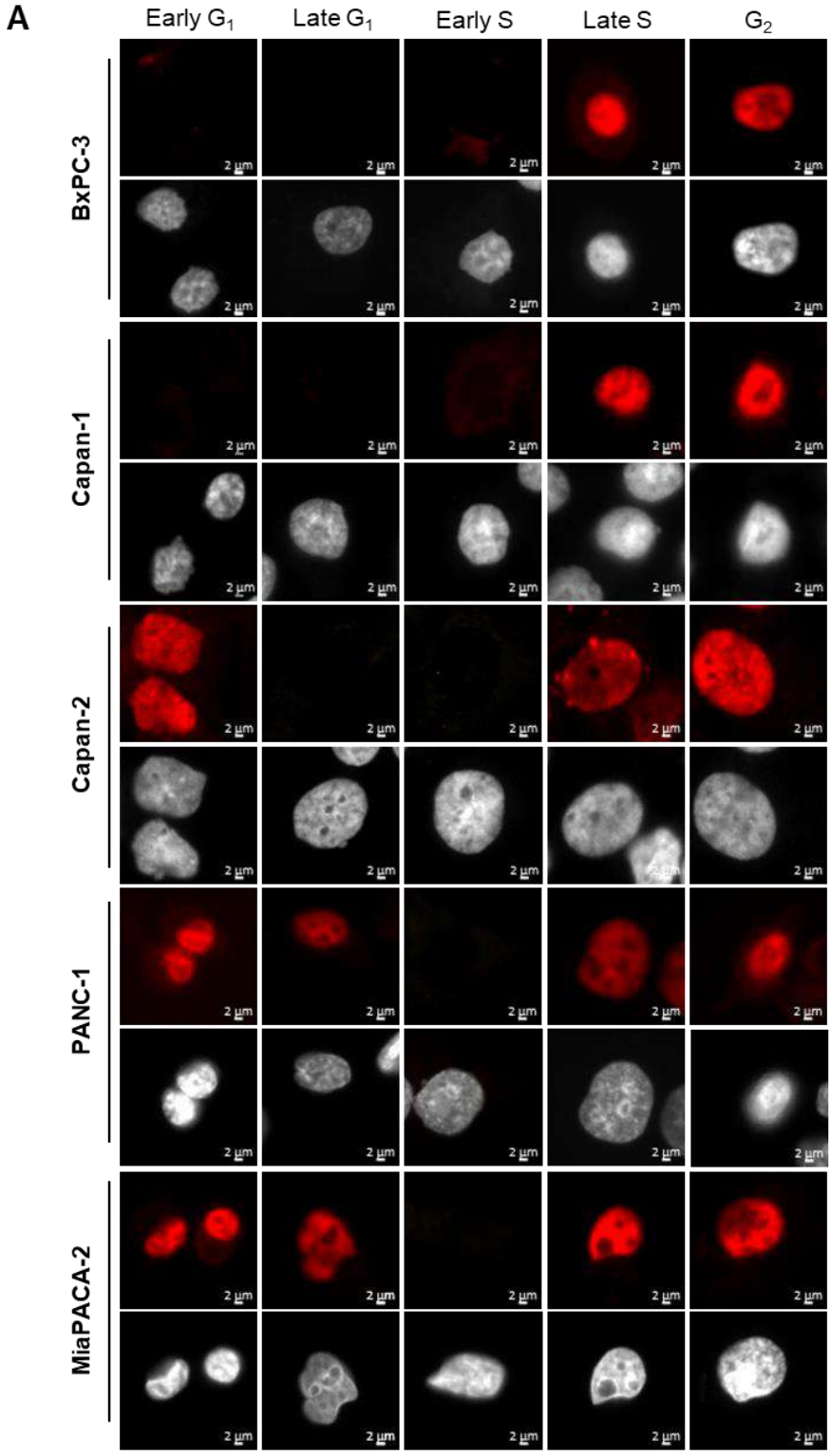

A- Representative images of TRIP12 protein cellular localization during the different phases of the cell cycle in asynchronous BxPC-3, Capan-1, Capan-2, PANC-1 and MiaPACA-2 cell population. The method to categorize cells in the different phases of the cell cycle is described in **Suppl Fig. S7**. Nuclei were counterstained with DAPI.

Figure 5

B

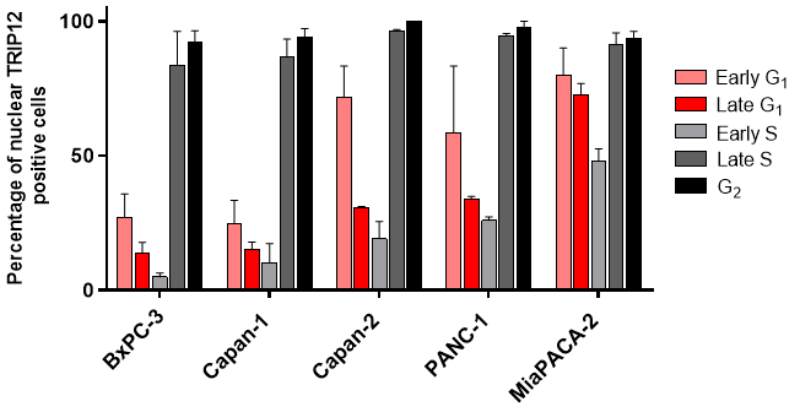

B- The percentage of nuclear TRIP12 positive cells in the different phase of the cell cycle was determined in indicated PDAC-derived cell lines by immuno-fluorescence as described in Material and Methods section. The graph represents the percentage of TRIP12 nuclear positive cells and expressed as the mean (±SEM) obtained over more than 500 cells from at least two separate experiments.

C

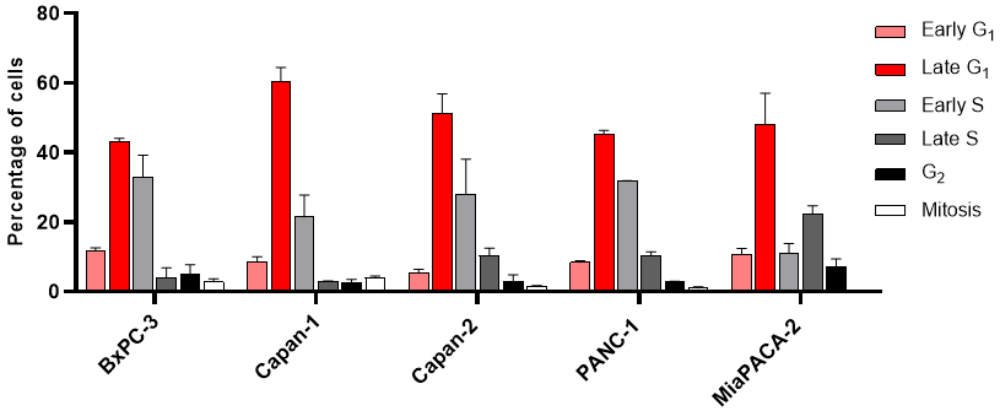

C- The distribution of asynchronous PDAC-derived cell lines in the different phases of cell cycle was determined by immuno-fluorescence as described in Material and Methods section. The graph represents the percentage of cells cells and expressed as the mean (±SEM) obtained over more than 700 cells from at least two separate experiments.

Figure 5

D

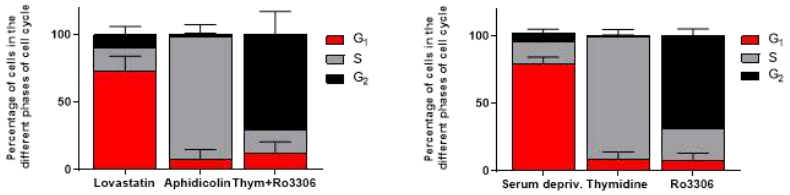

D- Cell cycle distribution of BxPC-3 and MiaPACA-2 enriched cell population in G_1, Early S and G_2 phases. Cells were enriched in the cell cycle phases following indicated treatments. Enrichment level was measured by flow cytometry after propidium iodide incorporation. The graph represents the percentage of cells in the different phases of the cell cycle and are expressed as the mean (±SEM) of at least three separate experiments.

E

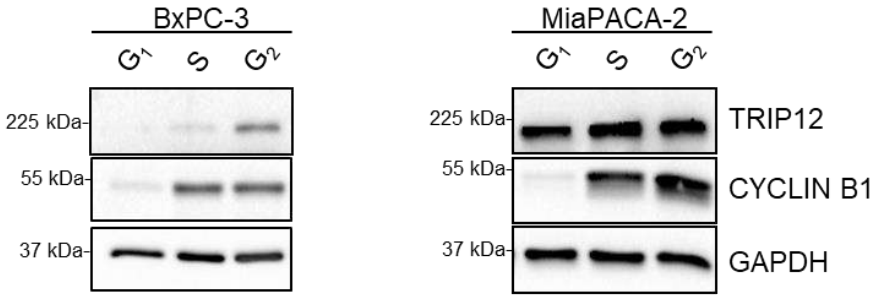

E- TRIP12 protein expression in BxPC-3 and MiaPACA-2 enriched cell population in G_1, Early S and G_2 phases was determined by Western blot analysis. CYCLIN B1 level was used control of enrichment. GAPDH level was used as loading control. The images were obtained from the same experiment and are representative of at least three separate experiments.

F

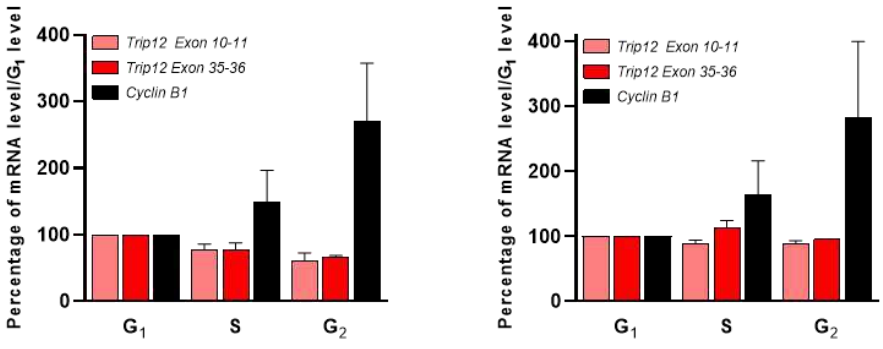

F- *Trip12* mRNA level in BxPC-3 and MiaPACA-2 enriched cell population in G_1, Early S and G_2 phases was determined by RT-qPCR. Two sets of primers (Exon 10-11 and Exon 35-36) were used to determine *Trip12* mRNA expression. *Gapdh*, *β-Actin* and *Cyclophilin A* mRNA levels were used for normalization. *Cyclin B1* mRNA level was used as control of enrichment. Results were obtained from at least three separate experiments and expressed as percentage (±SEM) of *Trip12* mRNA level in G_1 enriched cell population (set as 100%).

Figure 6

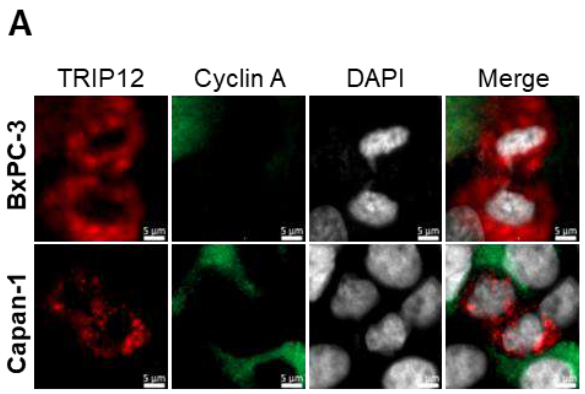

A- Representative images of TRIP12 cytoplasmic localization in BxPC-3 and Capan-1 cells in early G_1 phase by immunofluorescence. Nuclei were counterstained with DAPI.

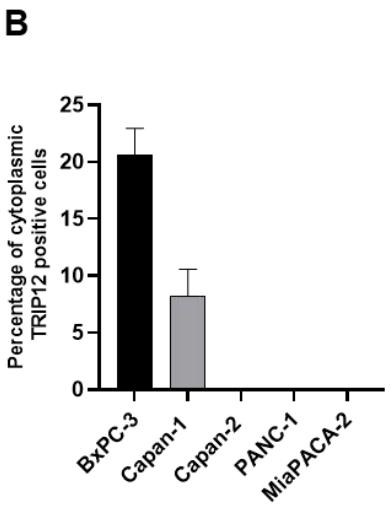

B- Percentage of TRIP12 cytoplasmic positive BxPC-3 and Capan-1 cells in early G_1 phase. The graph represents the mean (±SEM) of three separate experiments over more than 350 early G_1 cells.

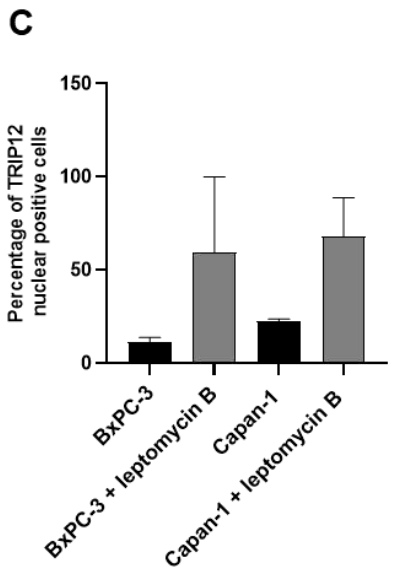

C- Percentage of TRIP12 nuclear positive BxPC-3 and Capan-1 cells in early G_1 phase treated with leptomycin B (50 ng/ml) or a vehicle for 20h was determined by immunofluorescence. Nuclei were counterstained with DAPI. The results are expressed as mean (±SEM) of two separate experiments on over 100 cells.

Figure 6

D

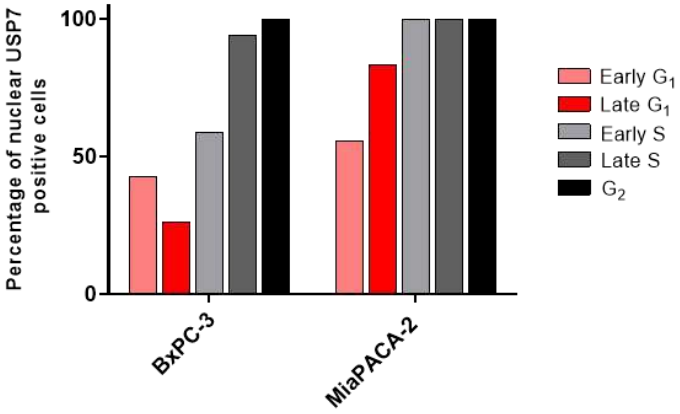

D- The percentage of nuclear USP7 positive cells in the different phase of the cell cycle was determined in MiaPACA-2 and BxPC-3 cell lines by immuno-fluorescence as described in Material and Methods section. The graph represents the percentage of USP7 nuclear positive cells and expressed as the mean (±SEM) obtained over more than 200 cells from one experiment.

E

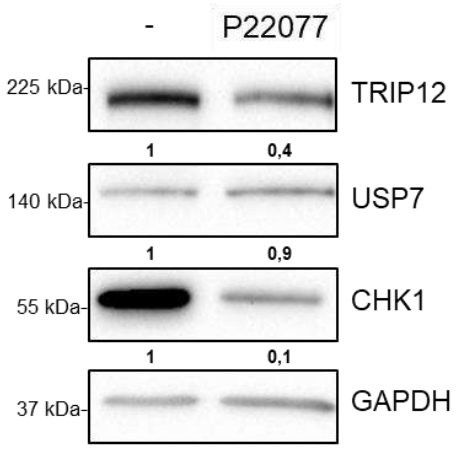

E- TRIP12 protein expression in MiaPACA-2 cell lines treated with USP7 inhibitor P22077 was determined by Western blot analysis. GAPDH protein level was used for normalization. The image is representative of at least three separate experiments. The quantification is expressed as the mean (±SEM) of three different experiments.

F

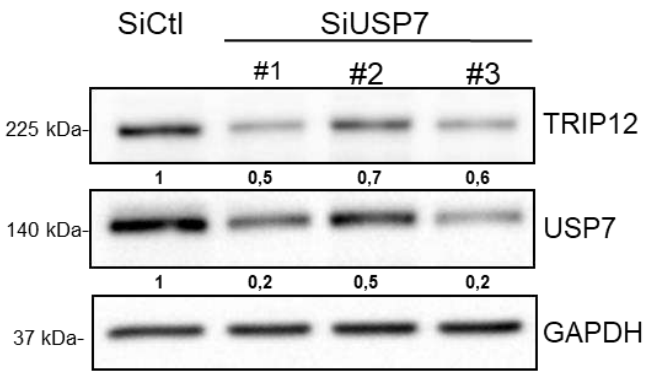

F- TRIP12 and USP7 protein expression in MiaPACA-2 cell lines transfected with siRNA targeting USP7 was determined by Western blot analysis. GAPDH protein level was used for normalization. The image is representative of at least three separate experiments. The quantification is expressed as the mean (±SEM) of three different experiments.

Figure 7

A

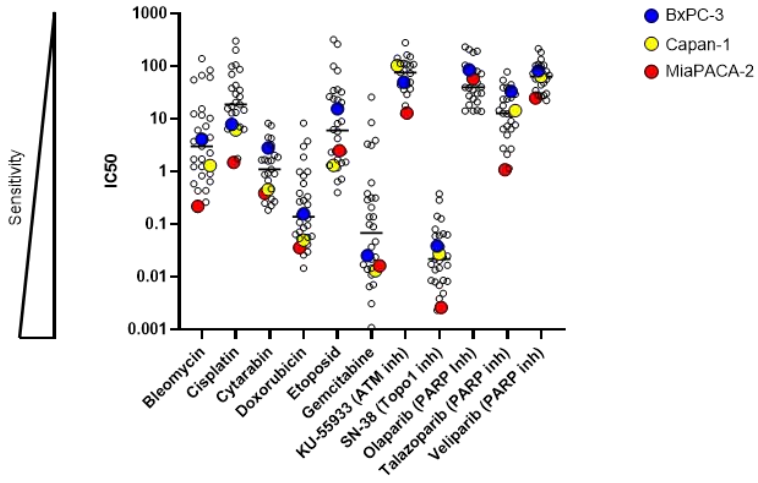

A- Sensitivity expressed as the half inhibitory concentration (IC50 in µM) of 30 PDAC-derived cell lines to the indicated drugs was obtained from Genomics of Drug Sensitivity in Cancer (www.cancerxgene.org) website. The different cell lines are represented as empty circles with the exception of BxPC-3, Capan-1 and MiaPACA-2 cell lines that are represented as blue, yellow and red filled circles, respectively.

B

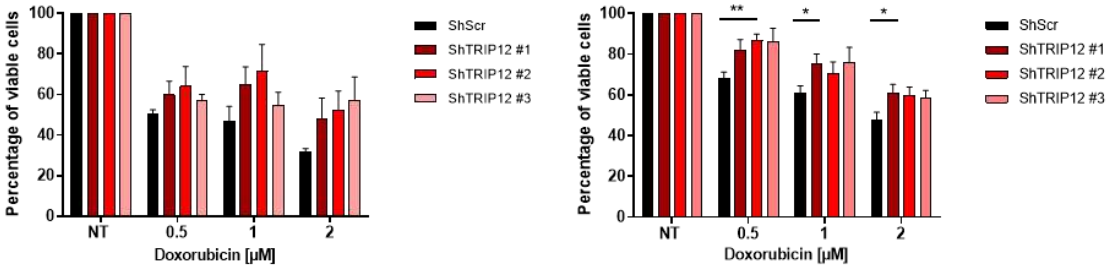

B- Doxorubicin sensitivity of TRIP12-depleted PANC-1 (left panel) and MiaPACA-2 cells (right panel) was measured by MTS assay. Cells were seeded and treated 24h later with the indicated doses of doxorubicin for 24h. The graph represents a percentage of viable cells compared to control MiaPACA-2 cells (ShScr) set as 100%. Results are expressed as mean (±SEM) obtained from at least three separate experiments.

SUPPLEMENTAL FIGURE LEGENDS

Fig. S1- Physical interaction networks of proteins encoded by the TRIP12 depleted-PANC-1 E2F target leading edge genes (n=138). The analysis was performed using STRING software. Nodes represent proteins. The edges indicate that the proteins are part of a physical complex. The line thickness indicates the strength of data. Colored nodes represent proteins that belong to the Gene Ontology biological processes indicated on the figure.

Fig. S2- Trip12 mRNA level in five PDAC-derived cell lines obtained from Broad Institute Cancer Cell Line Encyclopedia (CCLE) mRNA data (https://portals.broadinstitute.org/ccle). Results are expressed as arbitrary units (a.u.).

Fig. S3- Results of CGH array analysis of Trip12 gene in the indicated PDAC-derived cell lines. Copy number of Trip12 gene is compared in each human cell lines. The Trip12 gene region extends between 229,780 Kb and 229,900 Kb on chromosome 2q36.3 (visualized by the blue line).

Fig. S4- Graphical representation of human Trip12/FbxO36 promoter genomic localization obtained from UCSC genome browser (genome.ucsc.edu). the green box represents the localization of a CpG island containing 150 dinucleotides CG. Blue boxes indicate Trip12 and FbxO36 Exon 1 location GRCh38/hg38 assembly. Green histograms illustrate the level of conservation in 100 Vertebrates obtained by PhastCons software.

Fig. S5- Bisulfite mapping analysis of Trip12/FbxO36 bidirectional promoter. Each empty circles represents an unmethylated cytosine while a black represents a methylated cytosine. Grey circles corresponds to cytosines for which the methylation status could not be determined. Four clones for each cell lines were sequenced.

Fig. S6- Schematic representation of the short and long 3'-UTR forms of *Trip12* mRNA. PAS stands for consensus polyadenylation signals. The arrows indicate the position of the primers. The proportion of short and long forms of *Trip12* mRNA in different cell lines was determined by RT-qPCR. The results are expressed the mean (±SEM) of short and long forms as compared to total amount of *Trip12* mRNA (set as 1) and obtained from at least four separate experiments.

Fig. S7- Representative images of TRIP12 nuclear expression in BxPC-3 cell line in the different phases of the cell cycle was determined by immunofluorescence using TRIP12 antibody (Sigma). Nuclei were counterstained with DAPI. EdU and CYCLIN A-negative cells with small oblong-shape nucleus were considered in early G_1 phase. Cells in late G_1 phase and G_2 phase correspond to CYCLIN A/EdU nuclear negative cells and CYCLIN A nuclear positive/EdU negative cells, respectively. Cells in early S and late S phase correspond to EdU positive cells/CYCLIN A negative and positive nuclear cells, respectively.

Fig. S8- Cell cycle distribution of MiaPACA-2 treated with the USP7 inhibitor P22077 (25 µM) for 20h **(A)** or with three different USP7 siRNAs (50 nM) for 48h post-transfection **(B)** was measured by flow cytometry after propidium iodide incorporation. The graph represents the percentage of cells in the different phases of the cell cycle and are expressed as the mean (±SEM) of at least three separate experiments.

Figure S1

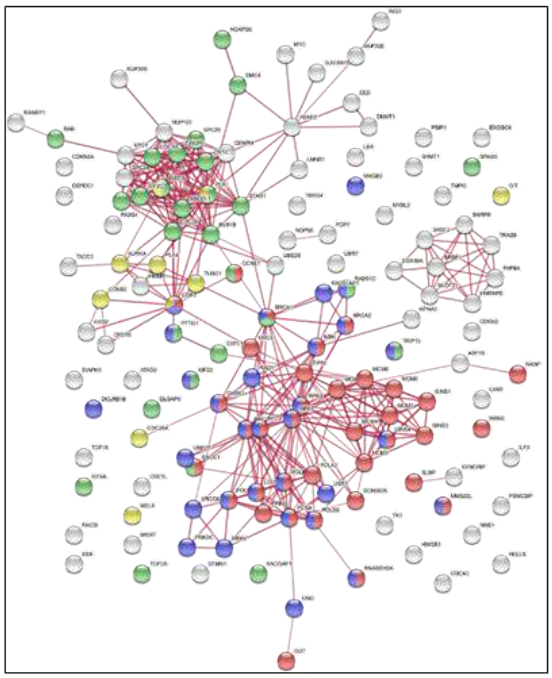

PANC-1 E2F leading genes (n=138)

Fig. S1- Physical interaction networks of proteins encoded by the TRIP12 depleted-PANC-1 E2F target leading edge genes (n=138). The analysis was performed using STRING software. Nodes represent proteins. The edges indicate that the proteins are part of a physical complex. The line thickness indicates the strength of data. Colored nodes represent proteins that belong to the Gene Ontology biological processes indicated on the figure.

Figure S2

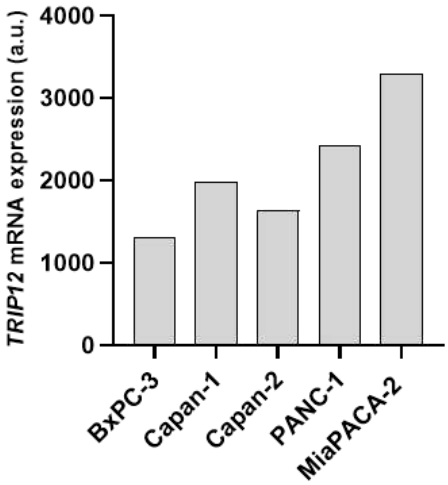

Fig. S2- Trip12 mRNA level in five PDAC-derived cell lines obtained from Broad Institute Cancer Cell Line Encyclopedia (CCLE) mRNA data (https://portals.broadinstitute.org/ccle). Results are expressed as arbitrary units (a.u.).

Figure S3

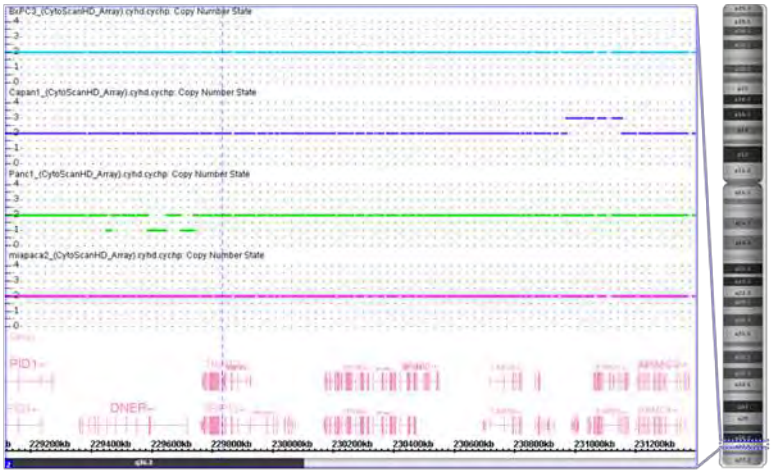

Fig. S3- Results of CGH array analysis of Trip12 gene in the indicated PDAC-derived cell lines. Copy number of Trip12 gene is compared in each human cell lines. The Trip12 gene region extends between 229,780 Kb and 229,900 Kb on chromosome 2q36.3 (visualized by the blue line).

Figure S4

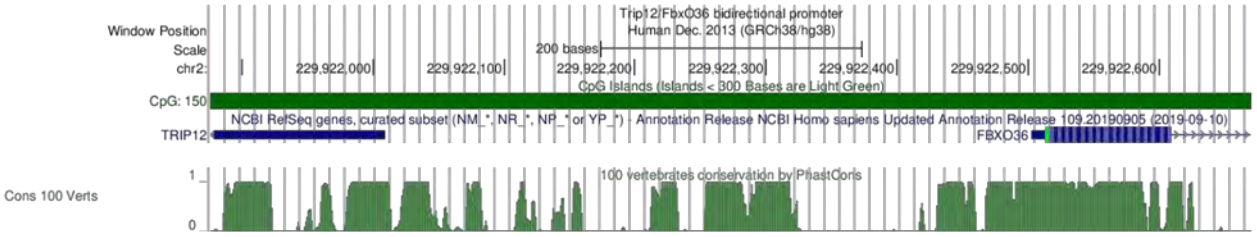

Fig. S4- Graphical representation of human Trip12/FbxO36 promoter genomic localization obtained from UCSC genome browser (genome.ucsc.edu). the green box represents the localization of a CpG island containing 150 dinucleotides CG. Blue boxes indicate Trip12 and FbxO36 Exon 1 location GRCh38/hg38 assembly. Green histograms illustrate the level of conservation in 100 Vertebrates obtained by PhastCons software.

Figure S5

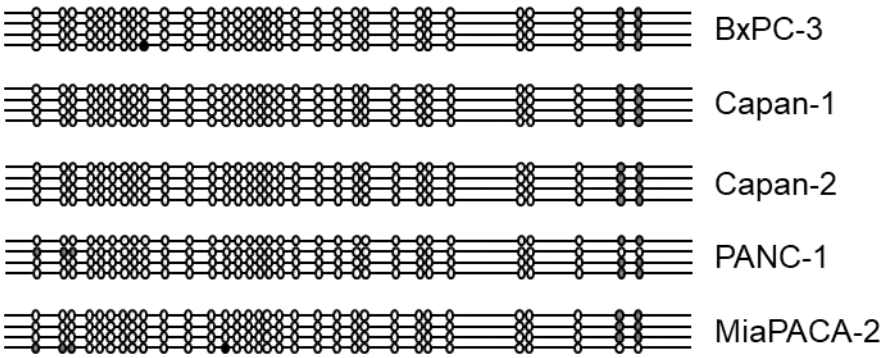

Fig. S5- Bisulfite mapping analysis of Trip12/FbxO36 bidirectional promoter. Each empty circles represents an unmethylated cytosine while a black represents a methylated cytosine. Grey circles corresponds to cytosines for which the methylation status could not be determined. Four clones for each cell lines were sequenced.

Figure S6

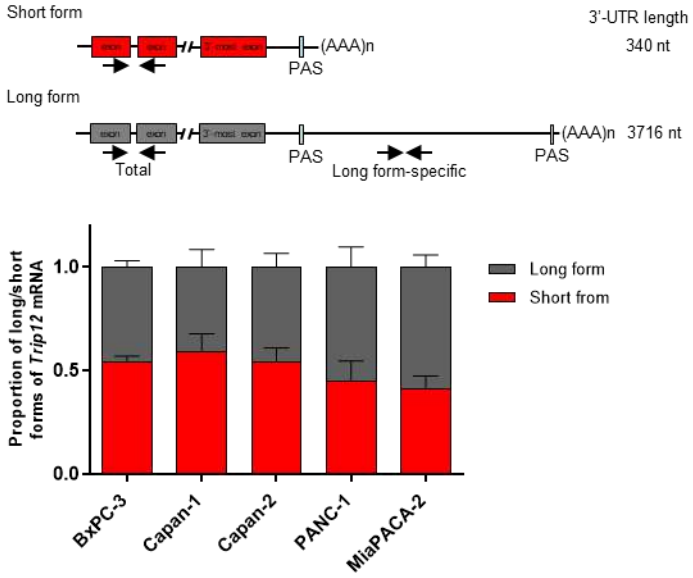

Fig S6- Schematic representation of the short and long 3'-UTR forms of *Trip12* mRNA. PAS stands for consensus polyadenylation signals. The arrows indicate the position of the primers. The proportion of short and long forms of Trip12 mRNA in different cell lines was determined by RT-qPCR. The results are expressed the mean (±SEM) of short and long form as compared to total amount of *Trip12* mRNA (set as 1) and obtained from at least four separate experiments.

Figure S7

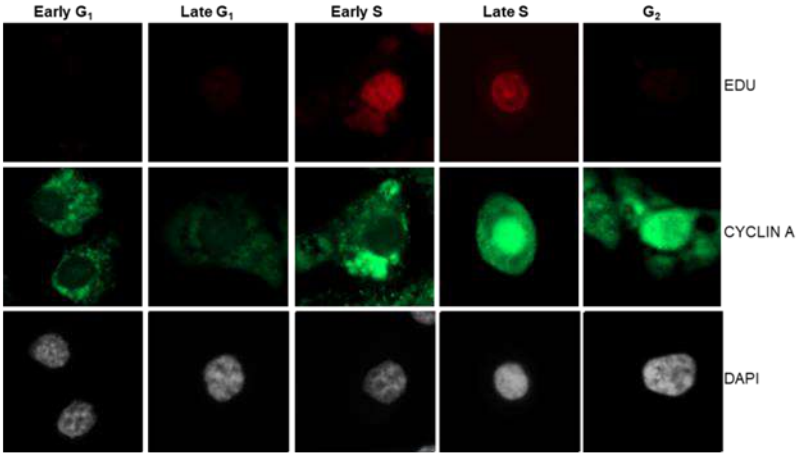

Fig. S7- TRIP12 nuclear expression in PDAC-derived cell lines in the different phases of the cell cycle was determined by immunofluorescence using TRIP12 antibody (Sigma). Nuclei were counterstained with DAPI. Cells with EdU and Cyclin A-negative and oblong-shape nucleus were considered in early G_1 phase. Cells in G_1 phase and G_2 phase correspond to CYCLIN A/EdU nuclear negative cells and CYCLIN A nuclear positive/EdU negative cells, respectively. Cells in early S and late S phase correspond to EdU positive cells/CYCLIN A negative and positive nuclear cells, respectively.

Figure S8

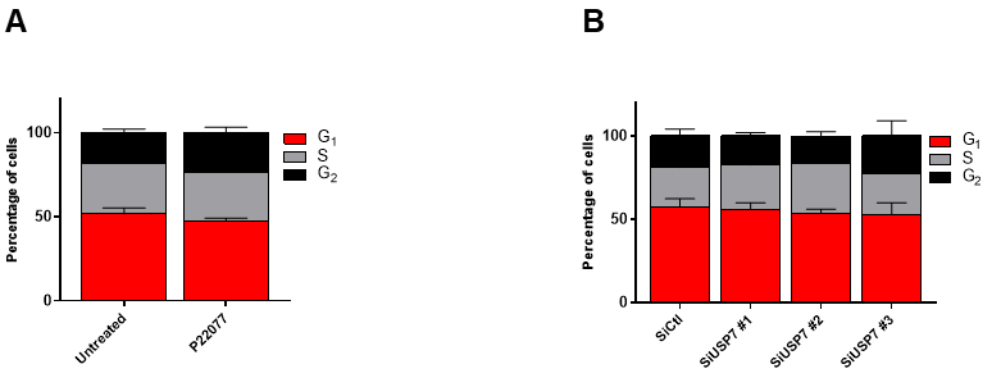

Fig. S8- - Cell cycle distribution of MiaPACA-2 treated with the USP7 inhibitor P22077 (25 µM) for 20h (A) or with three different USP7 siRNAs (50 nM) for 48h post-transfection (B) was measured by flow cytometry after propidium iodide incorporation. The graph represents the percentage of cells in the different phases of the cell cycle and are expressed as the mean (±SEM) of at least three separate experiments.

SUPPLEMENTAL TABLES

Suppl Table 1: Antibody list

Suppl Table 2: Primer list

Suppl Table 3: List of E2F target-genes

Supplemental Material and Methods.

Supplemental Table 1: List of antibodies.

Protein	Antibody	Dilution
USP7	Bethyl laboratories A300-033A	1/1000 (WB)
CHK1	Cell Signaling 2G1D5	1/1000 (WB)
PCNA	Santa Cruz Sc-56	1/500 (WB)
TRIP12	Bethyl laboratories A301-814A	1/1000 (IF and WB)
TRIP12	Sigma HPA036335	1/1000 (IF)
CYCLIN B1	Millipore MAB3684	1/1000 (IF and WB)
GAPDH	Santa Cruz sc-25778	1/2000 (WB)
Green Fluorescent Protein	Santa Cruz sc-9996	1/200 (IF)
CYCLIN A	GeneTex [6E6]	1/500 (IF)
CYCLIN A	GeneTex #2547	1/1000 (IF)
RNA POLYMERASE II Ser 5	AbCam [4H8]	ChIP assay
Acetylated K9 HISTONE H3	AbCam #6001	ChIP assay

Supplemental Table 2: List of primers.

Name	Forward (5' to 3')	Reverse (5' to 3')
RT-qPCR		
Trip12 exon 10-11	ATATTATGAACCATGCTTGTCGAG	CTCTGCCACATCAATACACTGAAT
Trip12 exon 35-36	TTCAGATTGGTGGACCTTCC	GGCTACAACTGGGTCGATGT
Trip12 3'-UTR	ATGGCAATTCCAGCAGCAAC	TAAATACCGGCCAGCCCAAG
Cyclin B1	CAAGCCCAATGGAAACATCTG	TTGCTCTTCCTCAAGTTGTCTC
Gapdh	CAATGACCCCTTCATTGACC	GTACTCGCTCCTGGAAGATG
β-Actin	AGATGTGGATCAGCAAGCAGGAGT	GCAATCAAAGTCCTCGGCCACATT
Cyclophilin A	GTCAACCCCACCGTGTTCTT	CTGCTGTCTTTGGGACCTTGT
Tmpo	AGAGTTGAGCACAATCAGAGCTA	TTAATGCCTGCAGAGGTCCG
Birc5	AGCCAAGAACAAAATTGCAAAGG	CGCACTTTCTCCGCAGTTTC
Tk1	CACAGAGAAGGAGGTCGAGGT	TTCTCTTTGTTGTCCGGCCC
Promoter cloning		
Trip12 promoter	AATTACCTAGTTAGGCCCCAAAGTCT	GTCGCTAAGACAACCAGGAAGG
Cxcr4 promoter	TACCGACCACCCGCAAACAG	TGGTAACCGCTGGTTCTCCA
ChIP PCR		
ChIP A	TGCGCCCCAATTACCTAGTT	TTACTGCCGCGCCACC
ChIP B	TCGCGGCGATGACACA	GGAGGAGCTGGAACAGAAAGTC
ChIP C	CTCCGTGGTAGCAGGAACTAATTC	GAACCCTGATCCGTGAAATTTC
ChIP D	CGCCGCCTAGCAAAGACTAT	CGCGGCTCGCACTTG
ChIP E	CCGGCTTCTTACCCGTAGAGT	CGGAGACGCCCGTTTTC
Deletion constructs		
TRIPmut1 (Trip12 +24)	GGCGGCGGCTCCGGGTACCTTCAATTATCAGC	GCTGATAATTGAAGGTACCCGGAGCCGCCGCC
TRIPmut2 F (Trip12 -111)	GGGCTCGTCCGCGGTACCGGCACCGCTG	CAGCGGTGCCGGTACCGCGGACGAGCCC
TRIPmut3 F (Trip12 – 249)	GGAGATCTACTTGGTACCCCTCCGCCGGGGTCAC	GTGACCCCGGCGGAGGGGTACCAAGTAGATCTCC
TRIP12mut 4-3 F(Trip -285)	CCCCCTCCCCTCCGTGGTACCAGGAACTAATTCCCC	GGGGAATTAGTTCCTGGTACCACGGAGGGGAGGGGG
TRIPmut4 F (Trip12 -389)	ATTTCACGGATCAGGGTACCCTAAGACCCTTGGAAGAGGG	CCCTCTTCCAAGGGTCTTAGGGTACCCTGATCCGTGAAAT
TRIP12 mut5 F (Fbx -48)	CAATTTAAACTAGGGTTTTGGTACCTTGACCCCAACCAAGC	GCTTGGTTGGGGTCAAGGTACCAAAACCCTAGTTTAAATTG
TRIP12 mut 3-2 F(Fbx -305)	GGCTCGACTCTCTCAGGTACCTCCGATCTCCGCCCGATC	GATCGGGCGGAGATCGGAGGTACCTGAGAGAGTCGAGCC
TRIP12 mut 2-1 F (Fbx -435)	TCCCCGCCTGCTCTGGTACCCTCGGGGAACTAC	GTAGTTCCCCGAGGGTACCAGAGCAGGCGGGGA
For bisulfite mapping		
Trip12 BS	GGGTTTTTTTAATTATTAGTTGAGT	TAAAATTTCCAACTCCAAATC

Supplemental Table 3: List of E2F target-genes

Level of expression of E2F-target genes (n=195) in TRIP12-depleted PANC-1 and MiaPACA-2 cell lines. Results are expressed as Log2-fold change compared to ShScr control cell lines and are the mean of four separate experiments. Up- and down-regulated genes are highlighted in red and in blue, respectively. Red and blue intensity is proportional to the level of up and down regulation, respectively.

	PANC-1	MiaPACA-2
CDC25B	1.938	0.817
WEE1	1.242	0.127
PAN2	0.875	0.530
RAD50	0.864	0.229
CDKN1B	0.713	0.962
MTHFD2	0.489	0.288
CDKN2C	0.459	0.076
IPO7	0.178	0.003
NAA38	0.177	0.044
LUC7L3	0.163	0.291
CDKN1A	0.131	-0.460
DCTPP1	0.048	0.234
PMS2	0.047	0.314
ASF1A	-0.015	-0.102
RPA2	-0.050	-0.179
POLE4	-0.060	-0.433
AK2	-0.061	-0.407
ORC2	-0.069	0.051
TIMELESS	-0.088	0.520
NAP1L1	-0.119	0.069
NUP153	-0.152	0.131
CBX5	-0.164	-0.402
EIF2S1	-0.166	-0.154
SMC6	-0.172	-0.159
MLH1	-0.185	0.653
BARD1	-0.192	-0.028
PRDX4	-0.210	-0.526
RAD21	-0.270	-0.021
PNN	-0.288	-0.328
TP53	-0.289	-0.413
PPP1R8	-0.294	-0.540
SMC1A	-0.299	-0.584
RBBP7	-0.300	-0.273
TUBB	-0.300	-0.356
CCP110	-0.310	-0.228
DCK	-0.315	-0.039
GSPT1	-0.325	-0.149
WDR90	-0.335	-0.233
CDK4	-0.357	0.180
EZH2	-0.376	-0.155
TFRC	-0.387	-0.524
PPM1D	-0.398	-0.141
HUS1	-0.399	na
HMGA1	-0.407	-0.206
POLD3	-0.408	-0.484
KIF18B	-0.411	-0.101
CHEK2	-0.432	-0.174
NOLC1	-0.446	-0.468
MXD3	-0.460	-0.023
SMC3	-0.470	-0.750
RFC1	-0.496	0.244
CTCF	-0.512	-0.407
H2AFX	-0.524	-0.811
PDS5B	-0.528	0.073
E2F8	-0.562	-0.736
PRPS1	-0.580	-0.259
SSRP1	-0.595	-0.400
SUV39H1	-0.607	-0.223
POP7	-0.609	-0.141
EED	-0.622	-0.631
GINS3	-0.632	-0.327
ZW10	-0.641	-0.453
RFC2	-0.648	0.024
SPC24	-0.651	-0.442
NUP107	-0.655	-0.199
UBR7	-0.655	0.236
MYC	-0.667	-0.266
SRSF1	-0.677	-0.858
UBE2S	-0.682	-0.303
H2AFZ	-0.682	-0.108
STMN1	-0.691	-0.295
XPO1	-0.695	-0.207
POLE	-0.696	0.087
RAN	-0.696	-0.189
PA2G4	-0.701	-0.371
TBRG4	-0.711	-0.021
DEK	-0.715	-0.412
MMS22L	-0.738	-0.362
CHEK1	-0.750	-0.653
HNRNPD	-0.758	-0.056
USP1	-0.763	-0.369
SYNCRIP	-0.764	-0.401
MCM7	-0.770	-0.538
RACGAP1	-0.773	-0.142
NME1	-0.784	-0.334
CKS1B	-0.797	-0.267
NUP205	-0.802	0.090
BRCA2	-0.815	-0.143
ING3	-0.820	-0.717
MCM3	-0.821	-0.081
NASP	-0.821	-0.506
STAG1	-0.829	-0.724
DNMT1	-0.837	-0.168
SRSF2	-0.843	-0.458
NUDT21	-0.855	-0.454
DCLRE1B	-0.859	-0.413
PAICS	-0.863	-0.268
SPAG5	-0.865	-0.167
DUT	-0.868	-0.417
XRCC6	-0.890	0.043
RAD1	-0.907	-0.248
CDC25A	-0.907	0.076
HMGB3	-0.926	-0.375
RPA1	-0.931	-0.455
NBN	-0.936	-0.159
UNG	-0.938	0.200
CCNE1	-0.944	0.324
SLBP	-0.947	-0.326
RPA3	-0.957	0.389
DONSON	-0.962	0.038
TRA2B	-0.980	-0.467
LBR	-0.982	-0.616
MELK	-0.983	0.005
RAD51AP1	-0.985	-0.248
POLA2	-0.998	-0.571
BRCA1	-1.014	-0.055
TCF19	-1.021	-0.108
CSE1L	-1.024	-0.218
MCM6	-1.035	-0.332
PRKDC	-1.036	-0.296
RNASEH2A	-1.047	0.077
ATAD2	-1.080	-0.216
SNRPB	-1.085	-0.202
TUBG1	-1.124	-0.085
UBE2T	-1.128	-0.024
POLD2	-1.157	0.209
KIF22	-1.166	0.199
TIPIN	-1.167	-0.526
DSCC1	-1.192	-0.804
LYAR	-1.194	-0.068
EXOSC8	-1.215	-0.125
HELLS	-1.255	-0.044
ILF3	-1.257	-0.503
TACC3	-1.266	-0.067
LMNB1	-1.279	-0.419
DDX39A	-1.279	-0.123
PSIP1	-1.289	0.111
PSMC3IP	-1.291	0.103
RANBP1	-1.297	-0.344
PHF5A	-1.315	-0.335
MCM2	-1.327	-0.316
PTTG1	-1.327	-0.434
RFC3	-1.332	-0.149
PRIM2	-1.337	-0.564
CDKN3	-1.339	-0.394
MKI67	-1.350	-0.946
NCAPD2	-1.353	-0.297
ASF1B	-1.363	-0.121
PLK4	-1.385	-0.721
CIT	-1.395	-0.215
MCM5	-1.431	-0.123
POLD1	-1.433	0.055
ORC6	-1.443	-0.524
BUB1B	-1.452	-0.487
KIF2C	-1.469	-0.309
SMC4	-1.474	-0.956
ESPL1	-1.477	-0.178
PCNA	-1.478	-0.224
KPNA2	-1.481	-0.471
MSH2	-1.491	-0.235
GINS1	-1.496	-0.090
TOP2A	-1.496	-0.203
ANP32E	-1.501	-0.694
LIG1	-1.542	0.279
DEPDC1	-1.605	-0.779
CDK1	-1.638	-0.383
CKS2	-1.654	-0.202
CDCA8	-1.658	-0.337
HMMR	-1.684	-0.473
RAD51C	-1.711	-0.532
MCM4	-1.726	-0.437
SHMT1	-1.732	-0.192
KIF4A	-1.735	-0.417
CDCA3	-1.736	-0.427
HMGB2	-1.748	0.070
MAD2L1	-1.761	-0.163
GINS4	-1.774	-0.578
DIAPH3	-1.777	-0.356
CENPE	-1.844	-0.229
AURKA	-1.849	-0.432
MYBL2	-1.864	-0.293
DLGAP5	-1.874	-0.499
TRIP13	-1.895	-0.654
SPC25	-1.915	-0.621
TK1	-1.939	-0.467
TMPO	-1.976	-1.013
PLK1	-2.005	-0.286
CDC20	-2.009	-0.489
CCNB2	-2.053	-0.151
CENPM	-2.056	-0.273
AURKB	-2.077	-0.335
BIRC5	-2.099	-0.359
RRM2	-2.460	-1.329
NOP56	-2.625	-0.248
CDKN2A	-3.884	-0.043

REFERENCES.

Alonso-de Vega, Ignacio, Yusé Martín, and Veronique A. J. Smits. 2014. "USP7 Controls Chk1 Protein Stability by Direct Deubiquitination." *Cell Cycle (Georgetown, Tex.)* 13 (24): 3921–26. https://doi.org/10.4161/15384101.2014.973324.

An, Chung-Il, Edward Ganio, and Nobuko Hagiwara. 2013. "Trip12, a HECT Domain E3 Ubiquitin Ligase, Targets Sox6 for Proteasomal Degradation and Affects Fiber Type-Specific Gene Expression in Muscle Cells." *Skeletal Muscle* 3 (1): 11. https://doi.org/10.1186/2044-5040-3-11.

Bailey, Peter, David K. Chang, Katia Nones, Amber L. Johns, Ann-Marie Patch, Marie-Claude Gingras, David K. Miller, et al. 2016. "Genomic Analyses Identify Molecular Subtypes of Pancreatic Cancer." *Nature* 531 (7592): 47–52. https://doi.org/10.1038/nature16965.

Bracken, Adrian P., Marco Ciro, Andrea Cocito, and Kristian Helin. 2004. "E2F Target Genes: Unraveling the Biology." *Trends in Biochemical Sciences* 29 (8): 409–17. https://doi.org/10.1016/j.tibs.2004.06.006.

Brunet, Manon, Claire Vargas, Dorian Larrieu, Jérôme Torrisani, and Marlène Dufresne. 2020. "E3 Ubiquitin Ligase TRIP12: Regulation, Structure, and Physiopathological Functions." *International Journal of Molecular Sciences* 21 (22). https://doi.org/10.3390/ijms21228515.

Cai, Jia-Bin, Guo-Ming Shi, Zhao-Ru Dong, Ai-Wu Ke, Hong-Hui Ma, Qiang Gao, Zao-Zhuo Shen, et al. 2015. "Ubiquitin-Specific Protease 7 Accelerates P14(ARF) Degradation by Deubiquitinating Thyroid Hormone Receptor-Interacting Protein 12 and Promotes Hepatocellular Carcinoma Progression." *Hepatology (Baltimore, Md.)* 61 (5): 1603–14. https://doi.org/10.1002/hep.27682.

Chang, Jae-Woong, Wei Zhang, Hsin-Sung Yeh, Ebbing P. de Jong, Semo Jun, Kwan-Hyun Kim, Sun S. Bae, et al. 2015. "MRNA 3'-UTR Shortening Is a Molecular Signature of MTORC1 Activation." *Nature Communications* 6 (June): 7218. https://doi.org/10.1038/ncomms8218.

Chen, Delin, Ning Kon, Jiayun Zhong, Pingzhao Zhang, Long Yu, and Wei Gu. 2013. "Differential Effects on ARF Stability by Normal versus Oncogenic Levels of C-Myc Expression." *Molecular Cell* 51 (1): 46–56. https://doi.org/10.1016/j.molcel.2013.05.006.

Chen, Delin, Jing Shan, Wei-Guo Zhu, Jun Qin, and Wei Gu. 2010. "Transcription-Independent ARF Regulation in Oncogenic Stress-Mediated P53 Responses." *Nature* 464 (7288): 624–27. https://doi.org/10.1038/nature08820.

Delpu, Yannick, Hubert Lulka, Flavie Sicard, Nathalie Saint-Laurent, Frédéric Lopez, Naïma Hanoun, Louis Buscail, Pierre Cordelier, and Jérôme Torrisani. 2013. "The Rescue of MiR-148a Expression in Pancreatic Cancer: An Inappropriate Therapeutic Tool." *PloS One* 8 (1): e55513. https://doi.org/10.1371/journal.pone.0055513.

Duconseil, Pauline, Marine Gilabert, Odile Gayet, Celine Loncle, Vincent Moutardier, Olivier Turrini, Ezequiel Calvo, et al. 2015. "Transcriptomic Analysis Predicts Survival and Sensitivity to Anticancer Drugs of Patients with a Pancreatic Adenocarcinoma." *The American Journal of Pathology* 185 (4): 1022–32. https://doi.org/10.1016/j.ajpath.2014.11.029.

Fabbro, Megan, Jose A. Rodriguez, Richard Baer, and Beric R. Henderson. 2002. "BARD1 Induces BRCA1 Intranuclear Foci Formation by Increasing RING-Dependent BRCA1 Nuclear Import and Inhibiting BRCA1 Nuclear Export." *The Journal of Biological Chemistry* 277 (24): 21315–24. https://doi.org/10.1074/jbc.M200769200.

Gatti, Marco, Ralph Imhof, Qingyao Huang, Michael Baudis, and Matthias Altmeyer. 2020. "The Ubiquitin Ligase TRIP12 Limits PARP1 Trapping and Constrains PARP Inhibitor Efficiency." *Cell Reports* 32 (5): 107985. https://doi.org/10.1016/j.celrep.2020.107985.

Georges, Anna, Edyta Marcon, Jack Greenblatt, and Lori Frappier. 2018. "Identification and Characterization of USP7 Targets in Cancer Cells." *Scientific Reports* 8 (1): 15833. https://doi.org/10.1038/s41598-018-34197-x.

Gudjonsson, Thorkell, Matthias Altmeyer, Velibor Savic, Luis Toledo, Christoffel Dinant, Merete Grøfte, Jirina Bartkova, et al. 2012. "TRIP12 and UBR5 Suppress Spreading of Chromatin

Ubiquitylation at Damaged Chromosomes." *Cell* 150 (4): 697–709. https://doi.org/10.1016/j.cell.2012.06.039.
Hank, Thomas, and Andrew S. Liss. 2018. "Recent Advances in Chromatin Mechanisms Controlling Pancreatic Carcinogenesis." *Epigenomes* 2 (2): 11. https://doi.org/10.3390/epigenomes2020011.
Hanoun, Naïma, Samuel Fritsch, Odile Gayet, Véronique Gigoux, Pierre Cordelier, Nelson Dusetti, Jérôme Torrisani, and Marlène Dufresne. 2014. "The E3 Ubiquitin Ligase Thyroid Hormone Receptor-Interacting Protein 12 Targets Pancreas Transcription Factor 1a for Proteasomal Degradation." *The Journal of Biological Chemistry* 289 (51): 35593–604. https://doi.org/10.1074/jbc.M114.620104.
Kamura, Takumi, Taichi Hara, Masaki Matsumoto, Noriko Ishida, Fumihiko Okumura, Shigetsugu Hatakeyama, Minoru Yoshida, Keiko Nakayama, and Keiichi I. Nakayama. 2004. "Cytoplasmic Ubiquitin Ligase KPC Regulates Proteolysis of P27(Kip1) at G1 Phase." *Nature Cell Biology* 6 (12): 1229–35. https://doi.org/10.1038/ncb1194.
Kent, Lindsey N., and Gustavo Leone. 2019. "The Broken Cycle: E2F Dysfunction in Cancer." *Nature Reviews. Cancer* 19 (6): 326–38. https://doi.org/10.1038/s41568-019-0143-7.
Keppler, Brian R., and Trevor K. Archer. 2010. "Ubiquitin-Dependent and Ubiquitin-Independent Control of Subunit Stoichiometry in the SWI/SNF Complex." *The Journal of Biological Chemistry* 285 (46): 35665–74. https://doi.org/10.1074/jbc.M110.173997.
Khan, Omar M., Jorge Almagro, Jessica K. Nelson, Stuart Horswell, Vesela Encheva, Kripa S. Keyan, Bruce E. Clurman, Ambrosius P. Snijders, and Axel Behrens. 2021. "Proteasomal Degradation of the Tumour Suppressor FBW7 Requires Branched Ubiquitylation by TRIP12." *Nature Communications* 12 (1): 2043. https://doi.org/10.1038/s41467-021-22319-5.
Kipreos, E. T., and M. Pagano. 2000. "The F-Box Protein Family." *Genome Biology* 1 (5): REVIEWS3002. https://doi.org/10.1186/gb-2000-1-5-reviews3002.
Larrieu, D., M. Brunet, C. Vargas, N. Hanoun, L. Ligat, L. Dagnon, H. Lulka, et al. 2020. "The E3 Ubiquitin Ligase TRIP12 Participates in Cell Cycle Progression and Chromosome Stability." *Scientific Reports* 10 (1): 789. https://doi.org/10.1038/s41598-020-57762-9.
Lee, K. M., C. Nguyen, A. B. Ulrich, P. M. Pour, and M. M. Ouellette. 2003. "Immortalization with Telomerase of the Nestin-Positive Cells of the Human Pancreas." *Biochemical and Biophysical Research Communications* 301 (4): 1038–44. https://doi.org/10.1016/s0006-291x(03)00086-x.
Liberzon, Arthur, Chet Birger, Helga Thorvaldsdóttir, Mahmoud Ghandi, Jill P. Mesirov, and Pablo Tamayo. 2015. "The Molecular Signatures Database (MSigDB) Hallmark Gene Set Collection." *Cell Systems* 1 (6): 417–25. https://doi.org/10.1016/j.cels.2015.12.004.
Molkentine, Jessica M., David P. Molkentine, Kathleen A. Bridges, Tongxin Xie, Liangpeng Yang, Aakash Sheth, Timothy P. Heffernan, et al. 2020. "Targeting DNA Damage Response in Head and Neck Cancers through Abrogation of Cell Cycle Checkpoints." *International Journal of Radiation Biology*, February, 1–8. https://doi.org/10.1080/09553002.2020.1730014.
Nishiyama, Atsuya, and Makoto Nakanishi. 2021. "Navigating the DNA Methylation Landscape of Cancer." *Trends in Genetics: TIG*, June, S0168-9525(21)00130-X. https://doi.org/10.1016/j.tig.2021.05.002.
Sahin, Ibrahim H., Maeve A. Lowery, Zsofia K. Stadler, Erin Salo-Mullen, Christine A. Iacobuzio-Donahue, David P. Kelsen, and Eileen M. O'Reilly. 2016. "Genomic Instability in Pancreatic Adenocarcinoma: A New Step towards Precision Medicine and Novel Therapeutic Approaches." *Expert Review of Gastroenterology & Hepatology* 10 (8): 893–905. https://doi.org/10.1586/17474124.2016.1153424.
Senft, Daniela, Jianfei Qi, and Ze'ev A. Ronai. 2018. "Ubiquitin Ligases in Oncogenic Transformation and Cancer Therapy." *Nature Reviews. Cancer* 18 (2): 69–88. https://doi.org/10.1038/nrc.2017.105.
Siegel, Rebecca L., Kimberly D. Miller, and Ahmedin Jemal. 2020. "Cancer Statistics, 2020." *CA: A Cancer Journal for Clinicians* 70 (1): 7–30. https://doi.org/10.3322/caac.21590.

Sipos, Bence, Simone Möser, Holger Kalthoff, Virag Török, Matthias Löhr, and Günter Klöppel. 2003. "A Comprehensive Characterization of Pancreatic Ductal Carcinoma Cell Lines: Towards the Establishment of an in Vitro Research Platform." *Virchows Archiv: An International Journal of Pathology* 442 (5): 444–52. https://doi.org/10.1007/s00428-003-0784-4.

Storz, Peter, and Howard C. Crawford. 2020. "Carcinogenesis of Pancreatic Ductal Adenocarcinoma." *Gastroenterology* 158 (8): 2072–81. https://doi.org/10.1053/j.gastro.2020.02.059.

Wakano, Clay, Jung S. Byun, Li-Jun Di, and Kevin Gardner. 2012. "The Dual Lives of Bidirectional Promoters." *Biochimica Et Biophysica Acta* 1819 (7): 688–93. https://doi.org/10.1016/j.bbagrm.2012.02.006.

Wang, L, P Zhang, D P Molkentine, C Chen, J M Molkentine, H Piao, U Raju, et al. 2017. "TRIP12 as a Mediator of Human Papillomavirus/P16-Related Radiation Enhancement Effects." *Oncogene* 36 (6): 820–28. https://doi.org/10.1038/onc.2016.250.

Zhang, Qiang, Yaqing Zhang, Joshua D. Parsels, Ines Lohse, Theodore S. Lawrence, Marina Pasca di Magliano, Yi Sun, and Meredith A. Morgan. 2016. "Fbxw7 Deletion Accelerates KrasG12D-Driven Pancreatic Tumorigenesis via Yap Accumulation." *Neoplasia* 18 (11): 666–73. https://doi.org/10.1016/j.neo.2016.08.009.

I. Article 2 : *"Loss of the E3 ubiquitin ligase TRIP12 inhibits Acinar to Ductal Metaplasia, Development of Pancreatic Intraepithelial Neoplasia and Proliferation of Tumor Cells in Mice"*

En préparation

Title: Loss of the E3 ubiquitin ligase TRIP12 inhibits Acinar to Ductal Metaplasia, Development of Pancreatic Intraepithelial Neoplasia and Proliferation of Tumor Cells in Mice

List of authors: M Brunet[1,2], C Vargas[1,2,*], M Fanjul[1,2,*], L Pieruccioni[3], H Lulka[1,2], F Capilla[4], V Gigoux[1,2], J Guillermet-Guibert[1,2], J Torrisani[1,2], M Dufresne[1,2,#]

Affiliations:

[1]-Centre de Recherches en Cancérologie de Toulouse, INSERM UMR1037, CEDEX 1, 31037 Toulouse, France
[2]-Université Toulouse III Paul-Sabatier, CEDEX 9, 31062 Toulouse, France
[3]-RESTORE Research Center, Université de Toulouse, INSERM, CNRS, EFS, ENVT, 31100 Toulouse, France
[4]-Experimental Histopathology Department, INSERM US006-CREFRE, Toulouse, France

* contributed equally
# corresponding author

Keywords:

Reprogramming, E3 ubiquitin ligase, preneoplastic lesions, pancreas, transdifferentiation

Abstract

The acinar cells are the most abundant cell type of the pancreas. Although specialized and dedicated to digestive enzyme production, they harbor a high plasticity. They are able to alter their identity and to undergo reversible ductal metaplasia through epigenetic silencing of acinar lineage gene program. Acinar to ductal cell metaplasia (ADM) becomes irreversible in the presence of oncogenic Kras mutations and leads to the formation of pancreatic intraepithelial neoplasia.

We demonstrate that the HECT E3 ubiquitin ligase TRIP12 (Thyroid hormone receptor interacting protein 12) is overexpressed in human pancreatic preneoplastic lesions and tumors. We show that a conditional deletion of TRIP12 in the pancreas during murine embryogenesis leads to a pancreatic lipomatosis suggesting pancreatic exocrine insufficiency. EGF induced-ADM is suppressed in pancreatic acini isolated from conditional Trip12 knockout mice model. In vivo, TRIP12-depleted acini are unable to develop ADM in response to pancreatic injury. An inactivation of TRIP12 prevents mutated Kras-induced PanIN formation in mouse pancreas and reduces the growth of pancreatic tumors when mutated P53 is concomitantly expressed.

Our study identifies TRIP12 as a master regulator of acinar fate and an important inducer of ductal identity in the adult pancreas. It highlights that TRIP12 is an essential factor of ADM and of initiation steps of pancreatic carcinogenesis.

Introduction

The mature exocrine pancreas comprises two types of epithelial cells. The acinar cells, the most abundant cell type, produce and secrete an extremely high level of digestive enzymes in pancreatic ducts daily. The acinar cells have been a model of terminal cellular differentiation with specialized cellular functions and organization dedicated to protein synthesis, transport, storage and exocytosis.[1] As such, they were thought to be irreversibly differentiated but numerous studies revealed their surprising plasticity as a defense mechanism against sustained stress as for example in the context of inflammation.[2–5] Ductal cells were originally thought to give rise to pancreatic ductal adenocarcinoma (PDAC) due to ductal differentiation of pancreatic precancerous lesions and tumors.

However, the cell at the origin of PDAC has been challenged and debated by experimental evidence providing insights in the plasticity of every pancreatic cell type (including endocrine cells) in the setting of neoplastic transformation. The most compelling studies used conditionally expressed mutant $Kras^{G12D}$ allele combined or not with inactivation of tumor suppressor genes in one particular adult individual pancreatic cell types in mice.[6–11] They demonstrated that cancer can originate from ductal and non-ductal cells of the mouse pancreas.

It has been known for decades that acinar cells lose their identity upon varying insults such as inflammation or in vitro culture through acinar-to-ductal metaplasia (ADM).[12–14] During this process, acinar cells dedifferentiate to an intermediate state with embryonic features and may acquire mesenchymal properties.[3,15] Subsequently, acinar cells transdifferentiate to adopt a ductal phenotype. ADM is reversible, can be induced by transient expression of reprogramming factors and is coupled to the silencing of acinar cell-related genes.[16–19] Numerous findings demonstrated that changes in acinar identity increase the susceptibility of cells to malignant transformation.[16,20–22] It is now widely accepted that acinar cells clearly contribute to the development of pancreatic intraepithelial (PanIN) preneoplastic lesions.

There is now a consensus on the importance of preserving a stable acinar cell differentiation program as a protective barrier against PDAC.[23–25] Acinar cell differentiation program has tumor suppressor properties by suppressing Kras function.[26] Acinar cell-specific gene expression is driven by PTF1a (Pancreas Transcription factor 1a) that is the main gatekeeper of acinar cell differentiation.[27,28] Silencing of acinar-cell related genes including *Ptf1a* is an initial epigenetic regulation step of ADM.[16,18,19] Maintaining or reintroducing PTF1a in the presence of $Kras^{G12D}$ and inflammation can prevent or reverse tumor initiation.[26,29,30]

Thyroid hormone receptor interactor protein 12 (TRIP12) is an HECT (Homologous to the E6-AP Carboxyl Terminus) type E3 ubiquitin ligase.[31] TRIP12 targets only a few substrates but they exert critical functions in cell-cycle progression, DNA damage response, cell differentiation, chromatin remodeling and chromatin dynamic. We previously demonstrated that TRIP12 is a chromatin associated protein regulating mitosis and that it targets PTF1a for proteasomal degradation.[32,33] We therefore hypothesized that TRIP12 plays a crucial role in PDAC and more particularly in regulating acinar cell fate in initiation steps of PDAC. We investigated the impact of conditional deletion of TRIP12 in mouse models for pancreatic regeneration, $Kras^{G12D}$-mediated cancer initiation and progression.

Materials and Methods

Mice – study approval – genotyping - treatments

To generate conditional Trip12 knockout mice, embryonic stem (ES) cell clones carrying the targeted allele (Trip12$^{tm1a(KOMP)Wtsi}$) were obtained from the KnockOut Mouse Project (KOMP) repository. Targeted ES cell clones (agouti C57BL/6 parental cell line JM8A3.N1) were microinjected into blastocysts of C57BL/6 (CIPHE, Centre d'Immunophénomique, Marseille, France) to generate mouse line Tm1a which was crossed with CIPHE Flippase mouse line to generate Trip12 $^{tm1c\ Ciphe}$ mice carrying the conditional floxed allele.

Mice were housed under specific pathogen-free conditions at the CREFRE (Centre Régional d'Exploration Fonctionnelle et de Ressources Expérimentales) animal facility (Toulouse, France). All animal studies were approved by the Ministère de l'Education Nationale, de l'Enseignement Supérieur et de la Recherche (APAFIS#3600-201512160838611v3) and performed in accordance with institutional guidelines. The following mouse strains were previously described: the LSL-Kras^{G12D} and LSL-p53^{R172H} knock-in mice were from the Mouse Models of Human Cancers Consortium repository (NCI-Frederick, USA), Pdx1-Cre were from DA Melton (Harvard University, Cambridge, MA, USA), Elastase Cre^{ERT2} (Elas-CreER) were from DA Stoffers (Philadelphia, PA, USA) and were kindly provided by Pr P Jacquemin (UCL, Belgium). ZSGreen mice (B6.Cg-Gt(ROSA)26Sor$^{tm6(CAG-ZsGreen1)Hze}$/J) were obtained from the Jackson Laboratory. Mice were interbred on mixed background (CD1/SV129/C57Bl6) to obtain Pdx1-Cre;Trip12$^{f/f}$ (CTT mice), Elas-CreER;Trip12$^{f/f}$ (ETT mice), LSL-Kras^{G12D};LSL-p53^{R172H};Trip12$^{f/f}$;Pdx1-Cre; (KPCTT mice) or LSL-Kras^{G12D};Trip12$^{f/f}$;Elas-CreER (KETT mice). To perform lineage tracing experiments, we generated ZsGreenCTT and ZsGreenETT. Control mice of CTT, ETT, KETT, KPCTT, ZsGreenCTT and ZsGreenETT lack the Trip12 floxed allele and are hereafter referred as Ctt, Ett, KEtt, KPCtt, ZsGreenCtt and ZsGreenEtt respectively.

For genotyping we used PCR protocols recommended by NCI for mutant Kras^{G12D} and p53^{R172H}, by the Jackson Laboratory for ZsGreen detection and by the CIPHE for the detection of Trip12 tm1c allele. Primer sequences used for Pdx1-Cre and Elas-CreER are listed in supplemental Table 1.

Seven week-old ETT and Ett mice were treated with tamoxifen (Sigma-Aldrich) dissolved in corn oil containing 10% ethanol at a concentration of 20 mg/ml. Mice received three intra-peritoneal (i.p.) injections (1 mg/15 g of body weight) on three consecutive days.

Acute pancreatitis was induced at 8 weeks of age by two sets of 6 hourly i.p. caerulein injections (50 µg/kg; Sigma-Aldrich) on alternating days separated by 24 hours after a fasting period of 12 hours. Mice were sacrificed 2, 24 and 120 hours from the end of the experiment. Blood and tissue samples were collected for further analyses. Amylase was measured in plasma (Phadebas). Glycemia was determined from tail blood using a glucose monitor (Accu-Chek Performa). Glucose (2 g/kg of body weight) was injected i.p. and glycemia measured at the indicated times.

Clinical samples

Surgically resected specimens from 27 patients were obtained from the department of pathology (Pr. J Selves, Cancer University Institute of Toulouse) following ethical procedures. They were immunostained with anti-TRIP12 (1:1000, Bethyl laboratories A301) using standard procedures.

Generation of mouse cancer cell lines

Tumor cells were isolated using the explant culture method. Briefly, the resected pancreatic tumors from KPCtt and KPCTT mice were cut into small pieces (0.5-1 mm^3). The tissue pieces were

rinsed in DMEM/F12 (Sigma) supplemented with penicillin (100 U/ml)/streptomycin (100 µg/ml) and transferred into wells of 6-well plates (4-6 pieces per well) containing 800 µl of culture medium (DMEM/F12 supplemented with 10% fetal calf serum (FCS) (Eurobio) and penicillin/streptomycin). The media were renewed every three days and the primary cultures were monitored for 15-35 days for epithelial cell outgrowth. The primary outgrowing epithelial cells were subcultured by trypsinization using a 0.05% trypsin - 0.02% EDTA solution and plated into 25-cm^2 flasks in DMEM/F12 supplemented with 10% fetal calf serum and penicillin/streptomycin. From the second passage, the cells were maintained in DMEM/F12 containing 4.5 g/l glucose, 10% FCS and penicillin/streptomycin. For the colony formation assay cells were seeded at 10^3 cells per 10 cm-plate. After 9-14 days, colonies were stained using 0,5% Cristal violet.

Embryos – optical clearing- segmentation

Mice were bred to obtain Pdx1-Cre;$Trip12^{f/f}$ (CTT) and control Ctt embryos. The day of vaginal plug is defined as E0.5. Adult mice were heavily anesthetized with an overdose of isofluorane. E13.5 and E15.5 embryos were collected in ice-cold phosphate buffer saline, one piece of tail was collected for further DNA extraction and genotyping. Embryos were fixed overnight at 4°C in 10% neutral buffered formalin and then again one hour at room temperature the next day. Fixed samples were washed in PBS for one hour and stored at 4°C. For optical clearing, fixed embryos were rinsed with PBS, included in 1% low-melting agarose (Life Technologies) and dehydrated with 100% methanol. They were cleared with the benzyl alcohol/benzyl benzoate (BABB) technique as previously described.[34] Briefly, embryos were first immersed in a 3/1/2 (v/v) methanol/benzyl alcohol/benzyl benzoate (BABB) solution during 30 min then cleared in 1/2 (v/v) benzyl alcohol/benzyl benzoate. Acquisitions were performed with selective plane illumination microscope (SPIM) technology. MacroSPIM microscope was used for acquisition at 561 nm. Autofluorescence was detected with a 609/57 nm filter and the exposure time was 400 ms. Segmentation of embryos was carried out using Amira software with a dual thresholding method to obtain the volume of the samples. Segmentation of pancreas and liver were done after cropping with Fiji software and using either Amira software or manual selection with appropriate thresholding.

Acinar cell isolation - in vitro acinar to ductal metaplasia formation

Mice were anesthetized with isofluorane and sacrificed by cervical dislocation. Pancreas were quickly resected, rinsed and 100 mg of the organ were placed in 5 ml of cold HBSS (Hank's balanced salt solution) containing 0.01% (w/v) STI (Soybean Trypsin Inhibitor, Sigma) and 1000 U of collagenase II (Thermofisher). Digestion was performed at 37°C during 20 minutes and mechanical dissociation every 5 minutes through 10 back-and-forth passages of the pancreatic tissue into sterile serological pipettes of decreasing size (25, 10, and 5 ml). Following multiple washes with HBSS supplemented with 5% FCS, 0.01% STI and 10 mM Hepes (pH 7.5), digested pancreatic tissue was pelleted by 400 rpm centrifugation, resuspended in DMEM culture medium containing 4.5 g/l glucose, 10% FCS, 10% penicillin-streptomycin mixture, 0.01% STI and filtered through 100 µm Nylon mesh. EGF (final concentration, 20 ng/ml) was added to the acinar suspension. An equal volume of neutralized rat tail collagen (RTC) type I (Corning) was added to the acinar cell suspension and 500µl pipetted into wells of 24-well plate precoated with 100 µl of neutralized RTC. Plates were placed at 37% and 5% CO2. After solidification of the RTC, 1 ml of DMEM culture medium (with above mentioned constituents) was added in each well. Medium was changed on day 1 and day 3. Acinar to ductal metaplasia was quantified using Fiji software.

Histologic analysis - immunohistochemistry and immunofluorescence

Whole embryos and pancreas were fixed in 10% neutral buffered formalin and embedded in paraffin. For histopathological analysis, pancreas were serially sectioned (3 µm) and stained with hematoxylin and eosin (H&E). Histopathological analysis of pancreas and scoring of tissue damage, were performed using representative serial H&E-stained sections (50 µm apart, at least two sections per pancreas). Immunostainings followed standard protocols. Antibodies used for immunohistochemical studies were the following: anti-cytokeratin 19 (rat monoclonal Troma III, developed by Rolf Kemler (Max-Planck Institute, Freiburg, Germany)) obtained from the Developmental Study Hybridoma Bank developed under the auspices of the NICHD and maintained by The University of Iowa, Department of Biology, Iowa City, IA 52242, anti-PTF1a[32], 1:1000), anti-PDX1 (1:1000, Abcam 47267), anti-TRIP12 (1:1000, Bethyl laboratories A301-814A or Sigma HPA036335), anti-E-Cadherin (BD Pharmingen 610181). Slides were imaged using a Hamamatsu Nanozoomer 2 slide scanner (Hamamatsu Photonics) or a Panoramic 250 flash II Scanner. Images were analyzed with caseViewer or QPath software.

RNA isolation - quantitative real-time PCR analysis

Total RNA was isolated from cell lines with Trizol® reagent (ThermoFisher) according to supplier's instructions. RNA concentration was measured with a NanoDrop® ND-1000 spectrophotometer (ThermoScientific). The RevertAid® minus H (company) kit was used according to the manufacturer's recommendations with 2 µg of total RNA. cDNA samples were diluted 1 into 100. qPCR duplicates were carried out using 2 µL of diluted cDNA in a 20 µL-reaction using Sso Fast EvaGreen reagent (BioRad) following supplier's instructions on a StepOne Plus™ Real-Time PCR system (Applied BioSystems). Relative amount of mRNA was calculated by the comparative threshold cycle (Ct) method as $2^{-\Delta Ct}$, where ΔCt=Ct target mRNA – Ct geometric mean of GAPDH, β-Actin and cyclophilin A (supplemental Table 1). Amplification efficacy was verified for every sets of primers.

Western-blotting

Cytosolic protein fraction of freshly prepared acinar cells was isolated using a 10 mM Tris-HCl, (pH 7.5) lysis buffer containing 1.5 mM $MgCl_2$, 5 mM KCl, 1 mM DTT, 0.5% Nonidet™-P40 and 0.5 mM PMSF supplemented with Protease Inhibitor Cocktail (Sigma-Aldrich). Soluble nuclear protein fraction was isolated using a 20 mM Tris-HCl (pH 7.5) lysis buffer containing 400 mM NaCl, 0.025% glycerol, 1.5 mM $MgCl_2$, 1 mM DTT, 0.5 mM PMSF, 0.2 mM EDTA and Protease Inhibitor Cocktail. Protein quantity was determined using Bradford assay. 30-50 µg of nuclear proteins were loaded onto a 10% SDS-PAGE and transferred on nitrocellulose membrane using TransBlot apparatus (BioRad). Membranes were subsequently incubated with TBS Tween-20® 0.01%, 5% fat milk for 1h and with indicated antibodies overnight at 4°C. Membranes were incubated with appropriate HRP-coupled secondary antibodies. Protein abundance was visualized using Clarity™ Western ECL substrate, ChemiDoc™ XRS+ device and ImageLab™ software (BioRad).

Statistical analysis

Data were analyzed by 2-tailed, unpaired Student's t-test using a multiple statistics Graph Pad Prism 9 software package and a difference was considered significant when p value was lower than 0.05. Number of independent experiments is indicated in the figure legends. *, ** and *** indicate a p value <0.05, 0.01 and 0.001, respectively. Gepia data were analyzed by Mantel-Cox test.

Supplemental Table 1

Name	Forward (5’ to 3’)	Reverse (5’ to 3’)
RT-qPCR		
Trip12	GACCCTGAAAGCAACCAGGA	AGAGGTGGTCATGCCAACAG
HPRT	TCAGTCAACGGGGGACATAAA	GGGGCTGTACTGCTTAACCAG
Cyclophilin A	TGTGCCAGGGTGGTGACTTTAC	TGGGAACCGTTTGTGTTTGG
18 S	TGTCTCAAAGATTAAGCCATGC	GCGACCAAAGGAACCATAAC
Amylase	CAGAGACATGGTGACAAGGTG	ATCGTTAAAGTCCCAAGCAGA
Lipase	GGCATTGTTGGTTAACGTTCT	AATTGCGTCCACAAACTGAG
Chymotrypsin	GCAAGACCAAATACAATGCCC	TGCGCAGATCATCACATCG
Mist1	TGGTGGCTAAAGCTACGTGT	CATAGCTCCAGGCTGGTTTT
CK19	CGTGCCGACATAGAGCGCCA	AGCTCAGATGGCCTTGGGGGT
HNF6	CCCTGGAGCAAACTCAAGTC	TGGACGTCTGTGAAGACCAG
SOX9	CTTCTGTGGGAGCGACAACTT	AGGGAGGGAAAACAGAGAACG
PDX1	CGGACATCTCCCCATACG	AAAGGGAGCTGGACGCGG
Genotyping		
PDX1-Cre	CCTGGACTACATCTTGAGTTGC	AGGCAAATTTTGGTGTACGG
Elas-CreER	CTCTGCTAACCATGTTCATGCCT	ACGCTAGAGCCTGTTTTG

Results

Trip12 is overexpressed in human pancreatic preneoplastic lesions and tumors.

We first investigated whether TRIP12 is associated with pancreatic cancer. To this purpose, we performed immunohistochemical analysis on human pancreatic tissue samples. TRIP12 is detected in the nucleus of exocrine and endocrine cells of healthy pancreas. Immunostaining intensity is weak and TRIP12 is heterogeneously present within acinar, ductal and islets structures **(Figure 1A)**. We found that TRIP12 is markedly overexpressed in pancreatic tumors **(Figure 1B).** This was supported by mRNA data from the Gene Expression Profiling Interactive Analysis (GEPIA) **(Figure 1C)**.

Overexpression of TRIP12 is observed at the earliest stage of the disease in low grade precancerous lesions **(Figures 1D and 1E)** supporting the hypothesis that TRIP12 plays a role in the initiation steps of PDAC. Interestingly, high Trip12 mRNA expression in tumors is associated with poorer patient survival suggesting that TRIP12 plays also a role during PDAC progression **(Figure 1F)**.

Trip12 deficiency during embryogenesis does not reveal major pancreatic abnormalities in embryos.

We examined the pattern of expression of TRIP12 in the murine pancreas in control mice. Similarly to human pancreas, Trip12 is heterogeneously present in the nuclei of murine acinar, duct cells and islet cells with a subset of cells that do not express TRIP12 **(Figure 2A)**. Since lethality was previously demonstrated in Trip12 knock-in mutant mice at the embryonic stage E11.5, we investigated the functional requirement of TRIP12 during pancreas development.[35] We crossed mice carrying floxed alleles of Trip12 gene with Pdx1-Cre mice to deplete TRIP12 protein expression in embryonic pancreatic progenitors **(Figure 2B)**. We analyzed embryos at E13.5 and E15.5. Embryos from the different expected genotypes were obtained according to the Mendelian ratio (Data not shown). A low expression of TRIP12 was detected in embryonic pancreas of wild-type embryos **(Figure 2C)**. We examined whether pancreas development was affected by the ablation of Trip12 gene in pancreatic progenitors using optical clearing of whole embryos for visualization of their pancreas at both embryonic stages. Quantification showed no differences in embryo and pancreas volumes between control and Trip12 knockout embryos **(Figure 2D)**. The expression pattern and intensity of PTF1a and Pdx1 in E13.5 and E15.5 TRIP12 deficient CTT embryos were similar to TRIP12-expressing controls **(Figure 2E)**. These data suggest that TRIP12 is dispensable for pancreatic development in mice.

Trip12 deficiency during embryogenesis reveals pancreatic abnormalities in adults.

Viable offspring was obtained. Pdx1-Cre;Trip12$^{f/f}$ (CTT) mice appear healthy and are indistinguishable in appearance from the Ctt control littermates. Pancreas of TRIP12 deficient CTT mice exhibit grossly normal morphology (Data not shown). Immunofluorescence staining confirmed a loss of TRIP12 in all pancreatic cell types and comparison of H&E showed no histological changes except a pancreatic steatosis in all TRIP12 deficient CTT mice examined at the age of 3-4 months **(Figure 3A)**. While body weight of TRIP12 deficient CTT and Ctt control mice are similar at all examined post-natal stages, we observed significant alterations of pancreas to body weight ratio starting at 30 days of age in males and over 3 months of age in females **(Figure 3B)**. We performed intraperitoneal glucose tolerance test to evaluate whether conditional TRIP12 depletion affects blood glucose homeostasis. Fasting glycemia and response to glucose overload are not significantly different in TRIP12 deficient CTT and control Ctt mice at the age of 1 to 3 months indicating that TRIP12 gene depletion in the pancreas does not affect endocrine function of young adults **(Figure 3C)**.

Although exocrine pancreatic tissue appeared normal, immunofluorescence and Western blot data revealed an increased PTF1a expression in TRIP12 deficient CTT acinar cells compared to control Ctt acini **(Figure 3D)**. This was consistent with our previous results that demonstrated PTF1a targeting by TRIP12.[32] In support of a post-translational role of TRIP12 in regulating PTF1a levels, PTF1a mRNA expression was unaffected by the ablation of TRIP12 **(Figure 3E)**. These data suggest a role of TRIP12 in acinar cell phenotype maintenance.

Trip12 deficiency in adult acinar cells does not alter acinar cell morphology.

Since Pdx1-expressing cells give rise to all the pancreatic lineages and adult cell types, we generated a conditional model with acinar-cell specific ablation of Trip12 gene to study the role of TRIP12 more specifically in these cells. We used Elas-CreER mice in which a conditional disruption of Trip12 gene in adult mice is induced by administration of tamoxifen **(Figure 4A)**. The Elas-CreER;Trip12$^{f/f}$ (ETT) TRIP12 deficient mice are macroscopically indistinguishable from Ett control mice. Their pancreas to body weight ratio significantly decreases at 5 months of age, 3 months after tamoxifen treatment **(Figure 4B**). They exhibit no macroscopic modifications of their pancreas and H&E staining showed similar pancreas phenotypes for control and TRIP12 deficient mice **(Figure 4C)**.

We combined an inducible deletion of Trip12 gene to a lineage tracing by using ZsGreen mice **(supplemental Figure S1)**. As expected from the Cre-activity pattern in Elas-CreER mice, ZsGreen expression is present in acinar cells but absent in duct cells and islet cells **(supplemental Figure 1)**. We further confirmed acinar Trip12 deletion by immunofluorescence and Western-blot in ETT isolated acinar cells **(Figure 4D)**. We observed increased immunostaining of PTF1a in TRIP12 deficient ETT acinar cells compared to Ett controls. These data indicate that TRIP12 is dispensable for acinar cell morphology in basal conditions.

Trip12 is required for ADM formation in vitro.

Acinar cells undergo acinar to ductal metaplasia (ADM), a reprogramming process to form metaplastic ducts in response to inflammation and/or Kras^{G12D} mutation that precedes the formation of PanIN arising from acinar cells. Given the elevated level of TRIP12 in these early-stage preneoplastic lesions and the repertoire of known TRIP12 functions, we investigated whether it plays a role in the regulation of acinar cell plasticity in response to injury. We used an established 3D acinar cell culture to model the conversion of acinar cells and a lineage tracing with the ZsGreen reporter allele to follow the fate of TRIP12-deficient cells. Acinar cells were isolated from pancreas of ZsGreenCtt and ZsGreenCTT mice **(Figure 5A)**. We also investigated the consequences of TRIP12 depletion in adult pancreas by using ZsGreenEtt and ZsGreenETT mice after tamoxifen induction of acinar-specific recombination **(Figure 5D)**. ADM was initiated by an addition of EGF. Control acinar cells expressing or not ZsGreen and TRIP12-depleted ZsGreen expressing cells from both mice models remain organized in small acinar cell clusters after one day of culture **(Figure 5B and 5E)**. We observed a lower level of acinar cell recombination in adult acinar cells than in embryonic pancreatic progenitors. Indeed, expression of ZsGreen is detected in almost 100% of cells when induced during embryogenesis **(Figure 5B)** but only in 30% when induced in adults **(Figure 5E)**. As expected, after 4 days of culture in the presence of EGF, both ZsGreenCtt and ZsGreenEtt control acini convert to ductal cyst structures with a single cellular layer surrounding an empty lumen **(Figures 5B and 5E)**. Importantly, ZsGreen expression has no impact on the viability of acinar cell 3D culture and does not prevent ADM in TRIP12-expressing ZsGreenEtt and ZsGreenCtt control acini. Unlike control TRIP12 expressing acini, TRIP12 deficient-acinar cells do not transdifferentiate into ductal cells. The ductal epithelium observed in both

ZsGreenCTT and ZsGreenETT TRIP12 deficient mice never contained ZsGreen expressing cells as shown in **Figure 5B** and **5E**. The absence of TRIP12 was linked to the presence of cell clusters of various sizes where sometimes a tiny lumen could be distinguished. In any cases, these cell clusters never resembled ductal cyst structures. Quantification of these cell clusters and of metaplastic ducts demonstrated that TRIP12 is required for acinar to ductal metaplasia **(Figures 5C and 5F)** and contributes to acinar cell plasticity.

Trip12 is required for ADM formation in vivo.

The 3D culture models that we used recapitulate acinar cell dedifferentiation similarly as how it occurs during pancreatitis. We therefore induced acute pancreatitis in control and TRIP12 knockout mice to investigate the role of TRIP12 in vivo. To avoid any still uncharacterized events linked to the absence of TRIP12 in embryonic pancreas, we used ETT and Ett mice and analyzed histological changes in response to pancreatic injury at three time points **(Figure 6A)**. Induction of pancreatitis was confirmed by an increase of the plasma amylase levels that is similar in both groups **(Figure 6B)**. Two hours after the last caerulein injection, pancreas of both genotypes are oedematous and infiltrated by immune cells **(Figure 5C)**. Vacuolization of acinar cells and distension of acinar lumens revealing initiation of ADM are observed in control mice and TRIP12 deficient mice. However, the response to injury is different in TRIP12-depleted acinar cells. They exhibit disruption in the acinar structure, mislocalization of the nuclei out of the basolateral pole and asymmetric and multilobed lumen. Alteration of the pancreas is more pronounced as the inflammatory process progresses. Analysis 24 hours after injury showed entire lobules of control mice with extensive ADM where acinar cells have lost polarity and adopted a columnar morphology similar to ductal cells. In contrast, TRIP12-depleted acini exhibit hypertrophy, one or more enlarged lumen but do not evolve towards a ductal phenotype. They are characterized by the presence of numerous vacuoles of different sizes that contain or not cellular or amorphous material **(Figure 5C)**. Five days after caerulein treatment, Ett tissue revert back to its original morphology while ETT pancreas retain several defects. Tissue disruption and vacuoles are still present suggesting that longer duration is required for a complete recovery in the absence of TRIP12 **(Figure 5C)**.

We examined the expression pattern of PTF1a, cytokeratin19 (CK19) and PDX1 by immunofluorescence at the same time-points **(Figures 6D and 6E)**. We used E-cadherin immunostaining to outline the cells. Pancreas of Ett control mice at the 2h show an increased CK19 staining in acinar cells compared to absence of expression in acinar cells of vehicle-treated mice. In accordance with ADM, CK19 expression peaks by day 1 and returns to basal levels at day 5. In contrast to vehicle-treated mice pancreas CK19 expression is detected 2h after caerulein treatment in TRIP12-depleted acini but at lower levels than in control mice at the same time point. CK19 expression does not increase by day 1 in the absence of TRIP12 confirming the altered differentiation response to caerulein. Unlike Ett control pancreas CK19 immunostaining is restricted to centroacinar lumen, it does not extend in basolateral location and is still observed by day 5, staining a subset of centroacinar lumen in ETT TRIP12 deficient pancreas **(Figures 6D and 6E)**.

The expression pattern of nuclear PTF1a and PDX1 during acute pancreatitis is altered by TRIP12 ablation. PTF1a expression in caerulein-treated Ett acinar cells is reduced 2h after the last injection, sharply increases by day 1 and decreases at basal level after 5 days. Immunofluorescence analysis revealed that PTF1a expression in vehicle-treated mice is increased in TRIP12-depleted acinar nuclei. A striking difference with Ett acinar cells is observed by day 5. Indeed, no PTF1a is detected in acinar cells in absence of TRIP12 **(Figure 6D)**. In vehicle-treated control and ETT pancreas, PDX1 is strongly

detected in the nucleus of endocrine cells but weakly in acinar cells. PDX1 expression strongly increases in Ett and ETT acinar cells one day after caerulein treatment. It is barely detectable by day 5 in control Ett acini but still overexpressed in TRIP12-depleted ETT acinar nuclei **(Figure 6E)**. These data show that TRIP12 is important for ADM formation in vivo and its depletion alters differentiation response to caerulein in mice.

TRIP12 collaborates with Kras to initiate pancreatic carcinogenesis.

Several studies showed that Kras oncogene expression in adult acinar cells initiates PDAC. We hypothesized that altered ADM that is observed in absence of TRIP12 have consequences on PDAC initiation. To investigate the role of TRIP12 in pancreatic carcinogenesis, we crossed Elas-CreER;Trip12$^{f/f}$ mice with LSL-Kras^{G12D} mice **(Figure 7A)**. Activation of Kras^{G12D} and loss of TRIP12 was achieved by administration of tamoxifen. Since promotion of ADM by caerulein accelerates Kras-induced PanIN formation, we also examined the effect of acute pancreatitis.[36] KEtt and KETT were treated or not with caerulein and sacrificed two or three months after tamoxifen treatment respectively **(Figure 7B)**. We observed no macroscopic changes between KEtt control and KETT TRIP12 deficient pancreas in both conditions. Histological analysis revealed the presence of rare ADM and low grade PanIN lesions in the pancreas of KEtt mice untreated with caerulein **(Figures 7C and 7D)**. PanIN lesions exhibit positive staining for alcian blue and are embedded in a fibrotic stroma **(Figure 7D**). No evidence of malignant or preneoplastic lesions is found in any of the KETT mice pancreas that exhibit normal acinar tissue and no fibrosis. Two months after acute caerulein KEtt mice develop large regions containing PanIN **(Figures 7C, and 7D)**. In contrast, pancreas of KETT TRIP12 deficient mice have no PanIN lesions nor ADM but exhibit vacuolized hypertrophied acinar cells **(Figure 7D)**.

These results demonstrate that inactivation of TRIP12 prevents oncogenic Kras-induced PanIN formation. They indicate that TRIP12 is an essential factor for initiation steps of pancreatic carcinogenesis. They also suggest that TRIP12 regulation of acinar cell plasticity is required for transformation by Kras oncogene.

TRIP12 depletion limits tumor growth.

TRIP12 is overexpressed in pancreatic tumors **(Figures 1B and 1C)**. Kaplan-Meier analysis of the patients survival stratified by expression level of TRIP12 shows that patients with a low TRIP12 expression exhibit a better survival than patients with a high TRIP12 expression **(Figure 1F)**. We previously demonstrated that TRIP12 exerts important functions during cell cycle and that a depletion of TRIP12 significantly inhibits cancer cell growth.[33] We hypothesized that TRIP12 influences PDAC growth and progression. We generated mouse cohorts of the consensus KPC mouse PDAC model combining oncogenic Kras with inactivation of p53 with or without TRIP12 ablation **(Figure 8A)**. Unexpectedly, survival of KPCTT mice is not significantly increased compared to that of KPC (**Figure 8B**). However, three KPCTT mice still survive at the age of 18 months. Clinical spectrum of the disease depicted in **Figure 8C** shows that metastases are more frequent in KPCtt control than in KPCTT TRIP12 deficient mice. Autopsy and histological analysis revealed that tumors replace the whole pancreas in the majority of KPC mice (3/4) while it is observed in 20% of KPCTT pancreas (1/5) **(Figure 8D)**.

We generated pancreatic cancer cell lines from tumors of KPC mice and from tumors of KPC mice with heterozygous and homozygous deletion of TRIP12 **(Figure 8E)**. **Figure 8F** shows that TRIP12 depletion does not inhibit the capacity of KPC cells to form colonies but significantly decreases the size of colonies. KPCTT cells were less proliferative than KPC cells **(Figure 8G)**. These results demonstrate that TRIP12 is required for pancreatic cancer cells growth.

Discussion – What remain to be done

In the present study, we provide several lines of evidence supporting a new key role of TRIP12 in the induction of ADM and the formation of PanIN. We demonstrate that TRIP12, which is expressed at low levels in the healthy pancreas, is markedly overexpressed in pancreatic preneoplastic pancreatic lesions and tumors. Using two conditional Trip12 knockout mice models, we reveal that TRIP12 expression is required for ADM formation. We also show that TRIP12 deficiency impedes the formation of ADM and PanIN in the presence of mutant Kras and reduces the growth of tumors when mutated P53 is concomitantly present.

We are aware that our findings are mainly descriptive. Therefore, this discussion will propose supplemental experiments to better understand the molecular mechanisms of action of TRIP12.

TRIP12 deletion during embryogenesis has a noticeable impact in adults causing pancreatic steatosis associated with reduced pancreas weight that may reflect impaired pancreatic exocrine function. Deficiency of UBR1, an E3 ubiquitin ligase of the N-end rule pathway which is part of the ubiquitin-proteasome system[37], induces similar defects in mouse pancreas and in Johansson-Blizzard Syndrome patients.[38,39] These alterations were not observed following TRIP12 invalidation in adult acinar cells. Since Trip12 deficiency in pancreatic progenitors does not reveal major pancreatic abnormalities in embryos, we hypothesize that TRIP12 is required for the proper implementation of the stimulus-secretion coupling of pancreatic acinar cells during embryogenesis. To further address the phenotype of TRIP12-deficient pancreas, we will assess the expression of digestive enzymes by immunostaining. The secretory response of isolated acinar cells to increasing doses of the secretagogue cholecystokinin will allow detection of impaired pancreatic exocrine function. These experiments will be performed in CTT and ETT TRIP12 deficient mice models and their respective TRIP12 expressing controls.

In physiological conditions, PTF1a mRNA expression remains unchanged supporting our previous demonstration of a post-translational regulation of PTF1a that does not operate in TRIP12-depleted acinar cells.[32] Acinar digestive enzymes encoding mRNA level controlled by PTF1A is unchanged while mRNA level of Sox9 and CK19 ductal markers decreases (Data not shown) suggesting that a change of the differentiation balance in favor of the acinar phenotype sets up in the absence of TRIP12. To validate this hypothesis, we propose to perform a complete transcriptomic profiling of RNA extracted from TRIP12-deficient and control acinar cells.

Our findings highlight the key role of TRIP12 for acinar cell plasticity and show that loss of a single protein blocks the reprogramming process in response to pancreatic injury. Of importance, TRIP12 deficiency also impedes the formation of ADM in presence of mutant $Kras^{G12D}$ indicating that TRIP12 is required for the transformation by the Kras oncogene. However, we will confirm the in vivo data by performing in vitro ADM with acinar cells obtained from Kras expressing TRIP12-deficient or control mice.

The role of epigenetic regulation in the initiation steps of PDAC is now demonstrated. Transient expression of reprogramming factors has been demonstrated to induce ADM.[16] The repression of acinar cell enhancers that reduces the expression of acinar cell transcription factors and increases expression of ductal genes is now recognized as an ADM inducer. Coherently, deletion of acinar-cell transcription factors leads to ADM.[25,26,40–42] Inversely, forced expression of these factors prevents ADM formation.[29,30] Increased PTF1a expression in Trip12 knockout acinar cells in basal conditions suggests that a repressive pathway is inhibited in these cells.

Several evidence support that TRIP12 ubiquitin ligase activity could contribute to repress acinar cell enhancers. During ADM, the epigenetic repression of acinar enzymes and transcription factors is initiated and maintained by the repressive histone marks H2AK119Ub (monoubiquitination of histone H2A on lysine119) and H3K27me3 (trimethylation of histone H3 on lysine27).[18,19] TRIP12 is known to mediate the proteolysis of ASXL1 a component of the Polycomb Repressive Deubiquitinase (PR-DUB) that deubiquitinates histone H2A.[43] Therefore, by preserving Polycomb gene silencing TRIP12 might contribute to the repression of acinar genes. Ablation of TRIP12 would prevent the epigenetic reprogramming of acinar cells and maintain the acinar program. We propose to validate this hypothesis by investigating the expression of the repressive marks H2AK119Ub and H3K27me3 and of ASXL1 during ADM in controls and TRIP12 knockout mice. The proposed repressive role of TRIP12 is also in agreement with the tight interaction of TRIP12 with the chromatin and our unpublished data showing that overexpression of TRIP12 contributes to chromatin condensation.[33] We propose to verify these assumptions by performing genome-wide chromatin immunoprecipitation DNA sequencing for TRIP12 in acinar cells (Chip-seq).

Finally, our results show that while needed for cancer initiation TRIP12 is dispensable for pancreatic tumors formation when the oncogenic Kras is associated with a loss of a tumor suppressor. Reduced growth and less metastases formation are preliminary arguments supporting the fact that tumors are different in absence of TRIP12. However, we need to perform a more detailed phenotypic and molecular analysis of TRIP12-deficient tumors. The pancreatic cell lines that we generated from the murine tumors will be useful tools for supplemental investigations including chemiosensitivity studies and expression analysis of epithelial, mesenchymal and progenitor markers.

The activity of the proteasome is required for the formation of PanIN.[44] To our knowledge, except for FBW7, the role of E3 ubiquitin ligases has been poorly investigated in pancreatic cancer initiation.[9] Our findings identify TRIP12 as an important inducer of ductal identity that plays an essential role in acinar-to-ductal reprogramming and in Kras-driven PanIN formation. Molecular mechanisms must be elucidated but our data may facilitate strategies aimed at preserving and/or regaining the acinar identity.

Acknowledgements

We thank F. Fiore for CIPHE service monitoring, all members of animal facility of CREFRE, Imag'IN platform and Pathology department of Institut Universitaire du Cancer de Toulouse, C. Segura from the histology platform of Institut des Maladies Métaboliques et Cardiovasculaires de Toulouse. We thank, Drs J. Rouquette (RESTORE Research Center), F. Larminat (Institut de Pharmacologie et de Biologie Structurale of Toulouse) and L. Bartholin (Centre de Recherche en Cancérologie of Lyon) for discussions.

Fundings

This project was funded by La Ligue Contre le Cancer and the Fondation Toulouse Cancer Santé. Manon BRUNET was funded by the University Paul Sabatier and La Ligue Contre le Cancer. Claire VARGAS was funded by the University Paul Sabatier of Toulouse.

Author contribution statement

M.B.: design of the work, acquisition, analysis and interpretation of data, writing of the manuscript
C.V.: acquisition of data
M.F.: acquisition of data
L.P.: acquisition of data
H.L.: acquisition of data
F.C.: acquisition of data
V.G.: substantial contributions to the conception
J.G.G: substantial contributions to the interpretation of data
J.T.: substantial contributions to the conception and interpretation of data
M.D.: conception and design of the work, acquisition, analysis and interpretation of data, writing of the manuscript

Figures legends

Figure 1: Trip12 is overexpressed in human pancreatic preneoplastic lesions and tumors

A. TRIP12 Immunohistochemistry on non-pathological pancreas (n=9). Scale bars: 300 µm (left), 50 µm (right).

B. Representative TRIP12 immunohistochemistry in human pancreatic adenocarcinoma (n=9). Scale bar: 300 µm.

C. Expression of Trip12 mRNA in pancreatic tumors (red, n=179) and normal pancreas (blue, n= 171), obtained from Gepia database.*p<0.05 (unpaired t-test).

D. Representative TRIP12 immunohistochemistry in sections of human pancreas containing PanINs (n= 27). Scale bar: 300 µm.

E. Quantification of TRIP12 positive nuclei in 78 non neoplastic and 537 neoplastic ducts from 9 PDAC samples, in 170 PanIN1, 62 PanIN2 and 29 PanIN3 from 21, 18 and 12 samples respectively. Each dot represents the mean percentage of TRIP12 positive nuclei in each quantified sample.

F. Kaplan Meyer survival plots of TRIP12 high (orange, n=89) and low (red, n=89) expressing PDAC patients. Data obtained from Gepia database.

Figure 2: Trip12 deficiency during embryogenesis reveals no major pancreatic abnormalities in embryos

A. Immunostaining of TRIP12 in adult wild-type mice pancreas. TRIP12 is expressed in acinar (A), ductal (D) and pancreatic endocrine cells in islets of Langerhans (I). Scale bar: 100 µm.

B. Schematic representation of the CTT mouse model. Cre recombinase expression is driven by the Pdx1 promoter. Yellow triangles indicate loxP sites.

C. Immunofluorescence staining of TRIP12 and PDX1 in pancreas of E13 and E15 embryos. Nuclei are counterstained with DAPI. Scale bars: 20 µm.

D. Quantification of the volumes of CTT (black bars, n=4) and Ctt (white bars, n=4) E13 and E15 embryos and their pancreas. Embryos were optical cleared and acquisition was performed with selective plane illumination microscope (SPIM) technology. Segmentations were carried out as described in Materials and Methods using AMIRA software. The volume of the liver of each embryo was also determined and used as a control parameter unaffected by TRIP12 depletion. The bars represent the means ± SD.

E. Immunofluoresence staining of PDX1 and PTF1a in CTT and Ctt E13 and E15 embryo. Nuclei are counterstained with DAPI. Scale bars: 100 µm.

Figure 3: Trip12 deficiency during embryogenesis reveals pancreatic abnormalities in adults

A. Immunofluorescence staining of TRIP12 in Ctt and CTT pancreas in acinar (A), ductal (D) and endocrine cells (I). Nuclei are counterstained with DAPI. Scale bars: 50 µm. H&E staining of Ctt and CTT adult mice pancreas. Scale bars: 200 µm.

B. Pancreas/body weight ratio of Ctt control mice and CTT TRIP12 knockout mice. Males and females are shown separately. Data are means ± SD, * p<0.05 and **p<0.01.

C. Glycemia after intraperitoneal glucose injection in control Ctt (bold lines) males (blue, n=27) and females (pink, n=6) and CTT TRIP12 knockout (dashed lines) males (blue, n=17) and females (pink, n=10) mice. Males and females were 1 to 3 months old.

D. Left: Immunostaining of PTF1a (red) in Ctt and CTT adult pancreas mice at the age of 3 months. Nuclei are counterstained with DAPI (blue). E cadherin staining (green) delimits the cells. Scale bars:

100 µm. Right panel: Western-blot analysis of protein extracted from Ctt and CTT isolated acinar cells showing protein levels of TRIP12 and PTF1a. PCNA was used as loading control.
E. qRT-PCR analysis of TRIP12 and PTF1a mRNA levels in Ctt (black bars) and CTT (white bars) isolated acinar cells (n=3). Data are expressed as percentage of expression in Ctt acinar cells normalized by HPRT, cyclophilin A and 18S genes expression.

Figure 4: Trip12 deficiency in adult acinar cells does not alter acinar cell morphology
A. Schematic representation of the ETT model where CreER recombinase expression is driven by the Elastase Cre^{ERT2} promoter and experimental approach. Yellow triangles indicate loxP sites.
B. Pancreas/body weight ratio, mouse and pancreas weight of control Ett (n=7) and TRIP12-depleted ETT mice (n=6). Data are means ± SEM, *indicates a p value <0.05.
C. H&E staining of Ett and ETT pancreas 4 months after tamoxifen treatment. Boxes indicate enlarged regions. Scale bars: 200 µm.
D. Left panel: Immunofluorescence staining of TRIP12 in Ett and ETT pancreatic acinar cells. Nuclei are counterstained with DAPI. Scale bars: 20 µm. Right panel: Western-blot analysis of protein isolated from ETT acinar cells. PCNA is used as loading control.
E. PTF1a Immunohistochemistry in TRIP12-depleted ETT acinar cells compared to Ett controls. Scale bars: 50 µm.

Figure 5: Trip12 is required for ADM formation in vitro
A. Schematic representation of the Pdx1-Cre; $ZsGreen^{f/f}$;$Trip12^{f/f}$ (ZsGreenCTT) and the Pdx1-Cre;$ZsGreen^{f/f}$ (ZsGreenCtt) mice.
B. Bright field and fluorescence images of acinar cell clusters and ductal cyst structures from isolated acinar cells from ZsGreenCtt and ZsGreenCTT pancreas on day 1 and on day 4 after isolation and treatment with EGF. Enlarged images are shown. Note the absence of fluorescence in the ductal cyst from ZsGreenCTT pancreas (red asterisk). Red # indicate ZsGreenCTT acinar cell clusters that do not undergo acinar to ductal metaplasia. Red arrows show the lumen of one abnormal ZsGreenCTT ductal structure. Scale bars: 50 µm.
C. Quantification of acinar cell clusters, ductal cyst structures and abnormal ductal structures (Uncompleted metaplasia: characterized by multilobed lumen, absence of ductal flat epithelium and presence of acinar cells) by day 4 after acinar cell isolation and treatment with EGF.
D. Schematic representation of the Elas-CreER;$ZsGreen^{f/f}$;$Trip12^{f/f}$ (ZsGreenETT) and the Elas-CreER;$ZsGreen^{f/f}$ (ZsGreenEtt) mice.
E. Bright field and fluorescence images of acinar cell clusters and ductal cyst structures from isolated acinar cells from ZsGreenEtt and ZsGreenETT pancreas on day 1 and on day 4 after isolation and treatment with EGF. Enlarged images are shown. Note the absence of fluorescence in the ductal cyst from ZsGreenETT pancreas (red asterisks). Red arrows show the lumen of one abnormal ZsGreenETT ductal structure. Scale bars: 50 µm.
F. Quantification of acinar cell clusters, ductal cyst structures and abnormal ductal structures (Uncompleted metaplasia: characterized by multilobed lumen, absence of ductal flat epithelium and presence of acinar cells) by day 4 after acinar cell isolation and treatment with EGF.

Figure 6: Trip12 is required for ADM formation in vivo
A. Experimental design of caerulein-induced acute pancreatitis in the ETT and Ett mice. Inactivation of TRIP12 is induced by injections of tamoxifen at the age of seven weeks. Controls are also treated with

tamoxifen. Pancreatitis is induced one week later. Mice are sacrificed 2 hours (0), 24 hours (1) and 5 days (5) from the last injection.

B. Plasma amylase levels of Ett (black bars, n=3) and ETT (white bars, n=3) were determined at 2h, 1 day or 5 days after the last injection. Values are means ± SEM.

C. H&E sections of Ett or ETT mice treated with vehicle or caerulein and analyzed at 2 h, 1 day and 5 days after the last injection. Enlarged boxes show acini (green frame), initiation of acinar–to-ductal metaplasia (orange frame), final acinar-to-ductal metaplasia (blue frame). Control Ett acinar cells exhibit central distended lumen at 2 hours that evolves towards a ductal phenotype by day 1. ETT acini appear disrupted (arrows) with mislocalized nuclei, do not transdifferentiate but exhibit vacuoles of various sizes (red frame). Scale bars: 200 µm.

D. PTF1a (orange) and CK19 expression (red) immunofluoresence at the indicated times after caerulein treatment. E cadherin (E-cad, green) is used to delimit cells. Scale bars: 50µm.

E. PDX1 (orange) and CK19 expression (red) immunofluoresence at the indicated times after caerulein treatment. E cadherin (E-cad, green) is used to delimit cells. Scale bars: 50 µm.

Figure 7: Trip12 collaborates with Kras to initiate pancreatic carcinogenesis in adult pancreas

A. Schematic representation of the KETT murine model. Yellow triangles indicate loxP sites. TRIP12 deletion and $Kras^{G12D}$ activation are induced by tamoxifen at the age of 7 weeks.

B. Experimental design. Tamoxifen is injected at 7 weeks and acute pancreatitis is induced or not one week later.

C. Clinical spectrum of disease in Kett and KETT mice treated or not with caerulein. N, proportion of mice with pancreatic preneoplastic lesions. F represents the frequency of lesions in examined pancreas sections: Low (L) <10% of the pancreas area exhibit lesions. P = percentage of cells within a specified lesion that stained positive for alcian blue and Sirius red (a = <10%, b=10-50%, c= >50% of the cells were positive). Na, not applicable.

D. Histological analysis of KEtt, and KETT mice treated or not with caerulein. Scale bars: 50µm.

Figure 8: TRIP12 depletion limits tumor growth

A. Schematic representation of the KPCtt and KPCTT models. Yellow triangles indicate loxP sites.

B. Survival of KPCtt and KPCTT mice.

C. Clinical spectrum of disease in KPCtt and KPCTT mice. *Three mice are still alive. Na, not applicable; N, number of mice with tumors; Y, Yes; N, no.

D. Representative macroscopic views of KPCtt (KPCtt-35) or KPCTT (KPCTT-28) pancreas at necropsy and H&E stainings. Scale bars: 1 000 µm.

E. TRIP12 protein expression in KPC, heterozygous KPCTt and homozygous knockout KPCTT cell lines was determined by Western-blot. PCNA is used as a loading control.

F. Colony formation assay of KPC, KPCTt and KPCTT cells. Cells were seeded at 10^3 cells per 10 cm-plate. After 9-14 days, colonies were stained using Cristal violet.

G. Cell proliferation of KPC, KPCTt and KPCTT cell lines. The results are expressed as growth percentage compared to T=0h and represent the mean ± SEM of three separate experiments.

Figure 1: Trip12 is overexpressed in human pancreatic preneoplastic lesions and tumors

A

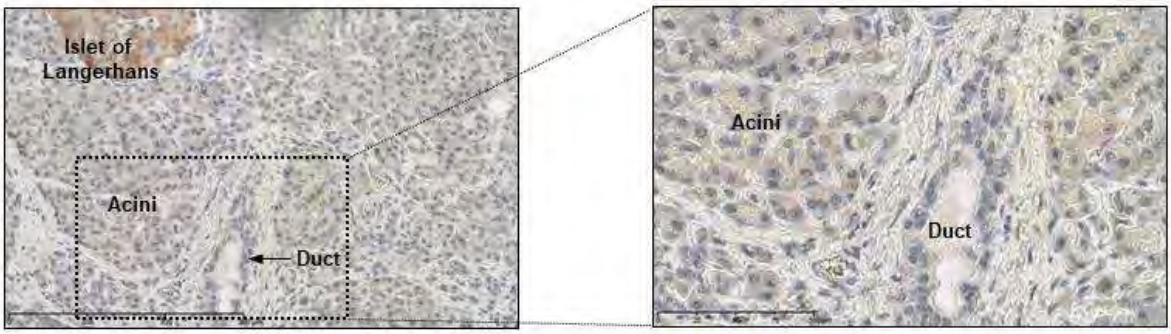

A. TRIP12 Immunohistochemistry on non-pathological pancreas (n=9). Scale bars: 300µm (left), 50µm (right).

B

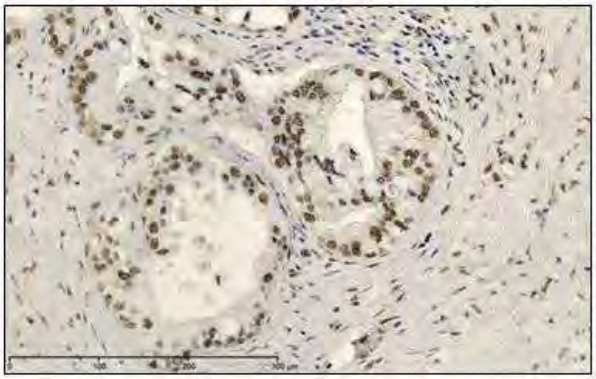

B. Representative TRIP12 immunohistochemistry in human pancreatic adenocarcinoma (n=9). Scale bar: 300µm.

C

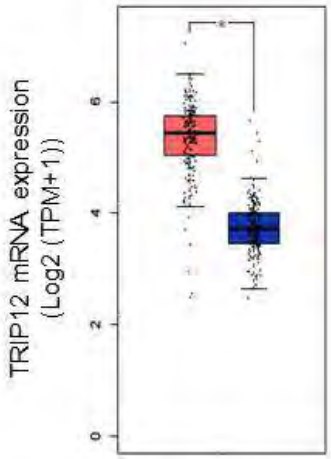

C. Expression of TRIP12 mRNA in pancreatic tumors (red, n=179) and normal pancreas (blue, n= 171), obtained from Gepia database .*p<0.05 (unpaired t-test).

Figure 1: Trip12 is overexpressed in human pancreatic preneoplastic lesions and tumors

D

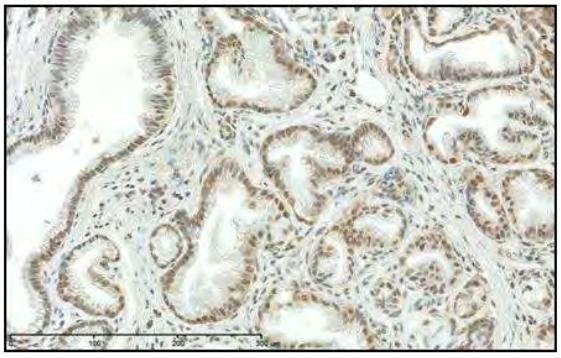

D. Representative TRIP12 immunohistochemistry in sections of human pancreas containing PanINs (n= 27). Scale bar: 300µm.

E

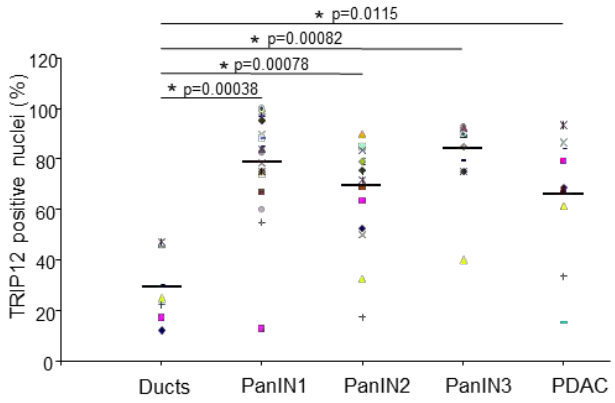

E. Quantification of TRIP12 positive nuclei in 78 non neoplastic and 537 neoplastic ducts from 9 PDAC samples, in 170 PanIN1, 62 PanIN2 and 29 PanIN3 from 21, 18 and 12 samples respectively. Each dot represents the mean percentage of TRIP12 positive nuclei in each quantified sample.

F

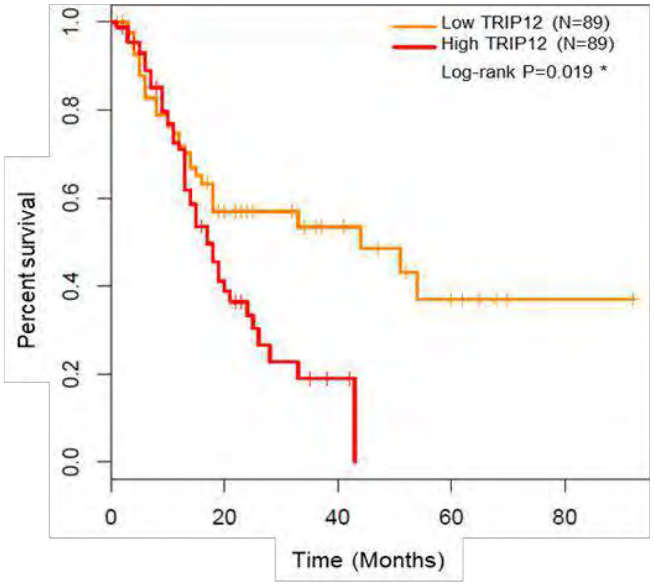

F. Kaplan Meyer survival plots of TRIP12 high (orange, n=89) and low (red, n=89) expressing PDAC patients. Data obtained from Gepia database.

Figure 2: Trip12 deficiency during embryogenesis reveals no major pancreatic abnormalities in embryos

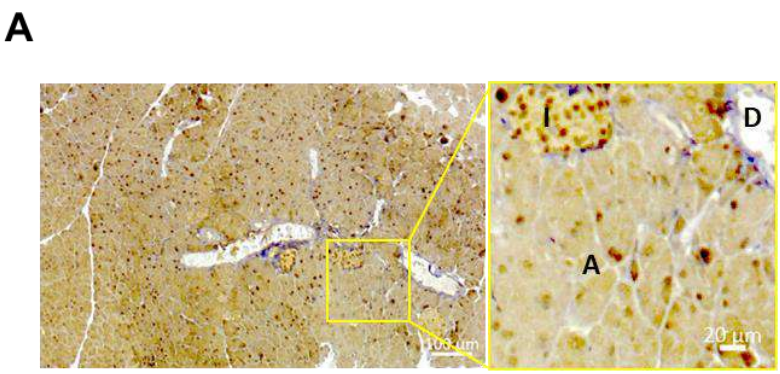

A. Immunostaining of TRIP12 in adult wild-type mice pancreas. TRIP12 is expressed in acinar (A), ductal (D) and pancreatic endocrine cells in islets of Langerhans (I). Scale bar: 100µm.

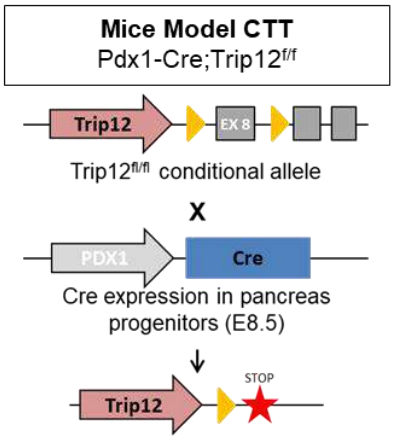

B. Schematic representation of the CTT mouse model. Cre recombinase expression is driven by the Pdx1 promoter. Yellow triangles indicate loxP sites.

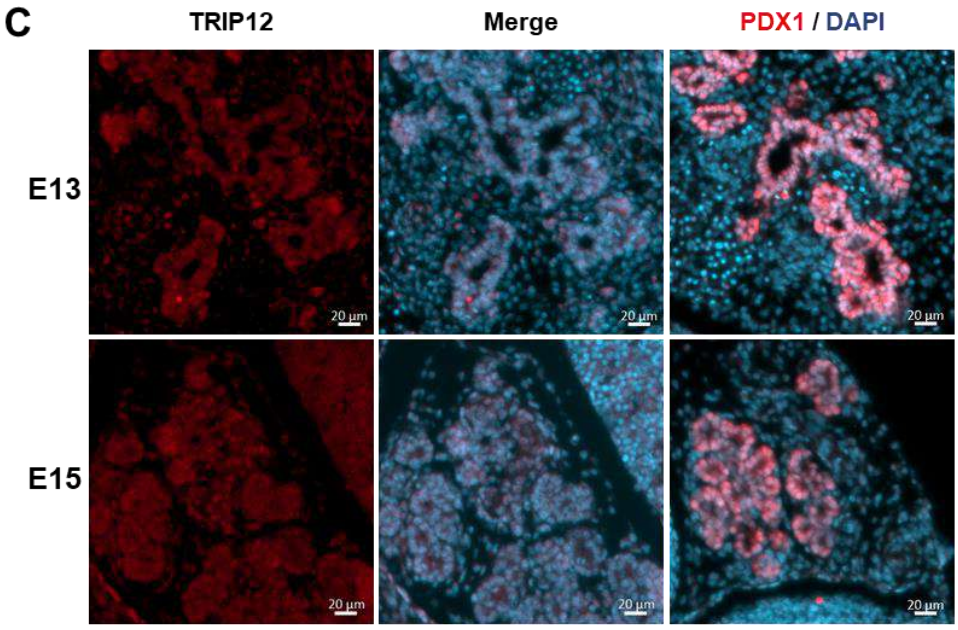

C. Immunofluorescence staining of TRIP12 and PDX1 in pancreas of E13 and E15 embryos. Nuclei are counterstained with DAPI. Scale bars: 20µm.

Figure 2: Trip12 deficiency during embryogenesis reveals no major pancreatic abnormalities in embryos

D

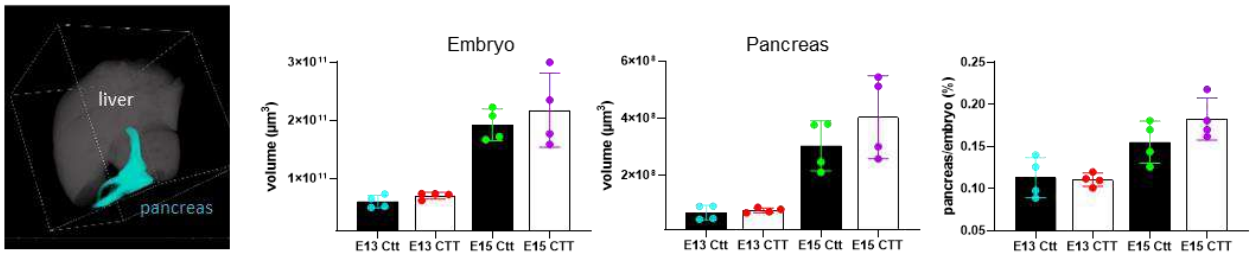

D. Quantification of the volumes of CTT (black bars, n=4) and Ctt (white bars, n=4) E13 and E15 embryos and their pancreas. Embryos were optical cleared and acquisition was performed with selective plane illumination microscope (SPIM) technology. Segmentations were carried out as described in experimental procedures using AMIRA software. The volume of the liver of each embryo was also determined and used as a control parameter unaffected by TRIP12 depletion. The bars represent the means ± SD.

E

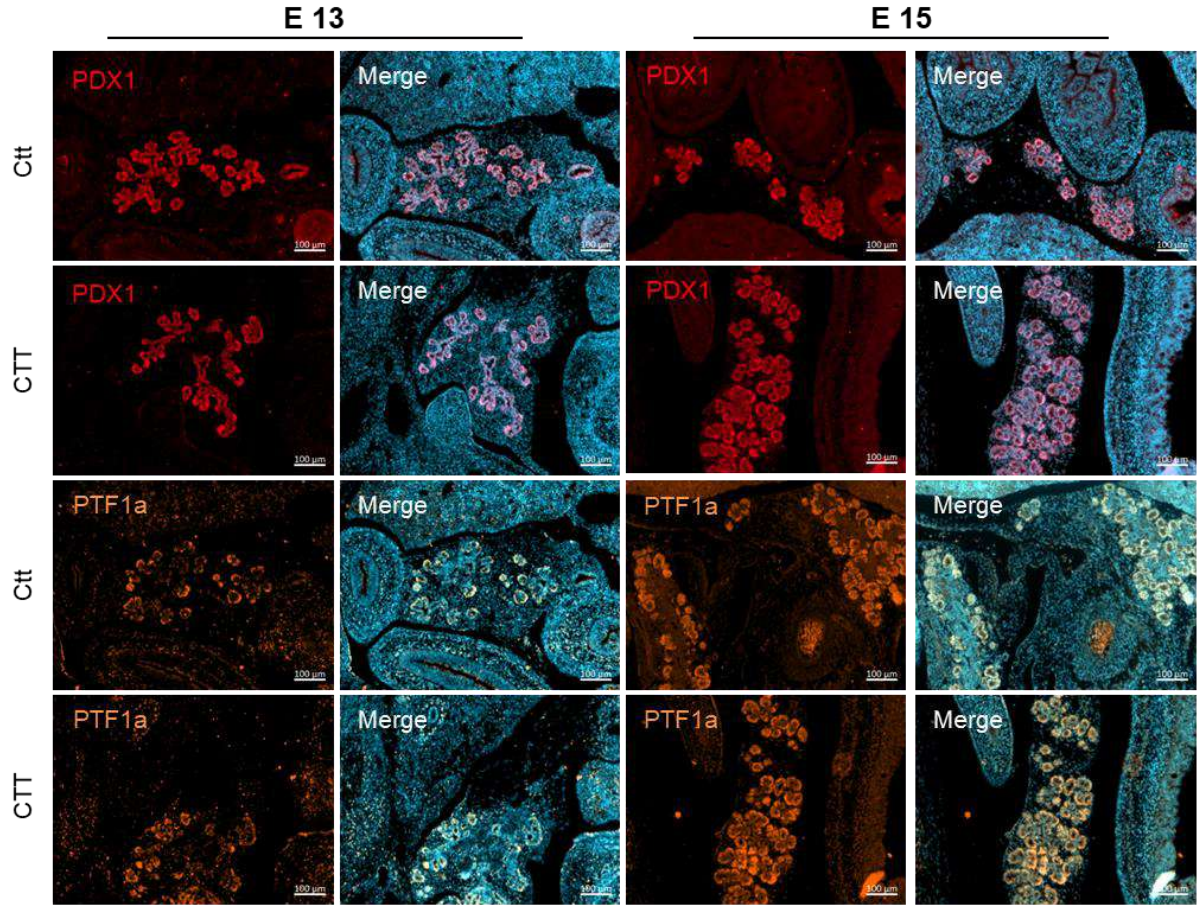

E. Immunofluoresence staining of PDX1 and PTF1a in CTT and Ctt E13 and E15 embryo. Nuclei are counterstained with DAPI. Scale bars: 100µm.

Figure 3: Trip12 deficiency during embryogenesis reveals pancreatic abnormalities in adults

A

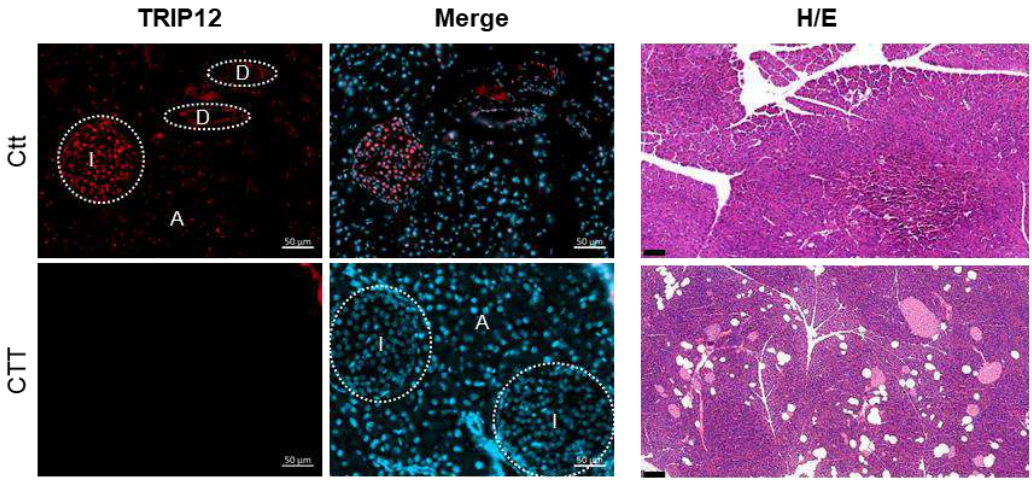

A. Immunofluorescence staining of TRIP12 in Ctt and CTT pancreas in acinar (A), ductal (D) and endocrine cells (I). Nuclei are counterstained with DAPI. Scale bars: 50µm. H&E staining of Ctt and CTT adult mice pancreas. Scale bars: 200µm.

B

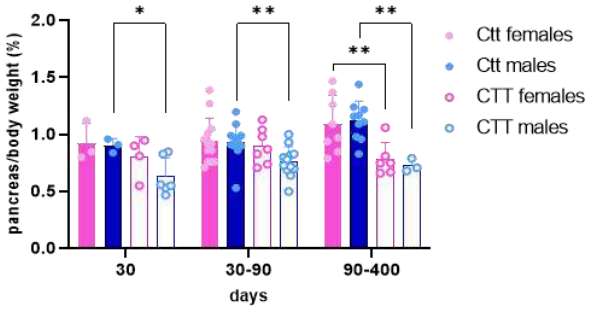

B. Pancreas/body weight ratio of Ctt control mice and CTT TRIP12 knockout mice. Males and females are shown separately. Data are means ± SD, * $p<0.05$ and ** $p<0.01$.

C

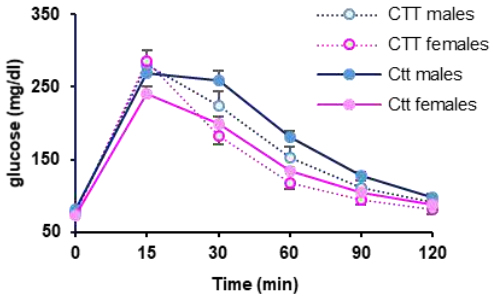

C. Glycemia after intraperitoneal glucose injection in control Ctt (bold lines) males (blue, n=27) and females (pink, n=6) and CTT TRIP12 knockout (dashed lines) males (blue, n=17) and females (pink, n=10) mice. Males and females were 1 to 3 months old.

Figure 3: Trip12 deficiency during embryogenesis reveals pancreatic abnormalities in adults

D

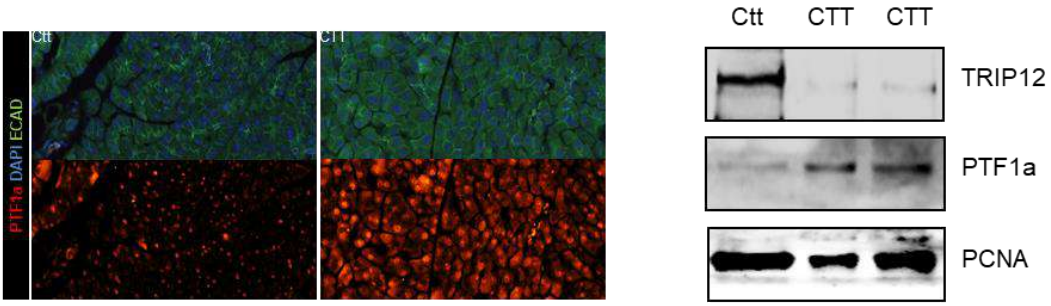

D. Left: Immunostaining of PTF1a (red) in Ctt and CTT adult pancreas mice at the age of 3 months. Nuclei are counterstained with DAPI (blue). E cadherin staining (green) delimits the cells. Scale bars: 100µm. Right panel: Western-blot analysis of protein extracted from Ctt and CTT isolated acinar cells showing protein levels of TRIP12 and PTF1a. PCNA was used as loading control.

E

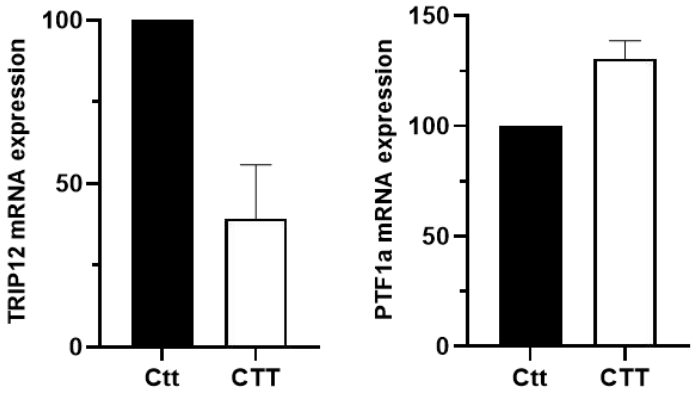

E. qRT-PCR analysis of TRIP12 and PTF1a mRNA levels in Ctt (black bars) and CTT (white bars) isolated acinar cells (n=3). Data are expressed as percentage of expression in Ctt acinar cells normalized by HPRT, cyclophilin A and 18S genes expression.

Figure 4: Trip12 deficiency in adult acinar cells does not alter acinar cell morphology

A

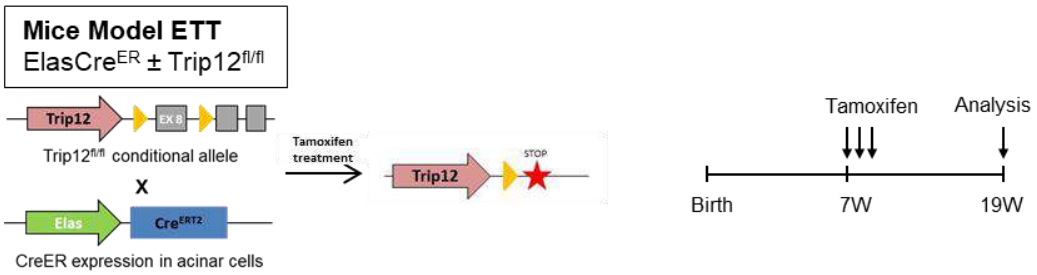

A. Schematic representation of the ETT model where CreER recombinase expression is driven by the Elastase Cre^{ERT2} promoter and experimental approach. Yellow triangles indicate loxP sites.

B

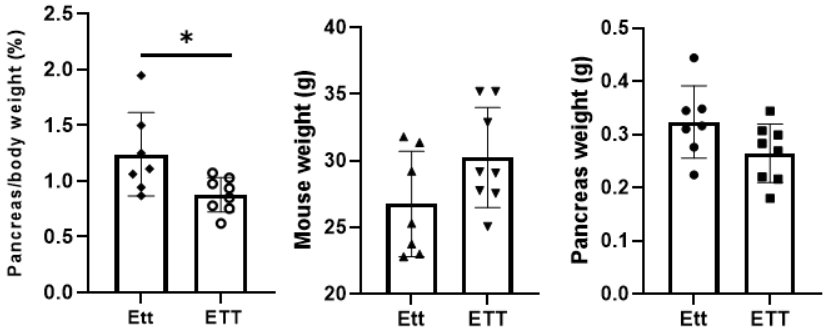

B. Pancreas/body weight ratio, mouse and pancreas weight of control Ett (n=7) and TRIP12-depleted ETT mice (n=6). Data are means ± SEM, *indicates a p value <0.05.

C

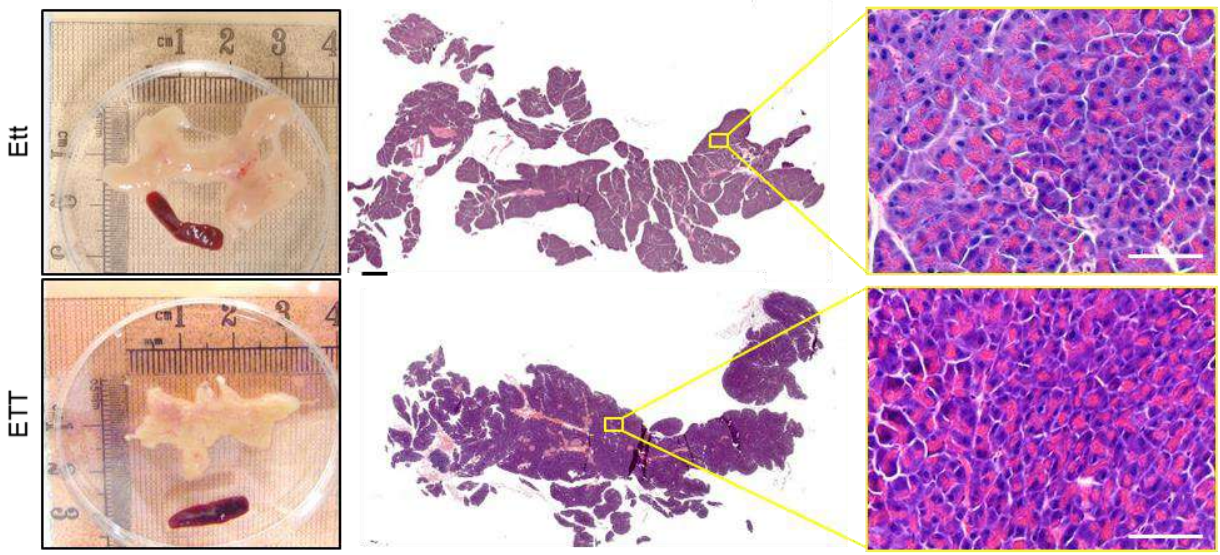

C. H&E staining of Ett and ETT pancreas 4 months after tamoxifen treatment. Boxes indicate enlarged regions. Scale bars: 200µm.

Figure 4: Trip12 deficiency in adult acinar cells does not alter acinar cell morphology

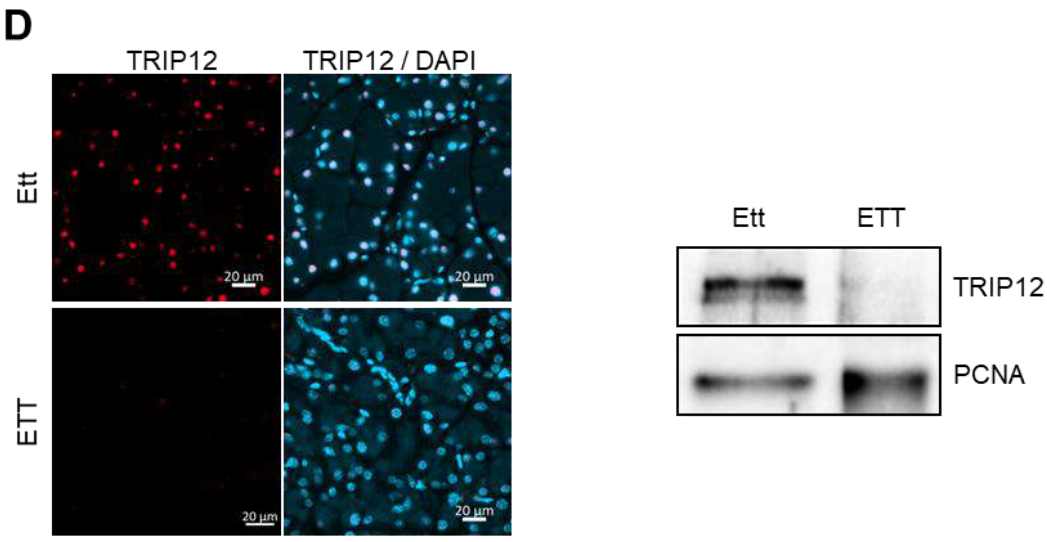

D. Left panel: Immunofluorescence staining of TRIP12 in Ett and ETT pancreatic acinar cells. Nuclei are counterstained with DAPI. Scale bars: 20µm. Right panel: Western-blot analysis of protein isolated from ETT acinar cells. PCNA is used as loading control.

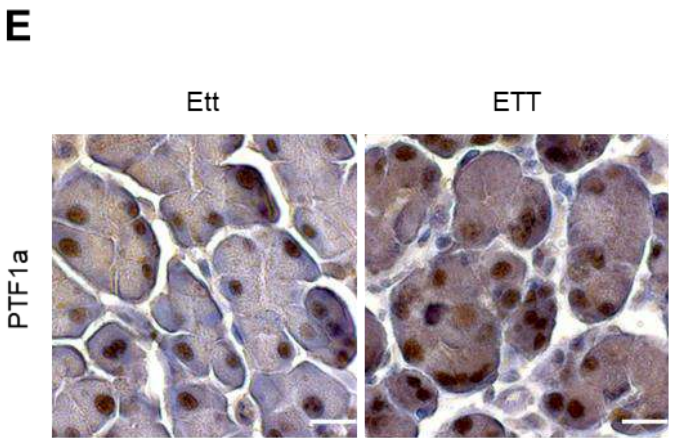

E. PTF1a Immunohistochemistry in TRIP12-depleted ETT acinar cells compared to Ett controls. Scale bars: 50µm.

Figure 5: Trip12 is required for ADM formation in vitro

A

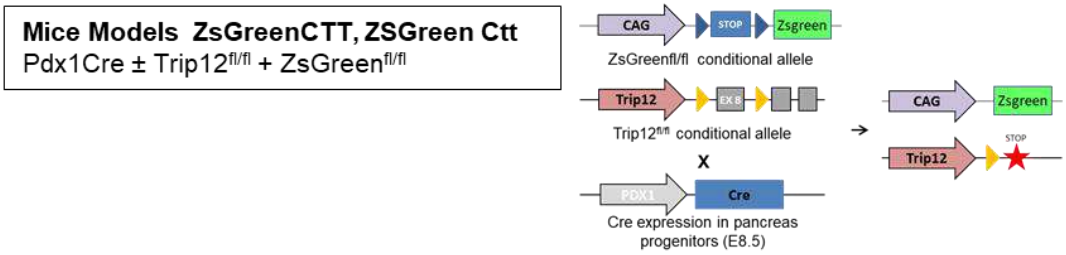

A. Schematic representation of the Pdx1-Cre;ZsGreen$^{f/f}$;Trip12$^{f/f}$ (ZsGreenCTT) and the Pdx1-Cre;ZsGreen$^{f/f}$ (ZsGreenCtt) mice.

B

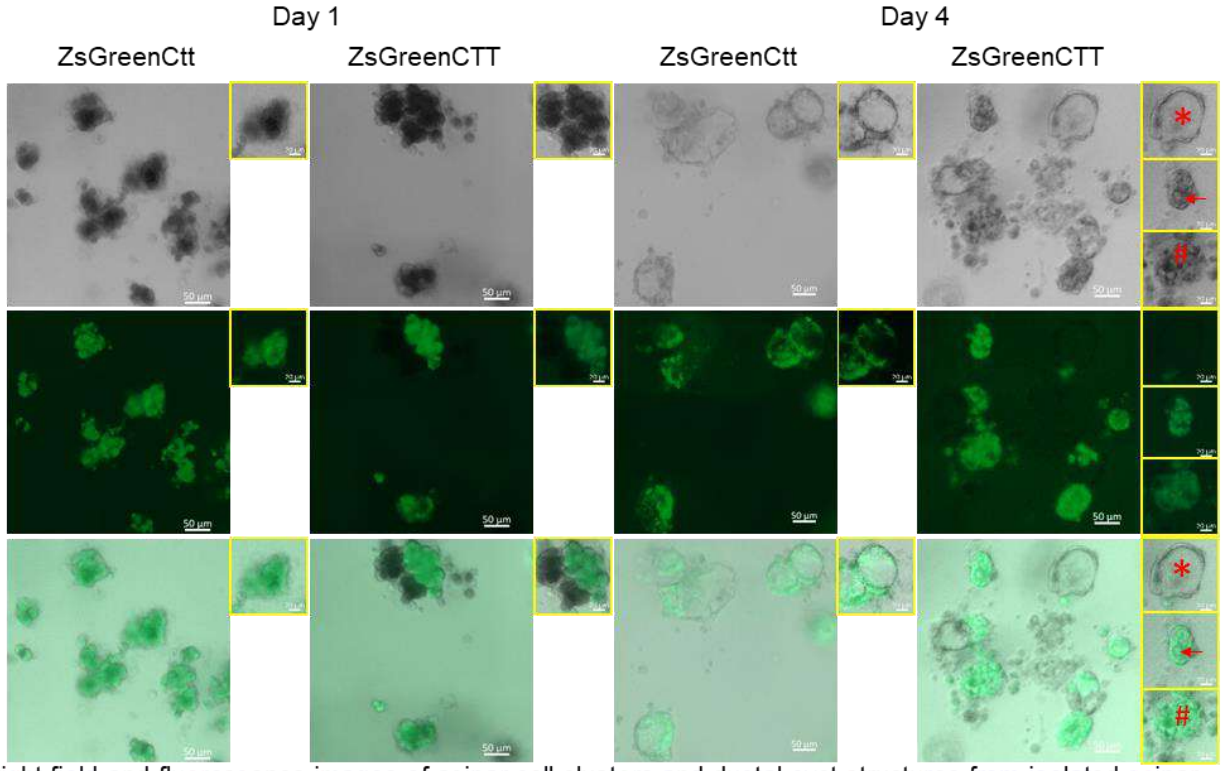

B. Bright field and fluorescence images of acinar cell clusters and ductal cyst structures from isolated acinar cells from ZsGreenCtt and ZsGreenCTT pancreas on day 1 and on day 4 after isolation and treatment with EGF. Enlarged images are shown. Note the absence of fluorescence in the ductal cyst from ZsGreenCTT pancreas (red asterisks). Red # indicate ZsGreenCTT acinar cell clusters that do not undergo acinar to ductal metaplasia. Red arrows show the lumen of one abnormal ZsGreenCTT ductal structure. Scale bars: 50µm.

C

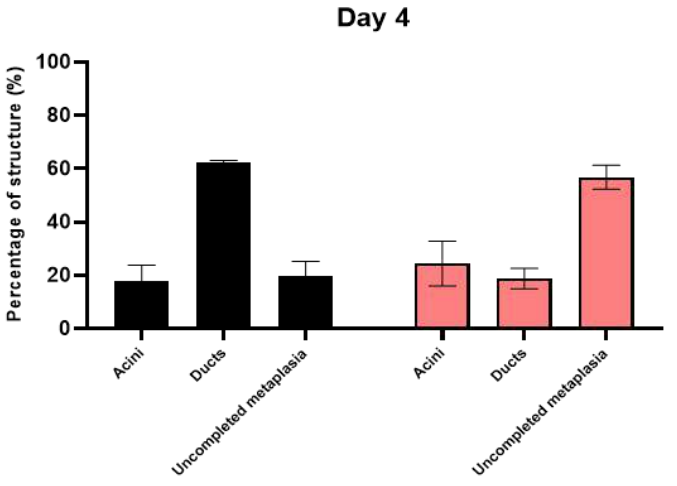

C. Quantification of acinar cell clusters, ductal cyst structures and abnormal ductal structures (Uncompleted metaplasia: characterized by multilobed lumen, absence of ductal flat epithelium and presence of acinar cells) by day 4 after acinar cell isolation and treatment with EGF.

Figure 5: Trip12 is required for ADM formation in vitro

D

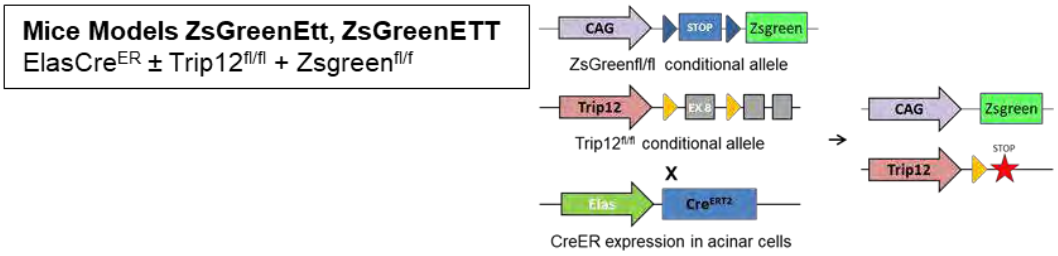

D. Schematic representation of the Elas-CreER;ZsGreen$^{f/f}$;Trip12$^{f/f}$ (ZsGreenETT) and the Elas-CreER;ZsGreen$^{f/f}$ (ZsGreenEtt) mice.

E

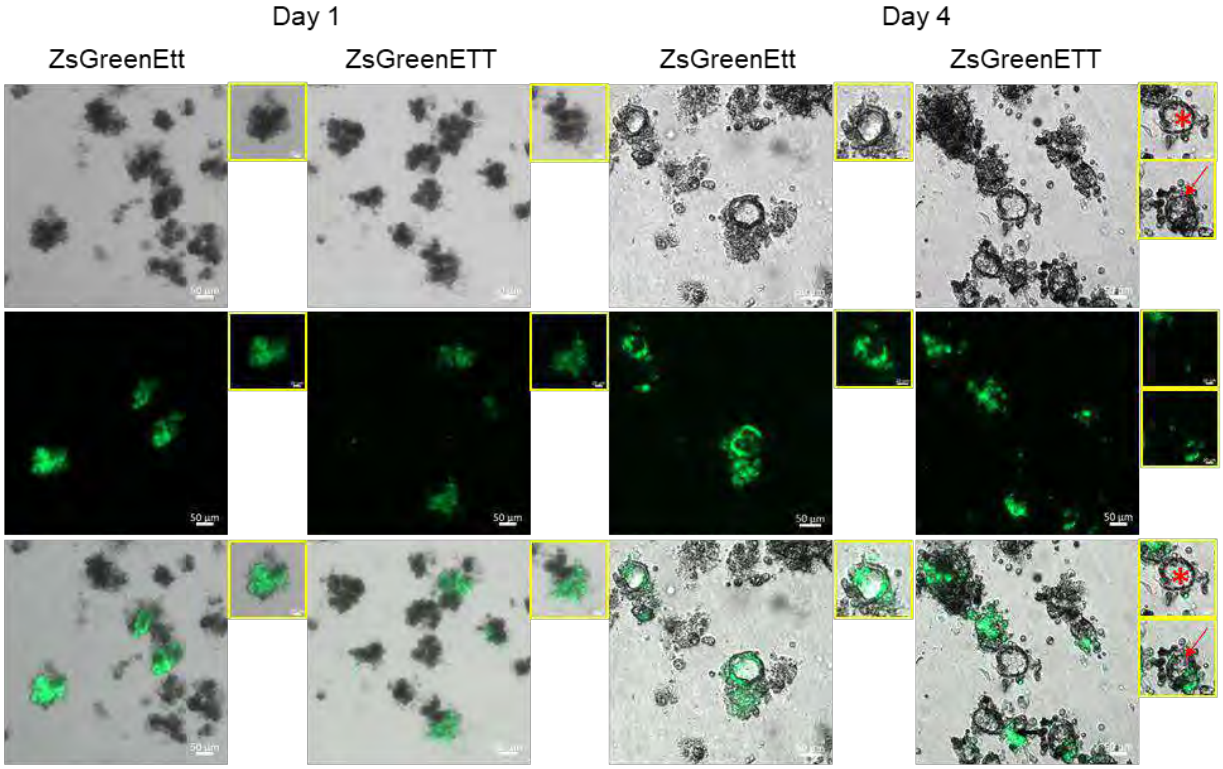

E. Bright field and fluorescence images of acinar cell clusters and ductal cyst structures from isolated acinar cells from ZsGreenEtt and ZsGreenETT pancreas on day 1 and on day 4 after isolation and treatment with EGF. Enlarged images are shown. Note the absence of fluorescence in the ductal cyst from ZsGreenETT pancreas (red asterisks). Red arrows show the lumen of one abnormal ZsGreenETT ductal structure. Scale bars: 50µm.

F

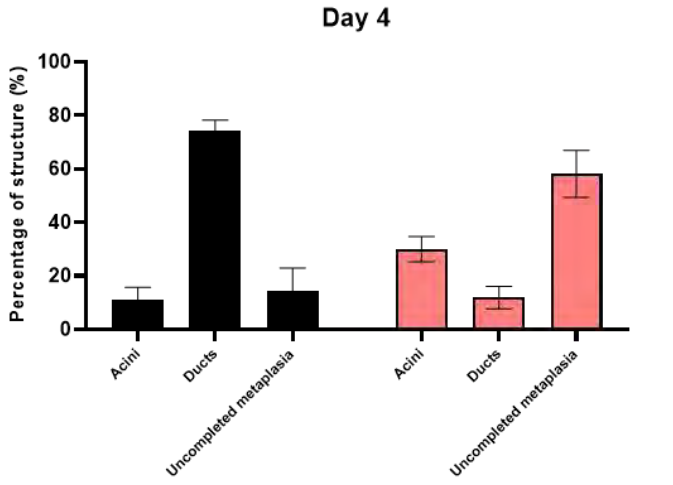

F. Quantification of acinar cell clusters, ductal cyst structures and abnormal ductal structures (Uncompleted metaplasia: characterized by multilobed lumen, absence of ductal flat epithelium and presence of acinar cells) by day 4 after acinar cell isolation and treatment with EGF.

Figure 6: Trip12 is required for ADM formation in vivo

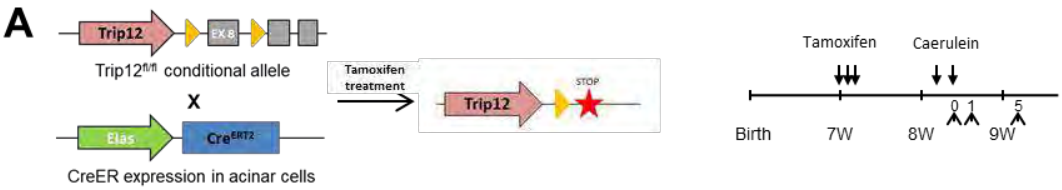

A. Experimental design of caerulein-induced acute pancreatitis in the ETT and Ett mice. Inactivation of TRIP12 is induced by injections of tamoxifen at the age of seven weeks. Controls are also treated with tamoxifen. Pancreatitis is induced one week later. Mice are sacrificed 2 hours (0), 24 hours (1) and 5 days (5) from the last injection.

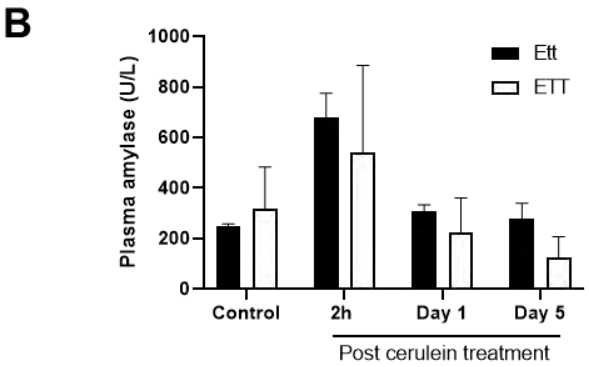

B. Plasma amylase levels of Ett (black bars, n=3) and ETT (white bars, n=3) were determined at 2h, 1 day or 5 days after the last injection. Values are means ± SEM.

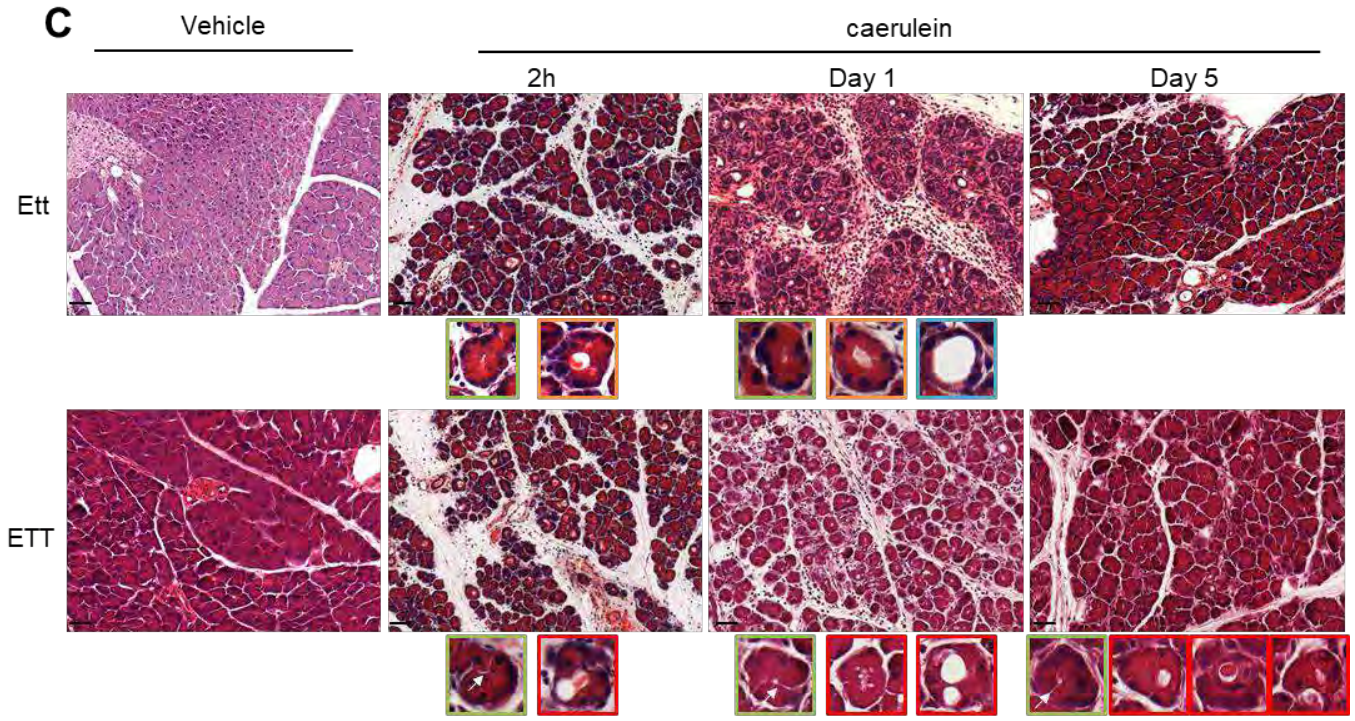

C. H&E sections of Ett or ETT mice treated with vehicle or caerulein and analyzed at 2 h, 1 day and 5 days after the last injection. Enlarged boxes show acini (green frame), initiation of acinar–to-ductal metaplasia (orange frame), final acinar-to-ductal metaplasia (blue frame). Control Ett acinar cells exhibit central distended lumen at 2 hours that evolves towards a ductal phenotype by day 1. ETT acini appear disrupted (arrows) with mislocalized nuclei, do not transdifferentiate but exhibit vacuoles of various sizes (red frame). Scale bars: 200µm.

Figure 6: Trip12 is required for ADM formation in vivo

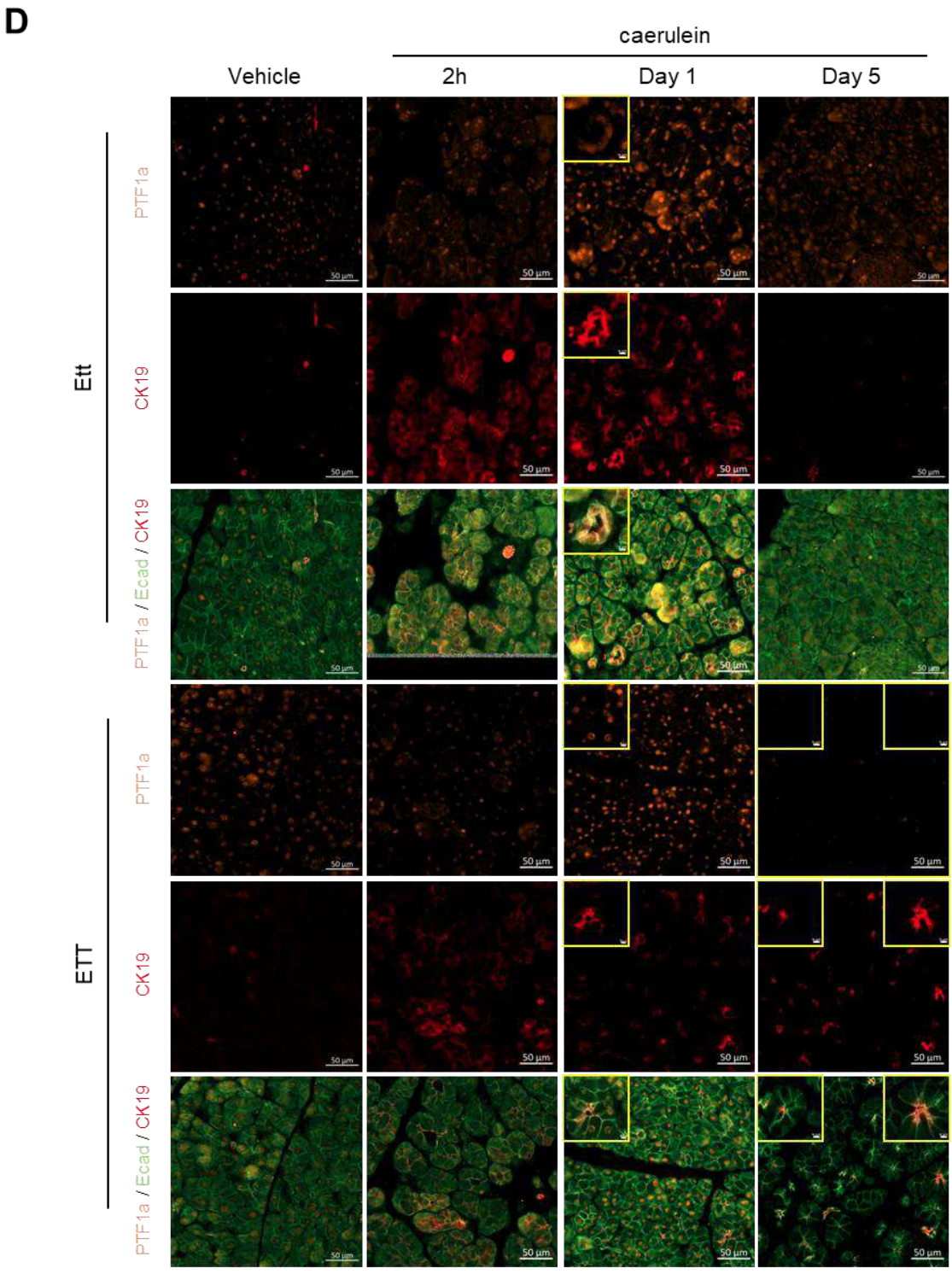

D. PTF1a (orange) and CK19 expression (red) immunofluoresence at the indicated times after caerulein treatment. E cadherin (E-cad, green) is used to delimit cells. Scale bars: 50µm.

Figure 6: Trip12 is required for ADM formation in vivo

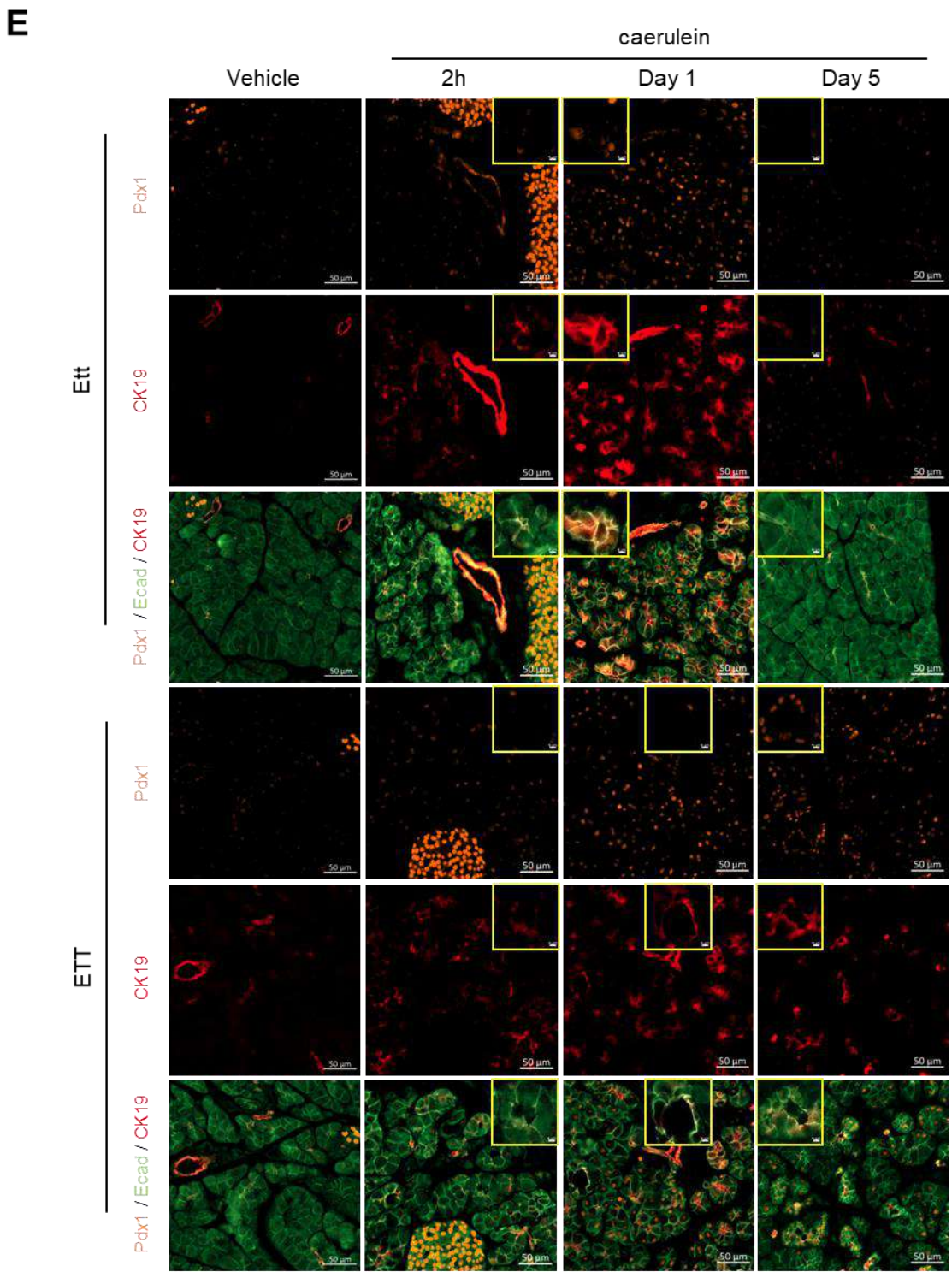

E. PDX1 (orange) and CK19 expression (red) immunofluoresence at the indicated times after caerulein treatment. E cadherin (E-cad, green) is used to delimit cells. Scale bars: 50µm.

Figure 7: Trip12 collaborates with Kras to initiate pancreatic carcinogenesis in adult pancreas

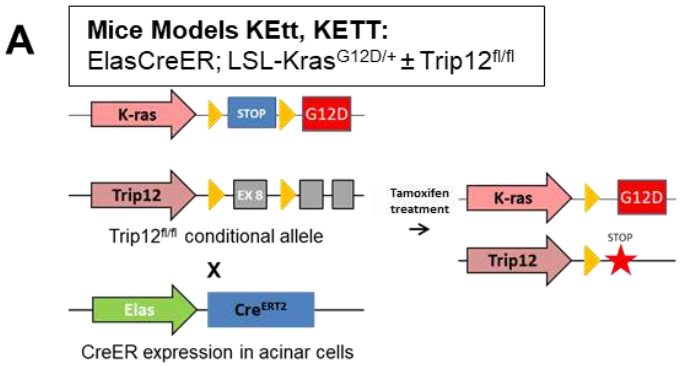

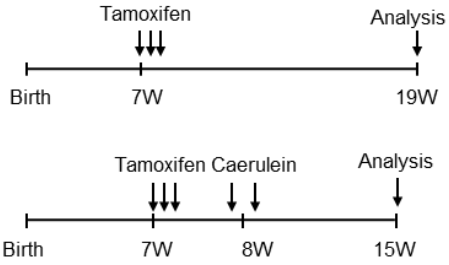

A. Schematic representation of the KETT murine model. Yellow triangles indicate loxP sites. TRIP12 deletion and Kras^{G12D} activation are induced by tamoxifen at the age of 7 weeks.

B. Experimental design. Tamoxifen is injected at 7 weeks and acute pancreatitis is induced or not one week later.

C

							Lesions		
Mouse ID	Treatement	Gender	Age	Body weight (g)	Pancreas weight (g)	Ratio (%)	N	F	P
KEtt-26	Tamoxifen	♂	3 months	36,3	0,411	1,13	2/3	Na	Na
KEtt-1018	Tamoxifen	♀	3 months	55,23	0,423	0,77		L	a
KEtt-1020	Tamoxifen	♀	3 months	59,03	0,283	0,48		L	a
KETT-1710	Tamoxifen	♂	3 months	28,26	0,287	1,02	0/3	Na	Na
KETT-1721	Tamoxifen	♂	3 months	26,2	0,321	1,23		Na	Na
KETT-1754	Tamoxifen	♀	3 months	23,34	0,336	1,44		Na	Na
KETT-1779	Tamoxifen	♀	3 months	23,32	0,344	1,48		Na	Na
KEtt-27	Tamoxifen and caerulein	♂	2 months	35,29	0,69	1,96	3/3	M	c
KEtt-32	Tamoxifen and caerulein	♀	2 months	29,54	0,397	1,34		L	c
KEtt-38	Tamoxifen and caerulein	♀	2 months	23,19	0,307	1,32		L	c
KETT-1555	Tamoxifen and caerulein	♂	2 months	29,97	0,408	1,36	0/3	Na	Na
KETT-1565	Tamoxifen and caerulein	♀	2 months	22,69	0,31	1,37		Na	Na
KETT-1571	Tamoxifen and caerulein	♀	2 months	20,46	0,316	1,54		Na	Na

C. Clinical spectrum of disease in Kett and KETT mice treated or not with caerulein. N, proportion of mice with pancreatic preneoplastic lesions. F represents the frequency of lesions in examined pancreas sections: Low (L) <10% of the pancreas area exhibit lesions. P = percentage of cells within a specified lesion that stained positive for alcian blue and Sirius red (a = <10%, b=10-50%, c= >50% of the cells were positive). Na, not applicable.

Figure 7: Trip12 collaborates with Kras to initiate pancreatic carcinogenesis in adult pancreas

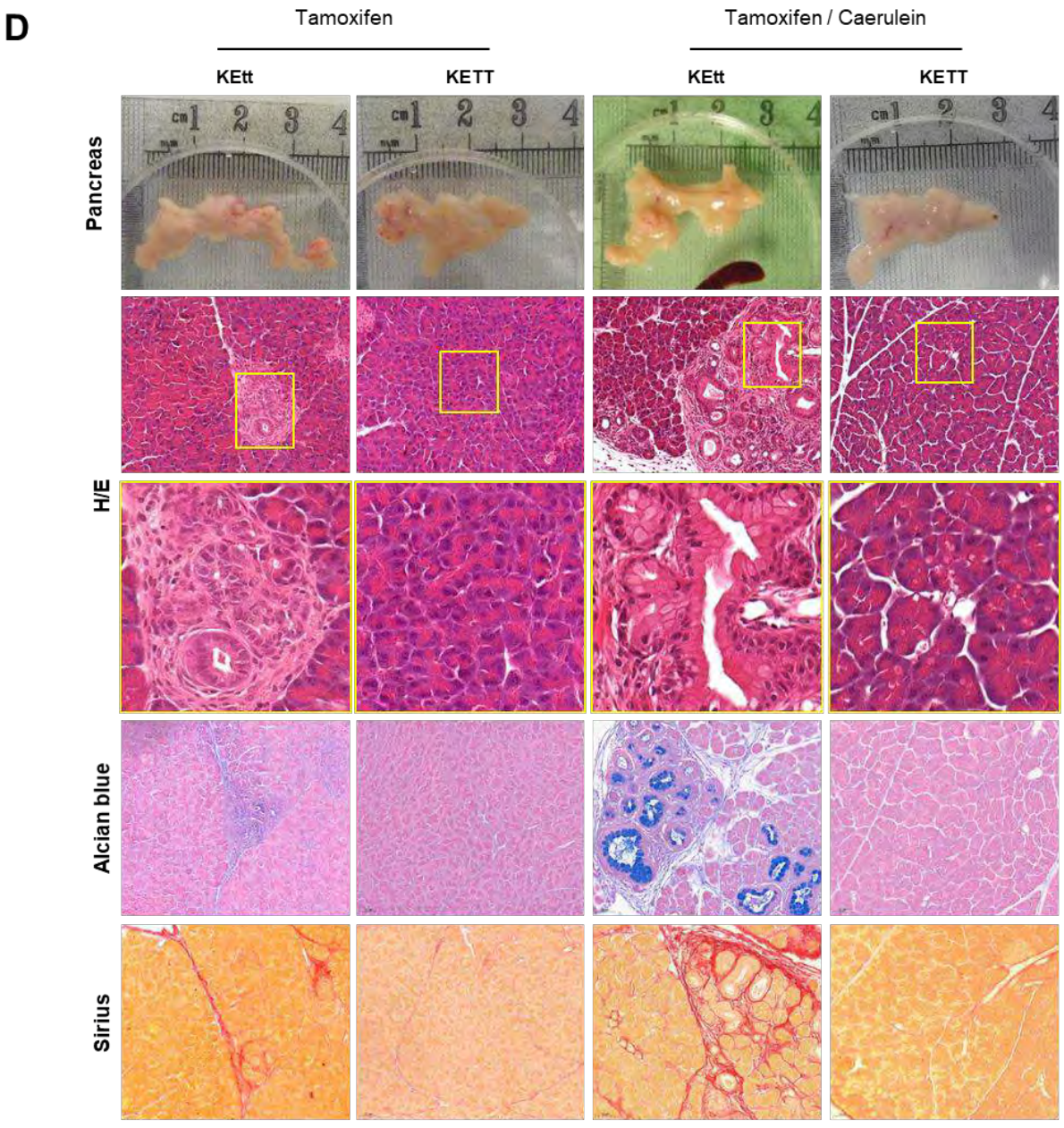

D. Histological analysis of KEtt, and KETT mice treated or not with caerulein. Scale bars: 50µm.

Figure 8: TRIP12 depletion limits tumor growth.

A

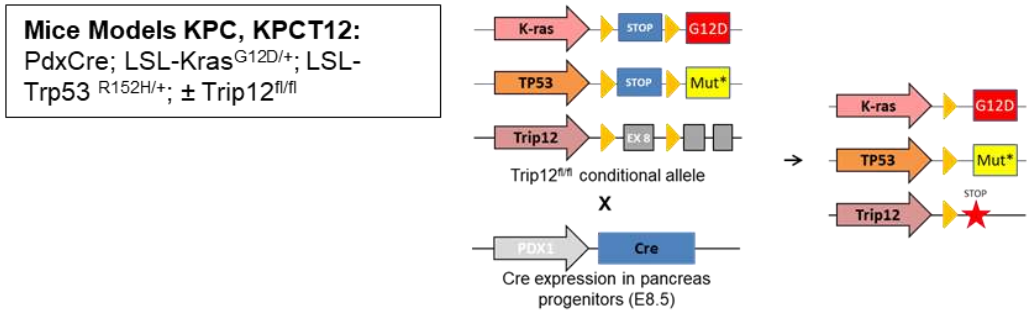

A. Schematic representation of the KPCtt and KPCTT models. Yellow triangles indicate loxP sites.

B

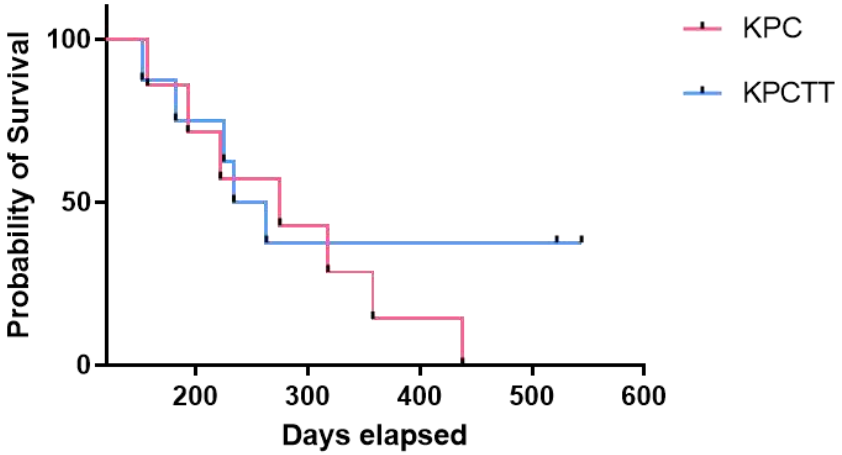

B. Survival of KPCtt and KPCTT mice.

C

						Tumors				
Mouse ID	Gender	Age (days)	Body weight (g)	tumor weight (g)	spleen weight (g)	N	Tumor localisation	Ascite	Metastases	Metastases localization
KPCtt-35	♀	275	30,36	2,57	0,397		Head and tail	Y	Y	Liver, kidneys, diaphragm, lungs
KPCtt-99	♀	193	19,22	0,92	0,121		Head	Na	Y	Kidneys
KPCtt-162	♀	222	20,97	2,33	0,194		Head	Na	Y	Liver
KPCtt-166	♀	157	22,30	2,31	0,307	6/7	Tail	Y	Y	Liver , kidneys, peritoneum
KPCtt-1801	♂	318	33,16	1,098	0,28		Head	N	N	
KPCtt-1936	♀	438	38,61	Na	Na		Na	N	N	
KPCtt-1937	♀	358	29,00	1,16	2,689		Head and tail	N	N	
KPCTT-21	♀	234	23,5	1,60	0,215		Na	Y	Y	Liver, Kidneys
KPCTT-28	♂	225	31,43	1,40	0,384		Tail	Y	N	
KPCTT-1762	♂	263	26,8	2,478	0,2		Tail	N	Y	Liver, Kidneys
KPCTT-1763	♂	182	32,16	1,044	0,271	5/8	Tail	N	N	
KPCTT-1858	♂	152	37,08	3,14	Na		Head	N	N	
KPCTT-1783	♂	544 *	Na	Na	Na		Na	Na	Na	
KPCTT-1905	♂	522 *	Na	Na	Na		Na	Na	Na	
KPCTT-1924	♂	522 *	Na	Na	Na		Na	Na	Na	

C. Clinical spectrum of disease in KPCtt and KPCTT mice. *Three mice are still alive. Na, not applicable; N, number of mice with tumors; Y, Yes; N, no.

Figure 8: TRIP12 depletion limits tumor growth

D

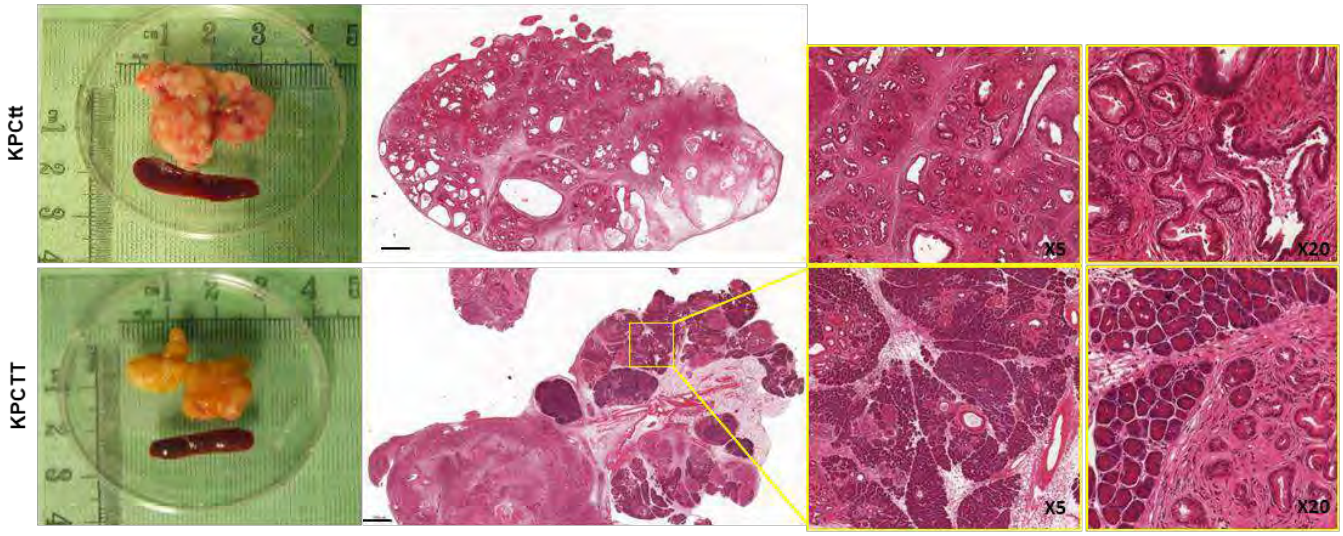

D. Representative macroscopic views of KPCtt (KPCtt-35) or KPCTT (KPCTT-28) pancreas at necropsy and H&E stainings. Scale bars: 1 000µm.

E

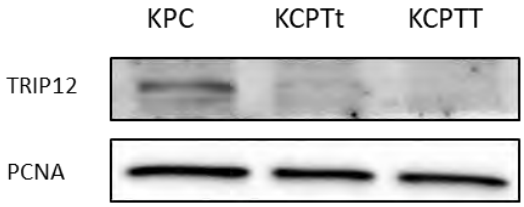

E. TRIP12 protein expression in KPC, heterozygous KPCTt and homozygous knockout KPCTT cell lines was determined by Western-blot. PCNA is used as a loading control.

F

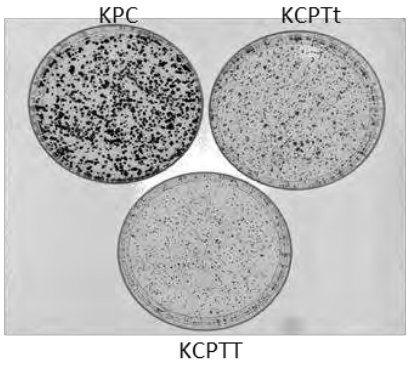

F. Colony formation assay of KPC, KPCTt and KPCTT cells. Cells were seeded at 10^3 cells per 10 cm-plate. After 9-14 days, colonies were stained using Cristal violet.

G

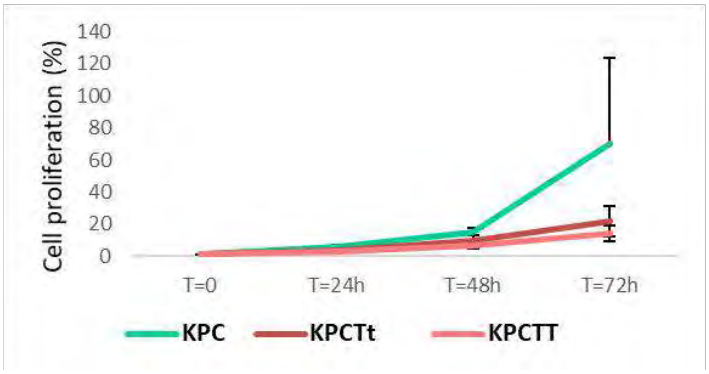

G. Cell proliferation of KPC, KPCTt and KPCTT cell lines. The results are expressed as growth percentage compared to T=0h and represent the mean ± SEM of three separate experiments.

Supplemental Figures

Figure S1. Expression of ZsGreen in the pancreas of ZsGreenETT mice. Elas-CreER expression induced by tamoxifen allows specific recombination in acinar cells. ZsGreen is expressed in acinar cells (A), but not in ductal (D) nor in islet cells (I). Nuclei are counterstained with DAPI. Scale bar: 50µm

Supplemental Figure

Figure S1

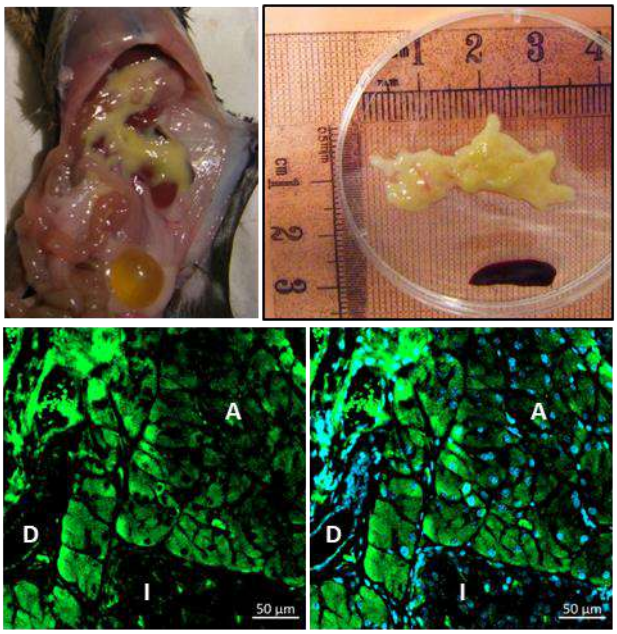

S1. Expression of ZsGreen in the pancreas of ZsGreenETT mice. Elas-CreER expression induced by tamoxifen allows specific recombination in acinar cells. ZsGreen is expressed in acinar cells (A), but not in ductal (D) nor in islet cells (I). Nuclei are counterstained with DAPI. Scale bar: 50µm

References

1. Jamieson, J. D. & Palade, G. E. Synthesis, intracellular transport, and discharge of secretory proteins in stimulated pancreatic exocrine cells. *J. Cell Biol.* **50**, 135–158 (1971).
2. Bockman, D. E. *et al.* Origin and development of the precursor lesions in experimental pancreatic cancer in rats. *Lab. Investig. J. Tech. Methods Pathol.* **83**, 853–859 (2003).
3. Pinho, A. V. *et al.* Adult pancreatic acinar cells dedifferentiate to an embryonic progenitor phenotype with concomitant activation of a senescence programme that is present in chronic pancreatitis. *Gut* **60**, 958–966 (2011).
4. Strobel, O. *et al.* In vivo lineage tracing defines the role of acinar-to-ductal transdifferentiation in inflammatory ductal metaplasia. *Gastroenterology* **133**, 1999–2009 (2007).
5. Kong, B. *et al.* Dynamic landscape of pancreatic carcinogenesis reveals early molecular networks of malignancy. *Gut* **67**, 146–156 (2018).
6. Gidekel Friedlander, S. Y. *et al.* Context-dependent transformation of adult pancreatic cells by oncogenic K-Ras. *Cancer Cell* **16**, 379–389 (2009).
7. Habbe, N. *et al.* Spontaneous induction of murine pancreatic intraepithelial neoplasia (mPanIN) by acinar cell targeting of oncogenic Kras in adult mice. *Proc. Natl. Acad. Sci. U. S. A.* **105**, 18913–18918 (2008).
8. Prévot, P.-P. *et al.* Role of the ductal transcription factors HNF6 and Sox9 in pancreatic acinar-to-ductal metaplasia. *Gut* **61**, 1723–1732 (2012).
9. Ferreira, R. M. M. *et al.* Duct- and Acinar-Derived Pancreatic Ductal Adenocarcinomas Show Distinct Tumor Progression and Marker Expression. *Cell Rep.* **21**, 966–978 (2017).
10. Quilichini, E. *et al.* Pancreatic Ductal Deletion of Hnf1b Disrupts Exocrine Homeostasis, Leads to Pancreatitis, and Facilitates Tumorigenesis. *Cell. Mol. Gastroenterol. Hepatol.* **8**, 487–511 (2019).
11. Lee, A. Y. L. *et al.* Cell of origin affects tumour development and phenotype in pancreatic ductal adenocarcinoma. *Gut* **68**, 487–498 (2019).
12. Arias, A. E. & Bendayan, M. Differentiation of pancreatic acinar cells into duct-like cells in vitro. *Lab. Investig. J. Tech. Methods Pathol.* **69**, 518–530 (1993).
13. Rooman, I. & Real, F. X. Pancreatic ductal adenocarcinoma and acinar cells: a matter of differentiation and development? *Gut* **61**, 449–458 (2012).
14. Vila, M. R., Lloreta, J. & Real, F. X. Normal human pancreas cultures display functional ductal characteristics. *Lab. Investig. J. Tech. Methods Pathol.* **71**, 423–431 (1994).
15. Fanjul, M. *et al.* Evidence for epithelial-mesenchymal transition in adult human pancreatic exocrine cells. *J. Histochem. Cytochem. Off. J. Histochem. Soc.* **58**, 807–823 (2010).
16. Shibata, H. *et al.* In vivo reprogramming drives Kras-induced cancer development. *Nat. Commun.* **9**, 2081 (2018).
17. Wei, D. *et al.* KLF4 Is Essential for Induction of Cellular Identity Change and Acinar-to-Ductal Reprogramming during Early Pancreatic Carcinogenesis. *Cancer Cell* **29**, 324–338 (2016).
18. Benitz, S. *et al.* Polycomb repressor complex 1 promotes gene silencing through H2AK119 mono-ubiquitination in acinar-to-ductal metaplasia and pancreatic cancer cells. *Oncotarget* **7**, 11424–11433 (2016).
19. Benitz, S. *et al.* Ring1b-dependent epigenetic remodelling is an essential prerequisite for pancreatic carcinogenesis. *Gut* **68**, 2007–2018 (2019).
20. Assi, M. *et al.* Dynamic Regulation of Expression of KRAS and Its Effectors Determines the Ability to Initiate Tumorigenesis in Pancreatic Acinar Cells. *Cancer Res.* **81**, 2679–2689 (2021).

21. Guerra, C. *et al.* Pancreatitis-induced inflammation contributes to pancreatic cancer by inhibiting oncogene-induced senescence. *Cancer Cell* **19**, 728–739 (2011).
22. Guerra, C. *et al.* Chronic pancreatitis is essential for induction of pancreatic ductal adenocarcinoma by K-Ras oncogenes in adult mice. *Cancer Cell* **11**, 291–302 (2007).
23. Kopp, J. L. *et al.* Identification of Sox9-dependent acinar-to-ductal reprogramming as the principal mechanism for initiation of pancreatic ductal adenocarcinoma. *Cancer Cell* **22**, 737–750 (2012).
24. Morris, J. P., Cano, D. A., Sekine, S., Wang, S. C. & Hebrok, M. Beta-catenin blocks Kras-dependent reprogramming of acini into pancreatic cancer precursor lesions in mice. *J. Clin. Invest.* **120**, 508–520 (2010).
25. Shi, G. *et al.* Maintenance of acinar cell organization is critical to preventing Kras-induced acinar-ductal metaplasia. *Oncogene* **32**, 1950–1958 (2013).
26. Krah, N. M. *et al.* The acinar differentiation determinant PTF1A inhibits initiation of pancreatic ductal adenocarcinoma. *eLife* **4**, (2015).
27. Hoang, C. Q. *et al.* Transcriptional Maintenance of Pancreatic Acinar Identity, Differentiation, and Homeostasis by PTF1A. *Mol. Cell. Biol.* **36**, 3033–3047 (2016).
28. Kawaguchi, Y. *et al.* The role of the transcriptional regulator Ptf1a in converting intestinal to pancreatic progenitors. *Nat. Genet.* **32**, 128–134 (2002).
29. Jakubison, B. L. *et al.* Induced PTF1a expression in pancreatic ductal adenocarcinoma cells activates acinar gene networks, reduces tumorigenic properties, and sensitizes cells to gemcitabine treatment. *Mol. Oncol.* **12**, 1104–1124 (2018).
30. Krah, N. M. *et al.* Prevention and Reversion of Pancreatic Tumorigenesis through a Differentiation-Based Mechanism. *Dev. Cell* **50**, 744-754.e4 (2019).
31. Brunet, M., Vargas, C., Larrieu, D., Torrisani, J. & Dufresne, M. E3 Ubiquitin Ligase TRIP12: Regulation, Structure, and Physiopathological Functions. *Int. J. Mol. Sci.* **21**, E8515 (2020).
32. Hanoun, N. *et al.* The E3 ubiquitin ligase thyroid hormone receptor-interacting protein 12 targets pancreas transcription factor 1a for proteasomal degradation. *J. Biol. Chem.* **289**, 35593–35604 (2014).
33. Larrieu, D. *et al.* The E3 ubiquitin ligase TRIP12 participates in cell cycle progression and chromosome stability. *Sci. Rep.* **10**, 789 (2020).
34. Gava, F. *et al.* 3D Model Characterization by 2D and 3D Imaging in t(14;18)-Positive B-NHL: Perspectives for In Vitro Drug Screens in Follicular Lymphoma. *Cancers* **13**, 1490 (2021).
35. Kajiro, M. *et al.* The E3 ubiquitin ligase activity of Trip12 is essential for mouse embryogenesis. *PloS One* **6**, e25871 (2011).
36. Carrière, C., Young, A. L., Gunn, J. R., Longnecker, D. S. & Korc, M. Acute pancreatitis accelerates initiation and progression to pancreatic cancer in mice expressing oncogenic Kras in the nestin cell lineage. *PloS One* **6**, e27725 (2011).
37. Hwang, C.-S., Shemorry, A., Auerbach, D. & Varshavsky, A. The N-end rule pathway is mediated by a complex of the RING-type Ubr1 and HECT-type Ufd4 ubiquitin ligases. *Nat. Cell Biol.* **12**, 1177–1185 (2010).
38. Zenker, M. *et al.* Deficiency of UBR1, a ubiquitin ligase of the N-end rule pathway, causes pancreatic dysfunction, malformations and mental retardation (Johanson-Blizzard syndrome). *Nat. Genet.* **37**, 1345–1350 (2005).

39. Liu, S. *et al.* Severe forms of Johanson-Blizzard syndrome caused by two novel compound heterozygous variants in UBR1: Clinical manifestations, imaging findings and molecular genetics. *Pancreatol. Off. J. Int. Assoc. Pancreatol. IAP Al* **20**, 562–568 (2020).
40. Zhu, L. *et al.* Inhibition of Mist1 homodimer formation induces pancreatic acinar-to-ductal metaplasia. *Mol. Cell. Biol.* **24**, 2673–2681 (2004).
41. Martinelli, P. *et al.* Gata6 is required for complete acinar differentiation and maintenance of the exocrine pancreas in adult mice. *Gut* **62**, 1481–1488 (2013).
42. von Figura, G., Morris, J. P., Wright, C. V. E. & Hebrok, M. Nr5a2 maintains acinar cell differentiation and constrains oncogenic Kras-mediated pancreatic neoplastic initiation. *Gut* **63**, 656–664 (2014).
43. Kweon, S.-M. *et al.* An Adversarial DNA N6-Methyladenine-Sensor Network Preserves Polycomb Silencing. *Mol. Cell* **74**, 1138-1147.e6 (2019).
44. Furuyama, T. *et al.* Proteasome activity is required for the initiation of precancerous pancreatic lesions. *Sci. Rep.* **6**, 27044 (2016).

Chapitre 3 : Discussion générale

L'adénocarcinome canalaire pancréatique a été initialement associé exclusivement aux cellules canalaires en raison de critères histologiques. Les lésions précancéreuses et les tumeurs pancréatiques différenciées ont en effet une morphologie canalaire. Néanmoins de nombreuses études ont révélé que les cellules acineuses longtemps considérées comme étant différenciées de manière irréversible ont une plasticité surprenante agissant en tant que mécanisme de défense contre un stress comme par exemple une inflammation. La compréhension des mécanismes qui préservent l'identité cellulaire est cruciale sur le plan fondamental et clinique. La perte de l'identité cellulaire peut constituer une étape préliminaire au développement tumoral.[284] In vitro, ces mêmes signaux pourraient être utilisés pour contrôler la reprogrammation cellulaire à l'origine d'un nouveau champ de recherche pour la médecine régénérative.[285]

L'E3 ubiquitine ligase TRIP12 est impliquée dans plusieurs processus biologiques majeurs altérés dans les cancers.[4] La première partie de mes travaux de thèse a permis de démontrer une hétérogénéité d'expression intertumorale de TRIP12 existant aussi entre les lignées cellulaires cancéreuses pancréatiques humaines. Mes résultats associent l'hétérogénéité d'expression de TRIP12 à une différence du niveau de transcription du gène et à une régulation de l'expression de la protéine au cours du cycle qui varie en fonction de la lignée cellulaire étudiée. Par ailleurs, mes données montrent que le niveau de TRIP12 dans les lignées cellulaires cancéreuses modifie leur sensibilité à un traitement qui induit des dommages de l'ADN.

Nous avons précédemment démontré que TRIP12 ubiquitine PTF1a, facteur de transcription essentiel du développement dont les propriétés de suppresseur de tumeur ont été démontrées en raison de son rôle de garant du phénotype des acini. Cependant, les fonctions de TRIP12 au cours du développement et à l'âge adulte dans le pancréas restent à ce jour méconnues. La seconde partie de mes travaux de thèse a mis en lumière son rôle dans l'homéostasie des cellules acineuses au cours de la MAC et dans l'initiation et la progression tumorale. Pour ce faire, le premier modèle murin d'invalidation conditionnelle de TRIP12 a été généré. En réponse à la déplétion de TRIP12, l'expression protéique de PTF1a est nettement augmentée en conditions physiologiques. En condition de stress, la MAC ne se produit pas en absence de TRIP12. Cela suggère que TRIP12 est nécessaire à la plasticité des cellules acinaires. Les résultats expérimentaux que j'ai obtenus restent descriptifs et nécessitent une analyse complémentaire afin d'élucider les mécanismes impliqués. De plus, nos données préliminaires obtenues dans un modèle murin exprimant l'oncogène $Kras^{G12D}$ montrent que la déplétion de TRIP12 bloque la MAC et la formation de PanIN. Cet effet n'est plus visible dans le cas où un suppresseur de tumeur est perdu conjointement à l'activation de Kras et les souris développent des PanIN et des tumeurs pancréatiques indépendamment de l'expression de TRIP12. Toutefois, les caractéristiques tumorales semblent différentes en absence de TRIP12, avec une prolifération nettement réduite.

I. Premier modèle murin d'invalidation conditionnelle de TRIP12

Pour étudier le rôle fonctionnel de TRIP12 dans le pancréas spécifiquement au cours des phases initiatrices du cancer du pancréas, il était nécessaire de développer un modèle murin invalidé pour cette protéine.

Cependant, l'étude de Kajiro et al., a démontré une létalité embryonnaire au stade E11.5 en réponse à l'expression constitutive d'un mutant inactif de TRIP12 dans tout l'embryon.[8] Les embryons de souris exprimant une protéine TRIP12 inactive présentent un retard de développement dès le stade E8.5, une diminution du nombre de somites au stade E9.5 conduisant à une létalité au stade E11.5, avec des malformations placentaires. La protéine TRIP12 est donc essentielle au bon développement de la souris.

Ne disposant d'aucune donnée sur l'impact de l'inactivation de TRIP12 sur le développement du pancréas, nous avons généré de manière concomitante deux modèles murins permettant l'invalidation conditionnelle de ce gène à l'âge embryonnaire ou à l'âge adulte. Dans les souris CTT, TRIP12 est perdue dès l'embryogenèse dans les cellules progénitrices exprimant PDX1, dans les souris ETT l'absence de TRIP12 est induite spécifiquement dans les cellules acineuses à l'âge adulte après injection de tamoxifène. Mes travaux montrent que la déplétion de TRIP12 dès l'embryogenèse n'est pas létale et ne semble pas délétère pour l'organogénèse du pancréas. Il ne semble pas y avoir d'altération de la fonction endocrine du pancréas. En revanche, l'altération de l'expression de TRIP12 perturbe le compartiment exocrine, puisque l'expression protéique de PTF1a, mais pas celle de son ARNm, est augmentée dans les souris invalidées pour TRIP12. Cette modification est également visible dans le modèle conduisant à la perte de TRIP12 dans les cellules acineuses. Ces résultats sont en accord avec nos précédents travaux montrant que TRIP12 participe à la dégradation de PTF1a.[9]

Ainsi, le développement de ces deux modèles a fourni des informations descriptives quant au rôle de TRIP12 au cours de l'organogenèse du pancréas jusqu'à l'âge adulte. Les conséquences de l'invalidation de TRIP12 au cours de l'embryogenèse mériteraient cependant d'être davantage explorées. Si aucune modification morphologique n'est associée aux cellules acineuses à l'âge adulte, nous avons observé une stéatose et une diminution du poids du pancréas du pancréas en absence de TRIP12 dans ce modèle. Ces résultats sont à rapprocher des données de la littérature qui montrent une anomalie similaire dans le pancréas d'enfants porteurs du syndrome de Johanson-Blizzard.[286] Ces enfants ont une mutation génétique pour UBR1, ubiquitine ligase impliquée dans le système protéolytique des résidus en N-terminal, qui se traduit par une insuffisance du pancréas exocrine. Cette pathologie est également associée à des malformations du visage et des retards mentaux. L'homologue de TRIP12 chez la levure, UFD4, collabore avec UBR1 dans ce système de dégradation des protéines.[287] Nous pouvons envisager qu'en réponse à la perte de TRIP12, le système protéolytique des résidus en N-

terminal peut être dérégulé, à l'origine de la stéatose reflet d'un dysfonctionnement du pancréas exocrine. Nous pouvons également supposer que la perte de TRIP12, comme celle d'UBR1, affecte l'homéostasie du pancréas exocrine et sa capacité de réponse aux stimuli délétères. L'analyse plus approfondie du compartiment exocrine (statut prolifératif et apoptose) et celle de sa fonction (expression des enzymes et capacité sécrétoire des cellules acineuses après stimulation du récepteur de la cholécystokinine) sont nécessaires afin d'identifier tout dysfonctionnement pouvant expliquer cette stéatose pancréatique. Nous savons également que TRIP12 contribue à la dégradation de FBW7 (F-box/WD repeat-containing protein 7),[56] protéine reconnaissant les substrats dans le complexe d'ubiquitine ligase SCF (SKP1, Cullin, F-box protein) et facteur important de la différenciation des cellules canalaires.[288] L'analyse plus fine du compartiment canalaire devra être réalisée. De façon intéressante des données préliminaires, qui seront à confirmer par des expériences complémentaires, montrent une tendance à la diminution de l'expression de l'ARNm de certains gènes canalaires tels que CK19, HNF6 et SOX9 en absence de TRIP12 **(Figure 26)** suggérant un éventuel contrôle au niveau transcriptomique.

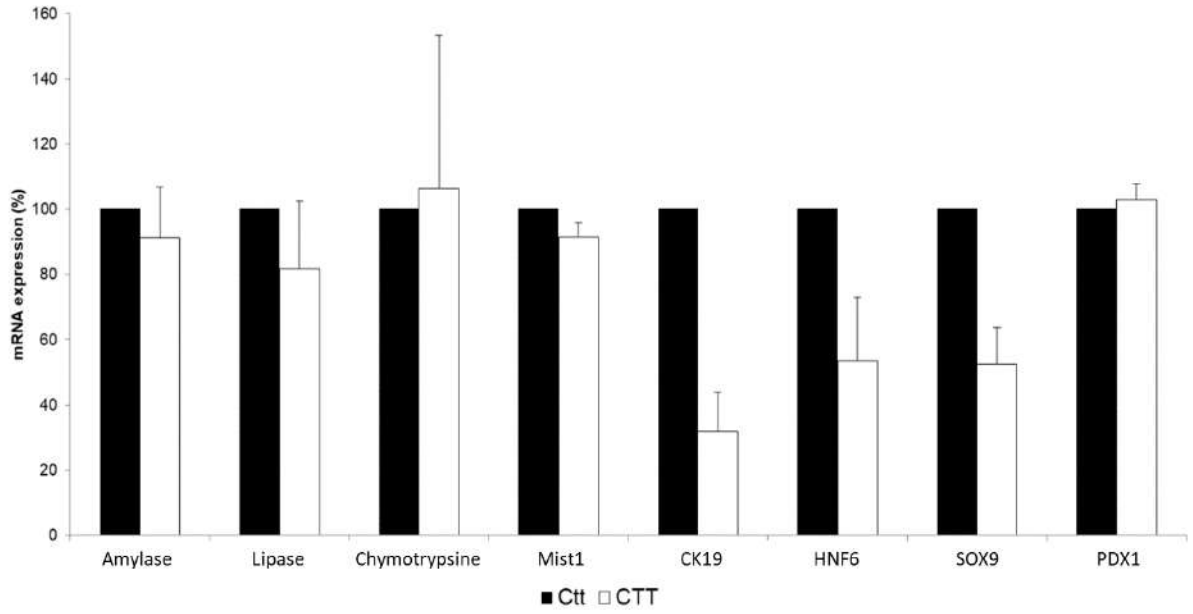

Figure 26 : Analyse transcriptomique des gènes acinaires et canalaires en réponse à la déplétion de TRIP12 dans des cellules acineuses isolées.
Les niveaux d'ARNm sont déterminés par RT- qPCR (n=2), les valeurs sont représentées en pourcentage par rapport à la condition contrôle « Ctt » et normalisées en fonction de trois gènes (HPRT, cyclophiline A, 18S).

Il sera donc essentiel d'analyser à large échelle le transcriptome des acini par RNAseq afin d'étudier les réseaux géniques altérés en réponse à la déplétion de TRIP12.

Enfin, au-delà de l'étude dans le pancréas, le nouveau modèle murin d'invalidation conditionnelle de TRIP12 pourrait être utilisé dans d'autres pathologies afin d'approfondir les voies moléculaires régies par TRIP12 dérégulées dans les troubles neurodéveloppementaux.[4] En effet, les

mutations du gène TRIP12 sont associées au trouble du spectre autistique et à des déficiences intellectuelles mais l'ensemble de ces études réalisées sur des cohortes de patients sont corrélatives.

II. Hétérogénéité d'expression de TRIP12 dans le pancréas à l'âge adulte.

Mes travaux de thèses ont permis de montrer une hétérogénéité d'expression protéique de TRIP12 dans les cellules pancréatiques murines en conditions basales à l'âge adulte. Les données disponibles dans le « Human Protein Atlas » (www.proteinatlas.org) appuient nos conclusions. Par ailleurs, en basal, l'expression de TRIP12 est régulée au cours du cycle cellulaire et contribue au bon déroulement de la mitose **(§ annexe II)**. Ainsi, il est probable que l'expression hétérogène de TRIP12 dans le pancréas soit en partie associée à sa régulation au cours du cycle cellulaire. Il sera intéressant de rechercher au sein du tissu pancréatique dans quelle phase du cycle cellulaire sont les cellules exprimant TRIP12. Selon notre hypothèse, seules les cellules qui se trouvent entre la fin de la phase S et la mitose devraient exprimer TRIP12.

Enfin, il a récemment été démontré que la population acineuse est hétérogène, composée de plusieurs sous-populations cellulaires ayant des capacités prolifératrices différentes.[223] Au vu de l'expression hétérogène de TRIP12 et sachant qu'elle participe à la prolifération cellulaire en régulant indirectement la voie P53, nous faisons l'hypothèse que son expression peut être corrélée à une sous-population cellulaire. Un co-marquage de TRIP12 et des marqueurs caractéristiques des sous-populations acineuses (positifs pour BMI1, Stamine ou DLCK1) pourra être réalisé afin de vérifier si TRIP12 est retrouvée préférentiellement dans une de ces sous-populations.

III. TRIP12, acteur dans la MAC, étape initiatrice du CP.

A. Caractérisation des structures « X »

Les analyses phénotypiques descriptives que nous avons menées dans nos modèles murins démontrent un rôle de TRIP12 dans la MAC in vivo et in vitro. En effet, en condition de stress ou en présence d'un oncogène, la perte de TRIP12 inhibe la capacité plastique des cellules acineuses et bloque la MAC. Ceci conduit à des modifications morphologiques des acini que nous n'avons pas caractérisées et que nous avons appelées structures « X ». Ces structures sont de plusieurs sortes, morphologiquement identifiées avec une lumière de grande taille qui peut être multilobée, une multitude de vacuoles caractéristiques d'acini stressés et une anomalie des jonctions des cellules acineuses. La pancréatite aiguë est associée à des défauts d'autophagie et au stress du réticulum endoplasmique (RE) à l'origine de la formation de vacuoles.[289] Certaines des structures « X » s'apparentent à des autophagosomes. Peu de travaux se sont intéressés au rôle du protéasome dans la pancréatite alors qu'il existe un lien étroit

entre ce système et le stress du RE, entre le protéasome et l'autophagie. Nous pouvons faire l'hypothèse que la perte de TRIP12 affecte le fonctionnement coordonné des systèmes de dégradation protéolytique et de recyclage activés en réponse au stress cellulaire qui est nécessaire au bon déroulement.[290] Une étude en microscopie électronique permettrait d'obtenir plus d'informations sur les structures « X ». En parallèle, l'analyse des marqueurs de l'autophagie (tels que LC3-I, LC3-II, Becline1, P62) et de ceux du stress du RE et de la réponse adaptative à ce stress, la réponse UPR (Unfolded Protein Response), au cours de la pancréatite sera indicatrice du mécanisme à l'origine des structures « X ». De même, leur caractérisation par immunofluorescence sur coupes ou lors de la MAC in vitro contribuera à leur identification.

B. Mécanisme d'action de TRIP12 dans la MAC

1) Rôle épigénétique

Au cours de la MAC, les acini subissent une réorganisation du génome, associée à une profonde modification de leur transcriptome avec pour conséquence un changement de phénotype **(§Chapitre 1 : Partie 2- II.C**). Nous avons démontré dans l'étude de Larrieu *et al.* que TRIP12 est une protéine nucléaire possédant un domaine intrinsèquement désordonné (IDR) dans la partie N-terminale. L'IDR est responsable de l'interaction forte de TRIP12 avec la chromatine. Les données préliminaires de l'équipe montrent que la surexpression du domaine IDR entraine une hypercompaction de la chromatine consolidant ainsi le rôle potentiel de TRIP12 dans l'organisation du génome.

De plus, l'activité catalytique de TRIP12 régule l'expression de protéines essentielles des complexes de remodelage de la chromatine telles que BAF57 appartenant au complexe SWI/SNF [55] et ASXL1 appartenant au complexe de déubiquitination PR-DUB.[54] L'interactome de TRIP12 montre également qu'elle est associée à SUZ2 et EZH2, deux régulateurs qui constituent le complexe PRC2 (Polycomb Repressive Complex 2) participant à la répression épigénétique des gènes en triméthylant l'histone H3 sur la lysine K27.

Au vu de ces éléments, indépendamment de son rôle sur l'expression de PTF1a, TRIP12 pourrait contribuer durant la MAC à la répression des gènes acinaires par son IDR et/ou son activité catalytique. Cela signifie que dans nos modèles d'études in vivo, en absence de TRIP12, l'inhibition de la MAC pourrait être causée par un blocage de la répression du programme de différenciation des cellules acineuses. Afin de vérifier notre hypothèse, il est dans un premier temps, envisageable de mesurer par IHC les marques répressives induites par le complexe polycomb tels que H2AK119ub et la tri-méthylation de l'H3K27 ou encore le niveau de ASXL1. En absence de TRIP12, ASXL1 ne serait pas dégradée par le protéasome, entrainant l'augmentation de son expression et favorisant la déubiquitination de l'histone H2AK119. Les travaux de Benitz *et al.* prouvent que l'ubiquitination de

cette histone par le complexe PRC1 est nécessaire pour réprimer l'expression de PTF1a lors de la MAC.[173] Ainsi, l'absence de TRIP12 réduirait la répression des gènes acinaires, stabilisant le programme de différenciation des acini se traduisant par un blocage de la métaplasie acino-canalaire.

Nous pouvons aussi supposer, étant donné les capacités de compaction de la chromatine de l'IDR de TRIP12 et son rôle sur le complexe SWI/SNF, qu'en son absence la chromatine serait sous une conformation relâchée. En effet, les formes libres de BAF57 ne seront pas ubiquitinées en absence de TRIP12 et seront alors disponibles pour interagir avec BAF155. Le complexe BAF155-BAF57 interagit avec BRG1 pour décompacter la chromatine. Ainsi, l'analyse de l'architecture du génome en présence ou non de TRIP12 par RNA-seq et CHIP-seq permettrait de mieux caractériser les régions ciblées et les modifications de chromatine qui dépendent de l'expression de TRIP12 au cours de la métaplasie acino-canalaire.

2) Régulation des masters gènes de la MAC

Mes travaux montrent que les souris déficientes pour TRIP12 ont un niveau de PTF1a augmenté ce qui est cohérent avec nos travaux précédents. Cependant, cinq jours après l'induction d'une pancréatite aiguë le niveau de PTF1a est nettement réduit dans les cellules acineuses qui n'expriment pas TRIP12 par rapport aux acini contrôles. Ceci est corrélé à l'augmentation de l'expression de PDX1 et associé à un marquage CK19 de la lumière des acini dans le modèle murin invalidé pour TRIP12. L'analyse à large échelle du transcriptome des acini par RNAseq au cours des différents stades de la MAC fournira les éléments de réponse permettant de comprendre les différences observées en absence de TRIP12 et de définir l'identité des cellules qui n'expriment pas TRIP12.

IV. Rôle de TRIP12 dans le développement des lésions prénéoplasiques

Les données générées durant ma thèse à partir des échantillons histologiques humains prouvent que le niveau d'expression de TRIP12 augmente dès l'apparition des lésions prénéoplasiques PanIN de bas grade et perdure dans les lésions de haut grade jusqu'au développement des tumeurs. Par ailleurs, l'étude des lignées cancéreuses pancréatiques humaines montre que l'expression de TRIP12 est très hétérogène d'une tumeur à l'autre. En effet, j'ai démontré une stratification des tumeurs pancréatiques en 3 sous catégories en fonction de l'expression de TRIP12 : faible, modérée, forte. Ces données sont en accord avec les données disponibles dans la base de données « Human Protein Atlas » (www.proteinatlas.org). De plus, l'hétérogénéité de cette E3 ligase est également visible dans d'autres types de cancers. Ainsi, il serait intéressant de vérifier si l'hétérogénéité d'expression de TRIP12 existe également au sein des lésions prénéoplasiques. Pour cela il faudrait associer le nombre de noyaux positifs pour TRIP12 mesurés dans les PanIN de grades différents à l'intensité du marquage comme dans l'article-1.

Par ailleurs, les données préliminaires de l'analyse de l'ARNm de TRIP12 dans les acini isolés de souris contrôles Ctt et dans les cellules tumorales issues du modèle murin KPCtt, montrent une augmentation de son expression dans les tumeurs **(Figure 27)**.

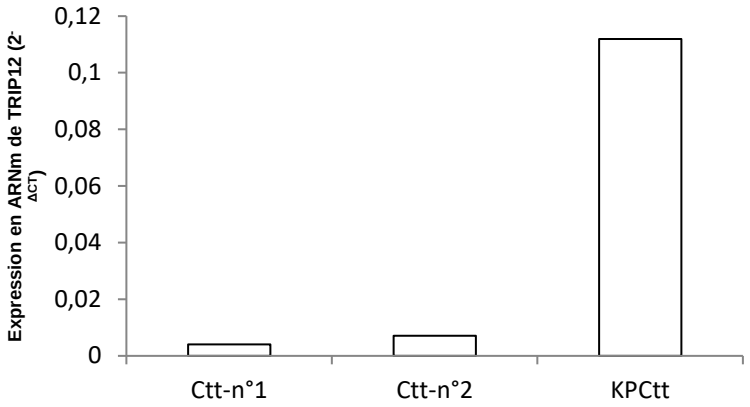

Figure 27 : Comparaison du niveau en ARNm de TRIP12 entre un tissu pancréatique acineux (Ctt) et la lignée tumorale (KPC).

Ces données doivent être reproduites afin d'assurer leur fiabilité et pourraient être complétées par une analyse de l'expression protéique de TRIP12. Elles sont cependant cohérentes avec l'analyse de l'expression de TRIP12 dans les modèles murins qui développent des lésions pré-néoplasiques en réponse à l'expression de l'oncogène $Kras^{G12D}$ (Données non montrées).

Nos modèles d'études précliniques pourraient servir à élucider le mécanisme responsable de la surexpression de TRIP12 dès les stades prénéoplasiques. Grâce aux résultats de notre première étude, nous pouvons envisager une régulation de l'activité du promoteur du gène Trip12. L'identification des facteurs de transcription responsables de la régulation transcriptomique restent méconnus. Cependant, l'analyse bioinformatique à l'aide du site Genomatix révèle l'existence de sites de liaison putatifs de nombreux facteurs de transcription. Dans le tableau suivant, seuls les facteurs de transcription pancréatiques sont référencés **(Figure 28)**.

Matrix Family	Detailed Family Information	Start position	End position	Anchor position	Strand	Core sim.	Matrix sim.	Sequence
HNF1	Hepatic Nuclear Factor 1	2	18	10	+	1	0,932	attacctaGTTAggccc
RREB	Ras-responsive element binding protein	16	30	23	+	1	0,805	cCCCAaagtctccgg
RREB	Ras-responsive element binding protein	70	84	77	+	1	0,89	cCCCAccccccccag
LEFF	LEF1/TCF	108	124	116	+	1	0,844	gttcctTCAAttatcag
NKXH	NKX homeodomain factors	107	125	116	-	1	0,907	gctgaTAATtgaaggaacc
BRNF	Brn POU domain factors	108	126	117	+	1	0,801	gttccttcaATTAtcagct
HOMF	Homeodomain transcription factors	108	126	117	+	1	0,954	gttccttcAATTatcagct
HOMF	Homeodomain transcription factors	109	127	118	-	1	0,954	cagctgaTAATtgaaggaa
SP1F	GC-Box factors SP1/GC	151	167	159	-	1	0,92	ggcacGGGCggaggcgc
EBOX	E-box binding factors	156	168	162	+	1	0,891	tccgccCGTGccg
SORY	SOX/SRY-sex/testis determinig and related HMG box factors	193	217	205	-	1	0,922	cgaggACAAagtagttccccgaggg
NR2F	Nuclear receptor subfamily 2 factors	197	221	209	-	1	0,825	agcccgaggaCAAAgtagttccccg
HOMF	Homeodomain transcription factors	216	234	225	+	1	0,851	cgggctcCGGTtacgggct
PAX6	PAX-4/PAX-6 paired domain binding sites	246	264	255	+	1	0,919	ccgGCACcgctgcctactg
HOMF	Homeodomain transcription factors	421	439	430	+	1	0,987	caggaaCTAAttccccctc
PAXH	PAX homeodomain binding sites	424	438	431	+	1	0,844	gaactAATTccccct
PDX1	Pancreatic and intestinal homeodomain transcription factor	424	442	433	-	0,76	0,863	cccgaggggGAATtagttc
SORY	SOX/SRY-sex/testis determinig and related HMG box factors	459	483	471	+	1	0,928	gctggaAATTtcacggatcagggtt
NR2F	Nuclear receptor subfamily 2 factors	460	484	472	+	0,857	0,823	ctggaaatttcacgGATCagggttc
PAX6	PAX-4/PAX-6 paired domain binding sites	466	484	475	+	0,818	0,862	atttcACGGatcagggttc
HNF1	Hepatic Nuclear Factor 1	556	572	564	-	0,76	0,831	aaaccctaGTTTaaatt
NR2F	Nuclear receptor subfamily 2 factors	567	591	579	-	0,762	0,826	ggttggggtcaaggGGCCaaaaccc
NR2F	Nuclear receptor subfamily 2 factors	569	593	581	-	1	0,867	ttggttggggTCAAgggccaaaac
INSM	Insulinoma associated factors	580	592	586	-	1	0,931	tggttGGGGtcaa
RREB	Ras-responsive element binding protein	584	598	591	+	1	0,904	cCCCAaccaagccc

Figure 28 : Liste des facteurs de transcription pancréatiques putatifs déterminée par analyse bio-informatique réalisée à l'aide du site Genomatix.

Parmi cette liste sont notamment retrouvés les facteurs PDX1 et HNF1 qui possèdent des sites de liaison localisés dans des régions conservées du promoteur TRIP12 et sont des facteurs de transcription fortement régulés au cours de la MAC et dans la tumorigénèse pancréatique.[118,184] De ce fait, l'étude comparative par séquençage de la chromatine immunoprécipitée (CHIP-Seq) et de l'ARN (RNA-seq) des acini contrôles, des lésions pré-néoplasiques et des tumeurs murines, permettrait de valider les données bio-informatiques prédictives et de définir l'implication de ces facteurs de transcription sur l'expression de l'ARNm de TRIP12 en conditions pathologiques.

Nous pouvons aussi envisager une régulation de l'expression de la protéine TRIP12 au cours du cycle cellulaire.[21] En effet, dans la première partie de mon projet de thèse, nous démontrons que contrairement aux lignées cellulaires exprimant faiblement TRIP12, les lignées cellulaires qui expriment modérément et fortement TRIP12 préservent son expression dans leur noyau en G_1. Le mécanisme pourrait faire intervenir la déubiquitinase USP7. L'interaction entre TRIP12 et USP7 est largement décrite au sein de la littérature notamment dans certains cancers pour stabiliser TRIP12.[37,86] Les données préliminaires réalisées sur les lignées cellulaire humaines après synchronisation dans chaque phase du cycle permettent de corréler l'expression protéique de TRIP12 et celle d'USP7 **(Figure 29)**.

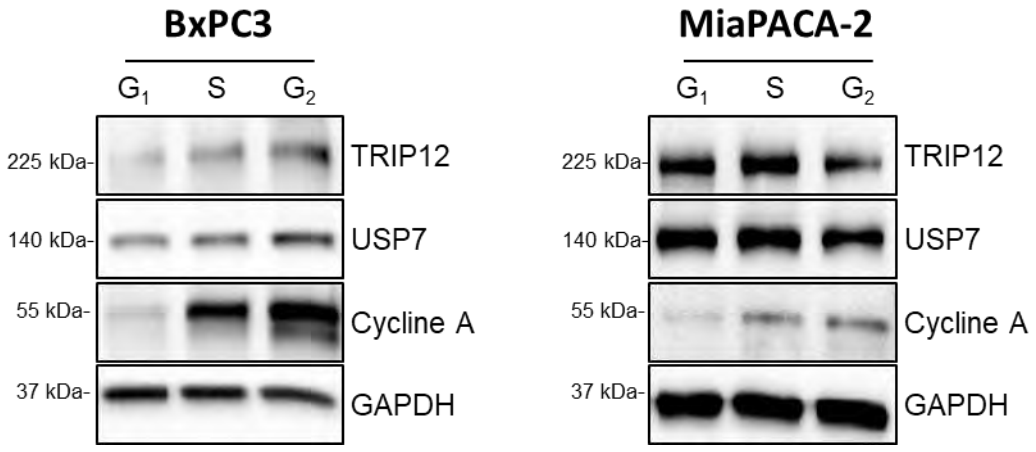

Figure 29 : Expression protéique de TRIP12 et d'USP7 dans les lignées BxPC3 et MiaPACA-2 dans les différentes phases du cycle cellulaire (G_1, S, G_2).
La cycline A est un contrôle de l'enrichissement de chaque phase, faiblement exprimé en phase G_1 pour atteindre un maximum en G_2.

Par ailleurs, l'expression importante de TRIP12 semble être associée à un défaut d'export cytoplasmique largement discuté dans l'article-1.

Or, il s'avère que la stabilité de TRIP12 en G_1 dans les lignées qui surexpriment TRIP12 est associée à l'augmentation d'USP7 dans cette même phase. Il serait possible que l'interaction entre TRIP12 et USP7 soit maintenue en G_1, stabilisant ainsi TRIP12 dans le noyau et l'empêchant d'être dégradée dans le cytoplasme par le protéasome. De plus, il est décrit que l'interaction entre USP7 et ses cibles peut être régulée par la phosphorylation des domaines d'interaction. Ceci est, par exemple, le cas de la protéine UHFR1 (Ubiquitin like with PHD and RING finger domains 1) phosphorylée sur son

domaine d'interaction avec USP7 durant la mitose par le complexe Cycline B1/CDK1. Cette phosphorylation empêche l'interaction entre USP7 et UHFR1 bloquant ainsi l'action de la déubiquitinase et permettant l'adressage d'UHFR1 au protéasome.[291] De manière similaire à UHFR1, TRIP12 est phosphorylée par CDK1 sur la sérine 424 pendant la mitose,[33] site correspondant au domaine d'interaction entre TRIP12 et USP7.[28] Ainsi, TRIP12 pourrait être phosphorylée spécifiquement pendant la mitose par CDK1, ne plus interagir avec USP7 pour un transfert vers le cytoplasme afin d'être dégradée par le protéasome. Cependant cette régulation pourrait être altérée dans les lignées où TRIP12 persiste en G_1.

Par ailleurs, dans les tumeurs pancréatiques humaines une corrélation existe entre l'expression de ces deux protéines dans les bases de données disponibles (GEPIA) et après analyse par immunofluorescence de leur expression sur TMA **(Figure 30)**.

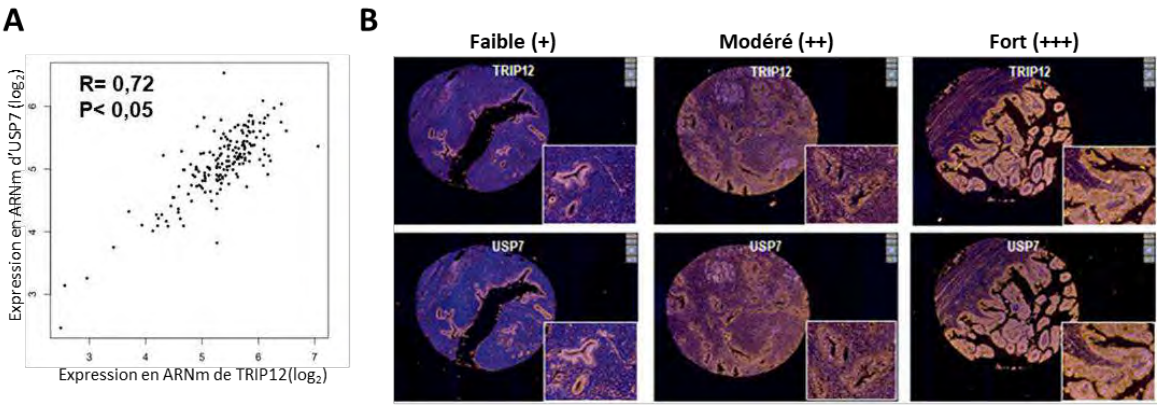

Figure 30 : Corrélation entre l'expression de TRIP12 et USP7 dans les tumeurs pancréatiques humaines.
(**A**) Expression de l'ARNm de TRIP12 corrélé à celle de l'ARNm d'USP7 dans les tumeurs pancréatiques humaines (données issues de GEPIA). (**B**) Expression protéique de TRIP12 et d'USP7 analysées par immunofluorescence sur TMA.

Ces données font de la déubiquitinase USP7 une cible intéressante qui nécessiterait une analyse plus approfondie pour comprendre le mécanisme à l'origine de la stabilité de TRIP12. Cependant, nous ne pouvons pas exclure une dégradation protéolytique de TRIP12 différente entre les lignées cellulaires. A ce jour, la protéine responsable de cette dégradation est inconnue.

V. Rôle de TRIP12 dans la tumorigénèse pancréatique

A. Impact sur la transformation cellulaire

Actuellement, de nouvelles pistes thérapeutiques sont envisagées visant à réactiver le programme de différenciation cellulaire afin d'inverser la transformation induite par l'expression des oncogènes.[232] En particulier, il a été démontré que la réintroduction de PTF1a dans des cellules cancéreuses pancréatiques humaines inhibe leur croissance.[235] Cependant, ce n'est pas le cas de toutes les lignées. Les lignées MiaPACA-2 et PANC-1 ne sont pas affectées par l'expression de PTF1a contrairement aux lignées SU8686 et SW1190 qui perdent leur capacité prolifératives.

Sachant que TRIP12 cible PTF1a et que les lignées MiaPACA-2 et PANC-1 ont un niveau protéique élevé de cette E3, il est probable que TRIP12 entraine la dégradation de PTF1a lors de sa réintroduction dans ces lignées. Notre hypothèse pourrait être confortée en vérifiant que les lignées SU8686 et SW1190 expriment peu TRIP12. Les données disponibles sur la lignée SU8686 indiquent des temps de prolifération et un état de différenciation modérés comme la lignée BxPC-3.[292] La perte de TRIP12 dans les lignées MiaPACA-2 et PANC-1 pourrait ainsi sensibiliser ces lignées à la réinduction de PTF1a et bloquer ainsi la croissance des cellules tumorales.

B. TRIP12, une cible thérapeutique potentielle

L'inhibition des E3 ligases ne semble pas être une bonne option thérapeutique. En effet, déjà testée en essai clinique,[293] elle ne permet pas d'améliorer le pronostic des patients.

Plusieurs études ont rapporté l'implication de TRIP12 dans le contrôle de la réparation des dommages à l'ADN. Cependant, les mécanismes impliqués et les conséquences sur la sensibilité à la chimiothérapie dépendent fortement du contexte cellulaire, des substrats de TRIP12 et du type de dommages à l'ADN (Chapitre 1 : partie 1).

Dans la première partie de mes travaux de thèse, j'ai observé qu'une expression élevée de TRIP12 dans des lignées cellulaires cancéreuses pancréatiques humaines est associée à une sensibilité plus élevée à différents types de médicaments. A l'inverse, la déplétion de TRIP12 diminue la sensibilité à la doxorubicine. De plus, nous démontrons que l'expression élevée de TRIP12 est principalement due à sa présence dans les cellules en phase G_1. La réparation correcte des dommages de l'ADN par NHEJ (Non-Homologous End-Joining) est majoritaire pendant cette phase afin de réparer les cassures de l'ADN apparues en fin de phase G_2 et au moment de la division cellulaire. Chez les patients exprimant fortement TRIP12, sa présence aberrante dans les cellules en phase G_1 pourrait potentiellement inhiber leur capacité de réparation des dommages à l'ADN par NHEJ, sensibilisant ainsi les cellules face à un traitement qui nécessite une réparation par ce système. A l'inverse, lorsque TRIP12 est faiblement exprimée, les systèmes de réparation par NHEJ ne sont pas réprimés réduisant l'efficacité du traitement créateur de cassures doubles brins.

De manière comparable aux données issues de l'article-1, dans la seconde partie du projet la prolifération cellulaire des lignées cancéreuses murines est nettement réduite lorsque TRIP12 est invalidée. Il sera intéressant d'analyser si la chimio-sensibilité de ces lignées murines dépend de l'expression de TRIP12 et d'élargir les analyses de chimio-sensibilité à d'autres agents inducteurs de cassures doubles brins de l'ADN. Les souris KPC surexprimant TRIP12, ayant des systèmes de réparation défectueux pourraient ensuite être traitées en combinant le traitement de référence (la gemcitabine) et la doxorubicine ou un autre agent. Par extrapolation les patients dont les tumeurs

expriment beaucoup TRIP12, pourraient éventuellement être traités avec cette combinaison thérapeutique.

Néanmoins, pour les patients dont la tumeur exprime faiblement TRIP12, un système de létalité synthétique serait à privilégier. D'après les données de Gatti *et al.* 2020., la perte de TRIP12 augmente la sensibilité des cellules cancéreuses aux inhibiteurs de PARP car TRIP12 dégrade PARP1 au niveau de la chromatine bloquant ainsi l'effet des inhibiteurs.[30] Ainsi, il serait intéressant d'analyser les capacités de réponse des lignées tumorales pancréatiques murines et humaines en fonction de l'expression de TRIP12 aux inhibiteurs de PARP. Alors que les lignées avec une faible expression de TRIP12 résistent aux agents inducteurs des cassures doubles brins, ces lignées seraient dans ce cas, plus sensibles aux inhibiteurs de PARP.

En conclusion, l'expression de la protéine TRIP12 pourrait être utilisée comme indicateur de la sensibilité aux médicaments pour orienter le traitement thérapeutique des patients porteur d'un CP.

Conclusion générale

Par des approches fonctionnelles qui reposent sur des modèles cellulaires et murins, mes travaux de thèse apportent des informations clefs sur le rôle d'une protéine ubiquitaire, qui lorsqu'elle est dérégulée perturbe à elle seule les mécanismes de MAC et l'homéostasie pancréatique, favorisant la mise en place des lésions pancréatiques précancéreuses. Sur le plan clinique, par extrapolation, je suggère que le niveau d'expression de TRIP12 soit utilisé comme biomarqueur pronostic de réponse aux traitements afin de stratifier les patients et d'optimiser la réponse thérapeutique en fonction de l'hétérogénéité de TRIP12.

L'ensemble des résultats issus de mes travaux de thèse seront les prérequis pour une étude plus approfondie dans le but d'identifier et de caractériser les mécanismes moléculaires qui dépendent de TRIP12 dans l'initiation et la progression du CP.

Annexes

I. Annexe 1 - Revue: « *E3 ubiquitin ligase TRIP12: regulation, struture and physiopathological functions* »

International Journal of
Molecular Sciences

MDPI

Review

E3 Ubiquitin Ligase TRIP12: Regulation, Structure, and Physiopathological Functions

Manon Brunet [1,2,†], Claire Vargas [1,2,†], Dorian Larrieu [1,2,†], Jérôme Torrisani [1,2,*,†] and Marlène Dufresne [1,2,*]

[1] Institut National de la Santé et de la Recherche Médicale, INSERM Unit 1037, Centre de Recherches en Cancérologie de Toulouse, CEDEX 1, 31 037 Toulouse, France; manon.brunet@inserm.fr (M.B.); claire.vargas@inserm.fr (C.V.); dorian.larrieu@gmail.com (D.L.)

[2] Université Toulouse III-Paul Sabatier, CEDEX 9, 31 062 Toulouse, France

* Correspondence: jerome.torrisani@inserm.fr (J.T.); marlene.dufresne@inserm.fr (M.D.); Tel.: +33-582-741-644 (J.T.); +33-582-741-643 (M.D.)

† These authors have contributed equally to this work.

Received: 25 September 2020; Accepted: 5 November 2020; Published: 12 November 2020

Abstract: The Thyroid hormone Receptor Interacting Protein 12 (TRIP12) protein belongs to the 28-member Homologous to the E6-AP C-Terminus (HECT) E3 ubiquitin ligase family. First described as an interactor of the thyroid hormone receptor, TRIP12's biological importance was revealed by the embryonic lethality of a murine model bearing an inactivating mutation in the *TRIP12* gene. Further studies showed the participation of TRIP12 in the regulation of major biological processes such as cell cycle progression, DNA damage repair, chromatin remodeling, and cell differentiation by an ubiquitination-mediated degradation of key protein substrates. Moreover, alterations of TRIP12 expression have been reported in cancers that can serve as predictive markers of therapeutic response. The *TRIP12* gene is also referenced as a causative gene associated to intellectual disorders such as Clark–Baraitser syndrome and is clearly implicated in Autism Spectrum Disorder. The aim of the review is to provide an exhaustive and integrated overview of the different aspects of TRIP12 ranging from its regulation, molecular functions and physio-pathological implications.

Keywords: TRIP12; E3 ubiquitin ligase; cancers; intellectual disorders

1. Introduction

Thyroid hormone Receptor Interacting Protein 12 cDNA was cloned from the human myeloid KG-1 cell line and named the unidentified KIAA0045 human gene. The deduced coding sequence of KIAA0045 showed partial identity to that of the *S. cerevisiae* UFD4 protein (Ubiquitin Fusion Degradation 4) [1]. Another study identified Thyroid hormone Receptor Interacting Protein 12 (TRIP12) as a member of the structurally and functionally related E3 ubiquitin ligases based on the identification of a domain homologous to the E6-associated protein carboxyl terminus (HECT domain), which is a protein that induces the ubiquitin-dependent degradation of P53 in the presence of the E6 protein from the papillomavirus [2].

TRIP12 was later characterized as a thyroid hormone receptor-interacting protein by the trap yeast interaction system to isolate proteins that interact with the ligand binding/dimerization/transcriptional activation domain of the rat TR-β1 (Thyroid Receptor-β1) [3]. Fifteen cDNAs encoding Thyroid hormone Receptor Interacting Proteins (TRIPs) were isolated. All the TRIPs interacted with the Thyroid hormone Receptor (TR), but only when thyroid hormone T3 was present (TRIP1 to TRIP11) or only when T3 was absent (TRIP12 to TRIP15). Protein sequences of the fifteen TRIPs are unrelated, but sequences similarities with known proteins and functional motifs were found for nine of them

based on blast alignment analyses with no demonstration of functional significance. The TRIP12 sequence was found to show 55% identity with the C-terminus of E6-associated protein, and more than a decade following its identification, TRIP12 was demonstrated to function as an E3 ubiquitin ligase [4]. Evidence of functional roles was later provided for the other TRIPs proteins (Supplemental Table). Among them, TRIP12 is the only TRIP family member bearing an E3 ubiquitin ligase activity.

The biological importance of TRIP12 was revealed by the embryonic lethality of a murine model bearing an inactivating mutation in the *TRIP12* gene [5]. Several molecular functions of TRIP12 in important cellular processes and signaling pathways have been demonstrated in recent years. Accumulating evidence indicate that TRIP12 ubiquitinates key proteins for cell homeostasis, regulates gene expression (See Section 5), and plays important roles in cancers and neurological diseases. Up to now, more than 58 publications related to TRIP12 have been referenced in PubMed, half of them in the last 5 years. We have recently contributed to broadening knowledge on the role of TRIP12 by discovering a new substrate essential for pancreatic acinar cells differentiation [6] and by demonstrating that TRIP12 is a new chromatin-associated protein with several implications in the cell cycle progression and in the maintenance of genome integrity [7]. Due to its implication in several important physiological and pathological processes, TRIP12 now emerges as a protein of interest for molecular mechanisms researches and as a potential new therapeutic target.

In this review, we attempt to comprehensively summarize the current knowledge from the literature and databases on TRIP12. This summary includes the gene and protein expression, the protein structure, the protein interactors and functions. We address the physio-pathological roles of TRIP12 in essential biological pathways in relation with some of its substrates. We also present the alterations of the *TRIP12* gene found in neurodevelopmental disorders and cancers as well as the alterations of TRIP12 protein expression in cancers, and their consequences. Finally, we discuss the potential role of TRIP12 as a therapeutic target and highlight the need for further research studies on this protein.

2. TRIP12 mRNA and Protein Expression

2.1. TRIP12 Gene Organization

In the human genome, the gene encoding for *TRIP12* mRNA is located on the long arm of chromosome 2 at the locus q36.3. It spreads over nearly 168 kb (Genome Browser (see Section Software and databases)). *TRIP12* mRNA expression is driven by a bidirectional promoter that also initiates the transcription of *FBXO36* (F-box Only protein 36) mRNA in a head-to-head opposite direction. Bidirectional promoters are often used to control genes sharing the same regulation or encoding proteins exhibiting a similar biological process [8]. The *FBXO36* gene encodes a protein that belongs to the F-box protein family. F-box is a ≈50 aa-domain that functions as a site for protein–protein interaction. Up to now, the functions of FBXO36 are unknown. In general, F-box proteins are part of SCF (SKP1, Cullin, F-box protein) ubiquitin ligase complexes, in which they bind to substrates for ubiquitin-mediated proteolysis [8,9]. This would be consistent with the fact that TRIP12 and FBXO36 expression are co-regulated. The 555 bp-bidirectional promoter is embedded in a 1753 bp long-CG-rich region also called CpG (Cytosine-phosphate-Guanosine) island, but the regulatory regions and methylation level of *TRIP12/FBXO36* promoter remain unstudied.

2.2. TRIP12 mRNA Expression

To date, 26 different *TRIP12* splicing mRNA variants have been identified (www.ncbi.nlm.nih.gov) (Table 1). Their length fluctuates from 9,065 (variant 4) to 10,492 nt (variant 20) with 41 to 43 exons with the exception of variants 24, 25, and 26 that contain only the first six (variants 24 and 25) or seven exons (variant 26) with a length of 5,951 (variant 26) to 6,052 nt (variant 25). Little is known regarding the expression level of the different splicing variants in human cells. It is suggested *TRIP12* mRNA transcripts are a mixture of all possible isoforms, although the variant NM_001284215.1 seems to be predominant in peripheral leukocytes [10]. For the long variants, while the 5′-Untranslated Region

(5′-UTR) is ≈180 nt-long, the 3′-Untranslated Region (3′-UTR) represents approximately one-third of the total mRNA length (≈3700 nt), which likely indicates a regulatory function for this region (Figure 1). In fact, the existence of a short (340 nt) and a long form (3716 nt) of *TRIP12* 3′-UTR mRNA was reported [11]. The different sites of transcriptional termination are explained by the presence of two consensus polyadenylation signals (Figure 1). These two variants display different translation efficiency in response to an activation of the mTORC (mammalian Target Of Rapamycin Complex 1) signaling pathway where the short form is more efficiently translated [11]. With reference to the Human Protein Atlas (see Section Software and databases), the expression of *TRIP12* mRNA is ubiquitous in human tissues even if levels of mRNA vary between tissues. For example, *TRIP12* mRNA is highly expressed in testis and in muscles but weakly expressed in pancreatic tissue [1,12,13].

Table 1. List of the human mRNA variants and protein isoforms of TRIP12.

mRNA Variant	Accession Number	mRNA Length	Exon Number	Protein Isoform	Protein ID	aa Number	Theoretical kDa
1	NM_001284214.2	10019	42	a	NP_001271143.1	2040	224
2	NM_001284215.2	9974	41	b	NP_001271144.1	2025	223
3	NM_004238.3	9875	41	c	NP_004229.1	1992	219
4	NM_001284216.2	9065	39	d	NP_001271145.1	1722	189
5	NM_001348315.2	10408	42	a	NP_001335244.1	2040	224
6	NM_001348316.2	10070	41	b	NP_001335245.1	2025	223
7	NM_001348317.1	9959	41	e	NP_001335246.1	2020	222
8	NM_001348318.2	10348	41	e	NP_001335247.1	2020	222
9	NM_001348319.1	10085	42	f	NP_001335248.1	2062	227
10	NM_001348320.2	10474	42	f	NP_001335249.1	2062	227
11	NM_001348321.1	10088	42	g	NP_001335250.1	2063	227
12	NM_001348322.1	10218	43	h	NP_001335251.1	2067	227
13	NM_001348323.3	10100	42	h	NP_001335252.1	2067	227
14	NM_001348324.2	10196	42	h	NP_001335253.1	2067	227
15	NM_001348325.2	10611	43	h	NP_001335254.1	2067	227
16	NM_001348326.2	10486	42	h	NP_001335255.1	2067	227
17	NM_001348327.2	10489	42	h	NP_001335256.1	2067	227
18	NM_001348328.1	10103	42	i	NP_001335257.1	2068	227
19	NM_001348329.2	10454	42	i	NP_001335258.1	2068	227
20	NM_001348330.2	10492	42	i	NP_001335259.1	2068	227
21	NM_001348331.1	9878	41	j	NP_001335260.1	1993	219
22	NM_001348332.1	9998	43	k	NP_001335261.1	2033	224
23	NM_001348333.1	10022	42	l	NP_001335262.1	2041	225
24	NM_001348335.1	5955	6	m	NP_001335264.1	440	48
25	NM_001348336.1	6052	6	m	NP_001335265.1	440	48
26	NM_001348334.1	5951	7	n	NP_001335263.1	411	45

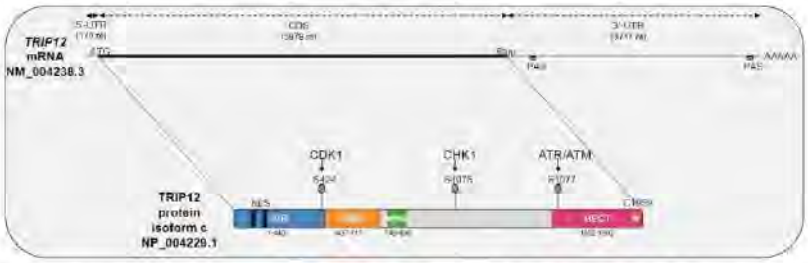

Figure 1. Schematic representation of Thyroid hormone Receptor Interacting Protein 12 (*TRIP12*) mRNA (NM_004238.3) and TRIP12 protein (isoform c, NP_004229.1) with functional domains, kinase associated-phosphorylated residues and cysteine catalytic site (yellow star). UTR: Untranslated Region, CDS: Coding Sequence, PAS: Poly-Adenylation Signal, AAA: Poly-adenylated tail, ATG: translation Start codon, Stop: translation Stop codon, NLS: Nuclear Localization Signal, S: serine residue, aa: amino acid, IDR: Intrinsically Disordered Regions, ARM: Armadillo repeats, HECT: Homologous to the E6-AP C-Terminus.

2.3. TRIP12 Protein Expression and Cellular Localisation

TRIP12 protein translation can occur from 26 different mRNA splicing variants (Table 1). This leads to the generation of 14 different TRIP12 protein isoforms (isoforms a to m) with a length comprised between 1722 aa and 2068 aa for the long isoforms a to l (Figure 2). The two short isoforms (m and n) contain only 440 and 411 aa, respectively. Multiple alignment analysis COBALT (Constraint-based Multiple Alignment Tool) (see Section Software and databases) reveals a high similarity between the long isoforms (Figure 2). The two most studied isoforms b and c (2025 and 1992 aa, respectively) only differ by a six aa deletion in the IDR domain and a 27 aa deletion in the WWE domain in the isoform c that potentially modifies the protein–protein interaction capacity of this isoform (see Section 3.2.). For further description of the TRIP12 protein, the 1992 aa isoform c (NP_004229.1) will be used as a reference. Even though several protein isoforms of TRIP12 potentially exist in human cells, it is still unknown whether the different isoforms are cell-specific or if they co-exist and in what proportion in the same type of cells. Unfortunately, commercially available antibodies are directed against epitopes that are common to the long isoforms of TRIP12 (except the isoform d). Therefore, they cannot discriminate the different long isoforms. However, immunostaining analysis using these antibodies reveals a nuclear localization of TRIP12 in several cell lines [7,14] and in human tissues (Human Protein Atlas). It can be explained by the presence of two putative bipartite variants of the classical basically Nuclear Localization Signals (NLS) (aa 73–94 and 136–152) (ELM software (see Section Software and databases)) (Figure 1). The importance of the N-terminal region in the maintenance of TRIP12 nuclear localization was demonstrated in our recent study [7]. Within the nucleus, two studies noted an absence of TRIP12 in the nucleoli [7,15].

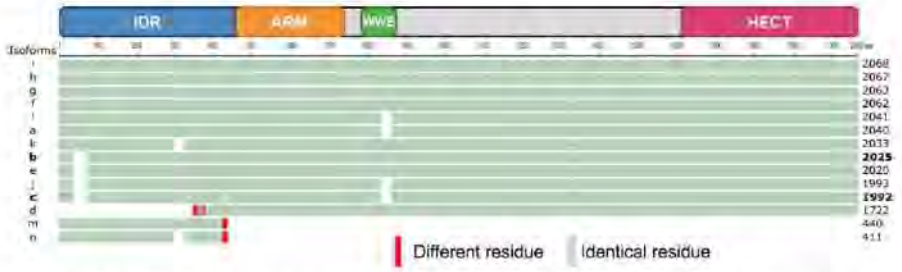

Figure 2. Schematic representation of a multiple alignment of human TRIP12 isoforms using the COBALT multiple alignment tool (see Section Software and databases). TRIP12 isoform i (2068 aa) was defined as the sequence of reference (master sequence). The two most studied isoforms b and c (and size) are written in bold. Residues in green are identical and in red are different. The different domains of TRIP12 are indicated above the alignment.

3. TRIP12 Protein Structure and Domains

TRIP12 is a large protein with an apparent molecular weight estimated between 189 and 227 kDa for the long forms (Table 1). It comprises several characterized protein domains: a catalytic HECT domain, two protein/protein interaction domains (WWE (Tryptophan-Tryptophan-Glutamate) and ARM (Armadillo repeats)), and a recently identified intrinsically disordered region (IDR) (Figure 1). These domains confer structure and functional roles to the protein. TRIP12 protein domains are conserved during evolution and are subject to post-translational modifications that likely modulate its structure and activity. Several studies reported HECT, ARM repeats, and WWE crystal structure of other proteins [16–18]. However, TRIP12 has yet to be recovered in crystal form to establish its complete 3D structure.

3.1. The HECT Domain

HECT domains (≈40 kDa) were first identified in the C-terminal part of the viral E6-AP protein; hence their name, Homologous to the E6-AP C-Terminus [2]. They are generally located in the C-terminal extremity of proteins and are constituted of two lobes: N-lobe domains (N-terminal end) and a C-lobe (C-terminal end) linked by a hinge domain [19,20]. The N-lobe is responsible for the interaction with the ubiquitin-conjugating enzyme E2 during the ubiquitination reaction (detailed in Section 4.1). The C-lobe carries the characteristic catalytic cysteine residue [21,22], which is highly conserved between species and essential to the ubiquitination reaction [2]. The TRIP12 HECT domain is located at residues 1552–1592, is structured in N and C-lobes, and contains a cysteine in position 1959 for which the replacement by an alanine residue abolishes TRIP12 ubiquitin ligase activity (Figure 1) [2,23]. Mechanistically, the 28 known HECT E3 ubiquitin ligases form an intermediate complex with ubiquitin before linking it to a lysine substrate via a thioester bond [20].

By ensuring the ubiquitin ligase catalytic activity, the HECT domain allows the implication of TRIP12 in different modes of protein degradation and signaling pathways (detailed in Sections 4 and 5).

3.2. The WWE Domain

A WWE domain is a globular region of ≈80 amino acids characterized by an enrichment with hydrophobic and aromatic residues in its two extremities and the conservation of two tryptophan residues (W) and one glutamate (E) [24]. The C- and N-terminal parts of WWE domains form β-sheets, while the central part is an α-helix. WWE domains are required for protein–protein interaction. They are essential for two families of proteins: E3 ubiquitin ligases (HECT, RING, and RING-H2 types) and in a sub-family of poly (ADP-ribose) polymerases (PARP). PARPs add multiple ADP-ribose moieties to protein targets (parylation) and participate in various cellular functions such as DNA repair and chromatin dynamics. The WWE domains were demonstrated as poly(ADP-ribose) (PAR) binding domains [25]. The WWE domain of TRIP12 is located between the residues 749 and 836 (InterProScan) [26] and is required for the interaction of TRIP12 with APP-BP1 (Amyloid Protein-Binding Protein 1) [4], PTF1a (Pancreas Transcription Factor 1a) [6], and parylated PARP1 (Poly-(ADP ribose) polymerase 1) [27] (Figure 1).

3.3. The Armadillo-Repeats Domain

Armadillo (ARM) repeat-containing proteins are characterized by the presence of imperfect tandem repeats of 42 hydrophobic amino acids. An ARM repeat is composed of three α-helices (H1, H2, and H3). Successive ARM repeats are able to assemble themselves to form a super-helix also named a solenoid. As such, ARM-repeat motifs are strongly implicated in protein/protein interactions. ARM repeat-containing proteins are involved in pleiotropic functions (cell/cell adhesion, cell signaling, cytoskeleton organization, nuclear trafficking, and ubiquitination) [28]. ARM repeats were first identified in the TRIP12 orthologues KAKTUS (*Arabidopsis thaliana*) and UFD4 (Ubiquitin Fusion Degradation 4) (*Saccharomyces cerevisiae*) (detailed in Section 4.3) [29,30]. The InterProScan database shows that ARM repeats are also present in the human TRIP12 protein. Slightly different ARM-repeat boundaries are found in this database; we arbitrarily chose to represent the smallest and the most quoted one between residues 437 and 715 (Figure 1). Functional studies demonstrated the role of ARM repeats of UFD4 in the recognition of the ubiquitin degradation signal (detailed in Section 4.3) of the substrates in *Saccharomyces cerevisiae* [30].

3.4. The IDR Domain

Intrinsically disordered regions (IDR) are common in the human proteome, whereby an estimated 44% of the proteome carries an IDR. These regions can be functional but interestingly lack a defined 3D conformation in physiological conditions [31]. The interaction of an IDR-containing protein with a partner can stabilize and/or fold the disordered region into a stable secondary structure. IDRs are

sequences enriched in basic, positively charged, and hydrophilic amino acids such as lysine (K), arginine (R), serine (S), and histidine (H). IDR-containing proteins are mostly involved in protein, DNA, and RNA binding/interaction [32–34]. Moreover, the presence of N-terminal IDRs is linked to DNA interaction [33–35]. We previously showed that TRIP12 interacts with chromatin through an IDR, which corresponds to the N-terminal quarter of the protein (aa 1–440) (Figure 1), and that the deletion of this domain leads to a loss of TRIP12 interaction with chromatin [7]. E3 ubiquitin ligases containing IDR structures are infrequent. Indeed, the IDEAL database (see Section Software and databases) references only 25 E3 ubiquitin ligases containing IDR among the ≈600 E3 ubiquitin ligases. According to the IDEAL (Intrinsically Disordered proteins with Extensive Annotations and Literature) database, TRIP12 IDR displays identity with well-characterized IDR-containing proteins such as MED1 (Mediator Complex Subunit 1, 25% of identity), AF9 (ALL1-Fused gene from chromosome 9, 23% of identity), and AF4/FMR2 (ALL1-Fused gene from chromosome 4/Fragile X Mental Retardation, 22% of identity). Numerous IDR-containing proteins are involved in transcription regulation [36], and these three proteins promote RNA polymerase II catalytic activity by being a coactivator (i.e., MED1) or by being part of the Super Elongation Complex (i.e., AF9, AF4/FMR2) [37,38]. Taken together with the discovery of TRIP12 chromatin interaction, TRIP12 may act as a new transcriptional regulator. Liu et al. described an APC (Adenomatous polyposis coli) domain, which is known to be positively charged and involved in microtubules interaction, within TRIP12 IDR [39]. However, the function of this APC domain was not further explored. It is also now well documented that IDRs can confer to proteins the particular biophysical property of the liquid-liquid phase separation (LLPS) by which two liquids form two different phases such as oil droplets in water [40,41]. This biophysical process was linked to genome organization and expression [42].

3.5. Conservation of TRIP12 Protein Domains during Evolution

TRIP12 orthologues were differently named depending on the species. For example, the TRIP12 orthologue is CTRIP (Circadian TRIP) in *Drosophila melanogaster*, KAKTUS (KAK also known as UPL3), in *Arabidopsis thaliana* (UniProt (see Section Software and databases)) and Ubiquitin Fusion Degradation protein 4 (UFD4) in *Saccharomyces cerevisiae* (UniProt). The size of TRIP12 orthologues also varies per species. The largest form is found in *Drosophila melanogaster* (3140 aa), while the smallest sequence is in *Saccharomyces cerevisiae* (1483 aa) (Figure 3). The TRIP12 amino-acid sequence is highly conserved in vertebrates, demonstrating 82% identity for the zebrafish to 97.7% for the mouse when compared to the human c isoform. This percentage of identity with the human sequence decreases in invertebrates, 38% for *Drosophila melanogaster*, 31.4% for *Arabidopsis thaliana*, 28% for *Schmidtea mediterranea*, and 27.2% for *Saccharomyces cerevisiae*. HECT and ARM-repeats domains are found in all species, whereas the WWE domain is found among all vertebrates and *Schmidtea mediterranea* but not in *Saccharomyces cerevisiae* and *Drosophila melanogaster*. The HECT domain, which is required for polyubiquitination, is present in less evolved species, underlying the importance of E3 ubiquitin ligase activity of TRIP12 during evolution. IDRs are fast evolving regions. Their evolution rate is higher than of structured domains due to the lack of 3D structure [31]. Highly conserved IDRs are often found in proteins involved in transcription regulation and DNA binding [31]. An N-terminal IDR is present in all the TRIP12 orthologues mentioned above. According to IUPred (see Section Software and databases), the TRIP12 IDR length varies from 1,042 aa in *Drosophila melanogaster* CTRIP to 117 aa in *Schmidtea mediterranea*. Vertebrate TRIP12 orthologues showed an IDR average size of 440 residues. Taken together, the high conservation of TRIP12 domains during evolution assumes essential functions for this protein in living organisms.

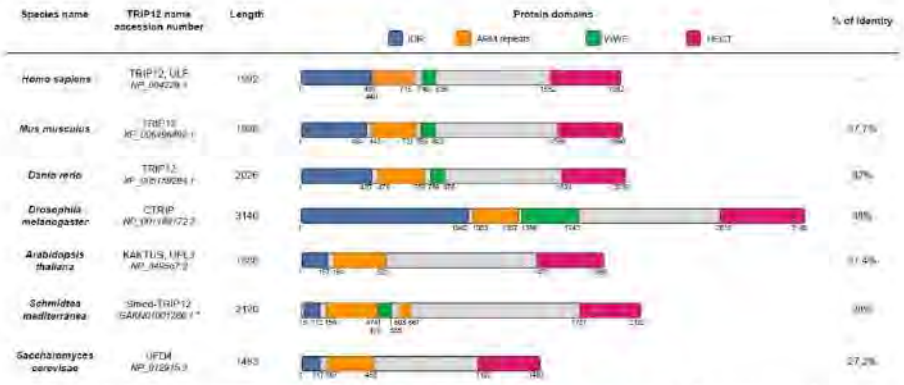

Figure 3. Schematic representation of protein domains in TRIP12 orthologues. Domain boundaries were defined using InterProScan analysis. Percentage of identity was determined by Emboss matcher (see Section Software and databases) pairwise sequence alignment (using *Homo sapiens* TRIP12 protein sequence as reference [43]). *: *Schmidtea mediterranea* cDNA sequence was manually corrected to perform the analysis.

3.6. Post-Translational Modifications of TRIP12

Similar to many other proteins, TRIP12 is post-translationally modified. The PhosphoSitePlus® database (see Section Software and databases) provides an exhaustive list of the post-translationally modified residues identified by mass spectrometry and other approaches (Figure 4). Among the modifications, the most abundant are the phosphorylation and the ubiquitination. TRIP12 can also be acetylated and mono-methylated. TRIP12 IDR is subject to abundant post-translational modifications, since it is a common feature of IDR domains [31], which is in contrast to the ARM repeats-domain that is poorly modified. Only few phosphorylation sites were attributed to specific kinases such as the serine S424, S1078, and S1577 to the kinases CDK1 (Cyclin Dependent Kinase 1), CHK1 (Checkpoint Kinase 1), and ATM/ATR (Ataxia-Telangiectasia-Mutated/Ataxia Telangiectasia and Rad3-related), respectively [44–46] (Figure 1). Despite two independent studies that reported the ubiquitination of TRIP12 [47,48] and numerous identified ubiquitinated residues, the ubiquitin ligases responsible for TRIP12 ubiquitination are unknown. Moreover, we cannot exclude that TRIP12 may exhibit functions of self-ubiquitination. It was demonstrated that the Ubiquitin-Specific Peptidase USP7 deubiquitinates and stabilizes the TRIP12 protein [47,48]. Despite numerous studies dedicated to TRIP12, none of the post-translational modifications are shown to function in the regulation of catalytic activity, interacting capacity, nor in the cellular localization of this E3 ubiquitin ligase.

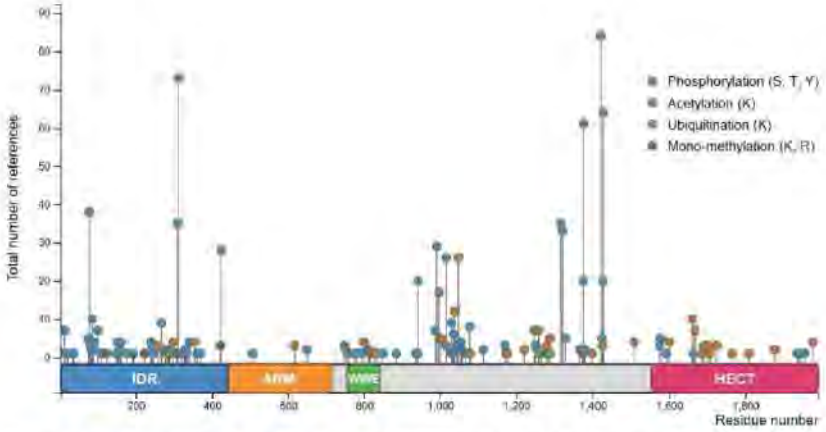

Figure 4. Post-translational modifications of TRIP12 (isoform c) adapted from PhosphoSitePlus® (see Section Software and databases). Total number of references represents the number of records in which this modification site was assigned using proteomic discovery mass spectrometry and using other methods. S stands for serine, T stands for threonine, Y stands for tyrosine, and K stands for lysine.

4. Functions of TRIP12 in Ubiquitin-Mediated Proteolysis

A detailed description of ubiquitination process, different ubiquitin ligase families, and functions are excellently reviewed elsewhere [20,49–51]. In this section, we will provide an overview of the essential information on TRIP12 actions in ubiquitin-dependent proteolytic pathways.

4.1. Ubiquitination

Ubiquitination is an essential ATP-requiring process leading to protein modification by the covalent conjugation of ubiquitin, which is a highly conserved 76 aa polypeptide (≈8.5 kDa) [49]. Although best known for targeting proteins to degradation by the 26S proteasome, ubiquitination is potentially linked to all cellular processes. Canonical ubiquitin conjugation involves the attachment of the C-terminal glycine 76 (G76) of ubiquitin (Ub) to the ε-amino group of a lysine on the protein substrate. Substrates can be either modified by a single ubiquitin on one (monoubiquitination) or more sites (multi-mono-ubiquitination) or by chains of ubiquitin [51]. In the case of poly (or multi) Ub chains, the C-terminal G76 of one Ub molecule is linked to the ε-NH_2 group of one of the seven lysines (K6, K11, K27, K29, K33, K48, or K63) of the preceding ubiquitin. The poly-Ub chains can have different lengths and topologies resulting in different consequences on the fate of the modified protein substrate. For instance, K48-linked polyubiquitination primes proteins for proteolytic destruction by the proteasome, whereas non-K48 linkages target proteins for various cellular functions and responses [50,51].

Ubiquitination is ensured by a three step-concerted action of three enzymes. An Ub-activating enzyme (E1) catalyzes the formation of a thiol-ester linkage between the C-terminal lysine G76 of Ub and the active cysteine (C) residue of E1; the Ub molecule is transferred to the cysteine of the Ub-conjugating enzyme (E2). E3 ligases are classified into three major classes, the RING (Really Interesting New Gene), the RBR (RING-between RING-RING), and the HECT ligases. For HECT and RBR E3 ligases, the transfer of Ub to the substrate lysine-amino group involves a thioester intermediate with a conserved cysteine in the catalytic site of the HECT domain or the Rcat domain, respectively [20]. The RING E3 ligases catalyze the direct transfer of ubiquitin from a thioester-linked E2-ubiquitin conjugate to a substrate [20]. In some cases, the cooperation of an additional E4 ubiquitin ligase, which may encode for independent ligase activity or enhance the processivity of the E3, is required.

To act as catalysts, E3s recruit their substrates for degradation by recognizing a specific portion in the protein sequence or degron. Ubiquitin conjugation can be reversed by deubiquitinating enzymes (DUBs) [52].

4.2. Known TRIP12 Substrates

Based on the literature, TRIP12 regulates the stability and promotes the proteolysis of nine protein substrates: ASXL1 (Additional Sex Combs Like 1) [53], USP7 (Ubiquitin-Specific Peptidase 7) [39], PTF1a (Pancreas Transcription Factor 1a) [6], SOX6 (SRY-Box Transcription Factor 6) [12], RNF168 (Ring Finger Protein 168) [14], BAF57 (BRG1-Associated Factor 57) also known as SMARCE1 (SWI/SNF Related, Matrix Associated, Actin-Dependent Regulator Of Chromatin, Subfamily E, Member 1) [54], P14/ARF (P14/Alternate Reading Frame) also known as CDKN2A (Cyclin Dependent Kinase Inhibitor 2A), for which TRIP12 was named ULF (Ubiquitin Ligase for ARF) [15], APP-BP1 (Amyloid Protein-Binding Protein 1) also known as NAE1 (NEDD8-Activating Enzyme E1 Subunit 1) [4] and PARP1 (Poly-(ADP ribose) polymerase 1) [27]. These proteins exert important functions in biological and/or pathological processes that will be outlined in Section 5.

The TRIP12 HECT domain (detailed in Section 3.4) is essential for the degradation of these proteins, but the role of TRIP12 as direct interacting E3 ligase is still questionable for ASXL1 [53] and RNF168 [14] for which experimental approaches that prove ubiquitination by TRIP12 are lacking. TRIP12 polyubiquitinates its substrates with the exception of APP-BP1, which is monoubiquitinated [4]. APP-BP1 polyubiquitination requires an additional E4 activity [4]. TRIP12 mediated-K48-linked polyubiquitination was demonstrated only for USP7 [39] and PTF1a [6]. While the interaction between the E3 ligase and its substrates was validated, the interaction domains of TRIP12 have been mapped only in few cases. Although these studies used different isoforms of TRIP12, they all emphasize the role of consensus protein/protein interaction domains of TRIP12. A region (aa 611–1259 of isoform c) that includes the WWE domain but not ARM repeats is responsible for the interaction with APP-BP1 [4]. A sequence of 577 aa (aa 234–810 of isoform a) preceding the WWE domains interacts with USP7 [39]. In addition, TRIP12 interacts with parylated PARP1 via its WWE (aa 797–911 of isoform a) domain. TRIP12 is freshly considered as an identified PAR-targeted ubiquitin ligase (PTUbL) controlling PARP1 turnover [27]. Finally, we demonstrated that PTF1a binds a region containing ARM repeats and the WWE domain (aa 446–1552 of isoform c) [6].

Interacting domains or ubiquitinated residues were identified for certain proteins regulated by TRIP12. A sequence of 80 aa within and flanking the central coiled-coil region of BAF57 was found to be critical for BAF57 stabilization and to contain lysine residues essential for ubiquitination [55]. The N-terminal part of Tumor necrosis factor-receptor associated factor (TRAF), also known as the Meprin And TRAF-C Homology (MATH) domain of USP7, is responsible for its interaction with TRIP12 [39]. We found that the lysine 312 of PTF1a is essential for its TRIP12-mediated degradation [6]. It was previously reported that the tumor suppressor ARF is a natural lysine-less protein that undergoes N-terminal polyubiquitination [56].

Intriguingly, TRIP12 targets several proteins that are unbound to their physiological binding partners. This is the case for BAF57, which is a subunit of the SWI/SNF (SWItch/Sucrose Non-Fermentable) chromatin remodeling complex (detailed in Section 5.4.) [54]. Most if not all SWI/SNF subunits are assembled into a complex for which maintenance of the stoichiometry is essential and no free subunits exist in the cell; otherwise, they are degraded. The stabilization and protection of BAF57 from proteasome-mediated degradation operates via protein–protein interaction with the BAF155 subunit [57]. TRIP12 was demonstrated to compete with BAF155 for BAF57 and to degrade only an unbound form of BAF57 [55]. The same type of interaction was found for the ubiquitination of the neddylation E1 enzyme subunit APP-BP1 [4]. In fact, TRIP12 does not interact with APP-BP1 in the heterodimeric form bound to Uba3 (Ubiquitin-Like Modifier-Activating Enzyme 3), which is the specific active E1 of the NEDD8 pathway. A similar scheme is described for ARF, which is stabilized and protected from TRIP12 ubiquitination when sequestered by nucleophosmin and

TRADD (NFR1-Associated Death Domain Protein) in the nucleolus (detailed in Section 5.2.) [15,58]. Indirect evidence suggests a similar mode of action for the degradation of RNF168 [14]. Indeed, the destabilization of RNF168 induced by a silencing of its binding partner HERC2 (HECT and RLD Domain Containing E3 Ubiquitin Protein Ligase 2) could be mitigated by a depletion of TRIP12. The TRIP12-ubiquitinated lysine 312 of PTF1a is located near the domain interacting with RBP (mammalian suppressor of Hairless) essential for the transcriptional activity of PTF1a. One may hypothesize that free PTF1a could be ubiquitinated, while binding to RBP could prevent TRIP12-mediated PTF1a degradation. Therefore, TRIP12 appears as a regulator of the balance between bound and unbound forms of its protein substrates to maintain them in their complexed forms.

4.3. Role of TRIP12 in Ubiquitin Fusion Degradation and N-Degron Pathways

TRIP12 is sequelogous to the UFD4 HECT E3 ligase, which catalyzes the ubiquitination of Ubiquitin Fusion Degradation (UFD) substrates in yeast [59]. These substrates are artificial fusion proteins consisting of an N-terminal uncleavable ubiquitin moiety that acts as a degron. The UFD pathway consists in the poly-ubiquitination of the uncleavable N-terminal ubiquitin. TRIP12 was shown to mediate the degradation of the aberrant form of ubiquitin named UBB^{+1} [60]. UBB^{+1} is a physiological human UFD substrate resulting from a dinucleotide deletion in the mRNA of the ubiquitin B gene. UBB^{+1} accumulates in the brain in neurodegenerative disorders [61]. The HECT E3 HUWE1 (HECT, UBA, and WWE domain containing E3 ubiquitin protein ligase 1) was reported to cooperate with TRIP12 for the degradation of UBB^{+1} [62]. Although the conservation of the UFD pathway from yeast to human attests its importance for proteolysis in cells, except for UBB^{+1}, no other native substrates have been identified. Most studies use artificial substrates for specific applications. In particular, enhanced immune response after UFD ubiquitination of antigens opens up interesting perspectives in the development of tumor vaccines [63].

The N-degron pathway (formerly N-end rule pathway) is another ubiquitin-dependent proteolytic pathway that regulates the half-life of proteins according to N-terminal degradation signals or N-degrons. UBR1, UBR2, UBR4, and UBR5 (ubiquitin protein ligase E3 component N-recognin) are the four E3s (or N-recognins) encoded by the mammalian genomes that can recognize Arg/N-degrons [64]. Interestingly, a study demonstrated that UBR1 and UFD4 E3s interact and cooperate to enhance substrate ubiquitination in both pathways in yeast [65]. This mutually cooperative physical interaction between E3s operating in parallel pathways are likely to be relevant to all eukaryotes and might apply to TRIP12 and UBR5 control of RNF168 accumulation [14].

5. The Physio-Pathological Roles of TRIP12

Proteomic approaches have allowed for the identification of several TRIP12 binding partners (Figure 5 and Table 2). However, the molecular function of only a restricted number of these interactions is known. Thus far, TRIP12 was implicated in the regulation of several important molecular pathways such as cell cycle progression, DNA damage repair (DDR), chromatin remodeling, and cell differentiation via a small number of identified protein interactors, which leaves wide open the field of investigation of molecular processes implicating TRIP12.

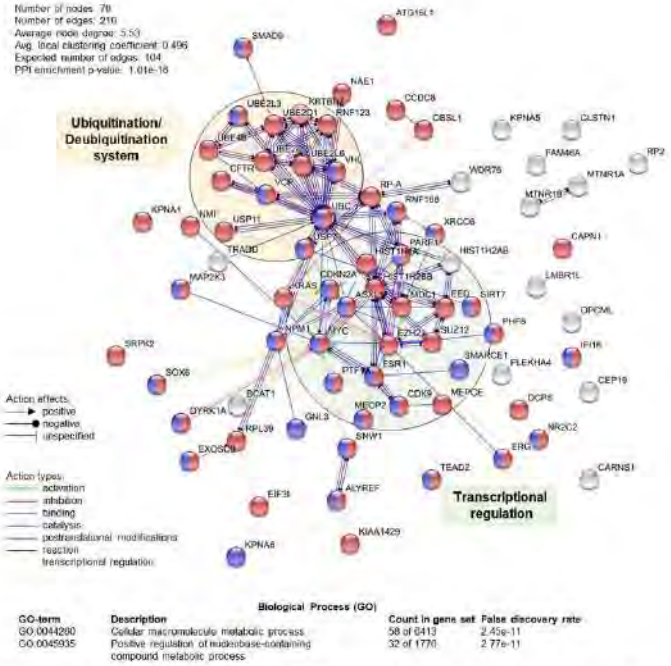

Figure 5. Schematic representation of human TRIP12-interacting protein–protein network ($n = 76$) and functional enrichment analysis using STRING software (see Section Software and databases). Network nodes represent proteins. Red nodes represent proteins belonging to cellular macromolecule metabolic process (GO term: 0044260), and purple nodes represent proteins belonging to the positive regulation of the nucleobase-containing compound metabolic process (GO-term: 0045935). Edges represent protein–protein molecular actions (indicated in the figure). Line shape indicates the predicted mode of action (indicated in the figure). Active interaction sources: text mining, experiments, databases, co-expression, neighborhood and co-occurrence. Minimum required interaction score: medium confidence (0.400). Green and orange filled circles indicate proteins implicated in "transcriptional regulation" and "ubiquitination/deubiquitination system", respectively.

Table 2. List of the different protein interactors of human TKJP12.

#	Interactor Gene	Interactor Name	Bait and/or Hit	Interaction Detection Method	Interaction Type	References
1	ALYREF	Aly/REF export factor	bait	aff tech	co-localization	[66]
2	**ASXL1**	**Additional Sex Combs-Like Protein 1**	bait	biochemical	ph ass	[59]
3	ATG16L1	Autophagy-related protein 16-like1	bait	aff tech	ph ass	[67]
4	BCAT1	Branched-chain-amino-acid aminotransferase	bait	ph ass	ph ass	[68,69]
5	CAPN1	Calpain-1 catalytic subunit	bait	aff tech	ph ass	[69]
6	CARNS1	Carnosine synthase 1	bait	two hybrid	dir int	[70]
7	CCDC8	Coiled-coil domain-containing protein 8	bait	aff tech	ph ass	[71]
8	CDK9	Cyclin-dependent kinase 9	bait, hit	aff tech	ph ass	[72]
9	**CDKN2A**	**Cyclin-Dependent Kinase Inhibitor 2A/p14ARF**	bait	aff tech, pd, ph ass	ph ass, dir int, ph int	[13,68,73–75]
10	CEP19	Centrosomal protein of 19 kDa	bait	biol	ph ass	[76]
11	CFTR	Cystic fibrosis transmembrane conductance regulator	bait	aff tech	ph ass	[77]
12	CLSTN1	Calsyntenin-1	bait	two hybrid	dir int	[70]
13	DCPS	Decapping scavenger enzyme	bait	aff tech	ph ass	[78]
14	DYRK1A	Dual specificity Tyrosine-phosphorylation-regulated kinase 1A	bait	aff tech	ph ass	[79]
15	EED	Embryonic ectoderm development protein	bait	aff tech	ph ass	[80]
16	EIF3I	Eukaryotic translation initiation factor 3 subunit I	bait	aff tech	ph ass	[65,69]
17	ERG	Transcriptional regulator ERG	bait	pd	dir int	[81]
18	ESR1	Estrogen receptor alpha	bait	aff tech	ph ass	[82]
19	EXOSC9	Exosome complex component RRP45	bait	aff tech	ph ass	[83]
20	EZH2	Histone-lysine N-methyltransferase	bait	aff tech	ph ass	[84]
21	FAM46A	HBV X-transactivated gene 11 protein	bait	aff tech	ph ass	[83]
22	GNL3	Guanine nucleotide-binding protein-like 3/Nucleostemin	hit	aff tech	ph ass, dir int, ph int	[79]
23	HIST1H2AB	Histone H2A	bait	aff tech	ph ass	[85]
24	HIST3H2BB	Histone H2B	bait	aff tech, biol	ph ass	[85,86]
25	HIST1H4A	Histone H4	bait	aff tech	ph ass	[85,87]
26	IFI16	Gamma-interferon-inducible protein 16	bait	aff tech	ph ass	[88]
27	KBTBD7	Kelch repeat and BTB domain-containing protein 7	bait	aff tech	ph ass	[67]
28	KIAA1429	Protein virilizer homolog	bait	aff tech	ph ass	[89]
29	KPNA1	Importin subunit alpha-5 (Karyopherin subunit alpha-1)	hit	aff tech	ph ass	[90]
30	KPNA5	Importin subunit alpha-6 (Karyopherin subunit alpha-5)	hit	aff tech	ph ass	[90]
31	KPNA6	Importin subunit alpha-7 (Karyopherin subunit alpha-6)	hit	aff tech	ph ass	[90]
32	KRAS	GTPase KRas	bait	aff tech	ph ass	[91]
33	LAMB1L	Limb development membrane protein 1-like	bait	aff tech	ph ass	[92]
34	MAP2K3	Dual specificity mitogen-activated protein kinase kinase 3	bait	aff tech	ph ass	[93]
35	MDC1	Mediator of DNA damage checkpoint protein 1	bait	aff tech	ph ass	[94]
36	MECP2	Methyl-CpG-binding protein 2	bait	aff tech	ph ass	[95]

Table 2. *Cont.*

#	Interactor Gene	Interactor Name	Bait and/or Hit	Interaction Detection Method	Interaction Type	References
37	MEPCE	7SK snRNA methylphosphate capping enzyme	bait	aff tech	ph ass	[72]
38	MTNR1A	Melatonin receptor type 1A	bait	two hybrid	dir int	[69]
39	MTNR1B	Melatonin receptor type 1B	bait	two hybrid	dir int	[69]
40	MYC	Myc proto-oncogene protein	bait, hit	aff tech, pd	ph ass, dir int	[15,95]
41	**NAE1**	**NEDD8-activating enzyme E1 regulatory subunit/APP-BP1**	hit	aff tech, enz study	ph ass, dir int	[4]
42	NMI	N-myc-interactor	bait, hit	aff tech, pd	ph ass, dir int	[74]
43	NPM	Nucleophosmin	bait, hit	aff tech, pd	ph ass, dir int	[96]
44	NR2C2	Nuclear receptor subfamily 2 group C member 2	bait	aff tech	ph ass	[97]
45	OBSL1	Obscurin-like protein 1	bait	aff tech	ph ass	[73]
46	OPCML	Opioid-binding protein/cell adhesion molecule	bait	aff tech	ph ass	[69]
47	**PARP1**	**Poly-(ADP Ribose) polymerase 1**	bait, hit	aff tech, pd, enz study	ph ass, dir int	[27]
48	PHF8	Histone lysine demethylase	bait	aff tech	ph ass	[80]
49	PLEKHA4	Pleckstrin homology domain containing, family member 4	bait	aff tech	ph ass	[96]
50	**PTF1A**	**Pancreas transcription factor 1 subunit alpha**	bait, hit	aff tech, FRET, two hybrid	ph ass, dir int, dir int	[6]
51	RNF123	E3 ring finger ubiquitin ligase 123	bait	aff tech	ph ass	[98]
52	**RNF168**	**E3 ring finger ubiquitin ligase168**	bait	aff tech	ph ass	[74]
53	RP2	Protein XRP2	bait	aff tech	ph ass	[66,69]
54	RPA	Replication protein A	bait	aff tech	ph ass	[100]
55	RPL39	60S ribosomal protein L39	hit	aff tech	ph ass	[96]
56	SIRT7	Sirtuin 7	bait	aff tech	ph ass	[101]
57	SMAD9	SMAD family member 9	bait	two hybrid	dir int	[102]
58	**SMARCE1**	**SWI/SNF-related matrix-associated actin-dependent regulator of chromatin subfamily E member 1/BAF57**	bait	aff tech	ph ass	[56]
59	SNW1	SNW domain-containing protein 1	bait	aff tech	ph ass	[103]
60	**SOX6**	**Transcription factor SOX-6**	bait, hit	enz study, aff tech, two hybrid	dir int, ph ass	[32]
61	SRPK2	SRSF protein kinase 2	bait	enz study	dir int	[104]
62	SUZ12	Polycomb protein SUZ12	bait	aff tech	ph ass	[96]
63	TEAD2	Transcriptional enhancer factor TEF-4	bait	aff tech	ph ass	[105]
64	TRADD	Tumor necrosis factor receptor type 1-associated DEATH domain	bait, hit	aff tech	ph ass	[58]
65	UBC	Ubiquitin-C	bait, hit	enz study, aff tech	dir int, ph ass	[86,106,107]
66	UBE2D1	Ubiquitin-conjugating enzyme E2 D1	hit	pd	dir int	[4,23,63,108]
67	UBE2D2	Ubiquitin-conjugating enzyme E2 D2	bait	pd	dir int	[108]
68	UBE2L3	Ubiquitin-conjugating enzyme E2 L3	bait, hit	pd	dir int	[108,109]
69	UBE2L6	Ubiquitin-conjugating enzyme E2 L6	bait	aff tech	ph ass	[86]
70	UBE4B	Ubiquitin conjugation factor E4 B	bait	pd	dir int	[2]

Table 2. *Cont.*

#	Interactor Gene	Interactor Name	Bait and/or Hit	Interaction Detection Method	Interaction Type	References
71	USP7	**Ubiquitin-specific-peptidase 7**	bait, hit	aff tech, ph ass	ph ass	[58,68,110,111]
72	USP11	Ubiquitin-specific peptidase 11	bait	aff tech	ph ass	[110]
73	VCP	Valosin-containing protein	bait	aff tech	ph ass	[112]
74	VHL	von Hippel-Lindau E3 ubiquitin ligase	bait	aff tech	ph ass	[85]
75	WDR76	WD repeat-containing protein 76	bait	aff tech	ph ass	[86]
76	XRCC6	X-ray repair cross-complementing protein	bait	biotd	ph ass	[113]

Human TRIP12 protein interactors based on Biogrid database (see Section Software and databases) and the literature. Interactors in bold ($n = 9$) were further characterized as TRIP12 ubiquitinated substrates. Proteins used to capture protein complexes in which TRIP12 was identified were designated as "bait". Hits are proteins detected only in the immunoprecipitation (IP) of the TRIP12 protein but not in a vector control IP. Aff tech: affinity techniques, biotd: biotin identification, dir int: direct interaction, enz study: enzymatic study, FRET: fluorescence resonance energy transfer, pd: pull down, ph ass: physical association and ph int: physical interact.

5.1. TRIP12 Protein Interactors

According to BioGrid resources (see Section Software and databases) and the literature, 76 unique proteins interact with human TRIP12 (Table 2). They were identified by different experimental approaches using either these proteins (n = 58), either TRIP12 (n = 7) or both as bait (n = 11). Among them, eight were further classified as TRIP12-ubiquitinated substrates (detailed in Section 4.2). A STRING protein–protein network and functional enrichment analyses (see Section Software and databases) reveals that 76% (58 out of 76) are implicated in cellular macromolecule metabolic process (red circles), which corresponds to proteins involved in the adding of low molecular mass protein units (i.e., ubiquitin) (Figure 5). In parallel, 42% (32 out of 76) are involved in the positive regulation of nucleobase-containing compound metabolism (purple circles), which corresponds to cellular processes that activate chemical reactions/pathways involving nucleic acid-related compounds. Moreover, we can clearly distinguish two protein-protein functional clusters including proteins involved in transcriptional regulation (i.e., PTF1a, EZH2, SUZ12, etc.) and in the ubiquitination/deubiquitination system (i.e., USP7, VHL, USP11, etc.). However, it is important to keep in mind that all the interactions of the TRIP12 with protein partners might depend on the type of cells, the stage of differentiation, or the cell cycle phase. Altogether, these analyses position TRIP12, via its interacting partners, as a potential central regulator of protein stability and genome expression.

5.2. Roles in Cell Cycle Progression

The P53 dependent-activating P14/ARF (P14/Alternative Reading Frame also known as CDKN2A (Cyclin-Dependent Kinase Inhibitor 2A)) pathway plays a major activating role in cell cycle progression. Chen et al. identified TRIP12 as the E3 ubiquitin ligase responsible for the degradation of ARF and renamed it ULF for Ubiquitin ligase for ARF [96]. TRIP12 decreases the stability of ARF after polyubiquitination and degradation by the proteasome. This leads to a proteasome-mediated destabilization of P53 by the E3 ubiquitin ligase MDM2 (Mouse Double Minute 2 homolog) and a cell cycle progression (Figure 6, left panel). The authors further showed the relationship between TRIP12 and two positive regulators of ARF: the nucleophosmin (NPM), a major component of nucleoli, and the transcription factor c-MYC. They reported that NPM sequestrates ARF in the nucleoli, isolating it from the ubiquitinating action of TRIP12 present only in the nucleoplasm (Figure 6, left panel). Then, they demonstrated that c-MYC enhances the ARF half-life by destabilizing the TRIP12/ARF nucleoplasmic complex (Figure 6, right panel). Therefore, the interaction of ARF with MDM2 prevents the ubiquitination-mediated degradation of P53, which in turn, induces a cell cycle arrest and apoptosis [114]. Later, the nucleostemin (also known as Guanine nucleotide-binding protein-like 3) was demonstrated to stabilize the NPM/ARF complex in the nucleoli and to destabilize the TRIP12/ARF complex in the nucleoplasm to inhibit ARF degradation by TRIP12 ubiquitination [75]. The translocation of TRADD (TNF-R Associated Death Domain Protein) from the cytoplasm to the nucleus was also shown to protect ARF from degradation by inhibiting its interaction with TRIP12 [58]. The participation of TRIP12 in cell cycle progression was assessed in non-cancerous cells subject to an oncogenic stress provoked by an overexpression of c-MYC [115]. Paradoxical properties of c-MYC overexpression have been reported in oncogenic processes [116]. Indeed, a mild expression of c-MYC stimulates cell proliferation, whereas a strong overexpression inhibits cell proliferation by activating the ARF/P53 response. In both cases, ARF mRNA levels were induced. However, the authors demonstrate that only a high concentration of c-MYC is able to inhibit the degradation of ARF mediated by TRIP12, which in turn leads to the activation of the ARF/P53 pathway and cell cycle arrest. Moreover, Kajiro et al. generated TRIP12 knock-in mutant mice by homozygous mutation in *TRIP12* exon 33 ($TRIP12^{mt/mt}$) disrupting the ubiquitin ligase activity [5]. This resulted in embryonic lethality at the embryonic stage E11.5. $TRIP12^{mt/mt}$ ES cells exhibited a significant decrease of growth rate caused by the abnormal induction of the cyclin-dependent kinase inhibitor P16 and ARF associated to a P53 protein increased stability. $TRIP12^{mt/mt}$ ES cells also display an abnormal accumulation in G_2/M and sub-G_1 phases. These data support that TRIP12 functions in the cell cycle control in vivo.

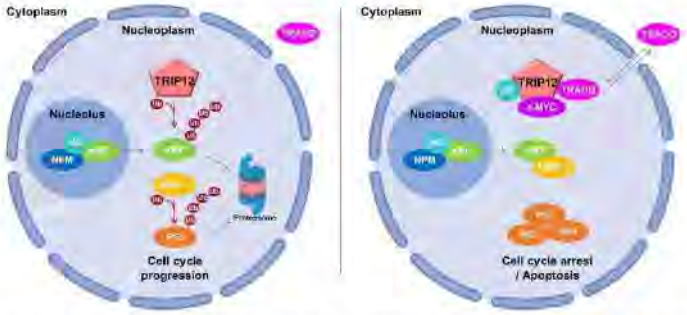

Figure 6. Schematic representation of TRIP12, ARF, and P53 pathway. On the left, TRIP12 controls ARF and indirectly P53 ubiquitination degradation by proteasome, while TRIP12 participates in cell cycle progression [58,75,96,115]. On the right, ARF is protected from TRIP12 when bound to nucleophosmin (NPM)/nucleostemin (NS) and localized in the nucleolus. Moreover, in the nucleoplasm, TRIP12 is sequestered by different proteins (in the presence of NS or TRADD and in high level c-MYC condition), blocking its interaction with ARF. ARF binds and inhibits MDM2, which leads to P53 accumulation and cell cycle arrest.

TRIP12 is tightly implicated in the control of cell cycle progression. Until very recently, little was known on cell cycle regulation of TRIP12 expression. We showed that the presence of TRIP12 in the nucleus strongly depends on the phase of the cell cycle. The TRIP12 protein appears in the nucleus in the late S phase and endures during the G_2 phase [7]. We found that while tightly bound to the chromosomes during mitosis, TRIP12 is rapidly degraded in the early G_1 phase and disappears in the nucleus in the late G_1 and early S phase. We further demonstrated that TRIP12 plays a role in phase S by controlling DNA replication timing. Via its chromatin-interacting IDR, TRIP12 coordinates mitotic entry and progression [7]. The important function of TRIP12 during mitosis was reinforced by mass spectrometry-based approaches showing that TRIP12 is specifically retained to mitotic chromatin [117]. With regard to variations to TRIP12 expression during the cell cycle, it would be important to reconsider TRIP12 molecular functions according to its presence or absence from the nucleus.

5.3. Roles in DNA Damage Response

5.3.1. Via the ARF/P53 Signaling Pathway

Oncogenic stimuli trigger the activation of checkpoints that delay or prevent tumorigenesis. The DNA damage repair (DDR) pathway and ARF protein are two major checkpoints that both act by the protein P53. Initially studied independently, the interconnection between these two checkpoints in tumorigenesis is gaining notoriety. For example, Velimezi et al. discovered that the key DDR kinase ATM negatively regulates the abundance of ARF with the implication of TRIP12 [118]. In response to DNA damage, the kinase ATM activates the protein phosphatase 1 (PP1), which in turn, dephosphorylates the nucleolar protein NPM (Figure 7). This dephosphorylation liberates ARF from NPM, rendering it susceptible to degradation via the action of TRIP12 in the nucleoplasm. Chen et al. further reported the contribution of TRIP12 in ARF degradation in response to DNA damage induced by doxorubicin [115]. The data showed that after DNA damage, the degradation of ARF is strongly attenuated in TRIP12 knockout mouse embryonic fibroblasts (MEFs). Another study identified the serine S1577 of TRIP12 (Figure 1) as phosphorylated by the kinases ATM/ATR, which suggests that post-translation modifications are possibly critical for a proper implication of TRIP12 in the DDR network [45].

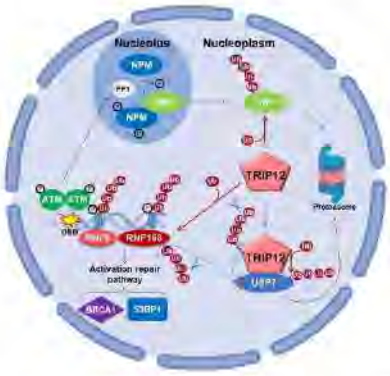

Figure 7. Schematic representation of TRIP12 in the DNA damage repair (DDR) pathway in response to DNA double-strand break (DSB) [14,39,115,118–121]. In response to double-strand breaks (DSB), ATM, RNF8, and RNF168 are recruited on the damage and trigger the propagation of the ubiquitination of H2A and H2AX far from the initial DNA lesions. TRIP12 controls the nuclear pool of RNF168 for the ubiquitination of chromatin after DNA disruption. Indeed, TRIP12 ubiquitinates and induces the degradation of RNF168 by the proteasome. TRIP12 controls Ubiquitin-Specific Peptidase 7 (USP7) ubiquitination, which in turn stabilizes it.

5.3.2. Via the Control of Histone Ubiquitination Spreading by RNF168

Histone ubiquitination plays a crucial role in the recruitment of proteins responsible for the detection and the repair of DNA damage. The E3 ubiquitin ligase RNF8 (Ring Finger Protein 8) initiates the ubiquitination of histones H2A and H2AX at the damaged sites (Figure 7) [119]. This priming of ubiquitination reaction is amplified by another E3 ubiquitin ligase, RNF168. The produced polyubiquitination (K63 chain) chain acts as a platform for the interaction of repair signaling factors, such as 53BP1 and the complex RAP80/BRCA1 (Receptor-Associated Protein 80/Breast Cancer 1) [122]. If not properly controlled, RNF168 over-amplifies the ubiquitination signal beyond the DNA breakage on neighboring chromatin, which can have dreadful consequences, notably by sequestrating the genome keepers 53BP1 (P53 Binding Protein 1) and BRCA1. The retention of 53BP1 and BRCA1 at a non-damaged DNA site prevents their recruitment at damaged DNA sites and subsequent repair. It was shown that TRIP12 and UBR5 are two proteins that prevent this over-amplification after the DNA damage induction of double-strand break (DSB) [14]. In physiological conditions, TRIP12 and UBR5 control the quantity of RNF168 required to restrain histone ubiquitination around DNA lesions (Figure 7). A depletion of TRIP12 and UBR5 provokes an accumulation of RNF168 to supra-physiological levels that amplifies histone ubiquitination beyond the DSB sites. Moreover, TRIP12 was demonstrated as the E3 ubiquitin ligase implicated in the stability of RNF168.

5.3.3. Via the Deubiquitinase USP7

It is accepted that the deubiquitinase USP7 plays a major role in the response of DNA damage by stabilizing the expression of key proteins such as P53 and RNF168 [120,121]. TRIP12 interacts with USP7 and polyubiquitinates (K48 chain) it to induce its degradation by the proteasome (Figure 7) [39]. Consequently, the TRIP12-mediated degradation of USP7 affects the stability of 53BP1 and CHK1 proteins, which are two important regulators of DDR regulated by USP7. Importantly, as mentioned in Section 3.6, the TRIP12 protein is also stabilized by USP7, suggesting a relevant interconnected feedback between these proteins. Taken together, these studies show that TRIP12 and USP7 mutually control their expression level. In addition, they both regulate the expression level of RNF168, which is

a key factor in DSB repair. This indicates that a fine-tuning of these three enzymes is certainly required to ensure a proper managing of DNA damage repair via RNF168 quantity control.

5.4. The Roles of TRIP12 in Chromatin Remodeling

5.4.1. Via the Control of SWI/SNF Complex Integrity

The level of chromatin compaction participates in highly dynamic processes such as transcription, DNA repair, and recombination. When the chromatin is compacted, genes are globally transcriptionally inactive due, in part, to a low accessibility of the transcriptional machinery to promoters [123]. The modification of chromatin compaction and consequently the modulation of transcriptional activity is partially controlled by the SWI/SNF complex [124]. It is a multi-protein complex constituted by a dozen sub-units. The sub-units BRG1 (hSWI/SNF Brahma-related Gene) and BRM-1 (BRachyury Modifier 1) ensure the ATPase catalytic activity. The function of the SWI/SNF complex is to remodel nucleosome positioning by sliding, inserting, or ejecting histone octamers into DNA in an ATPase-dependent manner. As such, it controls numerous cellular processes [125]. To reach an optimal efficiency, the SWI/SNF complex requires the presence of BAF proteins (BRG-1 associated factors), which interact with BRG-1. Therefore, the regulation of expression of BAF proteins by proteasome-dependent degradation is crucial. It was demonstrated that TRIP12 is the main E3 ubiquitin ligase that polyubiquitinates the free cellular pool of BAF57 (also known as SMARCE1 (SWI/SNF-related matrix-associated actin-dependent regulator of chromatin subfamily E member)) by a mechanism that we described in Section 4.2. [54]. Therefore, TRIP12 appears to be involved in a protein quality control system of the SWI/SNF complex. The TRIP12 mediated-degradation of BAF57 could affect the loading of SWI/SNF on its target genes and consequently disturb gene expression.

5.4.2. Via the Maintenance of Silenced Genes by the Polycomb Complex

Epigenetic modifications of DNA bases play a crucial role in the control of gene transcription. Most of these modifications were first identified in prokaryotes and then in higher eukaryotes. The methylation of the nitrogen atom in position 6 of an adenine (6mA) is the most frequent modification in prokaryotes. This modification was recently described in eukaryotes and particularly in vertebrates [126]. In mammals, the methyltransferase METTL44 (Methyltransferase Like 4) and the dioxygenase ALKBH4 (ALKB Homolog 4, Lysine Demethylase) are responsible for the deposit and the suppression of the 6mA on DNA, respectively [53]. In mammals, the 6mA is associated with epigenetic repressive marks such as the mono-ubiquitination on the K119 of histone H2A (K119 Ub-H2A) and the trimethylation on K27 of histone H3 (K27me3-H3). These repressive marks are used for silencing promoters during the stem cells differentiation and embryonic development. They are mainly added on the chromatin by the Polycomb Repressive Complexes (PRC1 and PRC2) [127,128]. These two marks are reversible. The K119 Ub-H2A is removed by the deubiquitinase complex PR-DUB (Polycomb Repressive-Deubiquitinase complex) formed by the proteins ASXL1 (Additional Sex Combs like 1) and BAP1 (BRAC1 Associated Protein 1) [129]. The BAP1 protein bears the deubiquitinase activity, and it is stabilized by ASXL1 [130]. Mass spectrometry based-proteomic analyzes identified the protein-protein interaction between TRIP12 and major components of PRCs such as SUZ12 (Polycomb protein SUZ12), EZH2 (Histone-lysine N-methyltransferase) [84] and EED (Embryonic Ectoderm Development protein) [80] but with no mechanistic findings. A recent study characterized the role of 6mA deposit and the implication of the E3 ubiquitin ligase TRIP12 in the maintenance of the repressive marks added by the Polycomb complex [53]. The addition of 6mA on PRC1/PRC2-inactivated genes leads to the recruitment of the PR-DUB complex. This recruitment on the chromatin leads to the degradation of the complex by TRIP12-mediated polyubiquitination of ASXL1 (discussed in Section 4.2.) and preserves the level of K119 Ub-H2A. A homozygous deletion of the *METTL4* gene in a murine model induces a decrease of 6mA deposit and provokes a craniofacial dysmorphism in a subset of pups. Interestingly, de novo nonsense mutations of the *ASXL1* gene were identified in patients

severe mental retardation, facial dysmorphism, and multiple renal cysts [141]. The identification of *TRIP12* among 10 new ID genes was later accomplished by meta-analysis of large-scale exome sequencing data of a combined cohort including 2104 patient-parent trios [142] where two different de novo heterozygous mutations in the *TRIP12* gene were identified in two unrelated patients.

Of importance, several de novo mutations (DNM) of the *TRIP12* gene were associated with a broader phenotype than ID in line with the overlap of genes and pathways involved in NDDs. Mutual comorbidities of ID and Autism Spectrum Disorder (ASD) also raised the question of whether *TRIP12* can be validated as a gene associated with ASD. Resequencing sixty-four ASD risk genes in two ASD cohorts newly identified mutations in the *TRIP12* gene, thus proposing that it could be a novel candidate gene for clinical follow-up [143,144]. Recent detailed clinical information characterizing the phenotype of 11 individuals with mild to moderate ID or learning disability finally demonstrated that *TRIP12* is a risk gene for ID with (8/11) or without ASD [10]. However, there is no correlation for the presence or absence of autistic features with the type of mutations in this study. Other typical clinical features of the *TRIP12*-associated spectrum such as unspecific craniofacial dysmorphism, speech delay, and seizures were reported in another cohort of nine pathogenic variants that further documented that *TRIP12* haploinsufficiency causes childhood-onset neurodevelopmental disorders [145]. Recent exome sequencing of Japanese trios and integrative analysis conducted by combining published DNM data identify *TRIP12* among 61 significant genes for ASD and suggest that it is a genuine disease-causative gene [146]. The *Trip12* gene is a high confidence gene for autism in the SFARI GENE database (see Section Software and databases).

Pathogenic *TRIP12* variants are now documented in gene variant databases related to human health LOVD (Leiden Open Variation Database (see Section Software and databases)) and ClinVar (Clinical Variation (see Section Software and databases)) and can be also found in ID/autism websites. According to the LOVD, most pathogenic variants (87%) have DNA changes in coding regions, 8% in spliced regions, 5% in multiple regions. These changes are substitutions (53%), deletions (29%), duplications (13%), and 5% of these variants have still unknown modifications. Consequences at the protein level include stop changes (32% of variants) and frame shifts (26%) generating premature termination, missense changes (18%), no protein production (8%), or unknown (16%). Selected variants are placed on the TRIP12 protein sequence according to the transcript variant 3, NM_004238.3 (Figure 8).

Figure 8. Schematic illustration of published *TRIP12* gene mutations in intellectual disorders. Mutations in blue are missense, mutations in orange are nonsense, mutations in black are frameshift. Mutations in green are located in splice donor sites. From [10,142–145].

Analysis was performed to identify protein/protein interaction networks and signaling pathways associated with a set of autism and ID genes. These frequently implicate neuronal signaling and development, chromatin remodeling, transcriptional regulation, mRNA splicing, ion transport, cell cycle, and microtubule cytoskeleton. They converge on neuronal and cognitive functions such as the regulation of synaptic transmission, learning, and memory [146–148]. To date, only one pilot study in *Drosophila melanogaster* investigated the role of TRIP12 using inducible RNA interference. This study reported no significant change in behavioral assay after *TRIP12* knock-down, suggesting no role in the development of the nervous system [148]. Given the important function for protein degradation in the nervous system, the synaptic plasticity, and the maintenance of neuronal structures, one might speculate that TRIP12 regulates the synaptic proteome. However, physiological roles of TRIP12 suggest

with Bohring–Opitz syndrome who display facial dysmorphism [131]. In humans, mutations of the *TRIP12* gene are also associated to craniofacial dysmorphism (detailed in Section 6.1). Therefore, we can speculate that an inactivation of TRIP12 could provoke an accumulation of ASXL1 and a stabilization of the PR-DUB complex that would subsequently alter the expression of genes implicated in facial development.

5.5. Roles in Cell Differentiation

Different studies have proven the strong involvement of TRIP12 in the cell differentiation. Differentiation is the process by which dividing cells change their functional or phenotypical type. It involves the coordinated regulation of genes by a multitude of cellular pathways. The first study showing the participation of TRIP12 in stem cells and regeneration mechanisms was performed in the freshwater planarian *Schmidtea mediterranea* [132]. *Schmidtea mediterranea* is a model for regeneration, stem cells, and the development of tissues. This worm is able to replace cell loss during normal cellular turnover or tissue loss through the regenerative capacity of adult stem cells called neoblasts. The authors demonstrated that 11 genes of HECT E3 ubiquitin ligases were expressed in neoblasts. Using RNA interference (RNAi), the authors showed that the TRIP12 orthologue also known as "smed-TRIP12" is essential for the establishment and the maintenance of posterior tissues.

TRIP12 displays another important function in the control in muscle fiber homeostasis. An et al. showed that the transcription factor SOX6 (SRY-Box Transcription Factor 6) is a target of TRIP12 in mammals. SOX6 is involved in muscle fiber homeostasis by the transcriptional repression of "slow switch muscle fiber" genes in fetal mice [133]. They showed that a TRIP12 knockdown in myotubes-derived cell lines leads to an increase of SOX6 protein levels and results in a dysregulation of muscle fiber homeostasis. TRIP12 binds to SOX6 protein, inducing its polyubiquitination and its degradation by the proteasome [12].

TRIP12 is also implicated in the homeostasis of pancreatic epithelial cells. We demonstrated that TRIP12 polyubiquitinates and provokes the degradation of the transcription factor PTF1a (Pancreas Transcription Factor 1a) by the proteasome [6]. PTF1a is a transcription factor that controls the expression of pancreatic acinar specific genes such as amylase and chymotrypsin genes. This factor is essential in pancreatic development and pancreatic cell homeostasis by maintaining the acinar phenotype. The expression of PTF1a is lost during acinar to ductal cells transdifferentiation [133,134]. PTF1a is also required for the specification of inhibitory neurons in various regions of the developing central nervous system including the spinal cord, brainstem, cerebellum, and retina [135–137]. Thus, it is possible that TRIP12 regulates neuronal specification via PTF1a degradation.

6. TRIP12 in Pathologies

6.1. Alterations of TRIP12 Gene in Autism and Intellectual Disability

TRIP12 (OMIM 604506 (Online Mendelian Inheritance in Man) (see Section Software and databases)) is a neurodevelopmental disorder (NDD)-associated gene. Several publications allowed its identification as a primary gene for Intellectual Disability (ID), which is the most common developmental disorder affecting 1–3% of the world's population. Most IDs are monogenic with 1,396 genes causing ID [138]. The *TRIP12* gene is referenced as a causative gene associated with Clark–Baraitser syndrome (CLABARS; OMIM617752), formerly autosomal-dominant mental retardation-49 (MRD49) in the OMIM database. Although originally thought to be an X-linked disorder [139], Clark-Baraitser syndrome was shown to have an autosomal dominant mode of inheritance [140]. In addition to mental retardation, craniofacial dysmorphism, behavioral psychiatric manifestations, and obesity are the main clinical features of the syndrome. CLABARS is caused by heterozygous mutation in the *TRIP12* gene.

The first indication of a putative role of the *TRIP12* gene in ID was the report of a large interstitial ≈5.6-Mb deletion on the long arm of chromosome 2 (2q36.2q36.3) in a 17-year-old girl. Twenty-four genes were located in the deleted fragment where *TRIP12* was disrupted. The phenotype included

its potential contribution to other essential pathways that are deregulated in ID pathologies. Therefore, additional functional analysis using relevant models is necessary to conclude a causal association between *TRIP12* gene variants and these diseases.

6.2. *Alterations of TRIP12 Gene, mRNA and Protein Expression, and Function in Cancers*

6.2.1. Alteration of *TRIP12* Gene in Cancers

The cBioPortal database (see Section Software and databases) provides the frequency of CNA (Copy Number Alteration) appearance in *TRIP12* gene in cancers [149,150]. It includes mutations, fusions, amplifications, deep deletions, and multiple alterations (Figure 9). On average, the *TRIP12* gene is altered in 1.84% of cancer patients (over 27,235 patients). This rate remains relatively weak compared to other genes, for instance, *TP53* (39.8%). *TRIP12* gene alteration frequency varies from 11.7% in endometrial carcinoma to 1.06% in glioblastoma patients. Up to now, 463 mutations have been located in the human *TRIP12* gene (Figure 10). These punctual alterations do not accumulate in hot spots but rather spread all along the protein sequence. Among them, 323 were classified as missense, 120 were classified as truncating mutation, and one arises from nucleotides insertion without an open reading frameshift. Additionally, 20 alterations result from a fusion between the *TRIP12* gene and other genes such as PID1 (PTB-containing, cubilin and LRP1-interacting protein) or KIF1A (Kinesin-like protein). However, a nonsense mutation is retrieved 10 times at the residue S1195 generating a truncated protein: six times in colon cancer, two times in uterine cancer, and once in lung and breast cancer. The main issue regarding *TRIP12* gene alterations and in particular point mutations is whether these mutations play a causal role in cancer initiation or progression ("driver" mutations) or if they only randomly appear during cancer establishment as a consequence of, for instance, DNA repair failure ("passenger" mutations).

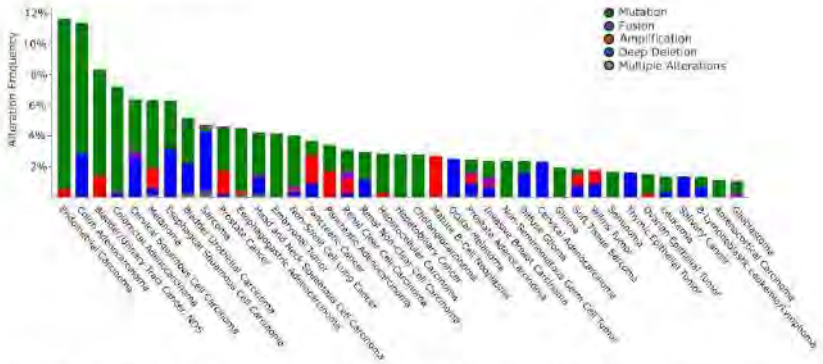

Figure 9. Copy number alterations (CNA) and mutations of the *TRIP12* gene in human cancers in cBioPortal (see Section Software and databases) obtained from 176 non-redundant studies containing more than 100 cases with both mutations and CNA data (27,235 patients and 28,253 samples). Only cancer types with more than 1% of altered cases are represented.

Only six publications have reported alterations in the *TRIP12* gene in cancers. Frameshift mutations of genes containing mononucleotide repeats are features of gastric and colorectal carcinomas with microsatellite instability (MSI). The *TRIP12* gene contains repetitions of seven adenines in exon 3 and seven thymidines in exon 24. In a cohort of 27 gastric and 32 colorectal cancer samples, Yoo et al. identified an adenine insertion in the exon 3-adenine repetition in one case of gastric cancer and a thymidine deletion in the exon 24-thymidine repetition in one case of colorectal cancer [151]. These frameshift mutations predict the formation of a truncated TRIP12 protein with no catalytic activity. Unfortunately, the authors did not investigate the functional consequences of this insertion.

Another study aiming to identify the genetic loci with an elevated risk of breast cancer related to menopausal hormone therapy (MHT) in post-menopausal women showed a strong linkage between a Single Nucleotide Polymorphism (SNP) located in the exon 1-2 intronic region of the *TRIP12* gene and MHT [152]. However, they were not successful in replicating *TRIP12* SNP × MHT interaction in an independent cohort. Corresponding analyses of public data of global RNA expression were obtained from 12 lung adenocarcinomas and six controls to identify mutated genes with high-frequency-risk expression [153]. They identified the *TRIP12* gene as the most frequently mutated (missense mutation on exon 16) (nine cases out of 12). A recent study reported somatic mutations of the *TRIP12* gene in three out 20 cases of HPV-positive anal squamous cell carcinoma (HPV-ASCC) [154]. A missense mutation, a frameshift internal deletion, and a nonsense mutation were identified on exons 3, 37, and 33, respectively. However, the functional consequences of these mutations were not further investigated. A RNA-seq analysis of 139 patients with pediatric Acute Myeloid Leukemia (AML) revealed the existence in one patient of a new gene rearrangement leading to the fusion between TRIP12 and NPM (nucleophosmin) proteins [155]. Although the properties of this new fusion protein were not further studied, the authors suggest that the TRIP12-NPM protein may inhibit the function of ARF. *TRIP12* somatic mutations at splice sites were identified in pancreatic cancer recurrence of two patients but not in matched originally resected primary tumor and were qualified as subclonal mutations [156].

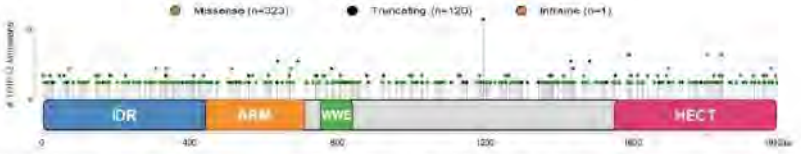

Figure 10. Schematic representation of mutations on the *TRIP12* gene in human cancers in cBioPortal (see Section Software and databases) obtained from 176 non-redundant studies containing more than 100 cases with both mutations and CNA data (27,235 patients and 28,253 samples). Mutation diagram circles are colored with respect to the corresponding mutation types indicated in the legend. In case of different mutation types at a single position, the color of the circle is determined with respect to the most frequent mutation type. Truncating mutations include nonsense, nonstop, frameshift deletion, frameshift insertion, and splice site. Inframe mutations include inframe deletion and inframe insertion.

Altogether, these studies suggest that although the *TRIP12* gene is found mutated in various type of tumors at variable frequencies, the functional consequences of these mutations in cancer development remain largely unidentified. Possible applications to detect these mutations as diagnostic, prognostic, or predictive still remain to be demonstrated.

6.2.2. Alteration of TRIP12 mRNA Expression in Cancers

If we refer to the Gepia2 database (see Section Software and databases), the *TRIP12* mRNA level compared to normal corresponding tissues varies depending on the type of cancer. Indeed, among 27 different types of cancer, the down-regulation of *TRIP12* mRNA is found in 12 cancer types compared to normal corresponding tissues but reached a statistical importance only in testicular germ cell tumors. In contrast, an overexpression of *TRIP12* mRNA is found in 15 types of cancer with a statistical significance for lymphoid neoplasm diffuse large B-cell lymphoma, thymoma and pancreatic adenocarcinoma (Figure 11). Of note, the *TRIP12* mRNA level is decreased in tumor types for which *TRIP12* mRNA is elevated in normal corresponding tissue, and inversely, it is up-regulated in tumors for which the *TRIP12* mRNA level is low in corresponding normal tissues (i.e., pancreatic adenocarcinoma). However, the mechanisms responsible for the alteration of *TRIP12* mRNA in tumor samples remain largely unknown. In certain types of cancer, a high level of *TRIP12* mRNA is associated with a shorter disease-free survival (i.e., bladder urothelial carcinoma, pancreatic adenocarcinoma), which suggests that the *TRIP12* mRNA level could be a useful prognostic marker. Additionally,

RNA-seq analysis of PBMC (Peripheral Blood Mononuclear Cells) obtained from a 47-year-old female patient with Acute Myeloid Leukemia (AML) with complete remission before and after induction therapy (fludarabine, cytarabine, and G-CSF (FLAG) protocol) revealed, among others, an exon 3 skipping in the *TRIP12* gene [157]. The authors claim that the alternative splicing of *TRIP12* mRNA could inhibit the TRIP12-mediated degradation of ARF, leading to an activation of the ARF/P53 signaling pathway and an induction of apoptosis of cell with aberrant growth. This process could contribute to the remission.

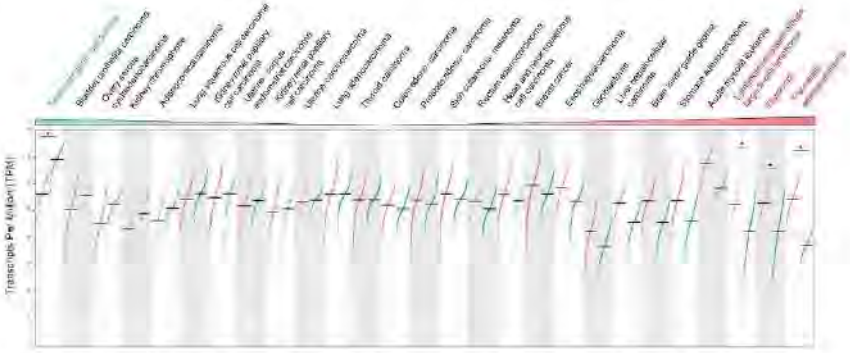

Figure 11. *TRIP12* mRNA expression level in 27 different types of cancer adapted from Gepia2 website (see Section Software and databases). Only tumor/normal tissue matched pairs with more than 25 cases were considered. Each dot represents a normal (green) or a tumor (red) sample. The horizontal black bar represents the mean. The *TRIP12* mRNA level was obtained by RNA-seq and expressed as transcripts per million (TPM). Cancer types in which *TRIP12* mRNA is statistically differentially expressed (ANOVA test with a q value < 0.01) are marked by an asterisk.

6.2.3. Alterations of TRIP12 Protein Expression in Cancers and Consequences

Available data on TRIP12 protein expression in cancer are much less abundant than those describing TRIP12 mRNA levels. The Human Protein Atlas indicates a heterogeneous expression of TRIP12 depending on cancer type with a high TRIP12 frequency in head-and-neck cancer, testis cancer, and glioma patients. Only a few molecular events leading to alterations of TRIP12 protein expression are known. For instance, Cai et al. demonstrated an overexpression of the deubiquitinase USP7 in hepatocellular carcinoma (HCC) tissues that is correlated with poor prognosis [47]. They showed that USP7 is required for the proliferation of HCC-derived cell lines. Mechanistically, the study reveals that USP7 overexpression stabilizes the TRIP12 protein, which in turn ubiquitinates and degrades ARF to promote HCC-derived cell proliferation. Interestingly, they established that the expressions of TRIP12 and/or USP7 are independent prognosis markers of HCC. *Helicobacter pylori* (*H. pylori*) is one of the most common human pathogens. This bacterium is recognized as the strongest identified risk factor for gastric malignancies. Horvat et al. demonstrated that infection by *H. pylori* of gastric cancer derived-cell lines induces TRIP12 protein expression through the implication of the virulence factor CagA (Cytotoxin-Associated Gene A) by a still unknown mechanism [158]. TRIP12 overexpression was observed in human gastric mucosa infected with *H. pylori*. The consequence of TRIP12-induced expression is a polyubiquitination-mediated degradation of ARF that leads to an inhibition of autophagy in gastric cells. Patients with human papillomavirus (HPV)-positive head and neck squamous cell carcinoma (HNSCC) have a better response to radiotherapy and higher overall survival rate than those with HPV-negative HNSCC. Indeed, HPV infection leads to P16 overexpression, which in turn provokes a destabilization of the TRIP12 protein by an unknown mechanism [159]. As TRIP12 is a DDR regulator (detailed in Section 5.3.), the down-regulation of TRIP12 sensitizes HPV-positive HNSCC to radiotherapy. Likewise, in 18 HPV-positive HNSCC patients, the overexpression of TRIP12

is associated with a poor survival rate. These results were confirmed recently by the same group [160]. Recently, Gatti et al. identified that the TRIP12 protein level could provide a useful marker for PARP inhibitors (PARPi) sensitivity [27]. Indeed, responses to this therapy are promising, but predictions based on PARP1 gene expression abundance and/or activity are not accurate enough. TRIP12 limits PARP1 presence at the chromatin by polyubiquitinating it and, as a consequence, it decreases the efficiency of PARP1 trapping by PARPi. Of importance, the TRIP12 protein level is negatively correlated with PARP1 protein abundance in two cohorts of breast and ovarian cancer patients.

We described in Section 5.2. the essential role of ARF in the activation of the P53 pathway and its degradation mediated by TRIP12. We also described how the nucleophosmin (NPM) protects ARF from TRIP12-mediated degradation by sequestrating it into the nucleoli [15]. The NPM gene is mutated in one-third of Acute myeloid leukemia (AML), which provokes the translocation of NPM protein into the cytoplasm and the loss of its capacity to maintain ARF localization in the nucleolus [96]. Combined with an overexpression of TRIP12, a frequent loss of NPM nucleolar localization strongly impedes the activation of the ARF/P53 pathway in AML-derived cells and favors their proliferation.

7. Conclusions and Perspectives

In this review, we provide a synthesis of the different knowledge on the E3 ubiquitin ligase TRIP12. First described as a thyroid hormone receptor interacting protein, it appears that the TRIP12 protein displays several important functions in essential cellular processes such as cell cycle progression, DNA damage repair, chromatin remodeling, and cell differentiation. Although the number of studies related to this E3 ubiquitin ligase is constantly growing, numerous aspects of its regulation and functions in physiology and pathologies are not entirely clear.

High-throughput sequencing analyses have determined the level of expression of *TRIP12* mRNA in a myriad of healthy and pathological human tissues such as cancers. However, the molecular mechanisms that regulate the production and the stability of *TRIP12* mRNA remain largely unknown. The same observation can be made for the post-translational regulation of TRIP12. Indeed, mass spectrometry approaches identified numerous post-translationally modified residues in TRIP12. Unfortunately, none of them have been linked to biological functions, even if three phosphorylation sites are attributed to specific kinases involved in cell cycle (CDK1) and DNA damage response (ATR/ATM, CHK1). We can speculate that these phosphorylated residues modify the protein-interacting properties or the ubiquitin ligase capacity of TRIP12, which in turn participates in cell cycle control and DDR. We could also envisage the possibility that TRIP12 phosphorylated residues result from the activity of kinases implicated in other signaling pathways (i.e., MAP kinases, PI3 kinases). The development of antibodies specific to TRIP12-phosphorylated residues is crucial to decipher the biological consequences of these post-translational modifications. Likewise, the identification of the ubiquitin ligase(s) responsible for the ubiquitinated residues of TRIP12 would certainly help to better perceive the regulation of the TRIP12 protein during the cell cycle. The anaphase-promoting complex/cyclosome (APC/C) system ubiquitinates several cell cycle-regulated proteins early after mitosis (i.e., CYCLIN A and B), thereby mediating degradation by the proteasome. TRIP12 possesses putative KEN box (aa 1496–1570/UniProt source) and Destruction boxes (aa 859–867 and aa 1546–1554/ELM resource) specifically recognized by the APC/C, system making this degradation system a legitimate candidate for the control of TRIP12 stability. To confirm these multiple hypotheses, a complete and exhaustive interactome/substratome of TRIP12 is required, keeping in mind that due to its ubiquitous expression, the interactome of TRIP12 will possibly vary depending on the cell type. We can logically expect other important cellular functions for this E3 ubiquitin ligase depending on the cell type or the cellular context.

This review raises questions, one of which is whether TRIP12 is an appropriate therapeutic target. In the case of cancers in which TRIP12 is overexpressed (i.e., pancreatic cancer) and given its role in the maintenance of a low level of P53 mediated by ARF degradation, it seems logical that the inhibition of TRIP12 could be a promising therapeutic strategy. The inhibition of TRIP12 ubiquitin ligase activity or

its interaction with protein partners might counteract the proliferation rate of cancer cells or sensitize them to chemotherapies (by affecting DNA damages repair induced by chemotherapies). To this purpose, the crystallization of the entire TRIP12 protein is a prerequisite to obtain the 3D structure of the protein to facilitate the screening and/or the design of specific inhibitors. PROTACs that are bifunctional molecules made up of an E3 ubiquitin ligase and a target protein connected via a linker could also be used to target TRIP12.

In pathological contexts where the *TRIP12* gene is mutated or truncated (numerous types of cancer and intellectual disorders), we do not yet understand whether the TRIP12 protein is indeed expressed or if the mRNA is degraded. If expressed, the functional consequences of mutated and truncated forms of TRIP12 in these pathologies are still unknown. We can only speculate that mutant proteins would act as dominant negative proteins, leading to an alteration of genome expression. The development of murine transgenic models expressing *Trip12* mutated forms could address these issues. Moreover, several truncating mutations identified in cancers and IDs theoretically lead to TRIP12 proteins lacking the HECT catalytic domain or protein–protein interacting domains (WWE/ARM). Therefore, therapeutic strategies inhibiting its catalytic activity or protein interaction might be useless or, even worse, deleterious for the patients.

To conclude, the TRIP12 protein is emerging as an important protein in several essential cellular processes as well as in pathological alterations. Uncovering the function of TRIP12 offers a glimpse for potential exciting therapeutic strategies. However, numerous aspects of its regulations and functions need to be better described prior to its application in therapeutic objectives.

8. Software and Data Bases

BioGrid: The Biological General Repository for Interaction Datasets (BioGrid) is an open access database that houses genetic and protein interactions curated from the primary biomedical literature for all major model organism species and humans (https://thebiogrid.org/).

cBioPortal: The cBio Cancer Genomics Portal is an open-access resource for the interactive exploration of multidimensional cancer genomics datasets, currently providing access to data from more than 5000 tumor samples from 20 cancer studies (www.cbioportal.org).

ClinVar: ClinVar is a public database of variant interpretations that has steadily grown to become the largest publicly available genetic variant database and provides an ever-growing resource to study genotype–phenotype correlations (https://www.ncbi.nlm.nih.gov/clinvar/).

COBALT: The constraint-based Multiple Alignment Tool is a multiple sequence alignment tool that finds a collection of pairwise constraints derived from conserved domain database, protein motif database, and sequence similarity, using RPS-BLAST, BLASTP, and PHI-BLAST. Then, pairwise constraints are incorporated into a progressive multiple alignment (www.ncbi.nlm.nih.gov/tools/cobalt/cobalt.cgi).

EMBOSS matcher: EMBOSS Matcher identifies local similarities in two input sequences using a rigorous algorithm based on Bill Pearson's lalign application (www.ebi.ac.uk).

ELM: The Eukaryotic Linear Motif resource is a computational biology resource for investigating short linear motifs (SLiMs) in eukaryotic proteins. It is currently the largest collection of linear motif classes with annotated and experimentally validated linear motif instances (http://elm.eu.org/).

Genome browser: A genome browser is a graphical interface for the display of information from a biological database for genomic data (www.genome.ucsc.edu).

Gepia2: The Gene Expression Profiling Interactive Analysis 2 web server is a valuable and highly cited resource for gene expression analysis based on tumor and normal samples from the TCGA and the GTEx databases (http://gepia2.cancer-pku.cn).

Human Protein Atlas: The Human Protein Atlas is a program with the aim to map all the human proteins in cells, tissues, and organs using an integration of various omics technologies, including antibody-based imaging, mass spectrometry-based proteomics, transcriptomics, and systems biology (www.proteinatlas.org).

IDEAL: Intrinsically Disordered proteins with Extensive Annotations and Literature is a collection of knowledge on experimentally verified intrinsically disordered proteins. IDEAL contains manual annotations by curators on intrinsically disordered regions, interaction regions to other molecules, post-translational modification sites, references, and structural domain assignments (www.ideal-db.org).

InterProScan: InterProScan is a tool that scans given protein sequences against the protein signatures of the InterPro member databases, currently—PROSITE, PRINTS, Pfam, ProDom, and SMART (https://www.ebi.ac.uk/interpro/).

IUPred: Intrinsically unstructured/disordered proteins have no single well-defined tertiary structure in their native, functional state. This server recognizes such regions from the amino acid sequence based on the estimated pairwise energy content (https://iupred.elte.hu/).

LOVD: The Leiden Variation Database is a free, flexible web-based open source database developed in the Leiden University Medical Center in the Netherlands, which is designed to collect and display variants in the DNA sequence. The focus of an LOVD is usually the combination between a gene and a genetic (heritable) disease (https://www.lovd.nl/).

OMIM: Online Mendelian Inheritance in Man is a comprehensive, authoritative compendium of human genes and genetic phenotypes that is freely available and updated daily (https://www.omim.org/).

PhosphoSitePlus®: PhosphoSitePlus® provides comprehensive information and tools for the study of protein post-translational modifications (PTMs) including phosphorylation, acetylation, and more (https://phosphosite.org/).

SFARI GENE: SFARI GENE is an evolving database for the autism research community that is centered on genes implicated in autism susceptibility (https://gene.sfari.org/).

STRING: Search Tool for the Retrieval of Interacting Genes/Proteins is a biological database and web resource of known and predicted protein–protein interactions. The STRING database contains information from numerous sources, including experimental data, computational prediction methods, and public text collections. It is freely accessible and it is regularly updated (https://string-db.org/).

UniProt: UniProt is the Universal Protein resource, a central repository of protein data created by combining the Swiss-Prot, TrEMBL and PIR-PSD databases. (www.uniprot.org).

Supplementary Materials: The following are available online at http://www.mdpi.com/1422-0067/21/22/8515/s1.

Author Contributions: M.B., C.V., D.L., J.T., M.D. conception, drafting, critical revising of the review (text, figures and tables). All authors have read and agreed to the published version of the manuscript.

Funding: University Paul Sabatier (Toulouse, France). Ligue Nationale contre le Cancer. Fondation Toulouse Cancer Santé (2018CS079). Ligue Régionale contre le Cancer (comité Haute-Garonne, comité Ariège). Institut National de la Santé et de la Recherche Médicale.

Acknowledgments: C. Vargas is funded by the University Paul Sabatier (Toulouse, France). M. Brunet is funded by the University Paul Sabatier (Toulouse, France) and the Ligue Nationale contre le Cancer. D. Larrieu was funded by the Ligue Nationale contre le Cancer. We thank the "Fondation Toulouse Cancer Santé" and the Ligue Nationale contre le Cancer (comité Haute-Garonne, comité Ariège) for financial support. We thank Dina Arvanitis (Inserm U1038, Institute of Cardiovascular and Metabolic Disease, Toulouse, France) for the critical reading of the manuscript. We apologize for all the studies that were not quoted in this manuscript due to a lack of space.

Conflicts of Interest: The authors declare no conflict of interest.

References

1. Nomura, N.; Nagase, T.; Miyajima, N.; Sazuka, T.; Tanaka, A.; Sato, S.; Seki, N.; Kawarabayasi, Y.; Ishikawa, K.-I.; Tabata, S. Prediction of the Coding Sequences of Unidentified Human Genes. II. The Coding Sequences of 40 New Genes (KIAA0041-KIAA0080) Deduced by Analysis of cDNA Clones from Human Cell Line KG-1. *DNA Res.* **1994**, *1*, 223–229. [CrossRef]
2. Huibregtse, J.M.; Scheffner, M.; Beaudenon, S.; Howley, P.M. A family of proteins structurally and functionally related to the E6-AP ubiquitin-protein ligase. *Proc. Natl. Acad. Sci. USA* **1995**, *92*, 2563–2567. [CrossRef]
3. Lee, J.W.; Choi, H.S.; Gyuris, J.; Brent, R.; Moore, D.D. Two classes of proteins dependent on either the presence or absence of thyroid hormone for interaction with the thyroid hormone receptor. *Mol. Endocrinol.* **1995**, *9*, 243–254.

4. Park, Y.; Yoon, S.K.; Yoon, J.-B. TRIP12 functions as an E3 ubiquitin ligase of APP-BP1. *Biochem. Biophys. Res. Commun.* **2008**, *374*, 294–298. [CrossRef]
5. Kajiro, M.; Tsuchiya, M.; Kawabe, Y.-I.; Furumai, R.; Iwasaki, N.; Hayashi, Y.; Katano, M.; Nakajima, Y.; Goto, N.; Watanabe, T.; et al. The E3 Ubiquitin Ligase Activity of Trip12 Is Essential for Mouse Embryogenesis. *PLoS ONE* **2011**, *6*, e25871. [CrossRef]
6. Hanoun, N.; Fritsch, S.; Gayet, O.; Gigoux, V.; Cordelier, P.; Dusetti, N.; Torrisani, J.; Dufresne, M. The E3 Ubiquitin Ligase Thyroid Hormone Receptor-interacting Protein 12 Targets Pancreas Transcription Factor 1a for Proteasomal Degradation. *J. Biol. Chem.* **2014**, *289*, 35593–35604. [CrossRef]
7. Larrieu, D.; Brunet, M.; Vargas, C.; Hanoun, N.; Ligat, L.; Dagnon, L.; Lulka, H.; Pommier, R.M.; Selves, J.; Jády, B.E.; et al. The E3 ubiquitin ligase TRIP12 participates in cell cycle progression and chromosome stability. *Sci. Rep.* **2020**, *10*, 1–17. [CrossRef] [PubMed]
8. Trinklein, N.D.; Aldred, S.F.; Hartman, S.J.; Schroeder, D.I.; Otillar, R.P.; Myers, R.M. An Abundance of Bidirectional Promoters in the Human Genome. *Genome Res.* **2003**, *14*, 62–66. [CrossRef] [PubMed]
9. Tekcham, D.S.; Chen, D.; Liu, Y.; Ling, T.; Zhang, Y.; Chen, H.; Wang, W.; Otkur, W.; Qi, H.; Xia, T.; et al. F-box proteins and cancer: An update from functional and regulatory mechanism to therapeutic clinical prospects. *Theranostics* **2020**, *10*, 4150–4167. [CrossRef] [PubMed]
10. Bramswig, N.C.; Lüdecke, H.-J.; Pettersson, M.; Albrecht, B.; Bernier, R.A.; Cremer, K.; Eichler, E.E.; Falkenstein, D.; Gerdts, J.; Jansen, S.; et al. Identification of new TRIP12 variants and detailed clinical evaluation of individuals with non-syndromic intellectual disability with or without autism. *Qual. Life Res.* **2017**, *136*, 179–192. [CrossRef]
11. Chang, J.-W.; Zhang, W.; Yeh, H.S.; De Jong, E.P.; Jun, S.; Kim, K.H.; Bae, S.S.; Beckman, K.; Hwang, T.H.; Kim, K.S.; et al. mRNA 3′-UTR shortening is a molecular signature of mTORC1 activation. *Nat. Commun.* **2015**, *6*, 7218. [CrossRef] [PubMed]
12. An, C.-I.; Ganio, E.; Hagiwara, N. Trip12, a HECT domain E3 ubiquitin ligase, targets Sox6 for proteasomal degradation and affects fiber type-specific gene expression in muscle cells. *Skelet. Muscle* **2013**, *3*, 11. [CrossRef] [PubMed]
13. Sadkowski, T.; Jank, M.; Zwierzchowski, L.; Oprzadek, J.; Motyl, T. Comparison of skeletal muscle transcriptional profiles in dairy and beef breeds bulls. *J. Appl. Genet.* **2009**, *50*, 109–123. [CrossRef] [PubMed]
14. Gudjonsson, T.; Altmeyer, M.; Savic, V.; Toledo, L.; Dinant, C.; Grøfte, M.; Bartkova, J.; Poulsen, M.; Oka, Y.; Bekker-Jensen, S.; et al. TRIP12 and UBR5 Suppress Spreading of Chromatin Ubiquitylation at Damaged Chromosomes. *Cell* **2012**, *150*, 697–709. [CrossRef] [PubMed]
15. Chen, D.; Shan, J.; Zhu, W.-G.; Qin, J.; Gu, W. Transcription-independent ARF regulation in oncogenic stress-mediated p53 responses. *Nat. Cell Biol.* **2010**, *464*, 624–627. [CrossRef]
16. Huber, A.H.; Nelson, W.J.; Weis, W.I. Three-dimensional structure of the armadillo repeat region of beta-catenin. *Cell* **1997**, *90*, 871–882. [CrossRef]
17. Ries, L.K.; Liess, A.K.L.; Feiler, C.G.; Spratt, D.E.; Lowe, E.D.; Lorenz, S. Crystal structure of the catalytic C-lobe of the HECT-type ubiquitin ligase E6AP. *Protein Sci.* **2020**, *29*, 1550–1554. [CrossRef]
18. Zweifel, M.E.; Leahy, D.J.; Barrick, D. Structure and Notch Receptor Binding of the Tandem WWE Domain of Deltex. *Structure* **2005**, *13*, 1599–1611. [CrossRef]
19. Sluimer, J.; Distel, B. Regulating the human HECT E3 ligases. *Cell. Mol. Life Sci.* **2018**, *75*, 3121–3141. [CrossRef]
20. Zheng, N.; Shabek, N. Ubiquitin Ligases: Structure, Function, and Regulation. *Annu. Rev. Biochem.* **2017**, *86*, 129–157. [CrossRef]
21. Huang, L. Structure of an E6AP-UbcH7 Complex: Insights into Ubiquitination by the E2-E3 Enzyme Cascade. *Science* **1999**, *286*, 1321–1326. [CrossRef] [PubMed]
22. Scheffner, M.; Huibregtse, J.M.; Vierstra, R.D.; Howley, P.M. The HPV-16 E6 and E6-AP complex functions as a ubiquitin-protein ligase in the ubiquitination of p53. *Cell* **1993**, *75*, 495–505. [CrossRef]
23. Wang, Y.; Argiles-Castillo, D.; Kane, E.I.; Zhou, A.; Spratt, D.E. HECT E3 ubiquitin ligases—Emerging insights into their biological roles and disease relevance. *J. Cell Sci.* **2020**, *133*, jcs228072. [CrossRef] [PubMed]
24. Aravind, L. The WWE domain: A common interaction module in protein ubiquitination and ADP ribosylation. *Trends Biochem. Sci.* **2001**, *26*, 273–275. [CrossRef]
25. Wang, Z.; Michaud, G.A.; Cheng, Z.; Zhang, Y.; Hinds, T.R.; Fan, E.; Cong, F.; Xu, W. Recognition of the iso-ADP-ribose moiety in poly(ADP-ribose) by WWE domains suggests a general mechanism for poly(ADP-ribosyl)ation-dependent ubiquitination. *Genes Dev.* **2012**, *26*, 235–240. [CrossRef]

26. Mitchell, A.L.; Attwood, T.K.; Babbitt, P.C.; Blum, M.; Bork, P.; Bridge, A.; Brown, S.D.; Chang, H.-Y.; El-Gebali, S.; Fraser, M.I.; et al. InterPro in 2019: Improving coverage, classification and access to protein sequence annotations. *Nucleic Acids Res.* **2018**, *47*, D351–D360. [CrossRef]
27. Gatti, M.; Imhof, R.; Huang, Q.; Baudis, M.; Altmeyer, M. The Ubiquitin Ligase TRIP12 Limits PARP1 Trapping and Constrains PARP Inhibitor Efficiency. *Cell Rep.* **2020**, *32*, 107985. [CrossRef]
28. Tewari, R.; Bailes, E.; Bunting, K.A.; Coates, J.C. Armadillo-repeat protein functions: Questions for little creatures. *Trends Cell Biol.* **2010**, *20*, 470–481. [CrossRef]
29. El Refy, A.; Perazza, D.; Zekraoui, L.; Valay, J.-G.; Bechtold, N.; Brown, S.; Hülskamp, M.; Herzog, M.; Bonneville, J.-M. The Arabidopsis KAKTUS gene encodes a HECT protein and controls the number of endoreduplication cycles. *Mol. Genet. Genom.* **2003**, *270*, 403–414. [CrossRef]
30. Ju, D.; Wang, X.; Xu, H.; Xie, Y. The armadillo repeats of the Ufd4 ubiquitin ligase recognize ubiquitin-fusion proteins. *FEBS Lett.* **2006**, *581*, 265–270. [CrossRef]
31. Van Der Lee, R.; Buljan, M.; Lang, B.; Weatheritt, R.J.; Daughdrill, G.W.; Dunker, A.K.; Fuxreiter, M.; Gough, J.; Gsponer, J.; Jones, D.T.W.; et al. Classification of Intrinsically Disordered Regions and Proteins. *Chem. Rev.* **2014**, *114*, 6589–6631. [CrossRef] [PubMed]
32. Toretsky, J.A.; Wright, P.E. Assemblages: Functional units formed by cellular phase separation. *J. Cell Biol.* **2014**, *206*, 579–588. [CrossRef] [PubMed]
33. Levy, Y. Intrinsically Disordered Regions as Affinity Tuners in Protein-DNA Interactions. *Biophys. J.* **2012**, *102*, 632a. [CrossRef]
34. Watson, M.; Stott, K. Disordered domains in chromatin-binding proteins. *Essays Biochem.* **2019**, *63*, 147–156. [CrossRef]
35. Vuzman, D.; Levy, Y. DNA search efficiency is modulated by charge composition and distribution in the intrinsically disordered tail. *Proc. Natl. Acad. Sci. USA* **2010**, *107*, 21004–21009. [CrossRef]
36. Sabari, B.R.; Dall'Agnese, A.; Boija, A.; Klein, I.A.; Coffey, E.L.; Shrinivas, K.; Abraham, B.J.; Hannett, N.M.; Zamudio, A.V.; Manteiga, J.C.; et al. Coactivator condensation at super-enhancers links phase separation and gene control. *Science* **2018**, *361*, eaar3958. [CrossRef]
37. Leach, B.I.; Kuntimaddi, A.; Schmidt, C.R.; Cierpicki, T.; Johnson, S.A.; Bushweller, J.H. Leukemia Fusion Target AF9 Is an Intrinsically Disordered Transcriptional Regulator that Recruits Multiple Partners via Coupled Folding and Binding. *Structure* **2013**, *21*, 176–183. [CrossRef]
38. Chen, Y.; Cramer, P. Structure of the super-elongation complex subunit AFF4 C-terminal homology domain reveals requirements for AFF homo- and heterodimerization. *J. Biol. Chem.* **2019**, *294*, 10663–10673. [CrossRef]
39. Liu, X.; Yang, X.; Li, Y.; Zhao, S.; Li, C.; Ma, P.; Mao, B. Trip12 is an E3 ubiquitin ligase for USP7/HAUSP involved in the DNA damage response. *FEBS Lett.* **2016**, *590*, 4213–4222. [CrossRef]
40. Banani, S.F.; Lee, H.O.; Hyman, H.O.L.A.A.; Rosen, S.F.B.M.K. Biomolecular condensates: Organizers of cellular biochemistry. *Nat. Rev. Mol. Cell Biol.* **2017**, *18*, 285–298. [CrossRef]
41. Posey, A.E.; Holehouse, A.S.; Pappu, R.V. Phase Separation of Intrinsically Disordered Proteins. *Methods Enzymol.* **2018**, *611*, 1–30. [CrossRef] [PubMed]
42. Gallego, L.D.; Schneider, M.; Mittal, C.; Romanauska, A.; Carrillo, R.M.G.; Schubert, T.; Pugh, B.F.; Köhler, A. Phase separation directs ubiquitination of gene-body nucleosomes. *Nat. Cell Biol.* **2020**, *579*, 592–597. [CrossRef] [PubMed]
43. Madeira, F.; Park, Y.M.; Lee, J.; Buso, N.; Gur, T.; Madhusoodanan, N.; Basutkar, P.; Tivey, A.R.N.; Potter, S.C.; Finn, R.D.; et al. The EMBL-EBI search and sequence analysis tools APIs in 2019. *Nucleic Acids Res.* **2019**, *47*, W636–W641. [CrossRef] [PubMed]
44. Blasius, M.; Forment, J.V.; Thakkar, N.; Wagner, S.A.; Choudhary, C.; Jackson, S.P. A phospho-proteomic screen identifies substrates of the checkpoint kinase Chk1. *Genome Biol.* **2011**, *12*, R78. [CrossRef]
45. Matsuoka, S.; Ballif, B.A.; Smogorzewska, A.; McDonald, E.R.; Hurov, K.E.; Luo, J.; Bakalarski, C.E.; Zhao, Z.; Solimini, N.; Lerenthal, Y.; et al. ATM and ATR Substrate Analysis Reveals Extensive Protein Networks Responsive to DNA Damage. *Science* **2007**, *316*, 1160–1166. [CrossRef]
46. Petrone, A.; Adamo, M.E.; Cheng, C.; Kettenbach, A.N. Identification of Candidate Cyclin-dependent kinase 1 (Cdk1) Substrates in Mitosis by Quantitative Phosphoproteomics. *Mol. Cell. Proteom.* **2016**, *15*, 2448–2461. [CrossRef]

47. Cai, J.-B.; Shi, G.-M.; Dong, Z.-R.; Ke, A.-W.; Ma, H.-H.; Gao, Q.; Shen, Z.-Z.; Huang, X.-Y.; Chen, H.; Yu, D.-D.; et al. Ubiquitin-specific protease 7 accelerates p14 ARF degradation by deubiquitinating thyroid hormone receptor-interacting protein 12 and promotes hepatocellular carcinoma progression. *Hepatology* **2015**, *61*, 1603–1614. [CrossRef]
48. Georges, A.; Marcon, E.; Greenblatt, J.; Frappier, L. Identification and Characterization of USP7 Targets in Cancer Cells. *Sci. Rep.* **2018**, *8*, 15833. [CrossRef]
49. Hershko, A.; Ciechanover, A. The Ubiquitin System. *Annu. Rev. Biochem.* **1998**, *67*, 425–479. [CrossRef]
50. McClellan, A.J.; Laugesen, S.H.; Ellgaard, L. Cellular functions and molecular mechanisms of non-lysine ubiquitination. *Open Biol.* **2019**, *9*, 190147. [CrossRef]
51. Swatek, K.N.; Komander, D. Ubiquitin modifications. *Cell Res.* **2016**, *26*, 399–422. [CrossRef] [PubMed]
52. Wilkinson, K.D. Regulation of ubiquitin-dependent processes by deubiquitinating enzymes. *FASEB J.* **1997**, *11*, 1245–1256. [CrossRef] [PubMed]
53. Kweon, S.-M.; Chen, Y.; Moon, E.; Kvederaviciute, K.; Klimasauskas, S.; Feldman, D.E. An Adversarial DNA N6-Methyladenine-Sensor Network Preserves Polycomb Silencing. *Mol. Cell* **2019**, *74*, 1138–1147.e6. [CrossRef] [PubMed]
54. Keppler, B.R.; Archer, T.K. Ubiquitin-dependent and Ubiquitin-independent Control of Subunit Stoichiometry in the SWI/SNF Complex. *J. Biol. Chem.* **2010**, *285*, 35665–35674. [CrossRef]
55. Hah, N.; Kolkman, A.; Ruhl, D.D.; Pijnappel, W.W.M.P.; Heck, A.J.R.; Timmers, H.T.M.; Kraus, W.L. A Role for BAF57 in Cell Cycle–Dependent Transcriptional Regulation by the SWI/SNF Chromatin Remodeling Complex. *Cancer Res.* **2010**, *70*, 4402–4411. [CrossRef]
56. Kuo, M.-L.; Besten, W.D.; Sherr, C.J. N-Terminal Polyubiquitination of the ARF Tumor Suppressor, A Natural Lysine-Less Protein. *Cell Cycle* **2004**, *3*, 1367–1369. [CrossRef]
57. Chen, J.; Archer, T.K. Regulating SWI/SNF Subunit Levels via Protein-Protein Interactions and Proteasomal Degradation: BAF155 and BAF170 Limit Expression of BAF57. *Mol. Cell. Biol.* **2005**, *25*, 9016–9027. [CrossRef]
58. Chio, I.I.C.; Sasaki, M.; Ghazarian, D.; Moreno, J.; Done, S.J.; Ueda, T.; Inoue, S.; Chang, Y.-L.; Chen, N.-J.; Mak, T.W. TRADD contributes to tumour suppression by regulating ULF-dependent p19Arf ubiquitylation. *Nat. Cell Biol.* **2012**, *14*, 625–633. [CrossRef]
59. Johnson, E.S.; Ma, P.C.M.; Ota, I.M.; Varshavsky, A. A Proteolytic Pathway That Recognizes Ubiquitin as a Degradation Signal. *J. Biol. Chem.* **1995**, *270*, 17442–17456. [CrossRef]
60. Park, Y.; Yoon, S.K.; Yoon, J.-B. The HECT Domain of TRIP12 Ubiquitinates Substrates of the Ubiquitin Fusion Degradation Pathway. *J. Biol. Chem.* **2008**, *284*, 1540–1549. [CrossRef]
61. Van Leeuwen, F.; De Kleijn, D.P.; Hurk, H.H.V.D.; Neubauer, A.; Sonnemans, M.A.; Sluijs, J.A.; Köycü, S.; Ramdjielal, R.D.; Salehi, A.; Martens, G.J.; et al. Frameshift mutants of beta amyloid precursor protein and ubiquitin-B in Alzheimer's and Down patients. *Science* **1998**, *279*, 242–247. [CrossRef] [PubMed]
62. Poulsen, E.G.; Steinhauer, C.; Lees, M.; Lauridsen, A.-M.; Ellgaard, L.; Hartmann-Petersen, R. HUWE1 and TRIP12 Collaborate in Degradation of Ubiquitin-Fusion Proteins and Misframed Ubiquitin. *PLoS ONE* **2012**, *7*, e50548. [CrossRef] [PubMed]
63. Setz, C.; Friedrich, M.; Hahn, S.; Dörrie, J.; Schaft, N.; Schuler, G.; Schubert, U. Just One Position-Independent Lysine Residue Can Direct MelanA into Proteasomal Degradation following N-Terminal Fusion of Ubiquitin. *PLoS ONE* **2013**, *8*, e55567. [CrossRef]
64. Varshavsky, A. N-degron and C-degron pathways of protein degradation. *Proc. Natl. Acad. Sci. USA* **2019**, *116*, 358–366. [CrossRef] [PubMed]
65. Hwang, C.-S.; Shemorry, A.; Auerbach, D.; Varshavsky, A. The N-end rule pathway is mediated by a complex of the RING-type Ubr1 and HECT-type Ufd4 ubiquitin ligases. *Nat. Cell Biol.* **2010**, *12*, 1177–1185. [CrossRef]
66. Havugimana, P.C.; Hart, G.T.; Nepusz, T.; Yang, H.; Turinsky, A.L.; Li, Z.; Wang, P.I.; Boutz, D.R.; Fong, V.; Phanse, S.; et al. A Census of Human Soluble Protein Complexes. *Cell* **2012**, *150*, 1068–1081. [CrossRef]
67. Arbogast, F.; Arnold, J.; Hammann, P.; Kuhn, L.; Chicher, J.; Murera, D.; Weishaar, J.; Muller, S.; Fauny, J.-D.; Gros, F. ATG5 is required for B cell polarization and presentation of particulate antigens. *Autophagy* **2018**, *15*, 280–294. [CrossRef]
68. Huttlin, E.L.; Ting, L.; Bruckner, R.J.; Gebreab, F.; Gygi, M.P.; Szpyt, J.; Tam, S.; Zarraga, G.; Colby, G.; Baltier, K.; et al. The BioPlex Network: A Systematic Exploration of the Human Interactome. *Cell* **2015**, *162*, 425–440. [CrossRef]

69. Huttlin, E.L.; Bruckner, R.J.; Paulo, J.A.; Cannon, J.R.; Ting, L.; Baltier, K.; Colby, G.; Gebreab, F.; Gygi, M.P.; Parzen, H.; et al. Architecture of the human interactome defines protein communities and disease networks. *Nat. Cell Biol.* **2017**, *545*, 505–509. [CrossRef]
70. Nakayama, M.; Kikuno, R.; Ohara, O. Protein-Protein Interactions between Large Proteins: Two-Hybrid Screening Using a Functionally Classified Library Composed of Long cDNAs. *Genome Res.* **2002**, *12*, 1773–1784. [CrossRef]
71. Hanson, D.; Stevens, A.; Murray, P.; Black, G.C.M.; Clayton, P.E. Identifying biological pathways that underlie primordial short stature using network analysis. *J. Mol. Endocrinol.* **2014**, *52*, 333–344. [CrossRef] [PubMed]
72. Jeronimo, C.; Forget, D.; Bouchard, A.; Li, Q.; Chua, G.; Poitras, C.; Thérien, C.; Bergeron, D.; Bourassa, S.; Greenblatt, J.; et al. Systematic Analysis of the Protein Interaction Network for the Human Transcription Machinery Reveals the Identity of the 7SK Capping Enzyme. *Mol. Cell* **2007**, *27*, 262–274. [CrossRef] [PubMed]
73. Lee, S.; Cho, Y.-E.; Kim, S.-H.; Kim, Y.-J.; Park, J.-H. GLTSCR2 promotes the nucleoplasmic translocation and subsequent degradation of nucleolar ARF. *Oncotarget* **2016**, *8*, 16293–16302. [CrossRef] [PubMed]
74. Li, Z.; Hou, J.; Sun, L.; Wen, T.; Wang, L.; Zhao, X.; Xie, Q.; Zhang, S.Q. NMI mediates transcription-independent ARF regulation in response to cellular stresses. *Mol. Biol. Cell* **2012**, *23*, 4635–4646. [CrossRef] [PubMed]
75. Lo, R.; Zhang, Y.; Dai, M.-S.; Sun, X.-X.; Zeng, S.X.; Lu, H. Nucleostemin stabilizes ARF by inhibiting the ubiquitin ligase ULF. *Oncogene* **2014**, *34*, 1688–1697. [CrossRef] [PubMed]
76. Gupta, G.D.; Coyaud, É.; Gonçalves, J.; Mojarad, B.A.; Liu, Y.; Wu, Q.; Gheiratmand, L.; Comartin, D.; Tkach, J.M.; Cheung, S.W.; et al. A Dynamic Protein Interaction Landscape of the Human Centrosome-Cilium Interface. *Cell* **2015**, *163*, 1484–1499. [CrossRef] [PubMed]
77. Wang, X.; Venable, J.; Lapointe, P.; Hutt, D.M.; Koulov, A.V.; Coppinger, J.; Gurkan, C.; Kellner, W.; Matteson, J.; Plutner, H.; et al. Hsp90 Cochaperone Aha1 Downregulation Rescues Misfolding of CFTR in Cystic Fibrosis. *Cell* **2006**, *127*, 803–815. [CrossRef]
78. Yamauchi, T.; Masuda, T.; Canver, M.C.; Seiler, M.; Semba, Y.; Shboul, M.; Al-Raqad, M.; Maeda, M.; Schoonenberg, V.A.; Cole, M.A.; et al. Genome-wide CRISPR-Cas9 Screen Identifies Leukemia-Specific Dependence on a Pre-mRNA Metabolic Pathway Regulated by DCPS. *Cancer Cell* **2018**, *33*, 386–400.e5. [CrossRef]
79. Guard, S.E.; Poss, Z.C.; Ebmeier, C.C.; Pagratis, M.; Simpson, H.; Taatjes, D.J.; Old, W.M. The nuclear interactome of DYRK1A reveals a functional role in DNA damage repair. *Sci. Rep.* **2019**, *9*, 1–12. [CrossRef]
80. Cao, Q.; Wang, X.; Zhao, M.; Yang, R.; Malik, R.; Qiao, Y.; Poliakov, A.; Yocum, A.K.; Li, Y.; Chen, W.; et al. The central role of EED in the orchestration of polycomb group complexes. *Nat. Commun.* **2014**, *5*, 1–13. [CrossRef]
81. Wang, S.; Kollipara, R.K.; Humphries, C.G.; Ma, S.-H.; Hutchinson, R.; Li, R.; Siddiqui, J.; Tomlins, S.A.; Raj, G.V.; Kittler, R. The ubiquitin ligase TRIM25 targets ERG for degradation in prostate cancer. *Oncotarget* **2016**, *7*, 64921–64931. [CrossRef] [PubMed]
82. Tarallo, R.; Bamundo, A.; Nassa, G.; Nola, E.; Paris, O.; Ambrosino, C.; Facchiano, A.; Baumann, M.; Nyman, T.A.; Weisz, A. Identification of proteins associated with ligand-activated estrogen receptor α in human breast cancer cell nuclei by tandem affinity purification and nano LC-MS/MS. *Proteom. Clin. Appl.* **2011**, *5*, 470. [CrossRef]
83. Hein, M.Y.; Hubner, N.C.; Poser, I.; Cox, J.; Nagaraj, N.; Toyoda, Y.; Gak, I.A.; Weisswange, I.; Mansfeld, J.; Buchholz, F.; et al. A Human Interactome in Three Quantitative Dimensions Organized by Stoichiometries and Abundances. *Cell* **2015**, *163*, 712–723. [CrossRef] [PubMed]
84. Oliviero, G.; Cagney, G.; Waston, A.; Streubel, G.; Jerman, E.; Andrews, D.; Doyle, B.; Munawar, N.; Wynne, K.; Crean, J.; et al. Dynamic Protein Interactions of the Polycomb Repressive Complex 2 during Differentiation of Pluripotent Cells. *Mol. Cell. Proteom.* **2016**, *15*, 3450–3460. [CrossRef]
85. Gilmore, J.M.; Sardiu, M.E.; Groppe, B.D.; Thornton, J.L.; Liu, X.; Dayebgadoh, G.; Banks, C.A.; Slaughter, B.D.; Unruh, J.R.; Workman, J.L.; et al. WDR76 Co-Localizes with Heterochromatin Related Proteins and Rapidly Responds to DNA Damage. *PLoS ONE* **2016**, *11*, e0155492. [CrossRef]
86. Lambert, J.-P.; Tucholska, M.; Go, C.; Knight, J.D.; Gingras, A.-C. Proximity biotinylation and affinity purification are complementary approaches for the interactome mapping of chromatin-associated protein complexes. *J. Proteom.* **2015**, *118*, 81–94. [CrossRef]
87. Nakamura, K.; Saredi, G.; Becker, J.R.; Foster, B.M.; Nguyen, N.V.; Beyer, T.E.; Cesa, L.C.; Faull, P.A.; Lukauskas, S.; Frimurer, T.; et al. H4K20me0 recognition by BRCA1–BARD1 directs homologous recombination to sister chromatids. *Nat. Cell Biol.* **2019**, *21*, 311–318. [CrossRef]

88. Diner, B.A.; Lum, K.K.; Javitt, A.; Cristea, I.M. Interactions of the Antiviral Factor Interferon Gamma-Inducible Protein 16 (IFI16) Mediate Immune Signaling and Herpes Simplex Virus-1 Immunosuppression. *Mol. Cell. Proteom.* **2015**, *14*, 2341–2356. [CrossRef]
89. Yue, Y.; Liu, J.; Cui, X.; Cao, J.; Luo, G.; Zhang, Z.; Cheng, T.; Gao, M.; Shu, X.; Ma, H.; et al. VIRMA mediates preferential m6A mRNA methylation in 3'UTR and near stop codon and associates with alternative polyadenylation. *Cell Discov.* **2018**, *4*, 1–17. [CrossRef]
90. Hauri, S.; Comoglio, F.; Seimiya, M.; Gerstung, M.; Glatter, T.; Hansen, K.; Aebersold, R.; Paro, R.; Gstaiger, M.; Beisel, C. A High-Density Map for Navigating the Human Polycomb Complexome. *Cell Rep.* **2016**, *17*, 583–595. [CrossRef]
91. Rosenbluh, J.; Mercer, J.; Shrestha, Y.; Oliver, R.; Tamayo, P.; Doench, J.G.; Tirosh, I.; Piccioni, F.; Hartenian, E.; Horn, H.; et al. Genetic and Proteomic Interrogation of Lower Confidence Candidate Genes Reveals Signaling Networks in β-Catenin-Active Cancers. *Cell Syst.* **2016**, *3*, 302–316.e4. [CrossRef] [PubMed]
92. Choi, J.H.; Zhong, X.; McAlpine, W.; Liao, T.-C.; Zhang, D.-W.; Fang, B.; Russell, J.; Ludwig, S.; Nair-Gill, E.; Zhang, Z.; et al. LMBR1L regulates lymphopoiesis through Wnt/β-catenin signaling. *Science* **2019**, *364*, eaau0812. [CrossRef] [PubMed]
93. Su, D.; Ma, S.; Shan, L.; Wang, Y.; Wang, Y.; Cao, C.; Liu, B.; Yang, C.; Wang, L.; Tian, S.; et al. Ubiquitin-specific protease 7 sustains DNA damage response and promotes cervical carcinogenesis. *J. Clin. Investig.* **2018**, *128*, 4280–4296. [CrossRef] [PubMed]
94. Benleulmi-Chaachoua, A.; Chen, L.; Sokolina, K.; Wong, V.; Jurisica, I.; Emerit, M.B.; Darmon, M.; Espin, A.; Stagljar, I.; Tafelmeyer, P.; et al. Protein interactome mining defines melatonin MT1receptors as integral component of presynaptic protein complexes of neurons. *J. Pineal Res.* **2015**, *60*, 95–108. [CrossRef] [PubMed]
95. Heidelberger, J.B.; Voigt, A.; Borisova, M.E.; Petrosino, G.; Ruf, S.; Wagner, S.A.; Beli, P. Proteomic profiling of VCP substrates links VCP to K6-linked ubiquitylation and c-Myc function. *EMBO Rep.* **2018**, *19*, e44754. [CrossRef]
96. Chen, D.; Yoon, J.-B.; Gu, W. Reactivating the ARF-p53 axis in AML cells by targeting ULF. *Cell Cycle* **2010**, *9*, 2946–2951. [CrossRef]
97. Yu, L.; Jearawiriyapaisarn, N.; Lee, M.P.; Hosoya, T.; Wu, Q.; Myers, G.; Lim, K.-C.; Kurita, R.; Nakamura, Y.; Vojtek, A.B.; et al. BAP1 regulation of the key adaptor protein NCoR1 is critical for γ-globin gene repression. *Genes Dev.* **2018**, *32*, 1537–1549. [CrossRef]
98. Shami Shah, A.; Batrouni, A.G.; Kim, D.; Punyala, A.; Cao, W.; Han, C.; Goldberg, M.L.; Smolka, M.B.; Baskin, J.M. PLEKHA4/kramer Attenuates Dishevelled Ubiquitination to Modulate Wnt and Planar Cell Polarity Signaling. *Cell Rep.* **2019**, *27*, 2157–2170.e8. [CrossRef]
99. Khanna, R.; Krishnamoorthy, V.; Parnaik, V.K. E3 ubiquitin ligase RNF 123 targets lamin B1 and lamin-binding proteins. *FEBS J.* **2018**, *285*, 2243–2262. [CrossRef]
100. Maréchal, A.; Li, J.-M.; Ji, X.Y.; Wu, C.-S.; Yazinski, S.A.; Nguyen, H.D.; Liu, S.; Jiménez, A.E.; Jin, J.; Zou, L. PRP19 Transforms into a Sensor of RPA-ssDNA after DNA Damage and Drives ATR Activation via a Ubiquitin-Mediated Circuitry. *Mol. Cell* **2014**, *53*, 235–246. [CrossRef]
101. Tsai, Y.-C.; Greco, T.M.; Boonmee, A.; Miteva, Y.; Cristea, I.M. Functional Proteomics Establishes the Interaction of SIRT7 with Chromatin Remodeling Complexes and Expands Its Role in Regulation of RNA Polymerase I Transcription. *Mol. Cell. Proteom.* **2012**, *11*, 60–76. [CrossRef] [PubMed]
102. Colland, F.; Jacq, X.; Trouplin, V.; Mougin, C.; Groizeleau, C.; Hamburger, A.; Meil, A.; Wojcik, J.; Legrain, P.; Gauthier, J.-M. Functional Proteomics Mapping of a Human Signaling Pathway. *Genome Res.* **2004**, *14*, 1324–1332. [CrossRef] [PubMed]
103. Lleres, D.; Denegri, M.; Biggiogera, M.; Ajuh, P.; Lamond, A.I. Direct interaction between hnRNP-M and CDC5L/PLRG1 proteins affects alternative splice site choice. *EMBO Rep.* **2010**, *11*, 445–451. [CrossRef] [PubMed]
104. Lipp, J.J.; Marvin, M.C.; Shokat, K.M.; Guthrie, C. SR protein kinases promote splicing of nonconsensus introns. *Nat. Struct. Mol. Biol.* **2015**, *22*, 611–617. [CrossRef]
105. Li, X.; Wang, W.; Wang, J.; Malovannaya, A.; Xi, Y.; Li, W.; Guerra, R.; Hawke, D.H.; Qin, J.; Chen, J. Proteomic analyses reveal distinct chromatin-associated and soluble transcription factor complexes. *Mol. Syst. Biol.* **2015**, *11*, 775. [CrossRef]
106. Baranes-Bachar, K.; Levy-Barda, A.; Oehler, J.; Reid, D.A.; Soria-Bretones, I.; Voss, T.C.; Chung, D.; Park, Y.; Liu, C.; Yoon, J.B.; et al. The Ubiquitin E3/E4 Ligase UBE4A Adjusts Protein Ubiquitylation and Accumulation at Sites of DNA Damage, Facilitating Double-Strand Break Repair. *Mol. Cell* **2018**, *69*, 866–878.e7. [CrossRef]

107. Mulder, M.P.; Witting, K.; Berlin, I.; Pruneda, J.N.; Wu, K.-P.; Chang, J.-G.; Merkx, R.; Bialas, J.; Groettrup, J.B.M.; Vertegaal, A.C.; et al. A cascading activity-based probe sequentially targets E1–E2–E3 ubiquitin enzymes. *Nat. Chem. Biol.* **2016**, *12*, 523–530. [CrossRef]
108. Schwarz, S.E.; Rosa, J.L.; Scheffner, M. Characterization of Human hect Domain Family Members and Their Interaction with UbcH5 and UbcH7. *J. Biol. Chem.* **1998**, *273*, 12148–12154. [CrossRef]
109. Pao, K.-C.; Wood, N.T.; Knebel, A.; Rafie, K.; Stanley, M.; Mabbitt, P.D.; Sundaramoorthy, R.; Hofmann, K.; Van Aalten, D.M.F.; Virdee, S. Activity-based E3 ligase profiling uncovers an E3 ligase with esterification activity. *Nat. Cell Biol.* **2018**, *556*, 381–385. [CrossRef]
110. Sowa, M.E.; Bennett, E.J.; Gygi, S.P.; Harper, J.W. Defining the Human Deubiquitinating Enzyme Interaction Landscape. *Cell* **2009**, *138*, 389–403. [CrossRef]
111. Georges, A.; Coyaud, E.; Marcon, E.; Greenblatt, J.; Raught, B.; Frappier, L. USP7 Regulates Cytokinesis through FBXO38 and KIF20B. *Sci. Rep.* **2019**, *9*, 2724. [CrossRef] [PubMed]
112. Yu, C.-C.; Yang, J.-C.; Chang, Y.-C.; Chuang, J.-G.; Lin, C.-W.; Wu, M.-S.; Chow, L.-P. VCP Phosphorylation-Dependent Interaction Partners Prevent Apoptosis in Helicobacter pylori-Infected Gastric Epithelial Cells. *PLoS ONE* **2013**, *8*, e55724. [CrossRef] [PubMed]
113. Abbasi, S.; Schild-Poulter, C. Mapping the Ku Interactome Using Proximity-Dependent Biotin Identification in Human Cells. *J. Proteome Res.* **2018**, *18*, 1064–1077. [CrossRef] [PubMed]
114. Junttila, M.R.; Evan, G.I. p53—A Jack of all trades but master of none. *Nat. Rev. Cancer* **2009**, *9*, 821–829. [CrossRef] [PubMed]
115. Chen, D.; Kon, N.; Zhong, J.; Zhang, P.; Yu, L.; Gu, W. Differential Effects on ARF Stability by Normal versus Oncogenic Levels of c-Myc Expression. *Mol. Cell* **2013**, *51*, 46–56. [CrossRef]
116. Murphy, D.J.; Junttila, M.R.; Pouyet, L.; Karnezis, A.; Shchors, K.; Bui, D.A.; Brown-Swigart, L.; Johnson, L.; Evan, G.I. Distinct Thresholds Govern Myc's Biological Output In Vivo. *Cancer Cell* **2008**, *14*, 447–457. [CrossRef]
117. Ginno, P.A.; Burger, L.; Seebacher, J.; Iesmantavicius, V.; Schübeler, D. Cell cycle-resolved chromatin proteomics reveals the extent of mitotic preservation of the genomic regulatory landscape. *Nat. Commun.* **2018**, *9*, 1–12. [CrossRef]
118. Velimezi, G.; Liontos, M.; Vougas, K.; Roumeliotis, T.; Bartkova, J.; Sideridou, M.; Dereli-Oz, A.; Kocylowski, M.; Pateras, I.S.; Evangelou, K.; et al. Functional interplay between the DNA-damage-response kinase ATM and ARF tumour suppressor protein in human cancer. *Nat. Cell Biol.* **2013**, *15*, 967–977. [CrossRef]
119. Mailand, N.; Bekker-Jensen, S.; Faustrup, H.; Melander, F.; Bartek, J.; Lukas, C.; Lukas, J. RNF8 Ubiquitylates Histones at DNA Double-Strand Breaks and Promotes Assembly of Repair Proteins. *Cell* **2007**, *131*, 887–900. [CrossRef]
120. Li, M.; Brooks, C.L.; Kon, N.; Gu, W. A Dynamic Role of HAUSP in the p53-Mdm2 Pathway. *Mol. Cell* **2004**, *13*, 879–886. [CrossRef]
121. Zhu, Q.; Sharma, N.; Qianzheng, Z.; Wani, G.; A Wani, A. USP7 deubiquitinase promotes ubiquitin-dependent DNA damage signaling by stabilizing RNF168. *Cell Cycle* **2015**, *14*, 1413–1425. [CrossRef]
122. Doil, C.; Mailand, N.; Bekker-Jensen, S.; Menard, P.; Larsen, D.H.; Pepperkok, R.; Ellenberg, J.; Panier, S.; Durocher, D.; Bartek, J.; et al. RNF168 Binds and Amplifies Ubiquitin Conjugates on Damaged Chromosomes to Allow Accumulation of Repair Proteins. *Cell* **2009**, *136*, 435–446. [CrossRef] [PubMed]
123. Felsenfeld, G.; Groudine, M. Controlling the double helix. *Nat. Cell Biol.* **2003**, *421*, 448–453. [CrossRef] [PubMed]
124. Roberts, C.W.M.; Orkin, S.H. The SWI/SNF complex—Chromatin and cancer. *Nat. Rev. Cancer* **2004**, *4*, 133–142. [CrossRef]
125. Vignali, M.; Hassan, A.H.; Neely, K.E.; Workman, J.L. ATP-Dependent Chromatin-Remodeling Complexes. *Mol. Cell. Biol.* **2000**, *20*, 1899–1910. [CrossRef] [PubMed]
126. Zhu, S.; Beaulaurier, J.; Deikus, G.; Wu, T.P.; Strahl, M.; Hao, Z.; Luo, G.; Gregory, J.A.; Chess, A.; He, C.; et al. Mapping and characterizing N6-methyladenine in eukaryotic genomes using single-molecule real-time sequencing. *Genome Res.* **2018**, *28*, 1067–1078. [CrossRef]
127. Kirmizis, A. Silencing of human polycomb target genes is associated with methylation of histone H3 Lys 27. *Genes Dev.* **2004**, *18*, 1592–1605. [CrossRef]
128. Wang, H.; Wang, L.; Erdjument-Bromage, H.; Vidal, M.; Tempst, P.; Jones, R.S.; Zhang, Y. Role of histone H2A ubiquitination in Polycomb silencing. *Nat. Cell Biol.* **2004**, *431*, 873–878. [CrossRef]

129. Scheuermann, J.C.; Alonso, A.G.D.A.; Oktaba, K.; Ly-Hartig, N.; McGinty, R.K.; Fraterman, S.; Wilm, M.; Muir, T.W.; Müller, J. Histone H2A deubiquitinase activity of the Polycomb repressive complex PR-DUB. *Nat. Cell Biol.* **2010**, *465*, 243–247. [CrossRef]
130. Kloet, S.L.; Makowski, M.M.; Baymaz, H.I.; Van Voorthuijsen, L.; Karemaker, I.D.; Santanach, A.; Jansen, P.W.; Di Croce, A.S.L.; Vermeulen, M. The dynamic interactome and genomic targets of Polycomb complexes during stem-cell differentiation. *Nat. Struct. Mol. Biol.* **2016**, *23*, 682–690. [CrossRef]
131. Hoischen, A.; Van Bon, B.W.; Rodríguez-Santiago, B.; Gilissen, C.; Vissers, L.E.L.M.; De Vries, P.; Janssen, I.; Van Lier, B.; Hastings, R.; Smithson, S.F.; et al. De novo nonsense mutations in ASXL1 cause Bohring-Opitz syndrome. *Nat. Genet.* **2011**, *43*, 729–731. [CrossRef] [PubMed]
132. Henderson, J.M.; Nisperos, S.V.; Weeks, J.; Ghulam, M.; Marín, I.; Zayas, R.M. Identification of HECT E3 ubiquitin ligase family genes involved in stem cell regulation and regeneration in planarians. *Dev. Biol.* **2015**, *404*, 21–34. [CrossRef] [PubMed]
133. Hagiwara, N.; Yeh, M.; Liu, A. Sox6 is required for normal fiber type differentiation of fetal skeletal muscle in mice. *Dev. Dyn.* **2007**, *236*, 2062–2076. [CrossRef] [PubMed]
134. Krah, N.M.; De La O, J.-P.; Swift, G.H.; Hoang, C.Q.; Willet, S.G.; Pan, F.C.; Cash, G.M.; Bronner, M.P.; Wright, C.V.; Macdonald, R.J.; et al. The acinar differentiation determinant PTF1A inhibits initiation of pancreatic ductal adenocarcinoma. *eLife* **2015**, *4*, e07125. [CrossRef]
135. Borromeo, M.D.; Meredith, D.M.; Castro, D.S.; Chang, J.C.; Tung, K.-C.; Guillemot, F.; Johnson, J.E. A transcription factor network specifying inhibitory versus excitatory neurons in the dorsal spinal cord. *Development* **2014**, *141*, 2803–2812. [CrossRef]
136. Lelièvre, E.; Lek, M.; Bolje, H.; Houille-Vernes, L.; Brajeul, V.; Slembrouck, A.; Roger, J.; Sahel, J.-A.; Matter, J.-M.; Sennlaub, F.; et al. Ptf1a/Rbpj complex inhibits ganglion cell fate and drives the specification of all horizontal cell subtypes in the chick retina. *Dev. Biol.* **2011**, *358*, 296–308. [CrossRef]
137. Millen, K.J.; Steshina, E.Y.; Iskusnykh, I.Y.; Chizhikov, V.V. Transformation of the cerebellum into more ventral brainstem fates causes cerebellar agenesis in the absence of Ptf1a function. *Proc. Natl. Acad. Sci. USA* **2014**, *111*, E1777–E1786. [CrossRef]
138. Ilyas, M.; Mir, A.; Efthymiou, S.; Houlden, H. The genetics of intellectual disability: Advancing technology and gene editing. *F1000Research* **2020**, *9*, 22. [CrossRef]
139. Mendicino, A.; Sabbadini, G.; Pergola, M.S. Clark—Baraitser syndrome: Report of a new case and review of the literature. *Clin. Dysmorphol.* **2005**, *14*, 133–135. [CrossRef]
140. Louie, R.J.; Friez, M.J.; Skinner, C.; Baraitser, M.; Clark, R.D.; Schwartz, C.E.; Stevenson, R.E. Clark-Baraitser syndrome is associated with a nonsense alteration in the autosomal gene TRIP12. *Am. J. Med Genet. Part A* **2019**, *182*, 595–596. [CrossRef]
141. Doco-Fenzy, M.; Landais, E.; Andrieux, J.; Schneider, A.; Delemer, B.; Sulmont, V.; Melin, J.-P.; Ploton, M.; Thevenard, J.; Monboisse, J.-C.; et al. Deletion 2q36.2q36.3 with multiple renal cysts and severe mental retardation. *Eur. J. Med. Genet.* **2008**, *51*, 598–607. [CrossRef] [PubMed]
142. Lelieveld, S.H.; Reijnders, M.R.F.; Pfundt, R.; Yntema, H.G.; Kamsteeg, E.-J.; De Vries, P.; De Vries, B.B.A.; Willemsen, M.H.; Kleefstra, T.; Löhner, K.; et al. Meta-analysis of 2104 trios provides support for 10 new genes for intellectual disability. *Nat. Neurosci.* **2016**, *19*, 1194–1196. [CrossRef] [PubMed]
143. Iossifov, I.; O'Roak, B.J.; Sanders, S.J.; Ronemus, M.; Krumm, N.; Levy, D.; Stessman, H.A.; Witherspoon, K.T.; Vives, L.; Patterson, K.E.; et al. The contribution of de novo coding mutations to autism spectrum disorder. *Nat. Cell Biol.* **2014**, *515*, 216–221. [CrossRef] [PubMed]
144. O'Roak, B.J.; Stessman, H.A.; Boyle, E.A.; Witherspoon, K.T.; Martin, B.; Lee, C.; Vives, L.; Baker, C.; Hiatt, J.B.; Nickerson, D.A.; et al. Recurrent de novo mutations implicate novel genes underlying simplex autism risk. *Nat. Commun.* **2014**, *5*, 1–6. [CrossRef]
145. Zhang, J.; Gambin, T.; Yuan, B.; Szafranski, P.; Rosenfeld, J.A.; Al Balwi, M.; Alswaid, A.; Al-Gazali, L.; Al Shamsi, A.M.; Komara, M.; et al. Haploinsufficiency of the E3 ubiquitin-protein ligase gene TRIP12 causes intellectual disability with or without autism spectrum disorders, speech delay, and dysmorphic features. *Qual. Life Res.* **2017**, *136*, 377–386. [CrossRef]
146. Takata, A.; Miyake, N.; Tsurusaki, Y.; Fukai, R.; Miyatake, S.; Koshimizu, E.; Kushima, I.; Okada, T.; Morikawa, M.; Uno, Y.; et al. Integrative Analyses of De Novo Mutations Provide Deeper Biological Insights into Autism Spectrum Disorder. *Cell Rep.* **2018**, *22*, 734–747. [CrossRef]

147. Ruzzo, E.K.; Pérez-Cano, L.; Jung, J.Y.; Wang, L.K.; Kashef-Haghighi, D.; Hartl, C.; Singh, C.; Xu, J.; Hoekstra, J.N.; Leventhal, O.; et al. Inherited and De Novo Genetic Risk for Autism Impacts Shared Networks. *Cell* **2019**, *178*, 850–866.e26. [CrossRef]
148. Stessman, H.A.F.; Xiong, B.; Coe, B.P.; Wang, T.; Hoekzema, K.; Fenckova, M.; Kvarnung, M.; Gerdts, J.; Trinh, S.; Cosemans, N.; et al. Targeted sequencing identifies 91 neurodevelopmental-disorder risk genes with autism and developmental-disability biases. *Nat. Genet.* **2017**, *49*, 515–526. [CrossRef]
149. Cerami, E.; Gao, J.; Dogrusoz, U.; Gross, B.E.; Sumer, S.O.; Aksoy, B.A.; Jacobsen, A.; Byrne, C.J.; Heuer, M.L.; Larsson, E.; et al. The cBio Cancer Genomics Portal: An Open Platform for Exploring Multidimensional Cancer Genomics Data: Figure 1. *Cancer Discov.* **2012**, *2*, 401–404. [CrossRef]
150. Gao, J.; Aksoy, B.A.; Dogrusoz, U.; Dresdner, G.; Gross, B.; Sumer, S.O.; Sun, Y.; Jacobsen, A.; Sinha, R.; Larsson, E.; et al. Integrative Analysis of Complex Cancer Genomics and Clinical Profiles Using the cBioPortal. *Sci. Signal.* **2013**, *6*, pl1. [CrossRef]
151. Yoo, N.J.; Park, S.W.; Lee, S.H. Frameshift mutations of ubiquitination-related genes HERC2, HERC3, TRIP12, UBE2Q1 and UBE4B in gastric and colorectal carcinomas with microsatellite instability. *Pathology* **2011**, *43*, 753–755. [CrossRef] [PubMed]
152. Hein, R.; Network, T.G.; Flesch-Janys, D.; Dahmen, N.; Beckmann, L.; Lindström, S.; Schoof, N.; Czene, K.; Mittelstraß, K.; Illig, T.; et al. A genome-wide association study to identify genetic susceptibility loci that modify ductal and lobular postmenopausal breast cancer risk associated with menopausal hormone therapy use: A two-stage design with replication. *Breast Cancer Res. Treat.* **2013**, *138*, 529–542. [CrossRef] [PubMed]
153. Li, G.; Yi, S.; Yang, F.; Zhou, Y.; Ji, Q.; Cai, J.; Mei, Y. Identification of mutant genes with high-frequency, high-risk, and high-expression in lung adenocarcinoma. *Thorac. Cancer* **2014**, *5*, 211–218. [CrossRef]
154. Cacheux, W.; Dangles-Marie, V.; Rouleau, E.; Lazartigues, J.; Girard, E.; Briaux, A.; Mariani, P.; Richon, S.; Vacher, S.; Buecher, B.; et al. Exome sequencing reveals aberrant signalling pathways as hallmark of treatment-naive anal squamous cell carcinoma. *Oncotarget* **2017**, *9*, 464–476. [CrossRef] [PubMed]
155. Shiba, N.; Yoshida, K.; Hara, Y.; Yamato, G.; Shiraishi, Y.; Matsuo, H.; Okuno, Y.; Chiba, K.; Tanaka, H.; Kaburagi, T.; et al. Transcriptome analysis offers a comprehensive illustration of the genetic background of pediatric acute myeloid leukemia. *Blood Adv.* **2019**, *3*, 3157–3169. [CrossRef] [PubMed]
156. Sakamoto, H.; Attiye, M.; Gerold, J.M.; Makohon-Moore, A.P.; Hayashi, A.; Hong, J.; Kappagantula, R.; Zhang, L.; Melchor, J.P.; Reiter, J.G.; et al. The Evolutionary Origins of Recurrent Pancreatic Cancer. *Cancer Discov.* **2020**, *10*, 792–805. [CrossRef] [PubMed]
157. Gao, P.; Jin, Z.; Cheng, Y.; Cao, X. RNA-Seq analysis identifies aberrant RNA splicing of TRIP12 in acute myeloid leukemia patients at remission. *Tumor Biol.* **2014**, *35*, 9585–9590. [CrossRef]
158. Horvat, A.; Noto, J.M.; Ramatchandirin, B.; Zaika, E.; Palrasu, M.; Wei, J.; Schneider, B.G.; El-Rifai, W.; Peek, R.M.; Zaika, A.I. Helicobacter pylori pathogen regulates p14ARF tumor suppressor and autophagy in gastric epithelial cells. *Oncogene* **2018**, *37*, 5054–5065. [CrossRef]
159. Wang, L.; Zhang, P.-J.; Molkentine, D.P.; Chen, C.; Molkentine, J.; Piao, H.; Raju, U.; Zhang, J.; Valdecanas, D.R.; Tailor, R.C.; et al. TRIP12 as a mediator of human papillomavirus/p16-related radiation enhancement effects. *Oncogene* **2016**, *36*, 820–828. [CrossRef]
160. Molkentine, J.M.; Molkentine, D.P.; Bridges, K.A.; Xie, T.; Yang, L.; Sheth, A.; Heffernan, T.P.; Clump, D.A.; Faust, A.Z.; Ferris, R.L.; et al. Targeting DNA damage response in head and neck cancers through abrogation of cell cycle checkpoints. *Int. J. Radiat. Biol.* **2020**, 1–8. [CrossRef]

II. Annexe 2 - Article : « *The E3 ubiquitin ligase TRIP12 participates in cell cycle progression and chromosome stability* »

www.nature.com/scientificreports

SCIENTIFIC REPORTS
nature research

OPEN

The E3 ubiquitin ligase TRIP12 participates in cell cycle progression and chromosome stability

D. Larrieu[1], M. Brunet[1], C. Vargas[1], N. Hanoun[1], L. Ligat[1], L. Dagnon[1], H. Lulka[1], R. M. Pommier[2], J. Selves[3], B. E. Jády[3], L. Bartholin[2], P. Cordelier[1], M. Dufresne[1] & J. Torrisani[1*]

Several studies have linked the E3 ubiquitin ligase TRIP12 (Thyroid hormone Receptor Interacting Protein 12) to the cell cycle. However, the regulation and the implication of this protein during the cell cycle are largely unknown. In this study, we show that TRIP12 expression is regulated during the cell cycle, which correlates with its nuclear localization. We identify an euchromatin-binding function of TRIP12 mediated by a N-terminal intrinsically disordered region. We demonstrate the functional implication of TRIP12 in the mitotic entry by controlling the duration of DNA replication that is independent from its catalytic activity. We also show the requirement of TRIP12 in the mitotic progression and chromosome stability. Altogether, our findings show that TRIP12 is as a new chromatin-associated protein with several implications in the cell cycle progression and in the maintenance of genome integrity.

TRIP12 (Thyroid Hormone Receptor Interacting Protein 12) is a 225 kDa HECT (Homologous to the E6-AP Carboxyl Terminus) domain-containing E3 ubiquitin ligase. It is also known as ULF (Ubiquitin Ligase for ARF)[1] and UFD4 (Ubiquitin Fusion Degradation) in S. cerevisae[2]. TRIP12 contains protein interacting WWE (tryptophan and glutamate conserved residues) and β-ARM (β-Armadillo) domains[3]. Several functions are attributed to TRIP12. For instance, it ubiquitinates APP-BP1 (Amyloid Precursor Protein-Binding Protein 1) and BAF57 (Brg1-Associated Factor 57) turn over and is therefore described as a sensor of SWI/SNF (SWItch/Sucrose Non-Fermentable) complex integrity[4,5]. TRIP12 is also known to control the histone ubiquitination after DNA breakage[6] and to contribute to p14/ARF (Alternate Reading Frame) degradation in response to DNA damage[7]. TRIP12 ensures the proteolysis of ASLX1 (Additional Sex Combs Like 1, Transcriptional Regulator), a regulatory component of the ubiquitin hydrolase BAP1 (BRCA1 Associated Protein 1)[8]. We showed that TRIP12 is implicated in the proteasome-mediated degradation of the transcription factor PTF1a (Pancreas specific Transcription Factor 1a) that plays an important role in the maintenance of the acinar phenotype in human pancreas[9]. TRIP12 is essential for cell viability as a homozygous mutation that disrupts the ubiquitin ligase activity leads to murine embryonic lethality[10]. Importantly, TRIP12 plays an important role in the cell cycle. For instance, $^{Trip12\ mt/mt}$ ES cells display reduced growth with increased expression of the p16/CDKN2A gene and an accumulation in G_2/M phase[10]. Moreover, by controlling the tumor suppressor protein p14/ARF, TRIP12 impacts TP53 protein level, a major regulator of the cell cycle[11]. TRIP12 expression is altered in several types of cancer, such as breast and pancreatic cancer[11]. High expression of TRIP12 is associated with poor prognosis in hepatocellular carcinoma after surgical resection[12]. TRIP12 is involved in radio-sensitization of head and neck squamous carcinoma[13]. TRIP12 mutations are also related to autism disorders[14] and intellectual disability[15].

Cell cycle progression is governed by sequentially organized events. Mitogen signaling pathways impose to the cell the exit of G_1 phase to duplicate its genome. The licensing of replication (Minute Chromosome Maintenance) to form the pre-replication complex (pre-RC). In S phase, the origins firing is dependent of the assembly of other proteins and the activity of CDKs (Cyclin Dependent Kinase). A multitude of additional factors are then recruited such as RPA (Replication Protein A), PCNA (Proliferating Cell Nuclear Antigen) and polymerases to

[1]Université de Toulouse, INSERM, Université Toulouse III-Paul Sabatier, Centre de Recherches en Cancérologie de Toulouse, Toulouse, France. [2]Université de Lyon, Université Claude Bernard Lyon 1, INSERM 1052, CNRS 5286, Centre Léon Bérard, Centre de recherche en cancérologie de Lyon, Lyon, 69008, France. [3]Laboratoire de Biologie Moléculaire Eucaryote du CNRS, UMR5099, Centre de Biologie Intégrative, Université Toulouse III-Paul Sabatier, Toulouse, Cedex 9, France. *email: jerome.torrisani@inserm.fr

constitute the fully functional replisome[16]. DNA replication is spatio-temporally ordered. Replication of euchromatin regions occurs in early S phase whereas heterochromatin regions in late S phase[17]. Subsequently, cells enter in a transition phase G_2 that ensures the complete DNA replication. In late G_2 phase, the initiation of mitosis is promoted by a complex comprising of the CYCLIN B1 and the Cyclin-Dependent Kinase 1 (CDK1)[18]. This complex is inhibited by the phosphorylation of Tyrosine 15 residue on CDK1 by the WEE1 kinase[19]. Chromatin condensation, separation of duplicated centrosomes and the recruitment of proteins to the kinetochores, all mark the prophase. The resulting release of chromosomes activates the Spindle Assembly Checkpoint (SAC) that controls the proper segregation of chromosomes and inhibits the Anaphase Promoting Complex/Cyclosome (APC/C) complex. In metaphase, the correct attachment of chromosomes to the kinetochores inhibits the SAC allowing for progression and ending of mitosis[20–22]. Mitotic dysfunction leads to chromosomal instability and aneuploidy favoring the initiation of cancer[23]. A prolonged activation of the SAC can provoke cell death or mitotic exit without separation of sister chromatids; named mitotic slippage. Improper separation of sister chromatids (anaphase bridges) induces the formation of micronuclei, which can be at the origin of DNA damages[24]. The succession of the different cell cycle phases requires a perfectly coordinated expression and activation of multiple proteins. This coordination is ensured by a multi-layer regulation including transcription, mRNA degradation, translation, post-translation modification and protein degradation[25]. For instance, protein expression of CYCLIN A begins in S phase, peaks during G_2 phase and dramatically declines in mitosis. It combines a tight coordination of transcription, mRNA translation and protein degradation.

Among the proteins that participate in cell cycle regulation, a significant proportion interacts with chromatin to modulate, for instance, the transcription (i.e.: transcription factors) and the chromatin structure (i.e.: histones, chromatin remodeling complexes, condensin). These proteins can bind to chromatin by recognition to a specific DNA consensus sequence *via* different DNA-binding domains. (i.e.: β-Helix-Loop-Helix, zinc fingers) but also *via* intrinsically disordered regions (IDR). IDRs are protein domains that lack a stable 3D structure under physiological conditions. IDRs can be predicted from the amino acid sequence according to their physicochemical properties[26]. They interact with DNA in a nucleotide sequence-independent manner, thereby modifying chromatin structure and regulating gene expression[27].

Our findings expose for the first time that TRIP12 protein expression is tightly regulated during cell cycle, and, that TRIP12 interacts with euchromatin through a new functional N-terminal domain. By means of this chromatin interaction, we further propose that TRIP12 participates in mitotic entry by controlling duration of DNA replication. We further demonstrate that TRIP12 is implicated in mitotic progression and in chromosome stability.

Results

TRIP12 expression is regulated during the cell cycle. The E3 ubiquitin ligase TRIP12 was shown to control the expression of important regulators of the cell cycle progression. However, the regulation of TRIP12 during the cell cycle is still unknown. To address this issue, HelaS3 cells were arrested at the G_1/S boundary and released in the cell cycle (Fig. 1A). The experiment showed a maximal percentage (10.1%) of cells in early mitosis 8 h after release and a maximal percentage of cells in G_1 phase (69.6%) 11 h after release. The level of *Trip12* mRNA was measured and did not fluctuate during the cell cycle kinetics (Fig. 1B). As a control, we measured the expression of *Cyclin B1* mRNA level that is known to be up-regulated in early S phase until G_2 phase[28]. Similarly, *Trip12* mRNA level did not vary in G_1-, early S- and G_2-phase-enriched cell populations unlike *Cyclin B1* mRNA (Fig. 1C,D), that confirms our results (Fig. 1B).

Next, TRIP12 protein level was measured following the same kinetics (Fig. 1E). Present in S phase, TRIP12 expression gradually increases to reach a maximal expression in G_2 phase and mitosis. Interestingly, TRIP12 protein level decreased to reach a minimal expression when cells enter in G_1 phase. TRIP12 protein level was also measured in enriched cell populations in G_1, early S, and G_2 phase (Fig. 1F). As expected, TRIP12 protein was barely detected in G_1 phase, appears in early S phase to reach a maximal expression in G_2 phase. These results clearly demonstrate that TRIP12 protein expression varies throughout the cell cycle while its mRNA remains at a constant level and, they suggest that TRIP12 protein is degraded during G_1 phase, or *Trip12* mRNA translation is tightly regulated, or a combination of both.

TRIP12 is a cell cycle-regulated nuclear protein associated with chromatin. We tested whether TRIP12 cell-cycle regulation correlated with its sub-cellular localization. First, we first showed that TRIP12 is a nuclear protein but it is not present in all cells (Figs. 2A,B and S1A). The specificity of TRIP12 nuclear staining was verified (Fig. S1B). Interestingly, TRIP12 nuclear staining did not colocalize with dense DAPI regions that correspond to peri-nuclear and peri-nucleolar heterochromatin regions (Fig. 2B), suggesting that TRIP12 preferentially colocalizes with euchromatin regions. TRIP12 nuclear localization was assessed during the cycle of asynchronous HelaS3 cells. We found that TRIP12 is barely detectable in late G_1 cells and appears in early S phase cells reaching a maximal detection in late S and G_2 cells (Fig. 2C). TRIP12 absent-cells observed in Fig. 2B correspond to cells in G_1 phase. It is known that euchromatin regions are replicated early during S phase and are stained homogenously after EDU incorporation. On the contrary, heterochromatin regions are replicated late in S phase and form punctiform staining with EDU. Interestingly, TRIP12 staining corresponds to DNA regions with homogenous and not punctiform EDU staining (Fig. 2C), corroborating the localization of TRIP12 on euchromatin regions (Fig. 2B). Cell cycle-dependent presence of TRIP12 in the nucleus was confirmed in G_1-, early S- and G_2-phase enriched cell populations (Figs. 2D and S1C). We clearly visualized TRIP12 association with chromatin in mitotic cells in which chromatin is subject to condensation and decondensation (Fig. 2E). TRIP12-chromatin association was also confirmed by chromatin-bound protein fractionation (Fig. 2F). The colocalization with chromatin during metaphase was also observed using a HA-tagged TRIP12 construct (Fig. S2A). Chromosome spreading experiments revealed that TRIP12 colocalizes with chromatin on full-length chromosomes (Figs. 2G and S2B).

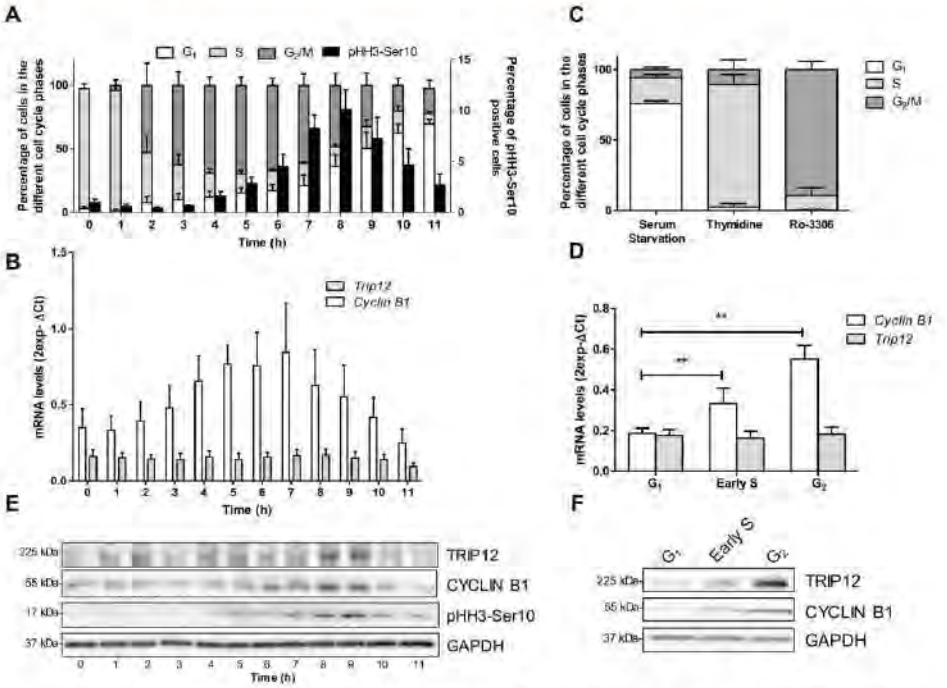

Figure 1. TRIP12 expression is regulated during the cell cycle. (**A**) Distribution of cells in the different phases of the cell cycle and the percentage of pHH3-Ser10 positive cells (black bars) were assessed by flow cytometry in HelaS3 cells arrested in early S phase using a double thymidine block and released in fresh medium for the indicated times. The bars represent the mean ± SEM obtained from three different experiments. (**B**) Expression level of *Trip12* and *Cyclin B1* mRNA was measured by RT-qPCR in HelaS3 cells arrested in early S phase using a double thymidine block and released in fresh medium for the indicated times. The bars represent the mean ± SEM of mRNA levels (expressed as $2^{exp-\Delta Ct}$) obtained from three different experiments. (**C**) Distribution of HelaS3 cells in the different phases of the cell cycle after serum starvation, double thymidine block and RO-3306 treatments was determined by flow cytometry. The bars represent the percentage expressed as a mean ± SEM obtained from three different experiments. (**D**) Expression level of *Trip12* and *Cyclin B1* mRNA was measured by RT-qPCR in HelaS3 cells were arrested in G_1, early S, and G_2 phase using serum starvation, double thymidine block and Ro-3306, respectively. The bars represent the mean ± SEM of mRNA levels (expressed as $2^{exp-\Delta Ct}$) obtained from three different experiments. ** indicates a p value < 0.01. (**E**) TRIP12, CYCLIN B1 and pHH3-Ser10 level was measured by Western blot analysis in HelaS3 cells arrested in early S phase using a double thymidine block and released in fresh medium for the indicated times. GADPH protein level was used as loading control. Images were obtained from the same experiment and representative of three different experiments. (**F**) TRIP12 and CYCLIN B1 levels were measured by Western blot analysis in HelaS3 cells arrested in G_1, early S and G_2 phase using serum starvation, double thymidine block and Ro-3306 treatments, respectively. GADPH protein level was used as loading control. Images were obtained from the same experiment and representative of three different experiments.

TRIP12 is associated with chromatin through a N-terminal intrinsically disordered region. We identified several IDRs in the TRIP12 sequence that could potentially act as chromatin interacting-domains, notably one in the N-terminus located between the amino-acids 1 and 440 (Fig. 3A). An analysis in metaphasic cells showed that TRIP12 colocalization with chromatin is mediated by its N-terminal IDR. Whereas the deletion of the C-terminal HECT domain (TRIP12(1-1552)-GFP) does not affect the capacity of the fusion protein to colocalize with chromatin, the deletion of the IDR (TRIP12(446-1992)-GFP) abolishes it (Fig. 3B). In parallel, the subcellular localization of full-length TRIP12-GFP and four TRIP12-GFP deletion constructs in cells in interphase led us to conclude that, similar to endogenous TRIP12, TRIP12(1-1992)-GFP localizes exclusively in the nuclear compartment. More importantly, the TRIP12(1-445)-GFP localizes in the nucleus demonstrating that the N-terminal IDR is sufficient for the nuclear localization of TRIP12; suggesting that this region contains a nuclear localization signal (Fig. 3C). Moreover, IDR alone can ensure a physical direct interaction with naked DNA (Fig. 3D) and the localization of GFP on full-length metaphasic chromosomes (Figs. S2A and S3B). The

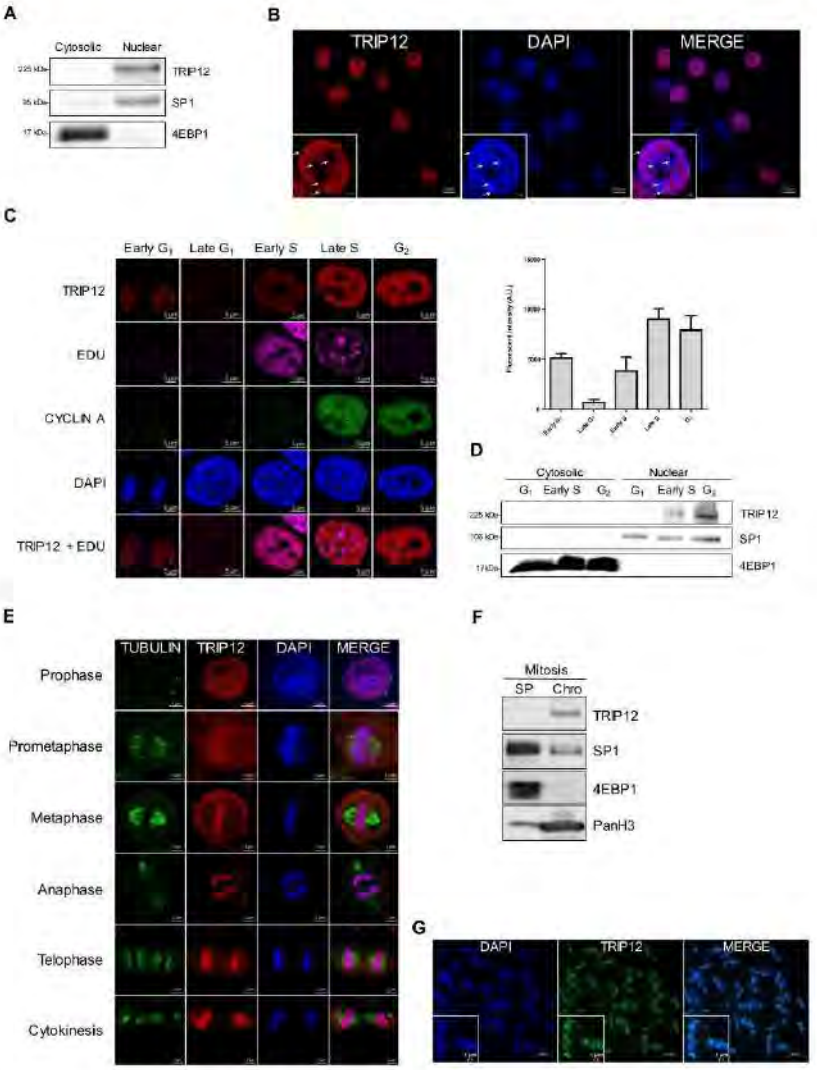

Figure 2. TRIP12 is a cell cycle-regulated nuclear protein associated with chromatin. (**A**) TRIP12 protein level in cytosolic and nuclear fractions of HelaS3 cells was measured by Western blot analysis. SP1 and 4EBP1 protein levels were used as purity controls of subcellular fractions. Images were obtained from the same experiment and representative of three different experiments. (**B**) TRIP12 subcellular localization in HelaS3 cells was determined by immunofluorescence using TRIP12 antibody (Sigma). The inset represents TRIP12 nuclear localization at a higher magnification. Nuclei were counterstained with DAPI. The white arrows indicate the peri-nucleolar and peri-nuclear heterochromatin regions. (**C**) TRIP12 nuclear expression in HelaS3 cells in the different phases of the cell cycle was determined by immunofluorescence using TRIP12 antibody (Sigma). Nuclei were counterstained with DAPI. Cells in G_1 phase and G_2 phase correspond to CYCLIN A/EDU nuclear negative cells and CYCLIN A nuclear positive/EDU negative cells, respectively. Cells in early G_1 correspond to G_1 cells with small oblong-shaped nucleus. Cells in early S and late S phase correspond to EDU positive cells/CYCLIN A negative and positive nuclear cells, respectively. The graph represents the mean TRIP12 expression (integrated density-background) ± SEM determined at least 200 cells using FIJI software. (**D**) Level of TRIP12 in cytosolic and nuclear protein fraction of G_1-, early S- and G_2-phase enriched HelaS3 cell populations was measured by Western blot analysis. SP1 and 4EBP1 protein levels were used as purity control of subcellular

fractions. Images were obtained from the same experiment and representative of three different experiments. (**E**) TRIP12 and γ-TUBULIN localization in HelaS3 cells in prophase, prometaphase, metaphase, anaphase, telophase and cytokinesis were visualized by immunofluorescence. Nuclei were counterstained with DAPI. (**F**) TRIP12 expression in soluble protein (SP) and chromatin-bound (Chro) protein fractions (40 µg for each fraction) obtained from nocodazole-treated mitotic HelaS3 cells was measured by Western blot analysis. As mitotic cells do not have nuclear membrane, SP fraction contains cytoplasmic and nuclear soluble proteins. SP1, 4EBP1 and panH3 protein levels were used as purity control of the different fractions. Images were obtained from the same experiment. (**G**) TRIP12 localization on metaphasic chromosomes was visualized by immunofluorescence using anti-TRIP12 antibody (Sigma) after chromosome spreading of HelaS3 cells treated with Ro-3306 and released in the cell cycle for 45 min. DNA was counterstained with DAPI. The inset represents a magnification of TRIP12 localization on two individual chromosomes.

colocalization of TRIP12 and its IDR with chromatin was confirmed in living cells (Figs. S3C). A more precise analysis of the IDR reveals that the region between the amino acids 107 and 325 ensures the interaction of TRIP12 with chromatin (Fig. S3D,E). Interestingly, cells that express a high level of the IDR construct display characteristic features of cells in prophase with condensed chromosomes covering the inner face of the nuclear membrane (Fig. S3F) even if they are not pHH3-Ser10 positive (Fig. S3G, bottom panel) as they should be a normal cell (Top panel). This suggests that TRIP12 *via* its IDR could participate in chromatin compaction.

Altogether, our experiments identify a new functional domain of TRIP12 that permits the association of the protein with chromatin.

A deregulated expression of TRIP12 affects cell division and mitotic entry. Given that TRIP12 expression and chromatin association are cell cycle dependent, we tested the consequences of a TRIP12 ectopic over-expression on cell fate during 48 h. We found that only 26.7% (8 out of 30) of TRIP12(1-1992)-GFP cells undergo two cell divisions or more (Figs. 4A and S4A,B) with a duration in interphase of 19.2 h (Fig. 4B). The remaining 73.7% (22 out of 30) fail to achieve a single division and die (Figs. 4A and S4A,B). Remarkably, this death occurs at a time (20.1 h) that mitosis should occur (Fig. 4B) suggesting that TRIP12 overexpression is deleterious for the mitotic division. This inhibitory effect on cell division was also observed after expression of an inactive mutant as well as several TRIP12 protein domains with the exception of the IDR of TRIP12 (Figs. 4A,B and S4A–E) suggesting that the mitotic inhibitory effect of TRIP12 is independent of chromosome binding and catalytic activity. We further demonstrated that TRIP12 over-expression diminishes the percentage of cells that enter in mitosis (Fig. 4C). When we focused on TRIP12(1-1992)-GFP expressing cells that undergo cell divisions (Fig. S4A), we noticed that TRIP12 over-expression significantly delays the entry into prophase 30 min after Ro-3306 release (Fig. 4D, Graph).

The inhibitory effect of TRIP12 over-expression on mitotic entry led us to investigate the consequences of a TRIP12 depletion on mitotic entry. Toward this end, TRIP12-depleted (ShTRIP12) and control (ShScr) cells were created using shRNAs (Fig. 5A,B). After Ro-3306 release (30 min), we microscopically observed an accelerated mitotic entry in TRIP12-depleted cells (Fig. 5C) that was associated to a higher percentage of cells in late prometaphase and metaphase (Fig. 5D). The accelerated mitotic entry was confirmed by flow cytometry-measurements of pHH3-Ser10 positive cells (Fig. 5E). A normal mitotic entry of TRIP12-depleted cells was restored by a transient expression of TRIP12 or the catalytic mutant but not by an expression of the IDR (Fig. S5A).

Altogether, these experiments reveal the important contribution of TRIP12 in mitotic entry as a deregulated expression of TRIP12 significantly impedes the proper setting of mitotic entry-regulatory mechanisms.

A shortened duration of DNA replication explains the accelerated mitotic entry of TRIP12-depleted cells. We next aimed to determine the causes of the accelerated mitotic entry of TRIP12-depleted cells. Mitotic entry is governed by a succession of events that leads to the condensation and the segregation of chromosomes into daughter cells. Among them, the Tyr15-dephosphorylation of CDK1 and the kinase WEE1-cytosolic translocation are essential[29,30]. In Ro-3306 cells, we simultaneously found a decreased level of phosphorylation on CDK1-Tyr15 in the nuclear fraction of TRIP12-depleted cells and a WEE1 translocation from the nuclear to the cytosolic fraction (Figs. 6A and S5B) which provokes the accelerated entry in prophase when the Ro-3306 is removed (Fig. S5C). It is reported that the cytosolic translocation of WEE1 is mediated by CYCLIN A nuclear import which begins early during S phase to allow DNA replication *via* the activation of the kinase CDK2[31,32]. We measured an increase in CYCLIN A expression in the nuclear fraction that is associated to a decreased expression in cytosolic fraction of these cells (Figs. 6B and S5D). This corroborates with a significant increased proportion of cells with CYCLIN A nuclear staining in TRIP12-depleted cells (Fig. 6C). The important role of CYCLIN A in DNA replication led us to investigate the status of DNA replication in CYCLIN A nuclear-positive cells. Our analyses revealed a higher percentage of TRIP12-depleted cells with achieved DNA replication (G_2-phase cells) and therefore set for mitotic entry (Fig. 6C). More importantly, these results strongly suggest that a TRIP12 depletion accelerates DNA replication. By measuring the duration of S phase, we verified that TRIP12-depleted cells have shortened S phase as compared to controls (Fig. 6D). Euchromatin regions are replicated early during S phase when heterochromatin regions are replicated in late S phase. Interestingly, we measured in EDU-positive asynchronous cells a higher proportion of cells in late S phase in TRIP12-depleted cells demonstrating that the depletion of TRIP12 specifically accelerates the DNA replication of euchromatin regions. This result is in accordance with the fact that TRIP12 preferentially colocalizes with euchromatin regions (Fig. 2B,C).

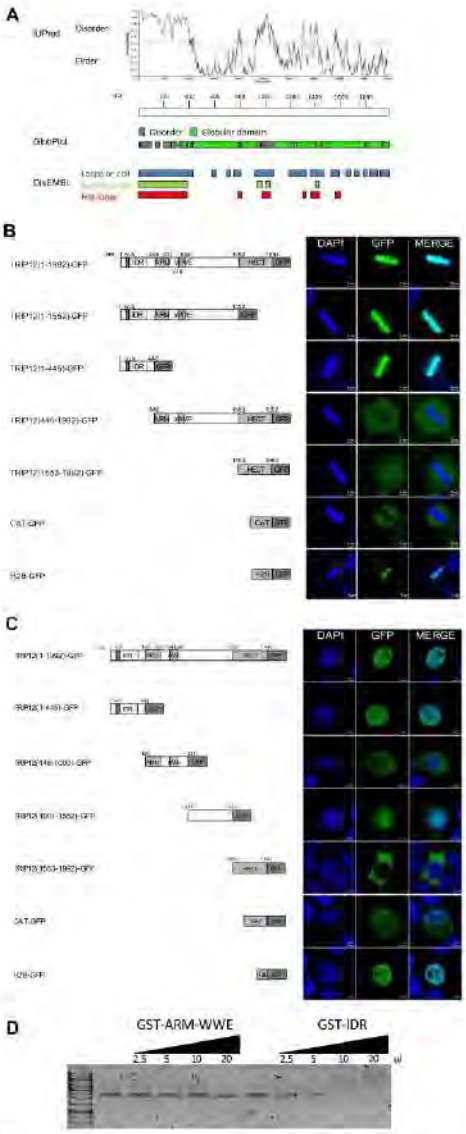

Figure 3. TRIP12 is associated with chromatin through a N-terminal intrinsically disordered region. (**A**) Prediction of intrinsically disordered and ordered regions in TRIP12 protein sequence (Protein accession number NP_004229.1) was determined using IUPred, GlobPlot and DisEMBL software. aa stands for amino acids. (**B**) GFP-fusion protein localization in metaphasic HelaS3 cells transfected with TRIP12 (1-1992), (1-1552), (1-445), (446-1992) and (1553-1992)-GFP constructs was visualized by immunofluorescence using an anti-GFP antibody. H2B-GFP and CAT-GFP constructs were used as controls. Nuclei were counterstained with DAPI. IDR stands for Intrinsically Disordered Region, NLS for Nuclear Localization Signal, ARM for β-Armadillo domain, WWE for tryptophan and glutamate enriched domain and HECT for Homologous to the E6-AP Carboxyl Terminus. Numbers indicate amino acids (aa) position. (**C**) GFP-fusion protein localization in interphasic HelaS3 cells transfected with TRIP12 (1-1992), (1-445), (446-1000), (1001-1552) and (1553-1992)-GFP constructs was analyzed by immunofluorescence using an anti-GFP antibody. H2B-GFP and CAT-GFP constructs were used as controls. Nuclei were counterstained with DAPI. IDR stands for Intrinsically

Disordered Region, ARM for β-Armadillo domain, WWE for tryptophan and glutamate enriched domain and HECT for Homologous to the E6-AP Carboxyl Terminus. Numbers indicate amino acids (aa) position. (**D**) Interaction of increasing amounts of GST-TRIP12-ARM-WWE(446-1000) and GST-IDR(1-325) with naked plasmid DNA visualized after migration on agarose gel.

A TRIP12 depletion prolongs the SAC activation, leads to chromosome segregation defects and cell growth inhibition. In addition to accelerate DNA replication, we observed that a TRIP12 depletion can lead to other cellular alterations such as a prolonged activation of the SAC. We observed that in control cells, the percentage of pHH3-Ser10 positive cells reaches a maximum at = 60 min before the physiological loss of pHH3-Ser10 at the metaphase-to-anaphase transition (Fig. 5E). In contrast, this percentage persists at a maximal level for 60 min (t = 30 min to t = 90 min) in TRIP12-depleted cells suggesting an inhibition of the metaphase/anaphase transition. This inhibition could be due to a prolonged activation of the SAC or a default of the APC/C complex. The use of reversine, a SAC inhibitor, proved a prolonged activation of the SAC in absence of TRIP12 (Fig. S5E). We confirmed the extended duration of prometaphase-metaphase by measuring a significantly increased duration of prometaphase (from invagination of the nuclear membrane) to metaphase in TRIP12-depleted cells (90.1 min) compared to control cells (53.5 min) (Fig. 7A,B). Additionally, we observed that TRIP12-depleted cells largely fail to transit from metaphase to anaphase (32.3% vs 3.7%). Among them, 36% exit mitosis by mitotic slippage and 64% die (Fig. 7C). Cell death and mitotic slippage are two processes by which cells overcome an extended arrest in prometaphase. A long term arrest in prometaphase and cohesion fatigue can lead to different chromosome segregation abnormalities such as the formation of chromosome laggings, anaphase bridges and alterations that are visible in interphasic cells such as micronuclei or giant nuclei (consequence of mitotic slippage). Among cells that achieve the metaphase-to-anaphase transition, our analysis revealed a higher percentage of chromosome lagging, anaphase bridges, micronuclei and giant nuclei in ShTRIP12 cells (Figs. 7D–E and S5F). These results indicate that TRIP12 also ensures the maintenance of chromosome integrity and therefore the stability of the genome.

The consequences of TRIP12 depletion on S phase duration, mitotic entry and progression led us to investigate the effects on cellular growth. Interestingly, a depletion of TRIP12 provokes a significant diminution of cell growth (30.3% after 72 h) *in vitro* (Fig. 7F) also visible by colony formation assay (Fig. 7G) and *in vivo* in SCID mouse model after sub-cutaneous injections (Fig. 7H). This reduced cell growth was associated to an accumulation of cells in G_2/M phase (Fig. 7I) that could be explained by the combination of the increased duration of prometaphase-metaphase (Fig. 7B) and the higher percentage of cells that exit mitosis by mitotic slippage with 4n DNA content (Fig. 7C). Moreover, this reduced growth is accompanied by an increased proportion of sub-G_1 cells (Fig. 7I) which could correspond to the TRIP12-depleted cells that die at the metaphase-to-anaphase transition (Fig. 7C).

Discussion

The E3 ubiquitin ligase TRIP12 was linked to the control of cell cycle regulators (*i.e.*: p14/ARF, p16/CDKN2A)[10]. In this study, we provide evidence that TRIP12 expression varies during the cell cycle and correlates with its nuclear localization. More importantly, we identify a functional N-terminal domain that confers to TRIP12 the capacity to strongly associate with euchromatin. We demonstrate the requirement of TRIP12 in mitotic entry by affecting the duration of S phase. Moreover, we reveal the implication of TRIP12 in the control of SAC activation, proper chromosome segregation and in cell proliferation.

In line with the implication in mitotic entry, TRIP12 over-expression and depletion alter initiation of mitosis. Therefore, fine-tuning of TRIP12 expression and/or activity is essential for the control of this phase. Similar observations are reported for other important mitotic proteins such as CYCLIN A. Indeed, CYCLIN A over-expression delays chromosome alignment and sister chromatid segregation[33]. The knock down of CYCLIN A by siRNA strategy delays the entry into mitosis by postponing cells in G_2 phase[34]. Although the mechanisms that govern its expression during the cell cycle need to be further studied, our findings indicate that *de novo Trip12* mRNA expression is not involved. These observations corroborate the *Whitfield et al.* study, which provides an exhausting list of HelaS3 mRNAs that fluctuate during cell cycle[35]. *Trip12* mRNA is not present in this list. It is plausible that induction of TRIP12 protein expression in S phase could be mediated by an IRES (Internal Ribosome Entry site) dependent-translational regulation as demonstrated for *Aurora A kinase* mRNA[36]. Comparative proteomics approaches during cell cycle identified TRIP12 as a newly synthetized protein in S phase which is in favor of a translational regulation of *TRIP12* mRNA during cell cycle[37]. Moreover, the disappearance of TRIP12 from the nucleus in G_1 phase-cells could imply its degradation by the proteasome mediated by APC/C-dependent ubiquitination as TRIP12 possesses putative KEN box (aa 1496–1570/UniProt source) and Destruction boxes (aa 859–867 and aa 1546–1554/ELM resource). This degradation mechanism may explain the decrease of TRIP12 expression. However, other actors that ensure TRIP12 stability remain to be identified. Similar to UHRF1, TRIP12 is stabilized by USP7[12]. During mitosis, CDK1 initiates UHRF1 degradation by phosphorylating the USP7-interacting domain[38]. The same mechanism could exist for TRIP12 degradation since a recent quantitative phospho-proteome approach identified serine 424 residue of TRIP12 as a CDK1 phosphorylation target[39]. Moreover, our preliminary results are in favor of a role of USP7 in the cell cycle regulation of TRIP12. Therefore, the variation of TRIP12 expression during cell cycle likely involves different layers of regulation including translation efficiency and protein stabilization.

Another pressing question is whether TRIP12 exerts its function in mitotic entry through its catalytic activity or by protein-protein interaction. Our observations favor a catalytically-independent function (Figs. 4A,B and S4A). However, these experiments were performed in the context of over-expressing the catalytic mutant. In this

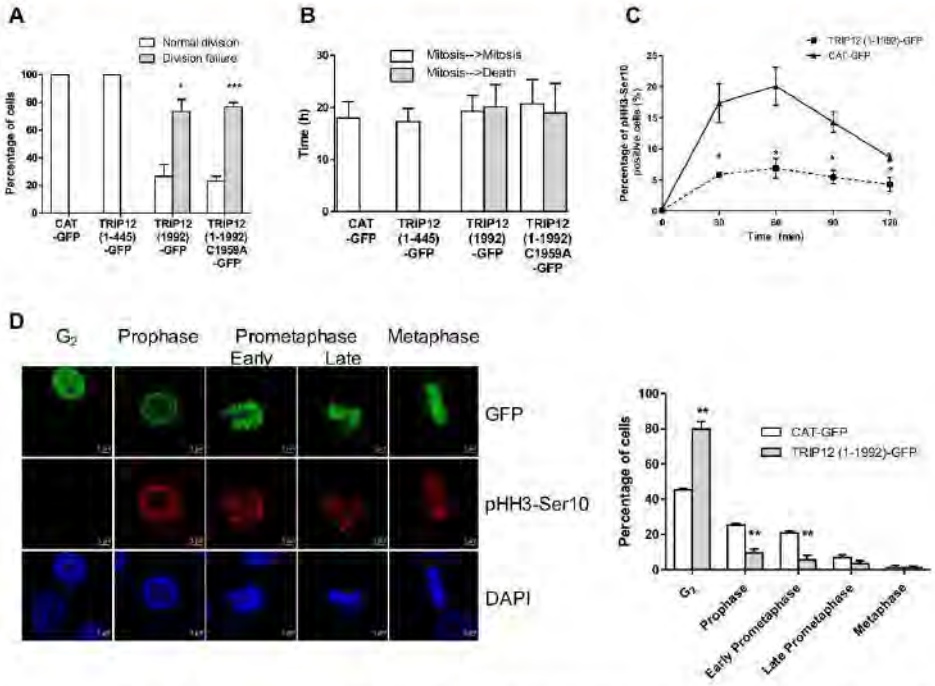

Figure 4. An over-expression of TRIP12 affects cell division by delaying mitotic entry. (**A**) The graph represents the percentage ± SEM of GFP-cells that overcome at least two cell divisions or die over a 48h-period. * and *** indicate a p value < 0.05 and < 0.001, respectively. (**B**) The graph represents the average duration ± SEM in interphase between two mitoses (white bars) and between mitosis and cell death (grey bars) in the different GFP positive cells. (**C**) Percentage of pHH3-Ser10 positive HelaS3 cells transfected with TRIP12(1-1992)-GFP or control CAT-GFP constructs and arrested by Ro-3306 treatment was assessed by flow cytometry after release in inhibitor free medium every 30 min for 2 h. The graph represents the mean ± SEM of three different experiments. * indicates a p value < 0.05. (**D**) Proportion of cells in G_2, prophase, early prometaphase, late prometaphase and metaphase in HelaS3 cells previously transfected with TRIP12(1-1992)-GFP or control CAT-GFP constructs was determined by immunofluorescence using anti-GFP (top panel) and anti-pHH3-Ser10 (middle panel) antibodies. Forty-eight hours after transfection, cells were arrested in G_2 phase by a Ro-3306 treatment and released in inhibitor free medium for 30 min. GFP-positive cells that were negative for pHH3-Ser10 staining were considered in G_2 phase. DNA was counterstained with DAPI. The graph represents the percentage of cells in the different phases expressed as mean ± SEM obtained from a minimum of 300 cells of three different experiments. ** indicates a p value < 0.01.

context, we show that an over-expression of several different TRIP12 domains (except the N-terminal domain) leads to an inhibition of cell division (Fig. S4A–E). In these conditions, we cannot entirely be certain that TRIP12 function in mitotic entry is independent of its catalytic activity. Moreover, TRIP12-GFP transfection leads to uncontrolled TRIP12 expression throughout all cell cycle phases whereas endogenous TRIP12 is tightly regulated during cell cycle. Formulation of a specific inhibitor of TRIP12 enzymatic activity would be required to definitely address this question.

We further demonstrate that TRIP12 interacts with chromatin *via* an IDR. IDRs are found in a multitude of proteins and participate in protein-, DNA-, or RNA-protein interactions[40,41]. DNA binding proteins are significantly enriched in disordered domains in Eukaryotes[12]. Many IDRs are functional, adopting a well-defined conformation upon interaction with target molecules. IDRs constitute important regulatory regions such as the N-terminal part of histones that are subject to numerous post-translational modifications to control the chromatin compaction[41]. To our knowledge, TRIP12 is the first demonstrated E3 ubiquitin ligase interacting with chromatin through an IDR domain. The staining on full-length chromosomes demonstrates that TRIP12 interacts through its IDR with the entire genome suggesting a widespread role of TRIP12 on genome organization and potentially on global gene expression.

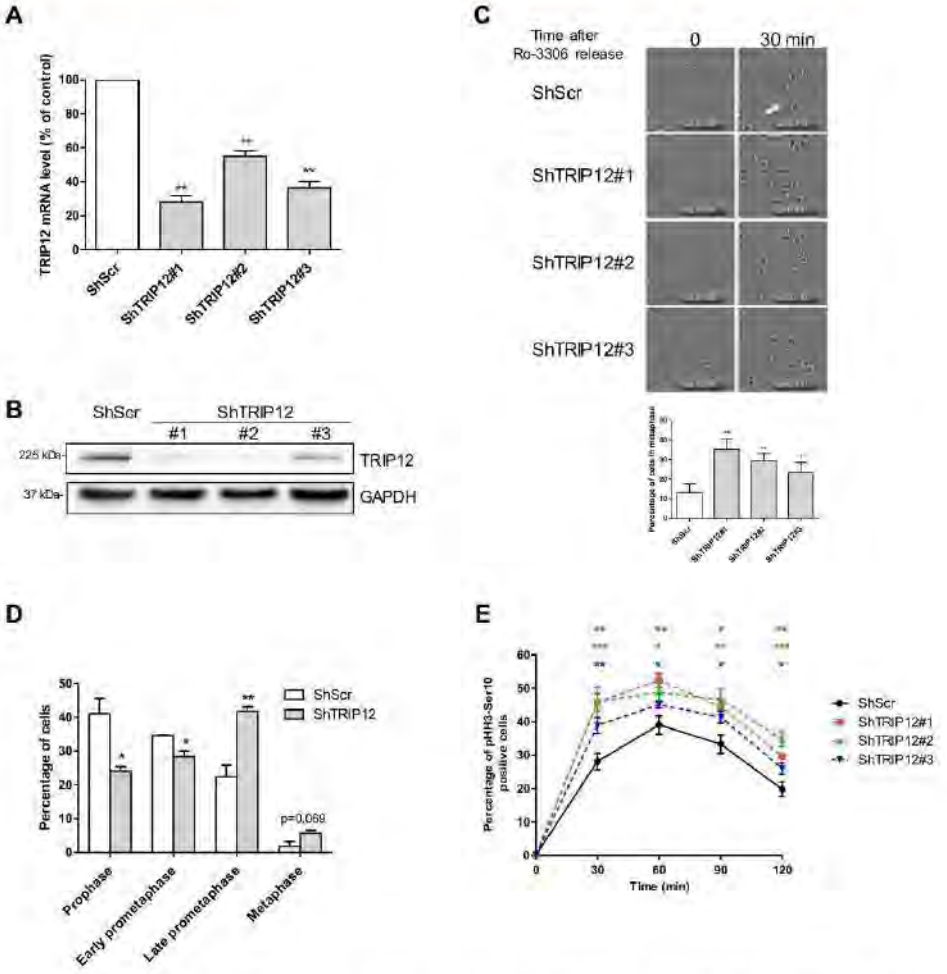

Figure 5. A TRIP12 depletion accelerates mitotic entry. (**A**) Expression of *Trip12* mRNA was determined by RT-qPCR in HelaS3 cells transduced with 3 shRNAs directed against *Trip12* mRNA (ShTRIP12) or scramble control shRNA (ShScr). *β-Actin*, *Gapdh* and *Cyclophilin* A mRNA level was used for normalization. Results are the mean ± SEM obtained from three different experiments and expressed as percentage of expression compared to ShScr control cells. ** indicates a p value < 0.01. (**B**) Expression of TRIP12 protein in HelaS3 ShTRIP12 and ShScr cells was determined by Western blot analysis. GAPDH protein level was used as loading control. Images were obtained from the same experiment and representative of three different experiments. (**C**) Percentage of cells in metaphase in TRIP12-depleted (ShTRIP12#1, #2 and #3) and control (ShScr) HelaS3 cells arrested by a Ro-3306 treatment and released in the cell cycle by medium replacement (t = 0) was determined by cell live microscopy. The graph represents the percentage of cells in metaphase phenotype expressed as mean ± SEM relatively to total number of cells. A cell was considered in metaphase phenotype when the equatorial plate was microscopically visualized. A representative cell in metaphase phenotype is indicated by the white arrow. The quantification was performed from 9 different fields from three different experiments representing an average of 650 analyzed cells. * and ** indicates a p value < 0.05 and 0.01, respectively. (**D**) Proportion of cells in prophase, early prometaphase, late prometaphase and metaphase in TRIP12-depleted (ShTRIP12#1) and control (ShScr) HelaS3 cells arrested by a Ro-3306 treatment and released in the cell cycle by medium replacement was determined by immunofluorescence using anti-pHH3-Ser10 antibody after 30 min. DNA was counterstained with DAPI. The graph represents the percentage of cells in the different steps of early mitosis expressed as mean ± SEM obtained from a minimum of 300 cells of three different experiments. * and ** indicate a p value < 0.05 and 0.01, respectively. (**E**) Percentage of pHH3-Ser10

positive cells in TRIP12-depleted (ShTRIP12) and control (ShScr) HelaS3 cells arrested in G_2 phase by a Ro-3306 treatment and released in the cell cycle by medium replacement was determined by flow cytometry at the indicated time. Three different ShTRIP12 (#1, #2 and #3) were used for these experiments. The results represent the mean ± SEM obtained from four different experiments. *, ** and *** indicate a p value < 0.05, 0.01 and 0.001, respectively.

We showed that TRIP12 depletion accelerates mitotic entry by shortening the DNA replication phase. DNA replication is a highly ordered process that ensures cells replicate their genome. It requires the sequential assembly of protein complexes such as the pre-replication complex, the pre-initiation complex and the replisome. TRIP12 could participate in the regulation of DNA replication by interacting or controlling the expression of replication complex components. Interestingly, TRIP12 was found in the RPA interactome[43]. Our personal comparative proteomic analysis (SWATH-MS) identified an increased expression of the cyclin dependent kinase CDK6 in TRIP12 depleted cells (Fig. S6A–C). It is known that CDK6 activity is a critical determinant of pre-RC assembly[44]. Therefore, TRIP12 could control DNA replication initiation by regulating CDK6 level. The progression through the different phases of DNA replication can also be controlled by chromatin structures[45]. Our data showed that TRIP12 IDR has the capacity to modify the chromatin structure when expressed at a high level (Fig. S3E,G). It is also reported that TRIP12 associates with chromatin remodeling complex components[4,46,47]. By modifying the structure of chromatin, TRIP12 could regulate S phase progression. In summary, it is likely that TRIP12 controls the duration of DNA replication by multiple complex mechanisms. Their complete discovery will require further investigations.

Our results strongly suggest that in addition to its role for the entry into mitosis, TRIP12 exerts other functions during the progression of mitosis. The interaction of TRIP12 on chromosomes could participate in regulating the kinetics of chromosome condensation or act as a competitor to other chromatin-interacting proteins. The identification of TRIP12 as a potential substrate of CDK1 could also support its role in chromosome condensation. Indeed, it is known that CDK1 substrates, such as CAP-D3 (Chromosome associated protein-D3), are implicated in this process[39,48]. Moreover, histone ubiquitination varies during cell cycle progression. Both histones H2A and H2B are ubiquitinated in S and G_2 phases, deubiquitinated in prophase and then reubiquinated in anaphase[49]. Also, the promoter of certain active genes remains ubiquitinated during the entire mitosis to facilitate their transcriptional reactivation in post-mitosis[50]. Although the ubiquitin ligase RNF20 is associated to genome ubiquitination, potentially TRIP12 also participates in this epigenetic modification of histones during mitosis.

Finally, our findings show that TRIP12 is localized and sequestered in the nucleus for a short duration. This strict temporal control may act to limit the period during which TRIP12 can exert its nuclear functions, precisely from S to early G_1. This is of particular importance for the TRIP12 inhibitory function on the DDR by promoting RNF168 degradation[9]. DDR is repressed during mitosis[51] and reactivated in G_1 phase to repair DNA damages that pass the G_2/M checkpoint or created during mitosis. Given its inhibitory role on DDR and nuclear localization during the cell cycle, TRIP12 could participate in the mechanisms of DDR inhibition during mitosis by interacting with chromatin and therefore by preventing chromatin accessibility to RNF168. In contrast, TRIP12 disappearance of the nucleus in G_1 phase could be part of DDR reactivation in the cell cycle.

In this study, we provide important findings on TRIP12 regulation and its implication in cell cycle progression. More importantly, we reveal for the first time its ability to interact with specific regions of the genome which can prefigure a critical role in the organization and the expression of the genome.

Materials and Methods

Cell culture and treatment. HelaS3 cells, HEK-293FT, HelaS3 H2B-dsRed were grown in DMEM 4.5 g/L glucose medium supplemented with 10% fetal calf serum (FCS), L-glutamine and antibiotics (Life Technologies) at 37 °C in humid atmosphere with 5% CO_2. HelaS3 and HEK-293FT were obtained from the American Type Culture Collection. The HelaS3 H2B-dsRed cell line was generated in the laboratory (see below). For serum starvation, HelaS3 cells were seeded at 80% of confluency and cultured in DMEM 4.5 g/L glucose medium supplemented with 0.5% FCS for 72 h. For double thymidine block, HelaS3 cells were grown in the presence of 2 mM thymidine (Sigma-Aldrich) for 18 h, then in fresh medium for 8 h and further grown with thymidine for another 18 h. Treatments are as follows: HelaS3 cells were cultured in the presence of 2 mM thymidine for 18 h, then in fresh medium for 5 h and treated with 100 ng/mL nocodazole (Sigma-Aldrich) for 5 h. HelaS3 cells were treated with 9 µM Ro-3306 (Tocris Bioscience) for 20 h; or, cells were treated with 500 nM reversine (Sigma-Aldrich) for 2 h. HeLaS3 cells were treated with 10 µM EDU for 15 min. The EDU incorporation was visualized using the Click-It™ EdU Alexa Fluor™ 647 Imaging kit (Life Technologies). The human pancreatic hPNE hTERT cell line was obtained from Dr M. Ouellette (University of Nebraska Medical Center, NE) and grown in DMEM 75% (Life Technologies)/M3 25% (InCell Biotech) medium supplemented with 10% FCS, L-glutamine and antibiotics (Life Technologies), 15 ng/ml EGF (Sigma-Aldrich) and 750 mg/ml puromycin. The human pancreatic cancer cell lines BxPC-3 and Capan-2 were obtained from the American Type Culture Collection and grown in RPMI medium supplemented with 10% FCS, L-glutamine and antibiotics (Life Technologies) at 37 °C in humid atmosphere with 5% CO_2.

Plasmids and transfection. The following lentivirus shRNA lentiviral plasmids were purchased from Sigma-Aldrich: pLKO1-TRC1 non mammalian shRNA control SHC002-target sequence CAACAAGATGAAGAGCACCAA, ShTRIP12#1 pLKO1-TRC1 TRCN0000022374-target sequence CCTGAGTCAAGGAAACATGTT, ShTRIP12#2 pLKO1-TRC1 TRCN0000022375-target sequence CCGGAGTTTGAATCCACCTTT and ShTRIP12#3 pLKO1-TRC1 TRCN0000273210-target sequence CCACTACTCAGTCACGTAAAT. HelaS3 cells

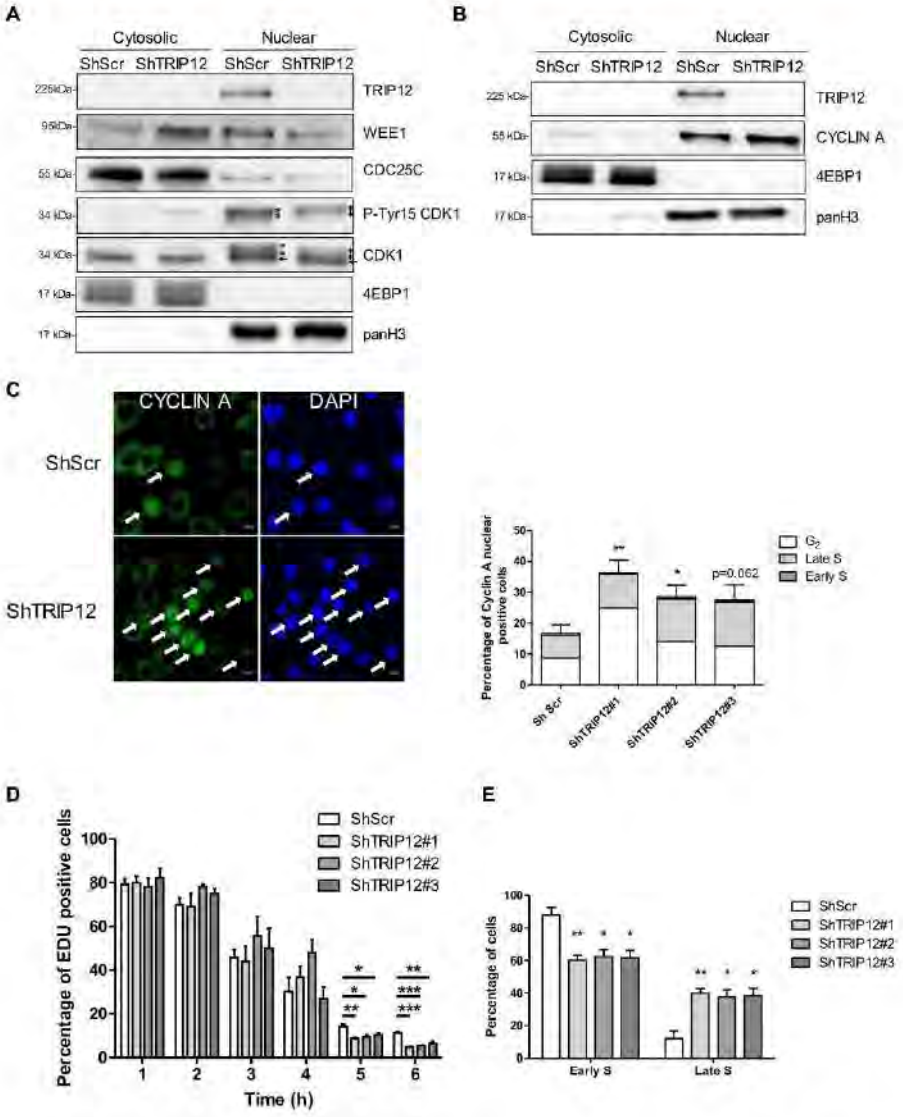

Figure 6. A shortened duration of DNA replication explains the accelerated mitotic entry of TRIP12-depleted cells. (**A**) TRIP12, WEE1, CDC25C and CDK1 protein and P-Try15-CDK1 phosphorylation levels in nuclear and cytosolic fractions of TRIP12-depleted and control HelaS3 cells after a Ro-3306 treatment were determined by Western blot analysis. 4EBP1 and panH3 protein levels were used as loading and purity controls. Images were obtained from the same experiment and representative of three different experiments. The asterisk and the arrow indicate the position of phosphorylated and non-phosphorylated forms of CDK1, respectively. (**B**) CYCLIN A level in nuclear and cytosolic fractions of TRIP12-depleted and control HelaS3 cells after Ro-3306 treatment was determined by Western blot analysis. 4EBP1 and panH3 protein levels were used as loading and purity controls. Images were obtained from the same experiment and representative of three different experiments. (**C**) CYCLIN A nuclear presence in TRIP12-depleted and control cells after RO-3306 treatment was determined by immunofluorescence. The image illustrates representative cells with nuclear CYCLIN A (white arrows) or not. The graph represents the percentage of cells expressed as mean ± SEM obtained from

three different experiments. Percentage of cells in G_2 phase (white bars), late S (light grey bars) and early S (dark grey bars) was determined by immunofluorescence using criteria defined in Fig. 2C. The bars represent the mean obtained from three different experiments. * and ** indicate a p value < 0.05 and 0.01, respectively. (**D**) Percentage of EDU positive cells in TRIP12-depleted (ShTRIP12) and control (ShScr) HelaS3 cells arrested in early S phase by a double thymidine block treatment and released in the cell cycle was determined by EDU incorporation at the indicated time. The graph represents the mean ± SEM obtained from a minimum of 2500 cells for each indicated time of three different experiments. *, ** and *** indicate a p value < 0.05, 0.01 and 0.001, respectively. (**E**) Percentage of early S and late S cells in EDU-positive TRIP12-depleted (ShTRIP12) and control (ShScr) HelaS3 cells was determined by immunofluorescence using criteria defined in Fig. 2C. The graph represents the mean ± SEM obtained from a minimum of 500 EDU-positive cells of three different experiments. * and ** indicate a p value < 0.05 and 0.01, respectively.

stably over-expressing histone H2B-dsRed fusion protein were generated after transient transfection of pcDNA$_3$/H2B-dsRed plasmid (kind gift from V. Lobjois, Advanced Technology Institute in Life Sciences of Toulouse, France) and selection with hygromycin (800 µg/mL). pENTA0045 plasmid containing TRIP12 cDNA (KIAA0045) was obtained from the Kasuka DNA Research Institute (Japan)[57]. TRIP12-GFP expressing vector was obtained by transferring TRIP12 cDNA into pCDNA™ 6.2/C-EmGFP-DEST vector (Life Technologies). TRIP12-GFP deletion constructs were generated by PCR amplification (Primers are listed in Supplemental Materials and Methods Table 1) followed by insertion into pDONR-201 or pDONR-221 (Life Technologies) using Gateway strategy. The different fragments were subsequently inserted in frame into pCDNA™6.2/C-EmGFP-DEST vector (Life Technologies) using the same strategy. Catalytically inactive TRIP12-GFP C1959A mutant was generated using Quik Change XL Site-Directed mutagenesis kit (Stratagene) and primers listed in Supplemental Materials and Methods Table 1. All plasmid sequences were verified by automatic sequencing. Chloramphenicol Acetyl Transferase (CAT)-GFP expressing vector pcDNA™6.2/C-EmGFP/GW/CAT was purchased from Life Technologies and used as control. Histone H2B (H2B)-GFP expressing plasmid was a gift from D Lières (Institute of Molecular Genetics of Montpellier, France). pSG5-HAx2-FLAG-TRIP12 plasmid was generated by PCR amplification (Primers are listed in Supplemental Materials and Methods Table 1) followed by insertion into the *Kpn* I and *EcoR* V sites of pcDNA$_3$ plasmid containing two HA tags, a TEV protease cleavage site and a FLAG motif upstream of the *Kpn* I site. TRIP12 cDNA fragment (1-325) and (446-1000) cloned in pDONR-201 were transferred in pET-60-DEST plasmid (Novagen) by Gateway strategy to generate GST-IDR(1-325) and GST-ARM-WWE(446-1000) plasmids. The different plasmids were transiently transfected in HelaS3 cells using JetPEI™ reagent (PolyPlus-Transfection) following manufacturer's recommendations with a N/P ratio of 5 or 10.

Lentiviral vector production and cell transduction. All replication defective, self-inactivating lentiviral vectors were generated in a BSL-3 facility (Vectorology platform, INSERM U1037, Toulouse, France) as previously described by Torrisani *et al.*[55]. Briefly, transient transfection of HEK-293FT cells with packaging and lentiviral vector plasmids were performed using LENTI-Smart INT kit (InvivoGen) following manufacturer's recommendations. All batches were verified replicative virus-free. Lentiviral vector concentrations were quantified by p24 ELISA (Innotest, Ingen, Paris). Cells were seeded at a density of 10^4 cells per well in a 48 well-dish. After 24 h, cells were incubated with 150 ng of p24-equivalent of lentiviral vectors in the presence of protamine sulfate (4 µg/mL) for 12 h. Transduced cells were selected for 3 weeks using puromycin (5 µg/mL-InvivoGen).

Subcellular fractionation and Western blot analysis. Cell pellets were incubated in 100 µM Tris-HCl (pH 7.5), 1,5 mM $MgCl_2$, 5 mM KCl, 5 mM DTT, 0,5% NP-40®, 0,5 mM PMSF and 10 µL/mL protease inhibitor (Sigma-Aldrich). After 10 min-incubation on ice, samples were centrifuged (15 min at 2 000 rpm, 4 °C). Supernatants containing cytosolic proteins were kept. After two washes, pellets were resuspended in RIPA (Radio-ImmunoPrecipitation Assay) buffer (Biotech) and centrifuged (20 min at 12 000 rpm, 4 °C), supernatants containing nuclear proteins were kept. The residual pellets were solubilized in RIPA buffer supplemented with 25 U micrococcal nuclease (Takara) and 1 mM DTT. After 20 min-incubation at 37 °C, the reaction was stopped using EDTA solution (44 mM final concentration). After sonication (2 cycles of 6 s, amplitude 40% with Vibra-Cell™ sonicator), samples were centrifuged (15 min at 12 000 rpm, 4 °C). Supernatants containing chromatin fraction were kept. For total protein, cell pellets were incubated in RIPA buffer supplemented with 10 µL/mL protease inhibitor (Sigma-Aldrich). After 15 min on ice, samples are centrifuged (15 min-12 000 rpm, 4 °C). Protein fractions were denaturated in Laemmli buffer after heating at 95 °C for 5 min. Proteins were separated by SDS-PAGE (Sodium Dodecyl Sulfate Polyacrylamide Gel Electrophoresis) and transferred onto nitrocellulose membrane (Bio-Rad) using TransBlot Turbo (Bio-Rad) apparatus. After membrane saturation and primary/secondary antibody incubation, protein expression was detected using Clarity™ Western ECL Substrate (Bio-Rad) and Chemi-Doc™ XRS$^+$ (Bio-Rad) apparatus. Signal intensities were quantified using Image Lab (Bio-Rad) software. Antibodies and dilution used for these experiments are listed in Supplemental Materials and Methods Table 2.

Flow cytometry. For cell cycle analyses, cells were fixed in 70% ethanol during the exponential growth phase for asynchronous HelaS3 cells or after treatment for enriched HelaS3 cell populations. Fixed cells were treated with RNAse A (10 µg/mL) and propidium iodide (20 µg/mL) (Sigma-Aldrich) for 15 min at 37 °C. TRIP12(1-1992)-GFP and H2B-GFP transfected cells were fixed with ethanol 70% and incubated with a pHH3-Ser10 antibody followed by Alexa Fluor® 555 anti-mouse secondary antibody. Data were acquired using the MACS Quant® VYB cytometer (Miltenyi Biotech) and analyzed with MACS Quant and ModFit software. Antibodies and dilution used for these experiments are listed in Supplemental Materials and Methods Table 2.

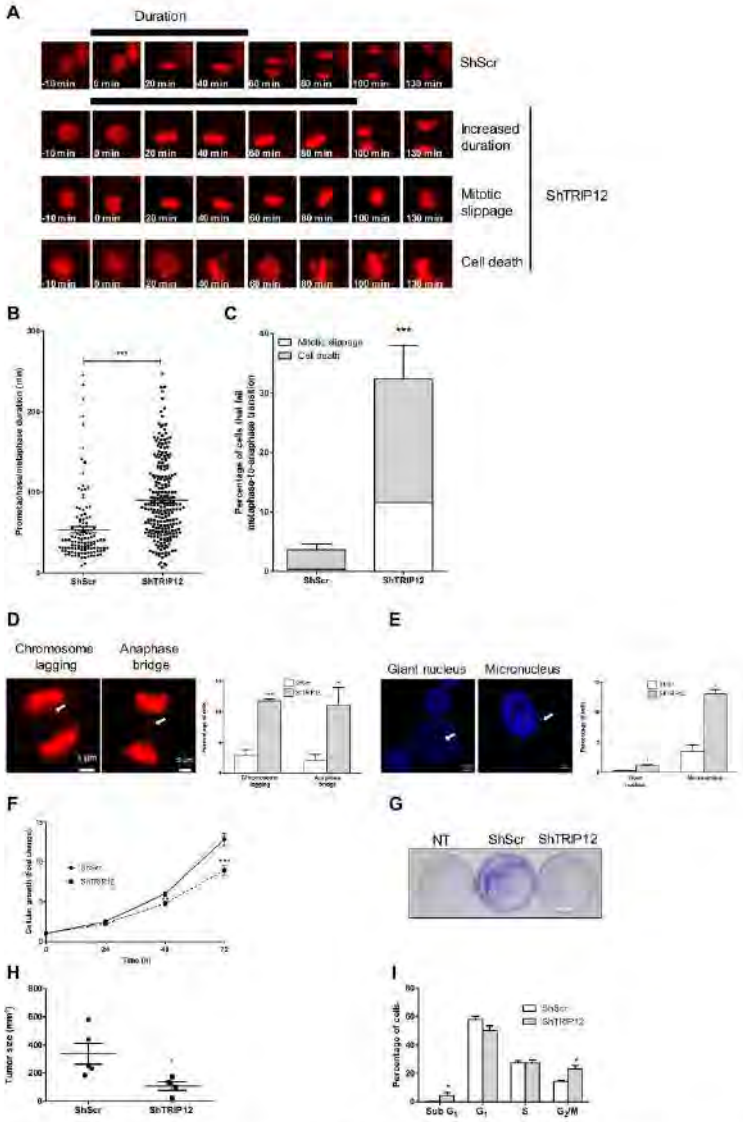

Figure 7. A TRIP12 depletion prolongs the SAC activation, leads to chromosome segregation defects and cell growth inhibition. (**A**) Representative images of the different fate of TRIP12-depleted cells during 140 min. TRIP12-depleted (ShTRIP12#1) and control (ShScr) H2B-dsRed HelaS3 were arrested by a Ro-3306 treatment. Cells were released in the cell cycle and followed by live microscopy for 6 h. The black bar represents the duration of prometaphase-metaphase. (**B**) Duration of prometaphase-metaphase was measured from the invagination of the nuclear membrane to the separation of sister chromatids in 125 control cells and 244 TRIP12#1-depleted cells. The horizontal bar represents the mean ± SEM from three different experiments. *** represents a p value < 0.001. (**C**) Percentage of cells that fail the transition metaphase-to-anaphase in TRIP12#1-depleted and control H2B-dsRed HelaS3 cells. The bars represent the mean ± SEM obtained from three different experiments. *** represents a p value < 0.001. Percentage of cells that exit mitosis *via* mitotic slippage (white bars) and cell death (grey bars). The bars represent the mean obtained from three different experiments. (**D**) Chromosome laggings and anaphase bridges in TRIP12-depleted and control H2B-dsRed HelaS3 cells arrested

by Ro-3306 treatment and released in the cell cycle were quantified by live cell microscopy. The images are representative of a chromosome lagging and an anaphase bridge observed in TRIP12-depleted H2B-dsRed HelaS3 cells. The graph represents the percentage of cells with chromosome segregation defects expressed as a mean ± SEM and obtained from 344 TRIP12-depleted and 251 control cells of three different experiments. * and *** indicate a p value < 0.05 and 0.001, respectively. (**E**) Micronucleus and giant nuclei in asynchronous TRIP12-depleted or control HelaS3 cells were quantified by immunofluorescence after DAPI staining. The graph represents the percentage of cells expressed as a mean ± SEM and obtained from a minimum of 10^3 cells of three different experiments. * indicates a p value < 0.05. (**F**) Cell growth of TRIP12-depleted and control cells was measured by cell counting. Cells were seeded at 5.10^3 cells/well of 6-wells plate and counted the day after (t = 0) and every 24 h the three following days. Results are expressed as fold change ± SEM relatively to t = 0. Results were obtained from 7 different experiments. ** and *** indicate a p value < 0.01 and 0.001, respectively. (**G**) Colony formation assay of HelaS3 cells transduced or not (NT) with ShScr and ShTRIP12 expressing lentiviral particles. Forty-eight hours after transduction, cells were seeded in a 10 cm-plate and selected with puromycin for 11 days. Colonies were fixed and counterstained with crystal violet. The images are representative of at least three different experiments. (**H**) *In vivo* tumor progression of TRIP12-depleted and control HelaS3 cells. Cells (10^6 cells) were sub-cutaneously injected into Scid mice (n = 5). After 5 weeks, mice were sacrificed and tumor volume was determined. Results are expressed in mm^3 ± SEM. * indicates a p value < 0.05. (**I**) Distribution of TRIP12-depleted and control cells in the cell cycle was determined by flow cytometry after propidium iodide incorporation. The percentage of cells in the different phases of the cell cycle is expressed as a mean ± SEM and was obtained from at least 7 different experiments. * indicates a p value < 0.05.

Cell proliferation. TRIP12-depleted and control HelaS3 cells were seeded in triplicate at a concentration of 5.10^4/well of 6 well-plate. After 24 h (t = 0), cells were counted using a Z1 Coulter® Particle Counter (Beckman Coulter™). Cells were counted after 24 h, 48 h and 72 h.

***In vivo* experiments.** Experimental procedures performed on mice were approved by the ethical committee of INSERM- CREFRE (National Institute of Health and Medical Research-Regional Center for Functional Exploration and Experimental Resources) and authorized by the French Ministry of Research: APAFIS#3600-2015121608386111v3. All experiments were performed in accordance with relevant guidelines and regulations. TRIP12-depleted and control HelaS3 cells (1.10^6 cells) were subcutaneously injected into SCID mice (n = 5). After 5 weeks, mice were euthanized and tumor volume was determined.

RNA extraction and RT-qPCR. Total RNA was isolated from HelaS3 cell lines with TRIzol® Reagent (Life Technologies) according to supplier's instructions. One to five µg of total RNA were reverse transcribed into cDNA using RevertAid H minus Reverse Transcriptase kit (Thermo-Scientific) according to manufacturer's recommendations. Duplicate RT-qPCR assays were carried out in a StepOnePlus™ Real-Time PCR System (Applied Biosystems) with SsoFast™ EvaGreen® supermix (Bio-Rad) and specific primers (see primers listed in Supplemental Materials and Methods 2). Relative quantity of mRNA was calculated by the comparative threshold cycle (CT) method as $2^{-\Delta CT}$, where ΔCT = CT *Trip12* mRNA − CT *Reference* mRNA. Three mRNAs of reference (*β-Actin, Gapdh and cyclophilin A*) were used for normalization. Primers are listed in Supplemental Materials and Methods Table 1.

Chromosome spreading. Cells were treated with 9 µM Ro-3306 for 20 h, washed with PBS and released in fresh medium for 45 min at 37 °C, or in medium supplemented with 100 µM nocodazole for 4 h. Mitotic cells were collected by brief treatment with trypsin, rinsed with PBS and swollen in hypotonic medium (10 mM KCl, 15% FCS) at 37 °C for 20 min. Cell preparations were fixed with a freshly made 75% ethanol, 25% glacial acetic acid solution overnight at 4 °C, dropped on glass slides and air-dried. Slides were stained with DAPI or processed for immunofluorescence (see below).

Naked DNA interaction. GST-IDR(1-325) and GST-WWE-ARM(446-1000) recombinant proteins were purified from BL21 bacteria and quantified. Increasing volumes of purified proteins were incubated with 100 ng of pENTR1A-GFP plasmid (made in laboratory) in Tris-HCl (pH 7.6) 10 mM-EDTA 1 mM buffer for 20 min at room temperature. Reactions were migrated on agarose gel 0.7% and visualized with ethidium bromide.

Immunofluorescence. Cells were grown on cover slips then subsequently fixed and permeabilized using with IntraStain™ reagent (DAKO) or methanol/0.1% Triton™ X-100. Cover slips were saturated using Protein block™ reagent (DAKO) for 30 min and then incubated with primary antibodies overnight at 4 °C. After several washes, cells were incubated with appropriate secondary Alexa Fluor®-488 anti-mouse, Alexa Fluor®-555 anti-mouse or Alexa Fluor®-555 anti-rabbit antibodies for 2 h at room temperature. Nuclei were counterstained with 1 µM DAPI for 5 min at room temperature. Cover slips were mounted on glass slides using Fluorescent Mounting Reagent/Medium (DAKO). Fluorescence was visualized using LSM 780 or 880 confocal microscope (Zeiss) with a 63x NA 1.4 oil-immersion objective and analyzed using Zen software (Zeiss). Antibodies and dilution used for these experiments are listed in Supplemental Materials and Methods Table 2. Images were quantified wit FIJI software.

Bioinformatic prediction of intrinsically disordered regions. Detection of intrinsically disordered region in TRIP12 protein sequence (NP_004229.1) was determined using the prediction software IUPred (iupred.enzim.hu)[54], GlobPlot (http://globplot.embl.de/)[55] and DisEMBL (dis.embl.de)[56].

Live cell microscopy. H2B-dsRed HelaS3 cells were treated with Ro-3306 and released in the cell cycle. Fluorescent images were acquired (Objective 20x) every minute for 6 h using a Zeiss motorized inverted Observer Z1 microscope, containing LED module Colibri. Filter combinations: GFP (38 HE) DsRed (43 HE) and DAPI (49) with the AxioCam MRm camera system. Time-lapse imaging of living cells was performed using Pecon-Zeiss incubation system for temperature (37 °C) and CO_2 (5%) controlled environment. Images were subsequently analyzed using ZEN SP2 software (Blue edition Zeiss). Transfected Ro-3306-treated HelaS3 cells released in the cell cycle were imaged every half-hour or hour using IncuCyte Zoom Kinetic Imaging System with a 10x objective.

SWATH-MS comparative proteomic analysis. Analysis of proteins was performed using a microLC system Ultimate 3000 (Dionex, Villebon sur Yvette, France) coupled to a Triple-TOF 5600 + (AB Sciex, Les Ullis, France) in the positive ion mode. Samples were first dissolved in 16 _L of buffer (5% ACN, 0.05% trifluoroacetic acid) and spiked with iRT calibration mix (Biognosys, Schlieren, France). The totality of the samples was then injected on a YMC-Pack Pro C18 column (3.0 mm _ 150 mm; 3 _m particle size) at a flow rate of 5 _L.min^{-1}. The run length was over 90 min with a gradient from 7% to 45% buffer B (buffer A: 0.1% formic acid, buffer B: 90% ACN, and 0.1% formic acid) in 70 min. The MS data were acquired with a SWATH mode. The source parameters were set as follows: IS at 5500 V, Cur gas at 25, GS1 at 5. The acquisition parameters were as follows: one 50 msec accumulation time MS scan followed by 50 variable SWATH windows each at 40 msec accumulation time for m/z 400–1250. Identification was determined using an in-house SWATH library created HelaS3 cells with MaxQuant software, Les Ulis, France) (FDR 1%). A mass accuracy of 20ppm on precursor ions was used, and 0.5 Da on the fragments. Cysteine carbamidomethylation, methionine oxidation, proline hydroxylation and serine, threonine and tyrosine phosphorylations were taken into account. Data treatment was done with Spectronaut Software 9.0, Les Ulis, France). Analysis of ShScr and ShTRIP12#1 HelaS3 cells was performed on three different transductions. For each peptide, a triplicate with a peptide quantity <5 and a standard error >60% of the mean was excluded from the analysis. For each replicate, the sum of the four most abundant peptides was calculated. The mean of ShTRIP12 triplicate was compared to the one of ShScr triplicate. Protein with a fold change >1.2 and <0.8 compared to ShScr cells were considered.

Statistical analysis. *In vitro* data were analyzed by 2-tailed, unpaired Student's t-test using a multiple statistics Graph Pad Prism 5 software package and a difference was considered significant when p valne was lower than 0.05. Mean values are given ± SEM. Number of independent experiments is indicated in the figure legends. *, ** and *** Indicate a p value < 0.05, 0.01 and 0.001, respectively.

Data availabilty

The datasets generated during and/or analyzed during the current study are available from the corresponding author on reasonable request.

Received: 23 September 2019; Accepted: 3 January 2020;
Published online: 21 January 2020

References

1. Chen, D., Yoon, J.-B. & Gu, W. Reactivating the ARF-p53 axis in AML cells by targeting ULF. *Cell Cycle Georget. Tex.* **9**, 2946–2951 (2010).
2. Xie, Y. & Varshavsky, A. UFD4 lacking the proteasome-binding region catalyses ubiquitination but is impaired in proteolysis. *Nat. Cell Biol.* **4**, 1003–1007 (2002).
3. Ju, D., Wang, X., Xu, H. & Xie, Y. The armadillo repeats of the Ufd4 ubiquitin ligase recognize ubiquitin-fusion proteins. *FEBS Lett.* **581**, 265–270 (2007).
4. Keppler, B. R. & Archer, T. K. Ubiquitin-dependent and ubiquitin-independent control of subunit stoichiometry in the SWI/SNF complex. *J. Biol. Chem.* **285**, 35665–35674 (2010).
5. Park, Y., Yoon, S. K. & Yoon, J.-B. TRIP12 functions as an E3 ubiquitin ligase of APP-BP1. *Biochem. Biophys. Res. Commun.* **374**, 294–298 (2008).
6. Gudjonsson, T. *et al.* TRIP12 and UBR5 suppress spreading of chromatin ubiquitylation at damaged chromosomes. *Cell* **150**, 697–709 (2012).
7. Chen, D. *et al.* Differential effects on ARF stability by normal versus oncogenic levels of c-Myc expression. *Mol. Cell* **51**, 46–56 (2013).
8. Kweon, S.-M. *et al.* An Adversarial DNA N6-Methyladenine-Sensor Network Preserves Polycomb Silencing. *Mol. Cell* https://doi.org/10.1016/j.molcel.2019.03.018 (2019).
9. Hanoun, N. *et al.* The E3 ubiquitin ligase thyroid hormone receptor-interacting protein 12 targets pancreas transcription factor 1a for proteasomal degradation. *J. Biol. Chem.* **289**, 35593–35604 (2014).
10. Kajiro, M. *et al.* The E3 ubiquitin ligase activity of Trip12 is essential for mouse embryogenesis. *PloS One* **6**, e23871 (2011).
11. Chen, D. *et al.* regulation in oncogenic stress-mediated p53 responses. *Nature* **464**, 624–627 (2010).
12. Cai, J.-B. *et al.* Ubiquitin-specific protease 7 accelerates p14(ARF) degradation by deubiquitinating thyroid hormone receptor-interacting protein 12 and promotes hepatocellular carcinoma progression. *Hepatol. Baltim. Md.* **61**, 1603–1614 (2015).
13. Wang, L. *et al.* TRIP12 as a mediator of human papillomavirus/p16-related radiation enhancement effects. *Oncogene* **36**, 820–828 (2017).
14. O'Roak, B. J. *et al.* Recurrent de novo mutations implicate novel genes underlying simplex autism risk. *Nat. Commun.* **5**, 5595 (2014).
15. Brunswig, N. G. *et al.* Identification of new TRIP12 variants and detailed clinical evaluation of individuals with non-syndromic intellectual disability with or without autism. *Hum. Genet.* **136**, 179–192 (2017).
16. Siddiqui, K., On, K. F. & Diffley, J. F. X. Regulating DNA replication in eukarya. *Cold Spring Harb. Perspect. Biol.* **5** (2013).
17. Lau, Y. F. & Arrighi, F. E. Studies of mammalian chromosome replication. II. Evidence for the existence of defined chromosome replicating units. *Chromosoma* **83**, 721–741 (1981).
18. Dunphy, W. G., Brizuela, L., Beach, D. & Newport, J. The Xenopus cdc2 protein is a component of MPF, a cytoplasmic regulator of mitosis. *Cell* **54**, 423–431 (1988).
19. Parker, L. L. & Piwnica-Worms, H. Inactivation of the p34cdc2-cyclin B complex by the human WEE1 tyrosine kinase. *Science* **257**, 1955–1957 (1992).

20. McLean, J. R., Chaix, D., Ohi, M. D. & Gould, K. L. State of the APC/C: organization, function, and structure. *Crit. Rev. Biochem. Mol. Biol.* **46**, 118–136 (2011).
21. Musacchio, A. & Salmon, E. D. The spindle-assembly checkpoint in space and time. *Nat. Rev. Mol. Cell Biol.* **8**, 379–393 (2007).
22. Pesin, J. A. & Orr-Weaver, T. L. Regulation of APC/C activators in mitosis and meiosis. *Annu. Rev. Cell Dev. Biol.* **24**, 475–499 (2008).
23. Ganem, N. J. & Pellman, D. Linking abnormal mitosis to the acquisition of DNA damage. *J. Cell Biol.* **199**, 871–881 (2012).
24. Crasta, K. *et al.* DNA breaks and chromosome pulverization from errors in mitosis. *Nature* **482**, 53–58 (2012).
25. Avinez, R., Shenoy, A., Elroy-Stein, O. & Geiger, T. Uncovering Hidden Layers of Cell Cycle Regulation through Integrative Multi-omic Analysis. *PLoS Genet.* **11**, e1005554 (2015).
26. van der Lee, R. *et al.* Classification of intrinsically disordered regions and proteins. *Chem. Rev.* **114**, 6589–6631 (2014).
27. Sabari, B. R. *et al.* Coactivator condensation at super-enhancers links phase separation and gene control. *Science* **361** (2018).
28. Pines, J. & Hunter, T. Isolation of a human cyclin cDNA: evidence for cyclin mRNA and protein regulation in the cell cycle and for interaction with p34cdc2. *Cell* **58**, 833–846 (1989).
29. Enders, G. H. Gauchos and ochos: a Wee1-Cdk tango regulating mitotic entry. *Cell Div.* **5**, 12 (2010).
30. Lindqvist, A., van Zon, W., Karlsson Rosenthal, C. & Wolthuis, R. M. F. Cyclin B1–Cdk1 activation continues after centrosome separation to control mitotic progression. *PLoS Biol.* **5**, e123 (2007).
31. Coverley, D., Laman, H. & Laskey, R. A. Distinct roles for cyclins E and A during DNA replication complex assembly and activation. *Nat. Cell Biol.* **4**, 523–528 (2002).
32. Li, C., Andrake, M., Dunbrack, R. & Enders, G. H. A bifunctional regulatory element in human somatic Wee1 mediates cyclin A/Cdk2 binding and Crm1-dependent nuclear export. *Mol. Cell. Biol.* **30**, 116–130 (2010).
33. den Elzen, N. & Pines, J. Cyclin A is destroyed in prometaphase and can delay chromosome alignment and anaphase. *J. Cell Biol.* **153**, 121–136 (2001).
34. De Boer, L. *et al.* Cyclin A/cdk2 coordinates centrosomal and nuclear mitotic events. *Oncogene* **27**, 4261–4268 (2008).
35. Whitfield, M. L. *et al.* Identification of Genes Periodically Expressed in the Human Cell Cycle and Their Expression in Tumors. *Mol. Biol. Cell* **13**, 1977–2000 (2002).
36. Dobson, T., Chen, J. & Krushel, L. A. Dysregulating IRES-Dependent Translation Contributes to Overexpression of Oncogenic Aurora A Kinase. *Mol. Cancer Res.* **11**, 887–900 (2013).
37. Chen, W., Smeekens, J. M. & Wu, R. Systematic study of the dynamics and half-lives of newly synthesized proteins in human cells. *Chem. Sci.* **7**, 1393–1400 (2016).
38. Ma, H. *et al.* M phase phosphorylation of the epigenetic regulator UHRF1 regulates its physical association with the deubiquitylase USP7 and stability. *Proc. Natl. Acad. Sci. USA* **109**, 4828–4833 (2012).
39. Petrone, A., Adamo, M. E., Cheng, C. & Kettenbach, A. N. Identification of Candidate Cyclin-dependent kinase 1 (Cdk1) Substrates in Mitosis by Quantitative Phosphoproteomics. *Mol. Cell. Proteomics MCP* **15**, 2448–2461 (2016).
40. Dyson, H. J. & Wright, P. E. Intrinsically unstructured proteins and their functions. *Nat. Rev. Mol. Cell Biol.* **6**, 197–208 (2005).
41. Peng, Z. & Kurgan, L. High-throughput prediction of RNA, DNA and protein binding regions mediated by intrinsic disorder. *Nucleic Acids Res.* **43**, e121 (2015).
42. Wang, C., Uversky, V. N. & Kurgan, L. Disordered nucleiome: Abundance of intrinsic disorder in the DNA- and RNA-binding proteins in 1121 species from Eukaryota, Bacteria and Archaea. *Proteomics* **16**, 1486–1498 (2016).
43. Marechal, A. *et al.* PRP19 transforms into a sensor of RPA-ssDNA after DNA damage and drives ATR activation via a ubiquitin-mediated circuitry. *Mol. Cell* **53**, 235–246 (2014).
44. Braden, W. A., McClendon, A. K. & Knudsen, E. S. Cyclin-dependent kinase 4/6 activity is a critical determinant of pre-replication complex assembly. *Oncogene* **27**, 7083–7093 (2008).
45. Demeret, C., Vassetzky, Y. & Mechali, M. Chromatin remodelling and DNA replication: from nucleosomes to loop domains. *Oncogene* **20**, 3086–3093 (2001).
46. Cao, Q. *et al.* The central role of EED in the orchestration of polycomb group complexes. *Nat. Commun.* **5**, 3127 (2014).
47. Oliviero, G. *et al.* Dynamic Protein Interactions of the Polycomb Repressive Complex 2 during Differentiation of Pluripotent Cells. *Mol. Cell. Proteomics MCP* **15**, 3450–3460 (2016).
48. Abe, S. *et al.* The initial phase of chromosome condensation requires Cdk1-mediated phosphorylation of the CAP-D3 subunit of condensin II. *Genes Dev.* **25**, 863–874 (2011).
49. Wu, R. S., Kohn, K. W. & Bonner, W. M. Metabolism of ubiquitinated histones. *J. Biol. Chem.* **256**, 5916–5920 (1981).
50. Arora, M. *et al.* Promoters active in interphase are bookmarked during mitosis by ubiquitination. *Nucleic Acids Res.* **40**, 10187–10202 (2012).
51. Giunta, S., Belotserkovskaya, R. & Jackson, S. P. DNA damage signaling in response to double-strand breaks during mitosis. *J. Cell Biol.* **190**, 197–207 (2010).
52. Nakajima, D. *et al.* Preparation of a set of expression-ready clones of mammalian long cDNAs encoding large proteins by the ORF trap cloning method. *DNA Res. Int. J. Rapid Publ. Rep. Genes Genomes* **12**, 257–267 (2005).
53. Torrisani, J. *et al.* let-7 MicroRNA transfer in pancreatic cancer-derived cells inhibits *in vitro* cell proliferation but fails to alter tumor progression. *Hum Gene Ther* **20**, 831–44 (2009).
54. Dosztányi, Z., Csizmók, V., Tompa, P. & Simon, I. The pairwise energy content estimated from amino acid composition discriminates between folded and intrinsically unstructured proteins. *J. Mol. Biol.* **347**, 827–839 (2005).
55. Linding, R., Russell, R. B., Neduva, V. & Gibson, T. J. GlobPlot: Exploring protein sequences for globularity and disorder. *Nucleic Acids Res.* **31**, 3701–3708 (2003).
56. Linding, R. *et al.* Protein disorder prediction: implications for structural proteomics. *Struct. Lond. Engl. 1993* **11**, 1453–1459 (2003).

Acknowledgements

D. Larrieu was funded by the Ligue Nationale contre le Cancer and M. Brunet by the University Paul Sabatier, Toulouse, France. This project was funded by the Ligue Régionale Midi-Pyrénées contre le Cancer and the "Fondation Toulouse Cancer Santé. The acquisition of Incucyte Zoom apparatus was funded by the Région Occitanie (#15052181). We thank the imaging, cytometry and geno-transcriptomics platforms of the Cancer Research Center of Toulouse (CRCT) and of the Institute of Cardiovascular and Metabolic Diseases of Toulouse (I2MC). We thank Drs P. Soubeyran (Cancer Research Center of Marseille), F. Larminat (Institute of Pharmacology and Structural Biology of Toulouse), A. Besson, S. Manenti, JS. Hoffmann research groups (CRCT) for ample scientific discussions, and D. Arvanitis (I2MC) for English proof reading of the manuscript.

Author contributions

D.L.: acquisition, analysis and interpretation of data, writing of the manuscript. M.B.: acquisition, analysis and interpretation of data. C.V.: acquisition, analysis and interpretation of data. N.H.: acquisition of data and analysis. L.L.: acquisition of data and analysis. L.D.: acquisition of data and analysis. H.L.: acquisition of data and analysis. RM.P.: acquisition of data and analysis. J.S.: substantial contributions to the conception B.J.: acquisition

of data. L.B.: substantial contributions to the conception. P.C.: substantial contributions to the conception. M.D.: conception and design of the work, acquisition, analysis and interpretation of data. J.T.: conception and design of the work, acquisition, analysis and interpretation of data, writing of the manuscript.

Competing interests

The authors declare no competing interests.

Additional information

Supplementary information is available for this paper at https://doi.org/10.1038/s41598-020-57762-9.

Correspondence and requests for materials should be addressed to J.T.

Reprints and permissions information is available at www.nature.com/reprints.

Publisher's note Springer Nature remains neutral with regard to jurisdictional claims in published maps and institutional affiliations.

Références bibliographiques

1. Oliviero, G. *et al.* Dynamic Protein Interactions of the Polycomb Repressive Complex 2 during Differentiation of Pluripotent Cells. *Mol. Cell. Proteomics MCP* **15**, 3450–3460 (2016).

2. Lee, J. W., Choi, H. S., Gyuris, J., Brent, R. & Moore, D. D. Two classes of proteins dependent on either the presence or absence of thyroid hormone for interaction with the thyroid hormone receptor. *Mol. Endocrinol.* **9**, 243–254 (1995).

3. Huibregtse, J. M., Scheffner, M. & Howley, P. M. Cloning and expression of the cDNA for E6-AP, a protein that mediates the interaction of the human papillomavirus E6 oncoprotein with p53. *Mol. Cell. Biol.* **13**, 775–784 (1993).

4. Brunet, M., Vargas, C., Larrieu, D., Torrisani, J. & Dufresne, M. E3 Ubiquitin Ligase TRIP12: Regulation, Structure, and Physiopathological Functions. *Int. J. Mol. Sci.* **21**, 8515 (2020).

5. Nomura, N. Prediction of the Coding Sequences of Unidentified Human Genes. II. The Coding Sequences of 40 New Genes (KIAA0041-KIAA0080) Deduced by Analysis of cDNA Clones from Human Cell Line KG-1. *DNA Res.* **1**, 223–229 (1994).

6. Huibregtse, J. M., Scheffner, M., Beaudenon, S. & Howley, P. M. A family of proteins structurally and functionally related to the E6-AP ubiquitin-protein ligase. *Proc. Natl. Acad. Sci. U. S. A.* **92**, 2563–2567 (1995).

7. Park, Y., Yoon, S. K. & Yoon, J.-B. TRIP12 functions as an E3 ubiquitin ligase of APP-BP1. *Biochem. Biophys. Res. Commun.* **374**, 294–298 (2008).

8. Kajiro, M. *et al.* The E3 Ubiquitin Ligase Activity of Trip12 Is Essential for Mouse Embryogenesis. *PLoS ONE* **6**, e25871 (2011).

9. Hanoun, N. *et al.* The E3 ubiquitin ligase thyroid hormone receptor-interacting protein 12 targets pancreas transcription factor 1a for proteasomal degradation. *J. Biol. Chem.* **289**, 35593–35604 (2014).

10. Masui, T. *et al.* Replacement of Rbpj With Rbpjl in the PTF1 Complex Controls the Final Maturation of Pancreatic Acinar Cells. *Gastroenterology* **139**, 270–280 (2010).

11. Krapp, A. *et al.* The bHLH protein PTF1-p48 is essential for the formation of the exocrine and the correct spatial organization of the endocrine pancreas. *Genes Dev.* **12**, 3752–3763 (1998).

12. Dufresne, M. *et al.* Id3 modulates cellular localization of bHLH Ptf1-p48 protein. *Int. J. Cancer* **129**, 295–306 (2011).

13. Krah, N. M. *et al.* The acinar differentiation determinant PTF1A inhibits initiation of pancreatic ductal adenocarcinoma. *eLife* **4**, e07125 (2015).

14. Chen, D., Shan, J., Zhu, W.-G., Qin, J. & Gu, W. Transcription-independent ARF regulation in oncogenic stress-mediated p53 responses. *Nature* **464**, 624–627 (2010).

15. Trinklein, N. D. *et al.* An abundance of bidirectional promoters in the human genome. *Genome Res.* **14**, 62–66 (2004).

16. Wakano, C., Byun, J. S., Di, L.-J. & Gardner, K. The Dual Lives of Bidirectional Promoters. *Biochim. Biophys. Acta* **1819**, 688–693 (2012).

17. Jin, J. *et al.* Systematic analysis and nomenclature of mammalian F-box proteins. *Genes Dev.* **18**, 2573–2580 (2004).

18. Tekcham, D. S. *et al.* F-box proteins and cancer: an update from functional and regulatory mechanism to therapeutic clinical prospects. *Theranostics* **10**, 4150–4167 (2020).

19. Chang, J.-W. *et al.* mRNA 3'-UTR shortening is a molecular signature of mTORC1 activation. *Nat. Commun.* **6**, 7218 (2015).

20. An, C.-I., Ganio, E. & Hagiwara, N. Trip12, a HECT domain E3 ubiquitin ligase, targets Sox6 for proteasomal degradation and affects fiber type-specific gene expression in muscle cells. *Skelet. Muscle* **3**, 11 (2013).

21. Larrieu D , Brunet M, Vargas C , Hanoun N , Ligat L , Dagnon L , Lulka H , Pommier R , Selves J , Beata J , Bartholin L , Cordelier P , Dufresne M, Torrisani J. The E3 ubiquitin ligase TRIP12 participates in cell cycle progression and chromosome stability. *Scientific reports, In press*.

22. Ju, D., Wang, X., Xu, H. & Xie, Y. The armadillo repeats of the Ufd4 ubiquitin ligase recognize ubiquitin-fusion proteins. *FEBS Lett.* **581**, 265–270 (2007).

23. Aravind, L. The WWE domain: a common interaction module in protein ubiquitination and ADP ribosylation. *Trends Biochem. Sci.* **26**, 273–275 (2001).

24. Park, Y., Yoon, S. K. & Yoon, J.-B. The HECT domain of TRIP12 ubiquitinates substrates of the ubiquitin fusion degradation pathway. *J. Biol. Chem.* **284**, 1540–1549 (2009).

25. Toretsky, J. A. & Wright, P. E. Assemblages: Functional units formed by cellular phase separation. *J. Cell Biol.* **206**, 579–588 (2014).

26. M, W. & K, S. Disordered domains in chromatin-binding proteins. *Essays Biochem.* **63**, (2019).

27. Vuzman, D. & Levy, Y. Intrinsically disordered regions as affinity tuners in protein-DNA interactions. *Mol. Biosyst.* **8**, 47–57 (2012).

28. Liu, X. *et al.* Trip12 is an E3 ubiquitin ligase for USP7/HAUSP involved in the DNA damage response. *FEBS Lett.* **590**, 4213–4222 (2016).

29. Tewari, R., Bailes, E., Bunting, K. A. & Coates, J. C. Armadillo-repeat protein functions: questions for little creatures. *Trends Cell Biol.* **20**, 470–481 (2010).

30. Gatti, M., Imhof, R., Huang, Q., Baudis, M. & Altmeyer, M. The Ubiquitin Ligase TRIP12 Limits PARP1 Trapping and Constrains PARP Inhibitor Efficiency. *Cell Rep.* **32**, (2020).

31. Huibregtse, J. M. A family of proteins structurally and functionally related to the E6-AP ubiquitin-protein ligase. 5.

32. Gudjonsson, T. *et al.* TRIP12 and UBR5 Suppress Spreading of Chromatin Ubiquitylation at Damaged Chromosomes. *Cell* **150**, 697–709 (2012).

33. Petrone, A., Adamo, M. E., Cheng, C. & Kettenbach, A. N. Identification of Candidate Cyclin-dependent kinase 1 (Cdk1) Substrates in Mitosis by Quantitative Phosphoproteomics. *Mol. Cell. Proteomics MCP* **15**, 2448–2461 (2016).

34. Blasius, M. *et al.* A phospho-proteomic screen identifies substrates of the checkpoint kinase Chk1. *Genome Biol.* **12**, R78 (2011).

35. Matsuoka, S. *et al.* ATM and ATR substrate analysis reveals extensive protein networks responsive to DNA damage. *Science* **316**, 1160–1166 (2007).

36. Cai, J.-B. *et al.* Ubiquitin-specific protease 7 accelerates p14 ^{ARF} degradation by deubiquitinating thyroid hormone receptor-interacting protein 12 and promotes hepatocellular carcinoma progression: HEPATOLOGY, Vol. XX, No. X, 2015. *Hepatology* **61**, 1603–1614 (2015).

37. Georges, A., Marcon, E., Greenblatt, J. & Frappier, L. Identification and Characterization of USP7 Targets in Cancer Cells. *Sci. Rep.* **8**, 15833 (2018).

38. Hershko, A. & Ciechanover, A. The ubiquitin system. *Annu. Rev. Biochem.* **67**, 425–479 (1998).

39. Pickart, C. M. Mechanisms underlying ubiquitination. *Annu. Rev. Biochem.* **70**, 503–533 (2001).

40. Varshavsky, A. N-degron and C-degron pathways of protein degradation. *Proc. Natl. Acad. Sci.* **116**, 358–366 (2019).

41. Wenzel, D. M., Lissounov, A., Brzovic, P. S. & Klevit, R. E. UbcH7 reactivity profile reveals Parkin and HHARI to be RING/HECT hybrids. *Nature* **474**, 105–108 (2011).

42. Scheffner, M., Nuber, U. & Huibregtse, J. M. Protein ubiquitination involving an E1-E2-E3 enzyme ubiquitin thioester cascade. *Nature* **373**, 81–83 (1995).

43. Lorenz, S. Structural mechanisms of HECT-type ubiquitin ligases. *Biol. Chem.* **399**, 127–145 (2018).

44. Spratt, D. E., Walden, H. & Shaw, G. S. RBR E3 ubiquitin ligases: new structures, new insights, new questions. *Biochem. J.* **458**, 421–437 (2014).

45. Zheng, N. & Shabek, N. Ubiquitin Ligases: Structure, Function, and Regulation. *Annu. Rev. Biochem.* **86**, 129–157 (2017).

46. Senft, D., Qi, J. & Ronai, Z. A. Ubiquitin ligases in oncogenic transformation and cancer therapy. *Nat. Rev. Cancer* **18**, 69–88 (2018).

47. Deng, L., Meng, T., Chen, L., Wei, W. & Wang, P. The role of ubiquitination in tumorigenesis and targeted drug discovery. *Signal Transduct. Target. Ther.* **5**, 1–28 (2020).

48. Swatek, K. N. & Komander, D. Ubiquitin modifications. *Cell Res.* **26**, 399–422 (2016).

49. McClellan, A. J., Laugesen, S. H. & Ellgaard, L. Cellular functions and molecular mechanisms of non-lysine ubiquitination. *Open Biol.* **9**, 190147 (2019).

50. Han, Y. G., Yun, M., Choi, M., Lee, S.-G. & Kim, H. TRAIP regulates Histone H2B monoubiquitination in DNA damage response pathways. *Oncol. Rep.* **41**, 3305–3312 (2019).

51. Wilkinson, K. D. Regulation of ubiquitin-dependent processes by deubiquitinating enzymes. *FASEB J.* **11**, 1245–1256 (1997).

52. Harrigan, J. A., Jacq, X., Martin, N. M. & Jackson, S. P. Deubiquitylating enzymes and drug discovery: emerging opportunities. *Nat. Rev. Drug Discov.* **17**, 57–78 (2018).

53. Ye, Y. *et al.* Polyubiquitin binding and cross-reactivity in the USP domain deubiquitinase USP21. *EMBO Rep.* **12**, 350–357 (2011).

54. Kweon, S.-M. *et al.* An Adversarial DNA N6-Methyladenine-Sensor Network Preserves Polycomb Silencing. *Mol. Cell* **74**, 1138-1147.e6 (2019).

55. Keppler, B. R. & Archer, T. K. Ubiquitin-dependent and Ubiquitin-independent Control of Subunit Stoichiometry in the SWI/SNF Complex. *J. Biol. Chem.* **285**, 35665–35674 (2010).

56. Khan, O. M. *et al.* Proteasomal degradation of the tumour suppressor FBW7 requires branched ubiquitylation by TRIP12. *Nat. Commun.* **12**, 2043 (2021).

57. Felsenfeld, G. & Groudine, M. Controlling the double helix. *Nature* **421**, 448–453 (2003).

58. Roberts, C. W. M. & Orkin, S. H. The SWI/SNF complex--chromatin and cancer. *Nat. Rev. Cancer* **4**, 133–142 (2004).

59. Chen, J. & Archer, T. K. Regulating SWI/SNF subunit levels via protein-protein interactions and proteasomal degradation: BAF155 and BAF170 limit expression of BAF57. *Mol. Cell. Biol.* **25**, 9016–9027 (2005).

60. Zentner, G. E. & Henikoff, S. Regulation of nucleosome dynamics by histone modifications. *Nat. Struct. Mol. Biol.* **20**, 259–266 (2013).

61. Wang, H. *et al.* Role of histone H2A ubiquitination in Polycomb silencing. *Nature* **431**, 873–878 (2004).

62. Cao, R. *et al.* Role of histone H3 lysine 27 methylation in Polycomb-group silencing. *Science* **298**, 1039–1043 (2002).

63. Scheuermann, J. C. *et al.* Histone H2A deubiquitinase activity of the Polycomb repressive complex PR-DUB. *Nature* **465**, 243–247 (2010).

64. Kloet, S. L. *et al.* The dynamic interactome and genomic targets of Polycomb complexes during stem-cell differentiation. *Nat. Struct. Mol. Biol.* **23**, 682–690 (2016).

65. Oliviero, G. *et al.* Dynamic Protein Interactions of the Polycomb Repressive Complex 2 during Differentiation of Pluripotent Cells. *Mol. Cell. Proteomics MCP* **15**, 3450–3460 (2016).

66. Cao, Q. *et al.* The central role of EED in the orchestration of polycomb group complexes. *Nat. Commun.* **5**, 3127 (2014).

67. Chen, D., Yoon, J.-B. & Gu, W. Reactivating the ARF-p53 axis in AML cells by targeting ULF. *Cell Cycle* **9**, 2946–2951 (2010).

68. Sherr, C. J. Divorcing ARF and p53: an unsettled case. *Nat. Rev. Cancer* **6**, 663–673 (2006).

69. Vousden, K. H. & Lu, X. Live or let die: the cell's response to p53. *Nat. Rev. Cancer* **2**, 594–604 (2002).

70. Chen, D. *et al.* Differential Effects on ARF Stability by Normal versus Oncogenic Levels of c-Myc Expression. *Mol. Cell* **51**, 46–56 (2013).

71. Carroll, P. A., Freie, B. W., Mathsyaraja, H. & Eisenman, R. N. The MYC transcription factor network: balancing metabolism, proliferation and oncogenesis. *Front. Med.* **12**, 412–425 (2018).

72. Aggarwal, B. B. Signalling pathways of the TNF superfamily: a double-edged sword. *Nat. Rev. Immunol.* **3**, 745–756 (2003).

73. Chio, I. I. C. *et al.* TRADD contributes to tumour suppression by regulating ULF-dependent p19Arf ubiquitylation. *Nat. Cell Biol.* **14**, 625–633 (2012).

74. Box, J. K. *et al.* Nucleophosmin: from structure and function to disease development. *BMC Mol. Biol.* **17**, (2016).

75. Lo, D. *et al.* Nucleostemin stabilizes ARF by inhibiting the ubiquitin ligase ULF. *Oncogene* **34**, 1688–1697 (2015).

76. Li, M. *et al.* Deubiquitination of p53 by HAUSP is an important pathway for p53 stabilization. *Nature* **416**, 648–653 (2002).

77. Li, M., Brooks, C. L., Kon, N. & Gu, W. A Dynamic Role of HAUSP in the p53-Mdm2 Pathway. *Mol. Cell* **13**, 879–886 (2004).

78. Ginno, P. A., Burger, L., Seebacher, J., Iesmantavicius, V. & Schübeler, D. Cell cycle-resolved chromatin proteomics reveals the extent of mitotic preservation of the genomic regulatory landscape. *Nat. Commun.* **9**, 4048 (2018).

79. Kim, W. Y. & Sharpless, N. E. The regulation of INK4/ARF in cancer and aging. *Cell* **127**, 265–275 (2006).

80. Reinhardt, H. C. & Schumacher, B. The p53 network: Cellular and systemic DNA damage responses in aging and cancer. *Trends Genet. TIG* **28**, 128–136 (2012).

81. Velimezi, G. *et al.* Functional interplay between the DNA-damage-response kinase ATM and ARF tumour suppressor protein in human cancer. *Nat. Cell Biol.* **15**, 967–977 (2013).

82. Challa, K. *et al.* Damage-induced chromatome dynamics link Ubiquitin ligase and proteasome recruitment to histone loss and efficient DNA repair. *Mol. Cell* **81**, 811-829.e6 (2021).

83. Mailand, N. *et al.* RNF8 ubiquitylates histones at DNA double-strand breaks and promotes assembly of repair proteins. *Cell* **131**, 887–900 (2007).

84. Panier, S. & Durocher, D. Regulatory ubiquitylation in response to DNA double-strand breaks. *DNA Repair* **8**, 436–443 (2009).

85. Doil, C. *et al.* RNF168 Binds and Amplifies Ubiquitin Conjugates on Damaged Chromosomes to Allow Accumulation of Repair Proteins. *Cell* **136**, 435–446 (2009).

86. Zhu, Q., Sharma, N., He, J., Wani, G. & Wani, A. A. USP7 deubiquitinase promotes ubiquitin-dependent DNA damage signaling by stabilizing RNF168. *Cell Cycle Georget. Tex* **14**, 1413–1425 (2015).

87. Wang, Z. *et al.* Recognition of the iso-ADP-ribose moiety in poly(ADP-ribose) by WWE domains suggests a general mechanism for poly(ADP-ribosyl)ation-dependent ubiquitination. *Genes Dev.* **26**, 235–240 (2012).

88. Wei, H. & Yu, X. Functions of PARylation in DNA Damage Repair Pathways. *Genomics Proteomics Bioinformatics* **14**, 131–139 (2016).

89. Ciccarone, F., Zampieri, M. & Caiafa, P. PARP1 orchestrates epigenetic events setting up chromatin domains. *Semin. Cell Dev. Biol.* **63**, 123–134 (2017).

90. Langelier, M.-F. & Pascal, J. M. PARP-1 mechanism for coupling DNA damage detection to poly(ADP-ribose) synthesis. *Curr. Opin. Struct. Biol.* **23**, 134–143 (2013).

91. Haince, J.-F. *et al.* Ataxia telangiectasia mutated (ATM) signaling network is modulated by a novel poly(ADP-ribose)-dependent pathway in the early response to DNA-damaging agents. *J. Biol. Chem.* **282**, 16441–16453 (2007).

92. Ménisser-de Murcia, J., Mark, M., Wendling, O., Wynshaw-Boris, A. & de Murcia, G. Early embryonic lethality in PARP-1 Atm double-mutant mice suggests a functional synergy in cell proliferation during development. *Mol. Cell. Biol.* **21**, 1828–1832 (2001).

93. Yoo, N. J., Park, S. W. & Lee, S. H. Frameshift mutations of ubiquitination-related genes HERC2, HERC3, TRIP12, UBE2Q1 and UBE4B in gastric and colorectal carcinomas with microsatellite instability. *Pathology (Phila.)* **43**, 753–755 (2011).

94. Li, G. *et al.* Identification of mutant genes with high-frequency, high-risk, and high-expression in lung adenocarcinoma. *Thorac. Cancer* **5**, 211–218 (2014).

95. Hein, R. *et al.* A genome-wide association study to identify genetic susceptibility loci that modify ductal and lobular postmenopausal breast cancer risk associated with menopausal hormone therapy use: a two-stage design with replication. *Breast Cancer Res. Treat.* **138**, 529–542 (2013).

96. Cacheux, W. *et al.* Exome sequencing reveals aberrant signalling pathways as hallmark of treatment-naive anal squamous cell carcinoma. *Oncotarget* **9**, 464–476 (2018).

97. Shiba, N. *et al.* Transcriptome analysis offers a comprehensive illustration of the genetic background of pediatric acute myeloid leukemia. *Blood Adv.* **3**, 3157–3169 (2019).

98. Gao, P., Jin, Z., Cheng, Y. & Cao, X. RNA-Seq analysis identifies aberrant RNA splicing of TRIP12 in acute myeloid leukemia patients at remission. *Tumor Biol.* **35**, 9585–9590 (2014).

99. Lee, K. K. *et al.* The oncogenic E3 ligase TRIP12 suppresses epithelial–mesenchymal transition (EMT) and mesenchymal traits through ZEB1/2. *Cell Death Discov.* **7**, 1–15 (2021).

100. Horvat, A. *et al.* Helicobacter pylori pathogen regulates p14ARF tumor suppressor and autophagy in gastric epithelial cells. *Oncogene* **37**, 5054–5065 (2018).

101. Kodaman, N. *et al.* Human and Helicobacter pylori coevolution shapes the risk of gastric disease. *Proc. Natl. Acad. Sci. U. S. A.* **111**, 1455–1460 (2014).

102. Wang, L. *et al.* TRIP12 as a mediator of human papillomavirus/p16-related radiation enhancement effects. *Oncogene* **36**, 820–828 (2017).

103. Pandol, S. J. The Exocrine Pancreas. *Colloq. Ser. Integr. Syst. Physiol. Mol. Funct.* **3**, 1–64 (2011).

104. Kern, H. Fine structure of the human exocrine pancreas. *Pancreas Biol. Pathobiol. Dis. 2nd Edn* pp 9-19 (1993).

105. Williams, J. A. Intracellular signaling mechanisms activated by cholecystokinin-regulating synthesis and secretion of digestive enzymes in pancreatic acinar cells. *Annu. Rev. Physiol.* **63**, 77–97 (2001).

106. Muallem, S., Kwiatkowska, K., Xu, X. & Yin, H. L. Actin filament disassembly is a sufficient final trigger for exocytosis in nonexcitable cells. *J. Cell Biol.* **128**, 589–598 (1995).

107. O'Konski, M. S. & Pandol, S. J. Effects of caerulein on the apical cytoskeleton of the pancreatic acinar cell. *J. Clin. Invest.* **86**, 1649–1657 (1990).

108. Grapin-Botton, A. Ductal cells of the pancreas. *Int. J. Biochem. Cell Biol.* **37**, 504–510 (2005).

109. Steward, M. C. & Ishiguro, H. Molecular and cellular regulation of pancreatic duct cell function. *Curr. Opin. Gastroenterol.* **25**, 447–453 (2009).

110. Cleveland, M. H., Sawyer, J. M., Afelik, S., Jensen, J. & Leach, S. D. Exocrine ontogenies: on the development of pancreatic acinar, ductal and centroacinar cells. *Semin. Cell Dev. Biol.* **23**, 711–719 (2012).

111. Gasslander, T., Ihse, I. & Smeds, S. The Importance of the Centroacinar Region in Cerulein-Induced Mouse Pancreatic Growth. *Scand. J. Gastroenterol.* **27**, 564–570 (1992).

112. Beer, R. L., Parsons, M. J. & Rovira, M. Centroacinar cells: At the center of pancreas regeneration. *Dev. Biol.* **413**, 8–15 (2016).

113. Whitcomb, D. C. & Lowe, M. E. Human Pancreatic Digestive Enzymes. *Dig. Dis. Sci.* **52**, 1–17 (2007).

114. Slack, J. M. Developmental biology of the pancreas. *Dev. Camb. Engl.* **121**, 1569–1580 (1995).

115. Lammert, E., Cleaver, O. & Melton, D. Induction of Pancreatic Differentiation by Signals from Blood Vessels. *Science* **294**, 564–567 (2001).

116. Pan, F. C. & Wright, C. Pancreas organogenesis: from bud to plexus to gland. *Dev. Dyn. Off. Publ. Am. Assoc. Anat.* **240**, 530–565 (2011).

117. Ahlgren, U., Jonsson, J. & Edlund, H. The morphogenesis of the pancreatic mesenchyme is uncoupled from that of the pancreatic epithelium in IPF1/PDX1-deficient mice. *Development* **122**, 1409–1416 (1996).

118. Miyatsuka, T. *et al.* Persistent expression of PDX-1 in the pancreas causes acinar-to-ductal metaplasia through Stat3 activation. *Genes Dev.* **20**, 1435–1440 (2006).

119. Jensen, J. *et al.* Control of endodermal endocrine development by Hes-1. *Nat. Genet.* **24**, 36–44 (2000).

120. Pa, S. *et al.* SOX9 is required for maintenance of the pancreatic progenitor cell pool. *Proc. Natl. Acad. Sci. U. S. A.* **104**, 1865–1870 (2007).

121. Kawaguchi, Y. *et al.* The role of the transcriptional regulator Ptf1a in converting intestinal to pancreatic progenitors. *Nat. Genet.* **32**, 128–134 (2002).

122. Haumaitre, C. *et al.* Lack of TCF2/vHNF1 in mice leads to pancreas agenesis. *Proc. Natl. Acad. Sci. U. S. A.* **102**, 1490–1495 (2005).

123. Hick, A.-C. *et al.* Mechanism of primitive duct formation in the pancreas and submandibular glands: a role for SDF-1. *BMC Dev. Biol.* **9**, 66 (2009).

124. Zhou, Q. *et al.* A Multipotent Progenitor Domain Guides Pancreatic Organogenesis. *Dev. Cell* **13**, 103–114 (2007).

125. Shih, H. P., Wang, A. & Sander, M. Pancreas Organogenesis: From Lineage Determination to Morphogenesis. *Annu. Rev. Cell Dev. Biol.* **29**, 81–105 (2013).

126. Kopinke, D. *et al.* Lineage tracing reveals the dynamic contribution of Hes1+ cells to the developing and adult pancreas. *Development* **138**, 431–441 (2011).

127. Kopp, J. L. *et al.* Sox9+ ductal cells are multipotent progenitors throughout development but do not produce new endocrine cells in the normal or injured adult pancreas. *Development* **138**, 653–665 (2011).

128. Murtaugh, L. C., Stanger, B. Z., Kwan, K. M. & Melton, D. A. Notch signaling controls multiple steps of pancreatic differentiation. *Proc. Natl. Acad. Sci. U. S. A.* **100**, 14920–14925 (2003).

129. Schaffer, A. E., Freude, K. K., Nelson, S. B. & Sander, M. Nkx6 Transcription Factors and Ptf1a Function as Antagonistic Lineage Determinants in Multipotent Pancreatic Progenitors. *Dev. Cell* **18**, 1022–1029 (2010).

130. Masui, T., Long, Q., Beres, T. M., Magnuson, M. A. & MacDonald, R. J. Early pancreatic development requires the vertebrate Suppressor of Hairless (RBPJ) in the PTF1 bHLH complex. *Genes Dev.* **21**, 2629–2643 (2007).

131. Rose, S. D., Swift, G. H., Peyton, M. J., Hammer, R. E. & MacDonald, R. J. The Role of PTF1-P48 in Pancreatic Acinar Gene Expression *. *J. Biol. Chem.* **276**, 44018–44026 (2001).

132. Holmstrom, S. R. *et al.* LRH-1 and PTF1-L coregulate an exocrine pancreas-specific transcriptional network for digestive function. *Genes Dev.* **25**, 1674–1679 (2011).

133. MacDonald, R. J., Swift, G. H. & Real, F. X. Transcriptional Control of Acinar Development and Homeostasis. in *Progress in Molecular Biology and Translational Science* vol. 97 1–40 (Elsevier, 2010).

134. Zhu, L. *et al.* Inhibition of Mist1 Homodimer Formation Induces Pancreatic Acinar-to-Ductal Metaplasia. *Mol. Cell. Biol.* **24**, 2673–2681 (2004).

135. Shih, H. P. *et al.* A Notch-dependent molecular circuitry initiates pancreatic endocrine and ductal cell differentiation. *Dev. Camb. Engl.* **139**, 2488–2499 (2012).

136. Wang, S. *et al.* Neurog3 gene dosage regulates allocation of endocrine and exocrine cell fates in the developing mouse pancreas. *Dev. Biol.* **339**, 26–37 (2010).

137. Shih, H. P. *et al.* A Notch-dependent molecular circuitry initiates pancreatic endocrine and ductal cell differentiation. *Development* **139**, 2488–2499 (2012).

138. Maestro, M. A. *et al.* Hnf6 and Tcf2 (MODY5) are linked in a gene network operating in a precursor cell domain of the embryonic pancreas. *Hum. Mol. Genet.* **12**, 3307–3314 (2003).

139. Solar, M. *et al.* Pancreatic exocrine duct cells give rise to insulin-producing beta cells during embryogenesis but not after birth. *Dev. Cell* **17**, 849–860 (2009).

140. De Vas, M. G. *et al.* Hnf1b controls pancreas morphogenesis and the generation of Ngn3+ endocrine progenitors. *Dev. Camb. Engl.* **142**, 871–882 (2015).

141. Puri, S. & Hebrok, M. *imaging*.

142. Slack, J. M. W. Metaplasia and transdifferentiation: from pure biology to the clinic. *Nat. Rev. Mol. Cell Biol.* **8**, 369–378 (2007).

143. De Lisle, R. C. & Logsdon, C. D. Pancreatic acinar cells in culture: expression of acinar and ductal antigens in a growth-related manner. *Eur. J. Cell Biol.* **51**, 64–75 (1990).

144. Hall, P. A. & Lemoine, N. R. Rapid acinar to ductal transdifferentiation in cultured human exocrine pancreas. *J. Pathol.* **166**, 97–103 (1992).

145. Vila, M. R., Lloreta, J. & Real, F. X. Normal human pancreas cultures display functional ductal characteristics. *Lab. Investig. J. Tech. Methods Pathol.* **71**, 423–431 (1994).

146. Fanjul, M. *et al.* Evidence for Epithelial–Mesenchymal Transition in Adult Human Pancreatic Exocrine Cells. *J. Histochem. Cytochem.* **58**, 807–823 (2010).

147. Githens, S. *et al.* Mouse pancreatic acinar/ductlar tissue gives rise to epithelial cultures that are morphologically, biochemically, and functionally indistinguishable from interlobular duct cell cultures. *Vitro Cell. Dev. Biol. - Anim.* **30**, 622–635 (1994).

148. Rooman, I., Heremans, Y., Heimberg, H. & Bouwens, L. Modulation of rat pancreatic acinoductal transdifferentiation and expression of PDX-1 in vitro. *Diabetologia* **43**, 907–914 (2000).

149. Jopling, C., Boue, S. & Izpisua Belmonte, J. C. Dedifferentiation, transdifferentiation and reprogramming: three routes to regeneration. *Nat. Rev. Mol. Cell Biol.* **12**, 79–89 (2011).

150. Means, A. L. *et al.* Pancreatic epithelial plasticity mediated by acinar cell transdifferentiation and generation of nestin-positive intermediates. *Development* **132**, 3767–3776 (2005).

151. Bouwens, L. Transdifferentiation versus stem cell hypothesis for the regeneration of islet beta-cells in the pancreas. *Microsc. Res. Tech.* **43**, 332–336 (1998).

152. Baeyens, L. *et al.* In vitro generation of insulin-producing beta cells from adult exocrine pancreatic cells. *Diabetologia* **48**, 49–57 (2005).

153. Lardon, J. *et al.* Plasticity in the adult rat pancreas: transdifferentiation of exocrine to hepatocyte-like cells in primary culture. *Hepatol. Baltim. Md* **39**, 1499–1507 (2004).

154. Houbracken, I. *et al.* Lineage tracing evidence for transdifferentiation of acinar to duct cells and plasticity of human pancreas. *Gastroenterology* **141**, 731–741, 741.e1–4 (2011).

155. Rooman, I. & Real, F. X. Pancreatic ductal adenocarcinoma and acinar cells: a matter of differentiation and development? *Gut* **61**, 449–458 (2012).

156. Murtaugh, L. C. & Keefe, M. D. Regeneration and repair of the exocrine pancreas. *Annu. Rev. Physiol.* **77**, 229–249 (2015).

157. Bockman, D. E. Morphology of the exocrine pancreas related to pancreatitis. *Microsc. Res. Tech.* **37**, 509–519 (1997).

158. Strobel, O. *et al.* In Vivo Lineage Tracing Defines the Role of Acinar-to-Ductal Transdifferentiation in Inflammatory Ductal Metaplasia. *Gastroenterology* **133**, 1999–2009 (2007).

159. Forsmark, C. E. Chronic pancreatitis and quality of life. *Dig. Liver Dis. Off. J. Ital. Soc. Gastroenterol. Ital. Assoc. Study Liver* **38**, 116–118 (2006).

160. Hyun, J. J. & Lee, H. S. Experimental Models of Pancreatitis. *Clin. Endosc.* **47**, 212–216 (2014).

161. Williams, J. A., Korc, M. & Dormer, R. L. Action of secretagogues on a new preparation of functionally intact, isolated pancreatic acini. *Am. J. Physiol.-Endocrinol. Metab.* **235**, E517-524 (1978).

162. Zaninovic, V., Gukovskaya, A. S., Gukovsky, I., Mouria, M. & Pandol, S. J. Cerulein upregulates ICAM-1 in pancreatic acinar cells, which mediates neutrophil adhesion to these cells. *Am. J. Physiol. Gastrointest. Liver Physiol.* **279**, G666-676 (2000).

163. Kong, B. *et al.* Dynamic landscape of pancreatic carcinogenesis reveals early molecular networks of malignancy. *Gut* **67**, 146–156 (2018).

164. Halangk, W. *et al.* Role of cathepsin B in intracellular trypsinogen activation and the onset of acute pancreatitis. *J. Clin. Invest.* **106**, 773–781 (2000).

165. Jensen, J. N. *et al.* Recapitulation of elements of embryonic development in adult mouse pancreatic regeneration. *Gastroenterology* **128**, 728–741 (2005).

166. Pinho, A. V. *et al.* Adult pancreatic acinar cells dedifferentiate to an embryonic progenitor phenotype with concomitant activation of a senescence programme that is present in chronic pancreatitis. *Gut* **60**, 958–966 (2011).

167. Iovanna, J. L., de la Porte, P. L. & Dagorn, J.-C. Expression of Genes Associated with Dedifferentiation and Cell Proliferation During Pancreatic Regeneration Following Acute Pancreatitis. *Pancreas* **7**, 712–718 (1992).

168. Gout, J. *et al.* Isolation and Culture of Mouse Primary Pancreatic Acinar Cells. *JoVE J. Vis. Exp.* e50514 (2013) doi:10.3791/50514.

169. Stanger, B. Z. & Hebrok, M. Control of cell identity in pancreas development and regeneration. *Gastroenterology* **144**, 1170–1179 (2013).

170. Rodolosse, A. *et al.* PTF1alpha/p48 transcription factor couples proliferation and differentiation in the exocrine pancreas [corrected]. *Gastroenterology* **127**, 937–949 (2004).

171. Campos, M. L. *et al.* ICAT is a novel Ptf1a interactor that regulates pancreatic acinar differentiation and displays altered expression in tumours. *Biochem. J.* **451**, 395–405 (2013).

172. Molero, X. *et al.* Pancreas transcription factor 1α expression is regulated in pancreatitis. *Eur. J. Clin. Invest.* **37**, 791–801 (2007).

173. Benitz, S. *et al.* Polycomb repressor complex 1 promotes gene silencing through H2AK119 mono-ubiquitination in acinar-to-ductal metaplasia and pancreatic cancer cells. *Oncotarget* **7**, 11424–11433 (2015).

174. von Figura, G., Morris, J. P., Wright, C. V. E. & Hebrok, M. Nr5a2 maintains acinar cell differentiation and constrains oncogenic Kras-mediated pancreatic neoplastic initiation. *Gut* **63**, 656–664 (2014).

175. Cobo, I. *et al.* Transcriptional regulation by NR5A2 links differentiation and inflammation in the pancreas. *Nature* **554**, 533–537 (2018).

176. Pin, C. L., Rukstalis, J. M., Johnson, C. & Konieczny, S. F. The bHLH transcription factor Mist1 is required to maintain exocrine pancreas cell organization and acinar cell identity. *J. Cell Biol.* **155**, 519–530 (2001).

177. Direnzo, D. *et al.* Induced Mist1 Expression Promotes Remodeling of Mouse Pancreatic Acinar Cells. *Gastroenterology* **143**, 469–480 (2012).

178. Johnson, C. L. *et al.* Activation of protein kinase Cδ leads to increased pancreatic acinar cell dedifferentiation in the absence of MIST1. *J. Pathol.* **228**, 351–365 (2012).

179. Shi, G. *et al.* Loss of the acinar-restricted transcription factor Mist1 accelerates Kras-induced pancreatic intraepithelial neoplasia. *Gastroenterology* **136**, 1368–1378 (2009).

180. Jia, D., Sun, Y. & Konieczny, S. F. Mist1 Regulates Pancreatic Acinar Cell Proliferation through p21CIP1/WAF1. *Gastroenterology* **135**, 1687–1697 (2008).

181. Grabliauskaite, K. *et al.* p21(WAF1) (/Cip1) limits senescence and acinar-to-ductal metaplasia formation during pancreatitis. *J. Pathol.* **235**, 502–514 (2015).

182. Prévot, P.-P. *et al.* Role of the ductal transcription factors HNF6 and Sox9 in pancreatic acinar-to-ductal metaplasia. *Gut* **61**, 1723–1732 (2012).

183. Kopp, J. L. *et al.* Identification of Sox9-dependent acinar-to-ductal reprogramming as the principal mechanism for initiation of pancreatic ductal adenocarcinoma. *Cancer Cell* **22**, 737–750 (2012).

184. Quilichini, E. *et al.* Pancreatic Ductal Deletion of Hnf1b Disrupts Exocrine Homeostasis, Leads to Pancreatitis, and Facilitates Tumorigenesis. *Cell. Mol. Gastroenterol. Hepatol.* **8**, 487–511 (2019).

185. Roy, N. *et al.* PDX1 dynamically regulates pancreatic ductal adenocarcinoma initiation and maintenance. *Genes Dev.* **30**, 2669–2683 (2016).

186. Zhang, W. & Liu, H. T. MAPK signal pathways in the regulation of cell proliferation in mammalian cells. *Cell Res.* **12**, 9–18 (2002).

187. Collins, M. A., Yan, W., Sebolt-Leopold, J. S. & Pasca di Magliano, M. MAPK signaling is required for dedifferentiation of acinar cells and development of pancreatic intraepithelial neoplasia in mice. *Gastroenterology* **146**, 822-834.e7 (2014).

188. Perera, R. M. & Bardeesy, N. Ready, set, go: the EGF receptor at the pancreatic cancer starting line. *Cancer Cell* **22**, 281–282 (2012).

189. Garcia-Carracedo, D. *et al.* Smad4 Loss Synergizes with TGFα Overexpression in Promoting Pancreatic Metaplasia, PanIN Development, and Fibrosis. *PLOS ONE* **10**, e0120851 (2015).

190. Means, A. L. *et al.* Overexpression of heparin-binding EGF-like growth factor in mouse pancreas results in fibrosis and epithelial metaplasia. *Gastroenterology* **124**, 1020–1036 (2003).

191. Ardito, C. M. *et al.* EGF receptor is required for KRAS-induced pancreatic tumorigenesis. *Cancer Cell* **22**, 304–317 (2012).

192. Shi, G. *et al.* Maintenance of acinar cell organization is critical to preventing Kras-induced acinar-ductal metaplasia. *Oncogene* **32**, 1950–1958 (2013).

193. Halbrook, C. J. *et al.* Mitogen-activated Protein Kinase Kinase Activity Maintains Acinar-to-Ductal Metaplasia and Is Required for Organ Regeneration in Pancreatitis. *Cell. Mol. Gastroenterol. Hepatol.* **3**, 99–118 (2017).

194. Manning, B. D. & Toker, A. AKT/PKB Signaling: Navigating the Network. *Cell* **169**, 381–405 (2017).

195. Baer, R. *et al.* Pancreatic cell plasticity and cancer initiation induced by oncogenic Kras is completely dependent on wild-type PI 3-kinase p110α. *Genes Dev.* **28**, 2621–2635 (2014).

196. Payne, S. N. *et al.* PIK3CA mutations can initiate pancreatic tumorigenesis and are targetable with PI3K inhibitors. *Oncogenesis* **4**, e169–e169 (2015).

197. Stanger, B. Z. *et al.* Pten constrains centroacinar cell expansion and malignant transformation in the pancreas. *Cancer Cell* **8**, 185–195 (2005).

198. Elghazi, L. *et al.* Regulation of pancreas plasticity and malignant transformation by Akt signaling. *Gastroenterology* **136**, 1091–1103 (2009).

199. Rooman, I. *et al.* Expression of the Notch signaling pathway and effect on exocrine cell proliferation in adult rat pancreas. *Am. J. Pathol.* **169**, 1206–1214 (2006).

200. Esni, F. *et al.* Notch inhibits Ptf1 function and acinar cell differentiation in developing mouse and zebrafish pancreas. *Development* **131**, 4213–4224 (2004).

201. Siveke, J. T. *et al.* Notch signaling is required for exocrine regeneration after acute pancreatitis. *Gastroenterology* **134**, 544–555 (2008).

202. Greer, R. L., Staley, B. K., Liou, A. & Hebrok, M. Numb regulates acinar cell dedifferentiation and survival during pancreatic damage and acinar-to-ductal metaplasia. *Gastroenterology* **145**, 1088-1097.e8 (2013).

203. Sharon, N. *et al.* Wnt Signaling Separates the Progenitor and Endocrine Compartments during Pancreas Development. *Cell Rep.* **27**, 2281-2291.e5 (2019).

204. Morris, J. P., Wang, S. C. & Hebrok, M. KRAS, Hedgehog, Wnt and the twisted developmental biology of pancreatic ductal adenocarcinoma. *Nat. Rev. Cancer* **10**, 683–695 (2010).

205. Zhang, Y. *et al.* Canonical wnt signaling is required for pancreatic carcinogenesis. *Cancer Res.* **73**, 4909–4922 (2013).

206. Wilson, B. G. & Roberts, C. W. M. SWI/SNF nucleosome remodellers and cancer. *Nat. Rev. Cancer* **11**, 481–492 (2011).

207. Tsuda, M. *et al.* The BRG1/SOX9 axis is critical for acinar cell–derived pancreatic tumorigenesis. *J. Clin. Invest.* **128**, 3475–3489 (2018).

208. von Figura, G. *et al.* The chromatin regulator Brg1 suppresses formation of intraductal papillary mucinous neoplasm and pancreatic ductal adenocarcinoma. *Nat. Cell Biol.* **16**, 255–267 (2014).

209. Sandoval, J. *et al.* Epigenetic Regulation of Early- and Late-Response Genes in Acute Pancreatitis. *J. Immunol. Baltim. Md 1950* **197**, 4137–4150 (2016).

210. Wang, W. *et al.* Purification and biochemical heterogeneity of the mammalian SWI-SNF complex. *EMBO J.* **15**, 5370–5382 (1996).

211. Chandler, R. L. *et al.* ARID1a-DNA interactions are required for promoter occupancy by SWI/SNF. *Mol. Cell. Biol.* **33**, 265–280 (2013).

212. Wang, W. *et al.* ARID1A, a SWI/SNF subunit, is critical to acinar cell homeostasis and regeneration and is a barrier to transformation and epithelial-mesenchymal transition in the pancreas. *Gut* **68**, 1245–1258 (2019).

213. Livshits, G. *et al.* Arid1a restrains Kras-dependent changes in acinar cell identity. *eLife* **7**, e35216 (2018).

214. Zhang, L. *et al.* Pancreas-Specific ARID1A Deficiency Promotes Acinar-to-Ductal Metaplasia and Elevates Interleukin-6 Expression in Experimental Pancreatitis Mode. (2021) doi:10.21203/rs.3.rs-326796/v1.

215. Simon, J. A. & Kingston, R. E. Mechanisms of Polycomb gene silencing: knowns and unknowns. *Nat. Rev. Mol. Cell Biol.* **10**, 697–708 (2009).

216. Benitz, S. *et al.* Polycomb repressor complex 1 promotes gene silencing through H2AK119 mono-ubiquitination in acinar-to-ductal metaplasia and pancreatic cancer cells. *Oncotarget* **7**, 11424–11433 (2016).

217. Benitz, S. *et al.* Ring1b-dependent epigenetic remodelling is an essential prerequisite for pancreatic carcinogenesis. *Gut* gutjnl-2018-317208 (2019) doi:10.1136/gutjnl-2018-317208.

218. Clair, J. M.-S. *et al.* EZH2 couples pancreatic regeneration to neoplastic progression. *Genes Dev.* **26**, 439–444 (2012).

219. Chen, N.-M. *et al.* Context-Dependent Epigenetic Regulation of Nuclear Factor of Activated T Cells 1 in Pancreatic Plasticity. *Gastroenterology* **152**, 1507-1520.e15 (2017).

220. Kalisz, M. *et al.* HNF1A recruits KDM6A to activate differentiated acinar cell programs that suppress pancreatic cancer. *EMBO J.* **39**, (2020).

221. Niu, N. *et al.* Loss of Setd2 promotes Kras-induced acinar-to-ductal metaplasia and epithelia-mesenchymal transition during pancreatic carcinogenesis. *Gut* **69**, 715–726 (2020).

222. Ogawa, S. *et al.* SETDB1 Inhibits p53-Mediated Apoptosis and Is Required for Formation of Pancreatic Ductal Adenocarcinomas in Mice. *Gastroenterology* **159**, 682-696.e13 (2020).

223. Wollny, D. *et al.* Single-Cell Analysis Uncovers Clonal Acinar Cell Heterogeneity in the Adult Pancreas. *Dev. Cell* **39**, 289–301 (2016).

224. Tosti, L. *et al.* Single nucleus RNA sequencing maps acinar cell states in a human pancreas cell atlas. *bioRxiv* 733964 (2019) doi:10.1101/733964.

225. Schlesinger, Y. *et al.* Single-cell transcriptomes of pancreatic preinvasive lesions and cancer reveal acinar metaplastic cells' heterogeneity. *Nat. Commun.* **11**, 4516 (2020).

226. Sangiorgi, E. & Capecchi, M. R. Bmi1 lineage tracing identifies a self-renewing pancreatic acinar cell subpopulation capable of maintaining pancreatic organ homeostasis. *Proc. Natl. Acad. Sci.* **106**, 7101–7106 (2009).

227. Westphalen, C. B. *et al.* Dclk1 Defines Quiescent Pancreatic Progenitors that Promote Injury-Induced Regeneration and Tumorigenesis. *Cell Stem Cell* **18**, 441–455 (2016).

228. Hingorani, S. R. *et al.* Preinvasive and invasive ductal pancreatic cancer and its early detection in the mouse. *Cancer Cell* **4**, 437–450 (2003).

229. Shi, C. *et al.* KRAS2 Mutations in Human Pancreatic Acinar-Ductal Metaplastic Lesions are Limited to those with PanIN: Implications for the Human Pancreatic Cancer Cell of Origin. *Mol. Cancer Res. MCR* **7**, 230–236 (2009).

230. Zhu, L., Shi, G., Schmidt, C. M., Hruban, R. H. & Konieczny, S. F. Acinar cells contribute to the molecular heterogeneity of pancreatic intraepithelial neoplasia. *Am. J. Pathol.* **171**, 263–273 (2007).

231. Guerra, C. & Barbacid, M. Genetically engineered mouse models of pancreatic adenocarcinoma. *Mol. Oncol.* **7**, 232–247 (2013).

232. Storz, P. Acinar cell plasticity and development of pancreatic ductal adenocarcinoma. *Nat. Rev. Gastroenterol. Hepatol.* **14**, 296–304 (2017).

233. Iacobuzio-Donahue, C. A. Genetic evolution of pancreatic cancer: lessons learnt from the pancreatic cancer genome sequencing project. *Gut* **61**, 1085–1094 (2012).

234. De La O, J.-P. *et al.* Notch and Kras reprogram pancreatic acinar cells to ductal intraepithelial neoplasia. *Proc. Natl. Acad. Sci. U. S. A.* **105**, 18907–18912 (2008).

235. Krah, N. M. *et al.* Prevention and Reversion of Pancreatic Tumorigenesis through a Differentiation-Based Mechanism. *Dev. Cell* **50**, 744-754.e4 (2019).

236. Grimont, A. *et al.* SOX9 regulates ERBB signalling in pancreatic cancer development. *Gut* **64**, 1790–1799 (2015).

237. Ray, K. C. *et al.* Epithelial Tissues Have Varying Degrees of Susceptibility to KrasG12D-Initiated Tumorigenesis in a Mouse Model. *PLoS ONE* **6**, e16786 (2011).

238. Guerra, C. *et al.* Chronic pancreatitis is essential for induction of pancreatic ductal adenocarcinoma by K-Ras oncogenes in adult mice. *Cancer Cell* **11**, 291–302 (2007).

239. Aichler, M. *et al.* Origin of pancreatic ductal adenocarcinoma from atypical flat lesions: a comparative study in transgenic mice and human tissues. *J. Pathol.* **226**, 723–734 (2012).

240. Yadav, D. & Lowenfels, A. B. The epidemiology of pancreatitis and pancreatic cancer. *Gastroenterology* **144**, 1252–1261 (2013).

241. Reichert, M., Blume, K., Kleger, A., Hartmann, D. & von Figura, G. Developmental Pathways Direct Pancreatic Cancer Initiation from Its Cellular Origin. *Stem Cells Int.* **2016**, 9298535 (2016).

242. Real, F. X. A “catastrophic hypothesis” for pancreas cancer progression1 1The author thanks J. Alguacil, D. Longnecker, N. Malats, X. Mayol, M. Porta, and A. Sodhi for valuable comments and suggestions to a prior version of this manuscript, as well as for many stimulating discussions and J. Franquesa for the artwork. *Gastroenterology* **124**, 1958–1964 (2003).

243. Sung, H. *et al.* Global Cancer Statistics 2020: GLOBOCAN Estimates of Incidence and Mortality Worldwide for 36 Cancers in 185 Countries. *CA. Cancer J. Clin.* **71**, 209–249 (2021).

244. Ferlay, J., Partensky, C. & Bray, F. More deaths from pancreatic cancer than breast cancer in the EU by 2017. *Acta Oncol. Stockh. Swed.* **55**, 1158–1160 (2016).

245. Siegel, R. L., Miller, K. D. & Jemal, A. Cancer statistics, 2020. *CA. Cancer J. Clin.* **70**, 7–30 (2020).

246. Jemal, A. *et al.* Cancer statistics, 2006. *CA. Cancer J. Clin.* **56**, 106–130 (2006).

247. McWilliams, R. R. *et al.* Risk Factors for Early-Onset and Very-Early-Onset Pancreatic Adenocarcinoma: A Pancreatic Cancer Case-Control Consortium (PanC4) Analysis. *Pancreas* **45**, 311–316 (2016).

248. Raimondi, S., Maisonneuve, P., Löhr, J.-M. & Lowenfels, A. B. Early onset pancreatic cancer: evidence of a major role for smoking and genetic factors. *Cancer Epidemiol. Biomark. Prev. Publ. Am. Assoc. Cancer Res. Cosponsored Am. Soc. Prev. Oncol.* **16**, 1894–1897 (2007).

249. GBD 2017 Pancreatic Cancer Collaborators. The global, regional, and national burden of pancreatic cancer and its attributable risk factors in 195 countries and territories, 1990-2017: a systematic analysis for the Global Burden of Disease Study 2017. *Lancet Gastroenterol. Hepatol.* **4**, 934–947 (2019).

250. He, J. *et al.* 2564 resected periampullary adenocarcinomas at a single institution: trends over three decades. *HPB* **16**, 83–90 (2014).

251. Wood, L. D. & Hruban, R. H. Pathology and molecular genetics of pancreatic neoplasms. *Cancer J. Sudbury Mass* **18**, 492–501 (2012).

252. Klein, A. P. Pancreatic cancer epidemiology: understanding the role of lifestyle and inherited risk factors. *Nat. Rev. Gastroenterol. Hepatol.* **18**, 493–502 (2021).

253. Bosetti, C. *et al.* Cigarette smoking and pancreatic cancer: an analysis from the International Pancreatic Cancer Case-Control Consortium (Panc4). *Ann. Oncol. Off. J. Eur. Soc. Med. Oncol.* **23**, 1880–1888 (2012).

254. Stolzenberg-Solomon, R. Z., Schairer, C., Moore, S., Hollenbeck, A. & Silverman, D. T. Lifetime adiposity and risk of pancreatic cancer in the NIH-AARP Diet and Health Study cohort. *Am. J. Clin. Nutr.* **98**, 1057–1065 (2013).

255. Lucenteforte, E. *et al.* Alcohol consumption and pancreatic cancer: a pooled analysis in the International Pancreatic Cancer Case-Control Consortium (PanC4). *Ann. Oncol. Off. J. Eur. Soc. Med. Oncol.* **23**, 374–382 (2012).

256. Solomon, S., Das, S., Brand, R. & Whitcomb, D. C. Inherited pancreatic cancer syndromes. *Cancer J. Sudbury Mass* **18**, 485–491 (2012).

257. Becker, A. E., Hernandez, Y. G., Frucht, H. & Lucas, A. L. Pancreatic ductal adenocarcinoma: risk factors, screening, and early detection. *World J. Gastroenterol.* **20**, 11182–11198 (2014).

258. Naudin, S. *et al.* Healthy lifestyle and the risk of pancreatic cancer in the EPIC study. *Eur. J. Epidemiol.* **35**, 975–986 (2020).

259. Huxley, R., Ansary-Moghaddam, A., Berrington de González, A., Barzi, F. & Woodward, M. Type-II diabetes and pancreatic cancer: a meta-analysis of 36 studies. *Br. J. Cancer* **92**, 2076–2083 (2005).

260. Chen, F., Roberts, N. J. & Klein, A. P. Inherited pancreatic cancer. *Chin. Clin. Oncol.* **6**, 58 (2017).

261. Del Chiaro, M., Segersvärd, R., Lohr, M. & Verbeke, C. Early detection and prevention of pancreatic cancer: is it really possible today? *World J. Gastroenterol.* **20**, 12118–12131 (2014).

262. Macdonald, S., Macleod, U., Campbell, N. C., Weller, D. & Mitchell, E. Systematic review of factors influencing patient and practitioner delay in diagnosis of upper gastrointestinal cancer. *Br. J. Cancer* **94**, 1272–1280 (2006).

263. Walter, F. M. *et al.* Symptoms and patient factors associated with diagnostic intervals for pancreatic cancer (SYMPTOM pancreatic study): a prospective cohort study. *Lancet Gastroenterol. Hepatol.* **1**, 298–306 (2016).

264. Neuzillet, C. *et al.* Pancreatic cancer: French clinical practice guidelines for diagnosis, treatment and follow-up (SNFGE, FFCD, GERCOR, UNICANCER, SFCD, SFED, SFRO, ACHBT, AFC). *Dig. Liver Dis.* **50**, 1257–1271 (2018).

265. Kamarajah, S. K., Burns, W. R., Frankel, T. L., Cho, C. S. & Nathan, H. Validation of the American Joint Commission on Cancer (AJCC) 8th Edition Staging System for Patients with Pancreatic Adenocarcinoma: A Surveillance, Epidemiology and End Results (SEER) Analysis. *Ann. Surg. Oncol.* **24**, 2023–2030 (2017).

266. Conroy, T. *et al.* FOLFIRINOX or Gemcitabine as Adjuvant Therapy for Pancreatic Cancer. *N. Engl. J. Med.* **379**, 2395–2406 (2018).

267. Hruban, R. H., Maitra, A., Kern, S. E. & Goggins, M. Precursors to pancreatic cancer. *Gastroenterol. Clin. North Am.* **36**, 831–849, vi (2007).

268. Robbins Basic Pathology PDF 10th Edition FREE Download [Direct Link] | Medicos Times. https://medicostimes.com/robbins-pathology-pdf/.

269. Maitra, A., Kern, S. E. & Hruban, R. H. Molecular pathogenesis of pancreatic cancer. *Best Pract. Res. Clin. Gastroenterol.* **20**, 211–226 (2006).

270. Redston, M. S. *et al.* p53 mutations in pancreatic carcinoma and evidence of common involvement of homocopolymer tracts in DNA microdeletions. *Cancer Res.* **54**, 3025–3033 (1994).

271. Hahn, S. A. *et al.* DPC4, a candidate tumor suppressor gene at human chromosome 18q21.1. *Science* **271**, 350–353 (1996).

272. Jones, S. *et al.* Core Signaling Pathways in Human Pancreatic Cancers Revealed by Global Genomic Analyses. *Science* **321**, 1801–1806 (2008).

273. Bailey, J. M. *et al.* p53 mutations cooperate with oncogenic Kras to promote adenocarcinoma from pancreatic ductal cells. *Oncogene* **35**, 4282–4288 (2016).

274. Collisson, E. A. *et al.* Subtypes of pancreatic ductal adenocarcinoma and their differing responses to therapy. *Nat. Med.* **17**, 500–503 (2011).

275. Moffitt, R. A. *et al.* Virtual microdissection identifies distinct tumor- and stroma-specific subtypes of pancreatic ductal adenocarcinoma. *Nat. Genet.* **47**, 1168–1178 (2015).

276. Bailey, P. *et al.* Genomic analyses identify molecular subtypes of pancreatic cancer. *Nature* **531**, 47–52 (2016).

277. Puleo, F. *et al.* Stratification of Pancreatic Ductal Adenocarcinomas Based on Tumor and Microenvironment Features. *Gastroenterology* **155**, 1999-2013.e3 (2018).

278. Thakur, R. & Singh, P. K. Molecular Subtypes of Pancreatic Cancer: A Proteomics Approach. *Clin. Cancer Res.* **27**, 3272–3274 (2021).

279. Campbell, P. J. *et al.* The patterns and dynamics of genomic instability in metastatic pancreatic cancer. *Nature* **467**, 1109–1113 (2010).

280. Shackleton, M., Quintana, E., Fearon, E. R. & Morrison, S. J. Heterogeneity in cancer: cancer stem cells versus clonal evolution. *Cell* **138**, 822–829 (2009).

281. Sakamoto, H. *et al.* The Evolutionary Origins of Recurrent Pancreatic Cancer. *Cancer Discov.* **10**, 792–805 (2020).

282. Zhang, Q. *et al.* Fbxw7 Deletion Accelerates KrasG12D-Driven Pancreatic Tumorigenesis via Yap Accumulation. *Neoplasia* **18**, 666–673 (2016).

283. Shibata, H. *et al.* In vivo reprogramming drives Kras -induced cancer development. *Nat. Commun.* **9**, 2081 (2018).

284. Roy, N. *et al.* Brg1 promotes both tumor-suppressive and oncogenic activities at distinct stages of pancreatic cancer formation. *Genes Dev.* **29**, 658–671 (2015).

285. Cherry, A. B. C. & Daley, G. Q. Reprogramming cellular identity for regenerative medicine. *Cell* **148**, 1110–1122 (2012).

286. Zenker, M. *et al.* Deficiency of UBR1, a ubiquitin ligase of the N-end rule pathway, causes pancreatic dysfunction, malformations and mental retardation (Johanson-Blizzard syndrome). *Nat. Genet.* **37**, 1345–1350 (2005).

287. Hwang, C.-S., Shemorry, A., Auerbach, D. & Varshavsky, A. The N-end rule pathway is mediated by a complex of the RING-type Ubr1 and HECT-type Ufd4 ubiquitin ligases. *Nat. Cell Biol.* **12**, 1177–1185 (2010).

288. Sancho, R., Gruber, R., Gu, G. & Behrens, A. Loss of Fbw7 Reprograms Adult Pancreatic Ductal Cells into α, δ, and β Cells. *Cell Stem Cell* **15**, 139–153 (2014).

289. Zhang, J. & Rouse, R. L. Histopathology and pathogenesis of caerulein-, duct ligation-, and arginine-induced acute pancreatitis in Sprague-Dawley rats and C57BL6 mice. *Histol. Histopathol.* **29**, 1135–1152 (2014).

290. Kwon, Y. T. & Ciechanover, A. The Ubiquitin Code in the Ubiquitin-Proteasome System and Autophagy. *Trends Biochem. Sci.* **42**, 873–886 (2017).

291. Ma, H. *et al.* M phase phosphorylation of the epigenetic regulator UHRF1 regulates its physical association with the deubiquitylase USP7 and stability. *Proc. Natl. Acad. Sci. U. S. A.* **109**, 4828–4833 (2012).

292. Deer, E. L. *et al.* Phenotype and Genotype of Pancreatic Cancer Cell Lines. *Pancreas* **39**, 425–435 (2010).

293. Wang, H., Cao, Q. & Dudek, A. Z. Phase II Study of Panobinostat and Bortezomib in Patients with Pancreatic Cancer Progressing on Gemcitabine-based Therapy. *ANTICANCER Res.* 5 (2012).